



HAL
open science

MATISSE Instrument Performance Report: Commissioning Report V2.0

R. G. Petrov, Fatmé Allouche, Stéphane Lagarde, Alexis Matter, Anthony Meilland, Florentin Millour, Bruno Lopez, James H. Leftley, Philippe Berio, Pierre Cruzalèbes, et al.

► **To cite this version:**

R. G. Petrov, Fatmé Allouche, Stéphane Lagarde, Alexis Matter, Anthony Meilland, et al.. MATISSE Instrument Performance Report: Commissioning Report V2.0. [Research Report] Version 2.0, European Southern Observatory. 2022. hal-03763766

HAL Id: hal-03763766

<https://hal.science/hal-03763766>

Submitted on 29 Aug 2022

HAL is a multi-disciplinary open access archive for the deposit and dissemination of scientific research documents, whether they are published or not. The documents may come from teaching and research institutions in France or abroad, or from public or private research centers.

L'archive ouverte pluridisciplinaire **HAL**, est destinée au dépôt et à la diffusion de documents scientifiques de niveau recherche, publiés ou non, émanant des établissements d'enseignement et de recherche français ou étrangers, des laboratoires publics ou privés.



MATISSE Consortium

UNS-OCA-CNRS, Nice, France
MPIA, Heidelberg, Germany
MPIfR, Bonn, Germany
NOVA, The Netherlands
ITAP, Kiel University, Germany
Vienna University, Vienna, Austria

Very Large Telescope MATISSE

MATISSE Instrument Performance Report: Commissioning Report

Doc. No.: VLT-TRE-MAT-15860-9141

Issue: 2.0

Date: 15/07/2022

Author(s):	R.G. Petrov, F. Allouche, S. Lagarde, A. Matter, A. Meilland, F. Millour, B. Lopez, J Leftley, Ph Berio, and the MATISSE commissioning team*	15/07/2022	
	Name	Date	Signature
Project Manager:	S. Lagarde	15/07/2022	
	Name	Date	Signature
Principal Investigator:	B. Lopez	15/07/2022	
	Name	Date	Signature

(*) The full list of commissioning team members can be found in annex 0 of this document



CHANGE RECORD

ISSUE	DATE	SECTION/PAGE AFFECTED	REASON/INITIATION/DOCUMENT/REMARKS
Draft 1.0	03/04/2020	All	Issue for iteration through the consortium
1.0	08/06/2020	All	
1.1	01/08/2020	1.5 p 10 and 5.6 p 51	Update on N coherent flux limits due to the coherent flux bias
		2.7 pp 18 to 22	New: coherent flux bias in N
		8 pp 57 to 63	Annex 8: justification of DRS options with illustrations
		8.1 p 57	ReplaceTel option
		8.2 p 59	Hampel filter option
		8.3 p 59	Effect of modulation and demodulation in N
		8.4 p 60	BCD calibration on Closure phase in L, M, N
		8.5 p 62	Spectral Binning
		8.6 p 63	Comparing LR-N and HR-N binned down to LR-N resolution
2.0	15/07/2022	10 p 70-71	New: examples near the limits
		All	Answers to AI of the punch list required for PAC
		Section 5.7	Inclusion of performances in N2 (10.5 um) and N3 (11.5 um) in fair seeing conditions
		Annex 6	Update of the commissioning runs and participants
		Annex 11	New annex about the VHR calibration in L and M band
		Annex 12	New annex containing the ETC plots of N2 and N3 bands
		Annex 13	New annex containing about the chopping frequency
		Annex 14	New annex containing about the influence of the BCD on the correlated flux
		Annex 15	New annex containing about the chromatic phase correction
Annex 16	New annex containing about the influence of the PWV on the visibility measurement		
Section 1.5 and Annex 17	Update of the proposed performances for MATISSE users		



MATISSE Instrument Performance Report:

Commissioning Report

Doc. :	VLT-TRE-MAT-15860-9141
Issue :	2.0
Date :	15.07.22
Page :	3 of 131

INTENTIONALLY LEFT BLANK

**Commissioning Report**

1	Introduction	9
1.1	Scope	9
1.1.1	<i>Scope of this commissioning report.....</i>	<i>9</i>
1.1.2	<i>Scope of the V2.0 update of this commissioning report.....</i>	<i>9</i>
1.2	Documents and Acronyms	9
1.2.1	<i>Applicable Documents</i>	<i>9</i>
1.2.2	<i>Reference Documents</i>	<i>9</i>
1.2.3	<i>Acronyms and usual symbols.....</i>	<i>10</i>
1.3	Content and structure of the report.....	10
1.4	Synthesis of Technical Specifications checked during commissioning.....	13
1.5	Synthesis of proposed performances for MATISSE users.....	14
2	Performance measurement methodology.....	15
2.1	Introduction	15
2.2	Fundamental noise error	15
2.2.1	<i>Computed prediction</i>	<i>15</i>
2.2.2	<i>Measured precision</i>	<i>16</i>
2.2.3	<i>Adjusting the ETC prediction to the measured precision.....</i>	<i>16</i>
2.3	Broad band calibration error from instrument and atmosphere variations.....	18
2.4	Broad band photometric errors.....	19
2.5	Sensitivity to seeing changes.....	20
2.6	Synthesis of broad band calibration errors	21
2.7	Update on the coherent flux BIAS in the N band	23
3	Operation and data reduction parameters	26
3.1	Acquisition OB.....	26
3.2	Observation OB.....	27
3.3	Data reduction parameters.....	27
4	Compliance with the technical specification	27
4.1	Operation specifications	27
4.1.1	<i>Number of telescopes and baselines</i>	<i>27</i>
4.1.2	<i>Observing modes</i>	<i>28</i>
4.1.3	<i>Sensitivity.....</i>	<i>28</i>
4.1.4	<i>Fringe Sensing.....</i>	<i>31</i>
4.1.5	<i>Observing time efficiency.....</i>	<i>32</i>
4.2	Compliance of measurement precision or accuracy with specifications.....	34
4.2.1	<i>Absolute visibility.....</i>	<i>34</i>
4.2.2	<i>Differential phase</i>	<i>36</i>
4.2.3	<i>Closure phase</i>	<i>37</i>
4.2.4	<i>Differential visibility.....</i>	<i>39</i>

**Commissioning Report**

5	Offered performances	40
5.1	Introduction	40
5.2	L band.....	42
5.2.1	Low Resolution	42
5.2.2	Medium Resolution	44
5.2.3	High Resolution	46
5.3	M band.....	48
5.3.1	Low Resolution	48
5.3.2	Medium Resolution	50
5.4	N1 band	51
5.4.1	Low Resolution	51
5.4.2	High Resolution	54
5.5	Summary table for the V1.1 version	56
5.5.1	L, M and N1 bands.....	56
5.6	Proposed performances in version 1.1	57
5.7	Complement to N-band performances: N2 and N3 bands	57
6	Annex: Commissioning runs and team	59
6.1	Commissioning runs.....	59
6.1.1	Operations (March 2018).....	59
6.1.2	Measurement accuracy in LR L&N (May 2018)	59
6.1.3	Higher spectral resolutions (July and September 2018)	59
6.1.4	Imaging and NAOMI update (December 2018)	60
6.1.5	M Band (April 2019).....	60
6.1.6	VHR (December 2019).....	60
6.1.7	GRA4MAT (from 2019 to 2022)	60
6.1.8	L band dispersive wheel recovery (February 2022)	60
6.1.9	Final update run (April 2022)	61
6.2	Commissioning Team	61
7	Annex: Observing parameters	62
7.1	Parameters of acquisition OB.....	62
7.2	Parameters of observation OB.....	62
7.2.1	DIT and NDIT.....	62
7.2.2	Chopping parameters	62
7.2.3	Spatial filters.....	63
7.2.4	Modulation.....	63
8	Annex: Data reduction options	64
8.1	ReplaceTel.....	64
8.2	Hampel filter	66

**Commissioning Report**

8.3	Modulation/demodulation	66
8.4	BCD calibration of closure phase.....	67
8.5	Spectral binning.....	69
8.6	HR-N binned to LR-N.....	69
9	Annex: Fundamental noise estimation	72
9.1	Expected fundamental noise from the Exposure Time Calculator.....	72
9.1.1	Visibility observable	72
9.1.2	Phase observables	73
9.1.3	Parameters and assumptions.....	74
9.2	Measured fundamental noise.....	74
10	Annex: examples of measures near the limits.....	77
11	ANNEX: VHR calibration in L and M band.....	79
12	ANNEX: N2 and N3 performance estimates	80
12.1	Low resolution.....	80
12.2	High resolution.....	82
13	ANNEX: chopping frequency	84
14	ANNEX: BCD influence on visibility	86
15	ANNEX: Chromatic Phase Correction	89
16	ANNEX: Impact of the PWV on visibility	93
17	ANNEX: Update of MATISSE standalone proposed performances.....	95
17.1	New measurements	95
17.2	Sensitivity limit updates from new measurements.....	96
17.3	Global synthesis of performances	97
18	ADDITIONAL MEMO: VHR and GRA4MAT MATISSE performances	99
19	ADDITIONAL MEMO: GRA4MAT with UTs	99
1	Scope.....	103
2	Summary of conclusions	103
2.1	Propositions.....	103
2.2	GRA4MAT operation limits	103
2.3	Coherent flux, closure phase and differential measures.....	103
2.4	Absolute visibility measures	103
2.5	Execution times with GRA4MAT.....	104
2.6	Future improvements.....	104
2.7	Data reduction of MATISSE data with GRA4MAT.....	104
3	GRA4MAT operation	105
3.1	Observation preparation	105

**Commissioning Report**

3.2	Operation sequence	105
3.3	MATISSE DITs with GRA4MAT	105
3.3.1	<i>In Low Resolution: DIT=1s</i>	105
3.3.2	<i>Higher spectral resolutions: DIT=10s</i>	106
4	Limits of MATISSE with GRA4MAT	106
4.1	Methodology	106
4.1.1	<i>Flux dependent calibration error.</i>	106
4.1.2	<i>Seeing dependent calibration error</i>	107
4.1.3	<i>Fundamental noise errors</i>	108
4.2	VHR mode	108
4.3	VHR-L differential phase: 20 Jy	109
4.4	VHR-L closure phase: 25 Jy	109
4.5	VHR-L Differential Visibility: 18 Jy	110
4.6	VHR-L illustration	110
4.7	VHR-M differential phase: 17 Jy	111
4.8	VHR-M closure phase: 25 Jy	111
4.9	VHR-M differential visibility: 15 Jy	112
4.10	HR-L Differential phase: 2 Jy	113
4.11	HR-L Closure phase: 3 Jy	113
4.12	HR-L Differential visibility: 3 Jy but SiPhot shift problem	114
4.13	HR-L illustration	115
4.14	MR-L Differential phase: 1 Jy	115
4.15	MR-L Closure phase: 1.5 Jy	116
4.16	MR-L Illustration	116
4.17	MR-M Differential phase	117
4.18	MR-M Closure phase	117
4.19	LR-L Differential phase: 0.17 Jy	118
4.20	LR-L Closure phase: 0.5 Jy	118
4.21	LR-M Differential phase: 0.7 Jy	119
4.22	LR-M Closure phase: 4 Jy	119
4.23	LR-M Illustration	120
5	Annex: transmission of VHR grisms	121
1	Scope	124
2	Summary of conclusions	124
2.1	Status of observations	124
2.2	Propositions	124



Commissioning Report

2.3	GRA4MAT operation limits	124
2.4	Coherent flux limit in the N	124
2.5	DIT for LM band observations with GRA4MAT on UTs	125
2.6	Absolute visibility measures	126
2.7	Execution times with GRA4MAT.....	127
2.8	Data reduction of MATISSE data with GRA4MAT.....	127
3	Targets successfully reduced in N with the K for N coherent flux bias correction.	128
4	Fringe jump rates as a function of observing conditions.....	131



1 INTRODUCTION

1.1 SCOPE

1.1.1 Scope of this commissioning report

- Show that the MATISSE performances measured during the commissioning are compliant with the contractual technical specifications.
- Update and consolidate the performances offered to the users of the MATISSE contractual modes.

1.1.2 Scope of the V2.0 update of this commissioning report

- Tackle the questions raised by ESO after the V1.1 and listed in the punch list of actions required for the PAC. The list is given in section 1.3.

1.2 DOCUMENTS AND ACRONYMS

1.2.1 Applicable Documents

AD Nr	Doc Nr	Doc Title	Issue	Date
AD1	VLT-SPE-ESO-15860-4820	MATISSE Technical Specifications	1	12.07.2011
AD2	VLT-SOW-ESO-15860-4819	MATISSE Statement of Work	1	12.07.2011

1.2.2 Reference Documents

RD Nr	Doc Nr	Doc Title	Issue	Date
RD1	VLT-VRM-MAT-15860-9029	MATISSE Verification Matrix (PAE)	5	24.05.2017
RD2	VLT-VRM-MAT-15860-9029	MATISSE Verification Matrix	6	08.06.2020
RD3	MAT-COM-2018-06-25	MATISSE Preliminary commissioning report	1	25.06.2018
RD4	MAT-COM-2018-08-05	MATISSE Performances from commissioning 1A&1B and proposed observing limits for P103	1	05.08.2018
RD5	MAT-COM-2019-02-01	Update of MATISSE performances after NAOMI implementation and the September and December commissioning runs	1	01.02.2019
RD6	MAT-COM-2019-02-22	Proposed update of MATISSE performances for P104	1	22.02.2019
RD7	MAT-COM-2019-07-31	MATISSE performances in the M band, L band update	1	31.07.2019
RD8	MAT-COM-2020-01-16	VHR and GRAMAT MATISSE performances update	1	16.01.2020
RD9	VLT-TRE-MAT-15860-9304	MATISSE Exposure Time Calculator Specifications	3	24.05.2017
RD10	VLT-PLA-MAT-15860-9140	MATISSE Test and Inspection report: AIV Report	2	08.07.2020
RD11	VLT-PLA-MAT-15860-9020	MATISSE Commissioning Plan	2	24.05.2017
RD12	VLT-TRE-MAT-15860-9135	MATISSE Instrument Performance Report	2	24.05.2017
RD13	VLT-TRE-MAT-15860-9007	MATISSE Performance Analysis Report	3	31.07.2012
RD14	VLT-TRE-MAT-15860-9141	MATISSE Commissioning report	1.1	01.08.2020



1.2.3 Acronyms and usual symbols

CfP	Call for Proposals
DIT	Detector integration time for one frame
DRS	Data reduction Software
NDIT	Number of frames in one exposure
PAC	Provisional Acceptance Chili
PAE	Preliminary Acceptance Europe
$V, V_{ij}, V(\lambda)$	Visibility, on the baseline ij , (as a function of wavelength)
$V_D, V_{Dij}, V_D(\lambda)$	Differential Visibility, on the baseline ij , (as a function of wavelength)
$\varphi, \varphi_{ij}, \varphi_{ij}(\lambda)$	Differential phase, on the baseline ij , (as a function of wavelength)
$\Psi, \Psi_{ijk}, \Psi_{ijk}(\lambda)$	Closure phase, on the triplet ijk , (as a function of wavelength)
$V_{cal}, V_{Dcal}, \varphi_{cal}, \Psi_{cal}$	Measures on calibrators

1.3 CONTENT AND STRUCTURE OF THE REPORT

The version 1.1 of this report, distributed in August 2020 was based on the MATISSE commissioning runs executed between March 2018 and March 2020. The list and key goals of each commissioning run are given in Annex 6.1. The commissioning team is presented in Annex 6.

The main goal of the commissioning is to show the operability and measure the performances of MATISSE with the VLTI on sky.

The methodology used to measure the precision and accuracy of MATISSE measurements is described in section 2.

The set of MATISSE observing and data reduction parameters that have been selected, optimized, and validated through the commissioning is presented in section 3. Annexes 7 and 8 detail the justification of the choices made for the key parameters.

Then, we present the measured performances of MATISSE with this optimized observing and data reduction parameters.

Section 44 shows that the performances of MATISSE are compliant with its contractual technical specifications described in the reference documents AD1 and AD2. Here, we discuss only the specifications that had to be checked on sky during the commissioning and were listed in the Verification Matrix agreed at the PAE of MATISSE (RD1). The compliance of MATISSE with all contractual specifications is shown in the PAC issue of the Verification Matrix (RD2). For the commodity of the reader, the following chapter (1.4) gives a synthetic list of these specifications and compliance validations. Then each specification and its validation are justified in the chapter of section 4, as indicated in the table of specifications.

The performances that we propose to offer to MATISSE users in the observing Call for Proposals (CfP) are described in section 5 and Annex 170, with a summary table in chapter



1.5. This report focuses on the contractual spectroscopic setups of MATISSE, defined in the technical specifications (AD1) and validated in the Verification Matrix (RD2).

Band	Range (μm)	LR	MR	HR
L	2.8-4.2	31.	499	979
M	4.5-5			NA
N	8-13	31.5	NA	218
N1	8.1-8.9			
N2	10-11			
N3	11-12			

MATISSE spectral bands and measured resolutions (from RD2 and RD10)

The performance estimates shown in the version 1.1 of this report are based on all the validated commissioning data, reprocessed with the Data Reduction Software (DRS) pipeline delivered to ESO in February 2020 (version 1.5.0). They update and most often confirm¹ or slightly improve the performances already offered by ESO for period P106 based on the various partial commissioning reports sent to ESO between June 2018 and January 2020 (reference documents RD3 to RD8).

In November 2019, we installed the Very High-Resolution (VHR) mode in L and M and we started commissioning it with the “GRA4MAT” extension based on the use of the GRAVITY Fringe Tracker for Observations with MATISSE. As it was agreed that these modes are not part of the PAC process, they are not addressed in this report. However, as these modes were already accepted by ESO and offered in the CfP for P106, the relevant commissioning report (RD8) sent to ESO in January 2020 and updated in February 2020, is appended in **Annex Erreur ! Source du renvoi introuvable.** of RD14. A brief discussion about the impact of GRA4MAT on coherent flux bias can also be found in section 2.7 where these biases are discussed.

There is no Technical Specification for the possibility to reconstruct images with MATISSE and the VLTI, but for the fact that MATISSE is a 4 telescopes instrument that delivers accurate closure phases. However, the MATISSE Statement of Work (AD2) requests, before the PAC, a proof that MATISSE can reconstruct images. This was achieved during the commissioning run of December 2018 and an example of image reconstruction is given in annex **Erreur ! Source du renvoi introuvable.** of RD14.

The version 1.1 of this commissioning report triggered a set of questions to be tackled before the PAC is granted to MATISSE. These questions are discussed in the present V2.0 update of the commissioning report which also updates some values based on the commissioning runs executed remotely after March 2020 and the Covid crisis interruption. In particular, we checked the performances of MATISSE after the repair of the DIL grating wheel (that sets the resolution modes in the L and M bands) that permitted the execution of the last commissioning runs for MATISSE standalone (see Annex 6 for the updated list of the commissioning runs).

1 The most substantial revision is an improvement of the limit for absolute visibility measurements in Low Spectral Resolution in the N band with ATs, from 28 Jy to 17 Jy.



Commissioning Report

The list of questions that had to be tackled before the PAC and that triggered this V2.0 update are:

1. Update the limiting performances for MATISSE standalone from the last commissioning runs.
2. Extend the evaluation of MATISSE performances to the full N band
3. Discuss the improvement of photometric measures
4. Update the chopping frequency requirements
5. Remove the signature of the BCD in the data
6. Provide a simple method to calibrate the LR differential phases and evaluate its performances
7. Provide a procedure for the spectral calibration of the VHR mode. This mode, also called High+, refers to the resolution ~ 3300 in L and M.
8. Discuss the influence of the water vapor content on the MATISSE measures.

Points 1, 2 and 3 triggered an update of the MATISSE performances to be presented to the general user, included in the summary table in section 1.5. The justification for the updates is briefly indicated in foot notes with some more details in annex 17.

The details of the evaluation of performances in the various N bands (point 2) is discussed in section 5.7.

The improvement of photometric measures (point 3) was already discussed in the version 1.1 of the report. They are based on data processing methods (we are now using the version 1.7.5) that include the possibility to replace a dubious photometric measurement by a combination of the other. This already triggered the shift from the 25-30 Jy limits in N offered to the users to the values 16.8-18.5 Jy proposed here based on detailed statistics on large data sample. We have recorded data for methods that could lead to further improvements but that require substantial Data Reduction changes that are longer term, post-Pac activities.

The update of the required chopping frequency (point 5) is discussed in Annex 13.

Removing the BCD signature (point 5) in the closure phase is a standard feature of the current version of the DRS that delivers a BCD calibrated closure phase to be used directly by the user. The removal of the BCD signature in the visibility and coherent flux measurements is the topic of the section 14 of this document.

The calibration of the differential phase (point 6) is described in section 15 of this document.

Points 7 and 8 are tackled in sections 11 and 16 of this document.



1.4 SYNTHESIS OF TECHNICAL SPECIFICATIONS CHECKED DURING COMMISSIONING

The following table gives the list of specifications that had to be checked during the commissioning.

Item	Name	Technical Specification	Performances	Section	Compliance
SP-1	Number of combined beams	4	4	4.1.1	C
SP-12	Visibility accuracy ² L (UT, 20Jy)	$\leq 7.5\%$	$\sigma_v/v = 0.25\%$	4.2.1	C
SP-13	Visibility accuracy N (UT, 20Jy)	$\leq 7.5\%$	$\sigma_v/v = 0.35\%$	4.2.1	C
SP-14	Visibility accuracy L (AT, 20Jy)	$\leq 7.5\%$	$\sigma_v/v = 0.8\%$	4.2.1	C
SP-15	Visibility accuracy N (AT, 20Jy)	$\leq 30\%$	$\sigma_v/v = 8.5\%$	4.2.1	C
SP-16	Differential phase L (UT, 20Jy)	$\leq 30\text{mrad}$	$\sigma_\phi = 14.5\text{mrad}$	4.2.2	C
SP-17	Differential phase L (AT, 20Jy)	$\leq 60\text{mrad}$	$\sigma_\phi = 14.5\text{mrad}$	4.2.2	C
SP-18	Differential phase N (UT, 20Jy)	$\leq 30\text{mrad}$	$\sigma_\phi = 1.5\text{mrad}$	4.2.2	C
SP-19	Differential phase N (AT, 20Jy)	$\leq 60\text{mrad}$	$\sigma_\phi = 9\text{mrad}$	4.2.2	C
SP-20	Closure phase L (UT, 20Jy)	$\leq 40\text{mrad}$	$\sigma_\phi = 4.9 \text{ mrad}$	4.2.3	C
SP-21	Closure phase L (AT, 20Jy)	$\leq 80\text{mrad}$	$\sigma_\phi = 5.4 \text{ mrad}$	4.2.3	C
SP-22	Closure phase N (UT, 20Jy)	$\leq 40\text{mrad}$	$\sigma_\phi = 8.5 \text{ mrad}$	4.2.3	C
SP-23	Closure phase N (AT, 20Jy)	$\leq 80\text{mrad}$	$\sigma_\phi = 21 \text{ mrad}$	4.2.3	C
SP-24	Sensitivity in L UT	$\text{SNR}_C \geq 3$ in coherence time for flux $\geq 0.75 \text{ Jy}$	$\text{SNR}_C=14.8$ for flux= 0.75Jy $\text{SNR}_C=3$, flux= 0.04 Jy	4.1.3	C
SP-25	Sensitivity in L AT	$\text{SNR}_C \geq 3$ in coherence time for flux $\geq 7.5 \text{ Jy}$	$\text{SNR}_C=14.8$, flux = 7.5 Jy $\text{SNR}_C=3$ for flux= 0.45 Jy	4.1.3	C
SP-26	Sensitivity in N UT	$\text{SNR}_C \geq 3$ in coherence time for flux $\geq 3 \text{ Jy}$	$\text{SNR}_C = 55.0$ for flux = 3 Jy $\text{SNR}_C=3$ for flux= 0.14 Jy	4.1.3	C
SP-27	Sensitivity in N AT	$\text{SNR}_C \geq 3$ in coherence time for flux $\geq 45 \text{ Jy}$	$\text{SNR}_C=45.8$ for flux= 45 Jy $\text{SNR}_C=3$ for flux= 2.7 Jy	4.1.3	C
SP-28	Differential visibility accuracy L (UT, 20Jy)	$\leq 1.5\%$	$\sigma_{\text{diff}}/v_{\text{diff}} = 0.25\%$	4.2.4	C
SP-29	Differential visibility accuracy N (UT, 20Jy)	$\leq 3\%$	$\sigma_{\text{diff}}/v_{\text{diff}} = 0.15\%$	4.2.4	C
SP-30	Differential visibility accuracy L (AT, 20Jy)	$\leq 5\%$	$\sigma_{\text{diff}}/v_{\text{diff}} = 0.25\%$	4.2.4	C
SP-31	Differential visibility accuracy N (AT, 20Jy)	$\leq 30\%$	$\sigma_{\text{diff}}/v_{\text{diff}} = 0.6\%$	4.2.4	C
SP-38	Fringe sensing accuracy (tracking in full L band in Low Resolution)	Accuracy better than (Coherence length)/2 at 0.1 Hz	Accuracy better than (Coherence length)/15 at $>1 \text{ Hz}$	4.1.4	C
SP-43	Observing time efficiency (for 6 calibrated measures)	$< 1\text{hr}$	ATs average = 55:14 UTs average = 56:36	4.1.5	C
SP-44	Observing modes	HighSens, SiPhot	Optimization: SiPhot in L and HighSens in N	4.1.2	C

2 We copy the « accuracy » specifications from the Technical Specification (AD1). We give the precision of calibrated measures that can be considered as the accuracy on the measure if the calibrator is perfectly unresolved ($V=1$, $V_{\text{diff}}=1$, $\phi_{\text{diff}}=0$, $\Psi=0$).



Column #1 is the verification matrix item number, column #2 the specification name, column #3 gives the specified value and #4 the commissioned value. Column #5 gives the section of that report where this value is justified. Column #6 confirms that MATISSE is very largely compliant on all items. The values given in column #4 were computed from datasets obtained under “fair” conditions, i.e. seeing=0.75±0.25 arcsec and $\tau_0=7\pm 2$ ms. The specifications in column #3 were defined at “0.7 arcsec seeing” without indications on the coherence time.

1.5 SYNTHESIS OF PROPOSED PERFORMANCES FOR MATISSE USERS

Here we summarize the performances that we propose to offer to MATISSE users in the CfPs. In agreement with Paranal MATISSE Instruments Scientists, the following table give the limits in coherent flux in Jy that allow to reach the following precisions on calibrated measurements, on all baselines, **in each spectral channel for each 1mn exposure**:

- Visibility: $\sigma_V = 0.1$
- Closure phase: $\sigma_\psi = 5^\circ$
- Differential phase: $\sigma_\phi = 4^\circ$
- Coherent flux SNR: $C/\sigma_C = 10$

For « Fair and Good » seeing conditions (seeing<0.9 arcsec, $\tau_0>5$ ms)³.

Limiting Coherent flux in Jy							
Telescopes	Resolution	Visibility		Closure Phase		Differential Phase	
		L	M	L	M	L	M
ATs	LOW	1.1	2.1	0.4	1.9	0.3	1.1
	MED	8.0	TBC ⁴	7.0	TBC	5.6	TBC
	HIGH	20.1	na	14.7	na	10.7	na
UTs	LOW	0.08	0.17	0.07	0.16	0.06	0.15
	MED	0.6	TBC ⁵	0.6	TBC	0.4	TBC
	HIGH	2.4	na	1.7	na	1.2	na

For « Poor » seeing conditions (seeing=0.9±0.2 arcsec and $\tau_0=3.6\pm 1.6$ ms)

Limiting Coherent flux in Jy							
Telescopes	Resolution	Visibility		Closure Phase		Differential Phase	
		L	M	L	M	L	M
ATs	LOW	2.8	4.0	0.4	1.5	0.3	1.1
	MED	8.0	TBC	7.0	TBC	5.6	TBC
	HIGH	31.4	na	14.7	na	10.7	na
UTs	LOW	0.1	0.15	0.07	0.16	0.06	0.15
	MED	0.6	TBC	0.6	TBC	0.4	TBC
	HIGH	3.8	na	1.7	na	1.3	na

3 The numbers for the « fair seeing » data set (seeing=0.75±0.2 arcsec and $\tau_0=7\pm 2$ ms) are very similar to those for a “good seeing” data set (seeing=0.55±0.1 arcsec and $\tau_0=8\pm 2$ ms). The limit between “good” and “bad” conditions for MATISSE is fundamentally set by $\tau_0\sim 4$ ms)

4 The MR-M band values were based on extrapolation from sparse data. We could not confirm these values as our new measurements are incoherent. We prefer to declare this values “TBC” until we obtain new data, hopefully in July 2022 if weather permits.

5 The values given in MR_M with UTs were estimated from the measured UT/AT flux ratio in M. As we could not confirm the AT values, the UT values are also declared “TBC”.

**For all conditions**

Limiting Coherent flux in Jy													
Telescopes	Resolution	Visibility			Closure Phase			Differential Phase Coherent Flux SNR			Combined Bias and fundamental noise limit on the CF		
		N1	N2	N3	N1	N2	N3	N1	N2	N3	N1	N2	N3
ATs	LOW	16.8	31.4	44.0	9,4	23.6	36.7	2,9	7.5	11.7	6	8	12
	HIGH	30.3	51.3	83.7	29.9	194	218	25,3	45.9	58.9	25,3	45.9	58.9
UTs	LOW	0.9	1.4	1.9	0.3	0.8	1.3	0.2	0.55	0.6	0.5	0.7	0.8
	HIGH	1.6	3.4	4.1	1.5	4.9	13.1	1.1	3.5	3.7	1.1	3.5	3.7

The coherent flux bias limits set by noise on the group delay correction have been estimated to be of the order of 5-6 Jy in N1 and 8-9 Jy in N3. As the group delay is estimated from the full N band, this bias is less dependent from the wavelength than the fundamental noise. In fact, it represents a specific limit only in and near N1, the other bands remaining dominated by fundamental noise. In HR-N, the fundamental noise completely dominates over the bias limit.

The justification of these numbers is given through the document. In the next section we summarize the methodology used to measure the performances of MATISSE.

2 PERFORMANCE MEASUREMENT METHODOLOGY

2.1 INTRODUCTION

Three elements are combined to evaluate the quality of MATISSE measurements.

- The variance of the error measurement due to fundamental noise.
- The variance of the calibration error on the visibility introduced by error on the photometric estimation, called the broad band photometric error
- The variance of the calibration error due to atmosphere + instrument changes between a science source and its calibrator.

As the results are calibrated measurements, the error combining fundamental noise and calibration error applies on the true measure, if the calibrator is perfectly unresolved, i.e. $V_{cal}(\lambda) = V_{Dcal}(\lambda) = 1$ and $\Psi(\lambda) = \varphi(\lambda) = 0$, and can hence be considered as a measurement accuracy. If the calibrator is resolved, the error must be divided by V_{cal} and combined with the uncertainty on the true value of the calibrator diameter and hence V_{cal} .

2.2 FUNDAMENTAL NOISE ERROR

2.2.1 Computed prediction

The Exposure Time Calculator (ETC) computes the measurement errors as a function of the coherent flux due to:

- The source photon noise
- The detector read-out noise
- The background photon noise

The ETC is described in the document RD9, and a summary of this description is given in Annex 0 for the comfort of the reader.

Commissioning Report

2.2.2 Measured precision

The error bars on the measures given by the pipeline are sensitive to the fundamental noise and to variations of the instrumental response during the exposure. To isolate the contribution of fundamental noise we measure a dispersion of the measures in the wavelength direction, after fitting the measure $M(\lambda)$ by a 2nd degree polynomial and subtracting the fit:

$$\sigma_c = rms\{M(\lambda) - fit[M(\lambda)]\}$$

The fit removes all calibration biases that affect globally the measurement. This procedure is explained with some additional details in annex 9.2.

2.2.3 Adjusting the ETC prediction to the measured precision.

The figure 2.2.3.a below shows the ETC prediction (straight full lines) for three different sets of instrument parameters (in particular the expected transmission, over-plotted on the measured precisions of a large number of one-minute exposures from many observations. The ETC plot can be then adjusted to the measurements, to fit through the median distribution of points. Finally, the fitted ETC curve can be used to obtain the variance (or standard deviation) of the fundamental noise error as a function of the coherent flux.

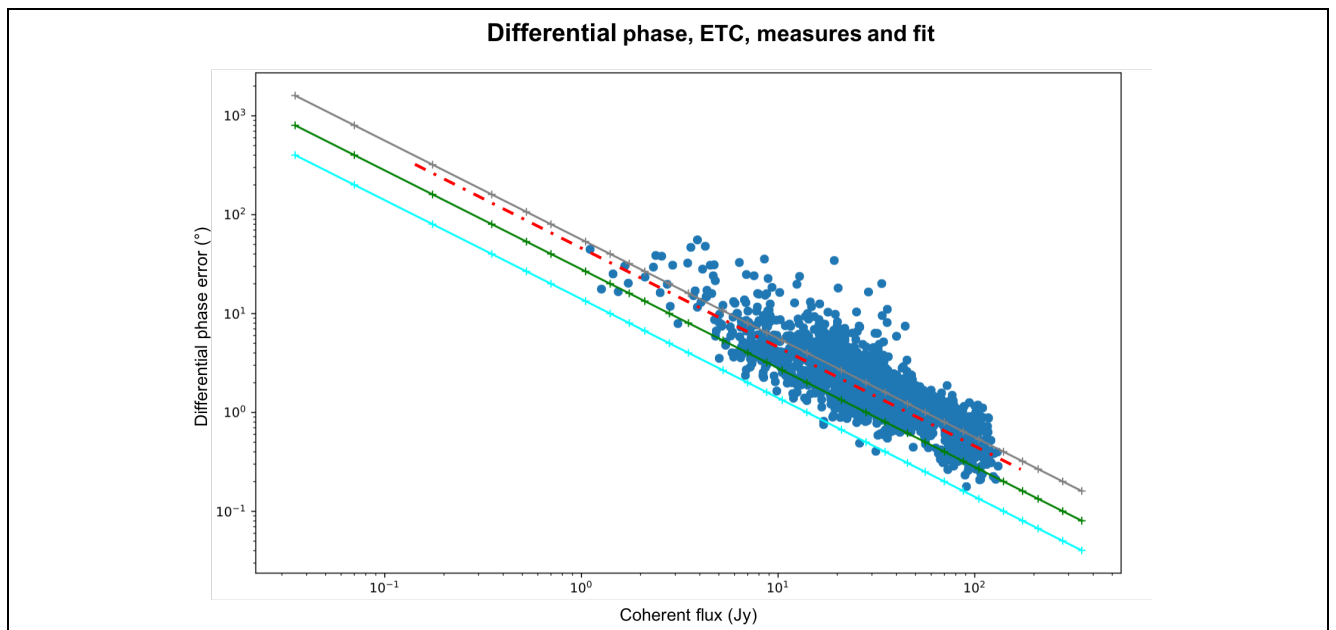


Figure 2.2.3.a: fundamental noise error on the differential phase as a function of the source coherent flux (from RD5), for N band LR observations with ATs between 8 and 9 μm in December 2018 (plot from RD5).

The full lines are the ETC prediction for three different values of the instrument exact transmission (the central one being the best expectation after AIV). Each blue point represents the precision of one actual exposure of one minute. All baselines and many observations with a range of different conditions are merged (there is no significant difference between baselines). The red dot-dashed line represents the adaptation of the computed ETC to fit the median distribution of measures.

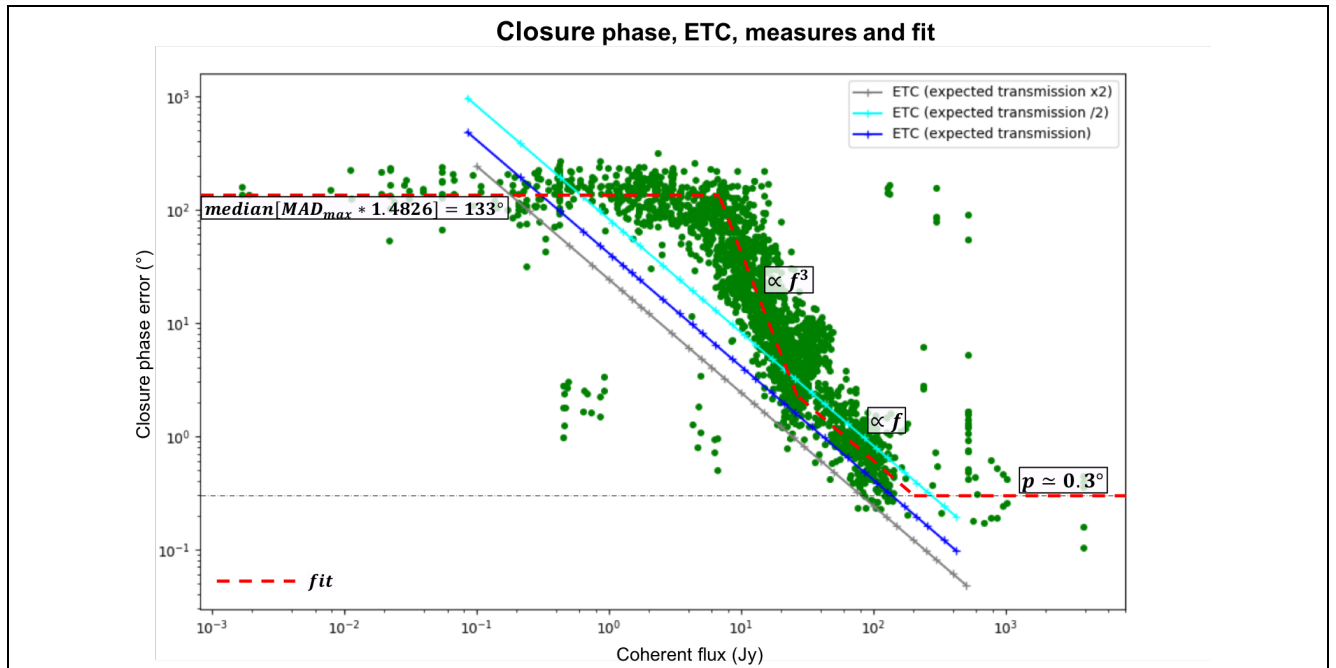


Figure 2.2.3.b: fundamental noise error on the closure phase as a function of the source coherent flux (from RD5). The dots, straight and dashed lines have the same meaning than in figure 2.2.3.a. In the case of the Closure Phase the computed ETC is valid only for bright sources or small phase errors, as explained in annex 9.1.2. A better fit of the measures is obtained by a sum of $1/f$ and $1/f^2$ functions. In addition, we have often to include an upper, low flux plateau on phase measurements, corresponding to phase randomly distributed between $\pm\pi$. And we have also often to insert a high flux plateau, corresponding to high accuracy measures that cannot be improved on brighter targets. These two plateaux never impact the specified precision at 20 Jy, nor the limiting sensitivity.

2.3 BROAD BAND CALIBRATION ERROR FROM INSTRUMENT AND ATMOSPHERE VARIATIONS

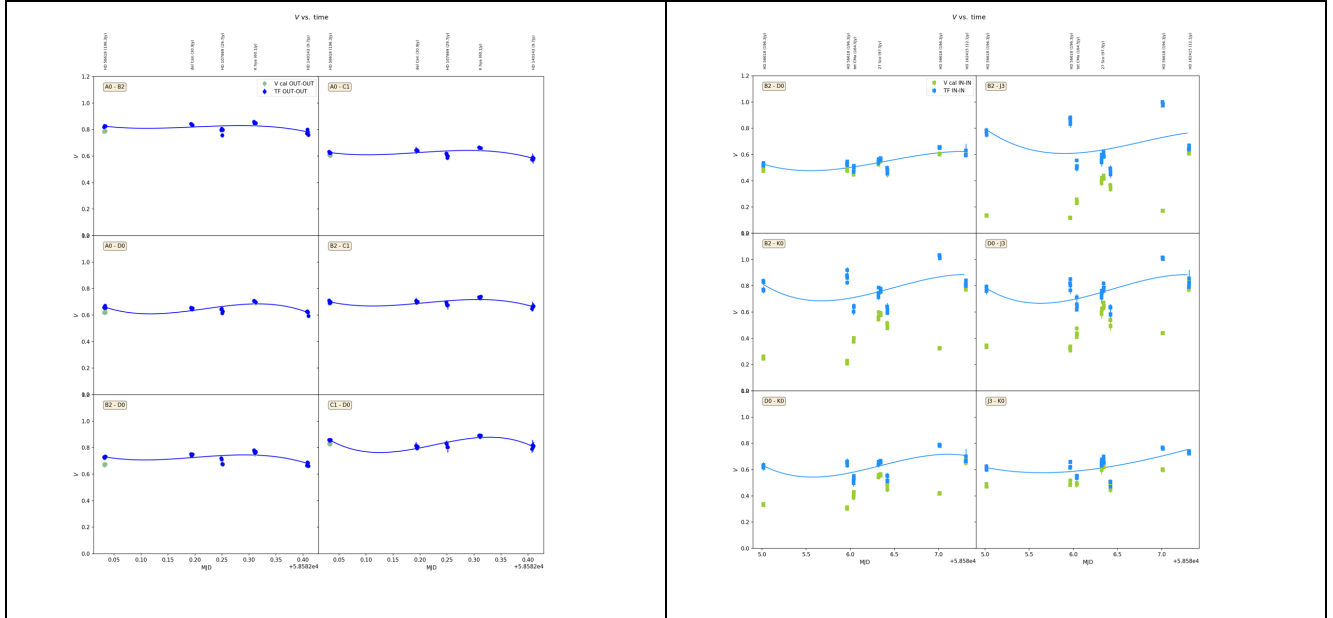


Figure 2.3: Example of TF(time) i.e. calibrator visibility corrected from the calibrator diameter, in LR-N, for a good night (left) and a bad night (right). The rms of the difference between the measures and the fit is an estimate of the broad band calibration error.

The broad band calibration error due to seeing variations is considered to be independent of the source flux. It is estimated from “Transfer Function”, i.e. plots of the instrument visibility as a function of time on bright calibrators, to reduce the sensitivity to the source flux. These transfer functions are fitted by 2nd or 3rd order polynomial functions and the standard deviation of the difference between the values and the fit is considered as an approximation of the single OB calibration error. In the first commissioning runs, we made also statistics on calibrator triplets to evaluate the accuracy of a Cal-Sci-Cal calibrations. It was shown [RD3] that the two methods give quite similar results. We performed these statistics on nights with good, fair, and poor seeing. The results are summarized in the following table:

Visibility Calibration Errors from Seeing and Instrument Changes (Standard Deviation on Broad Band Visibility Measurements)						
	L		M		N	
	Visibility	Closure Phase ^o	Visibility	Closure Phase ^o	Visibility	Closure Phase ^o
	FAIR conditions : Seeing = 0.74 as $\tau_0 = 6.8$ ms					
σ_C	0.021	0.26	0.02	0.24	0.02	0.49
	GOOD conditions: Seeing = 0.56 as $\tau_0 = 7.5$ ms					
σ_C	0.02	0.16	0.015	0.15	0.015	0.29
	BAD conditions: Seeing = 0.96 as $\tau_0 = 3.2$ ms					
σ_C	0.08	0.30	0.05	0.25	0.045	1.75

2.4 BROAD BAND PHOTOMETRIC ERRORS

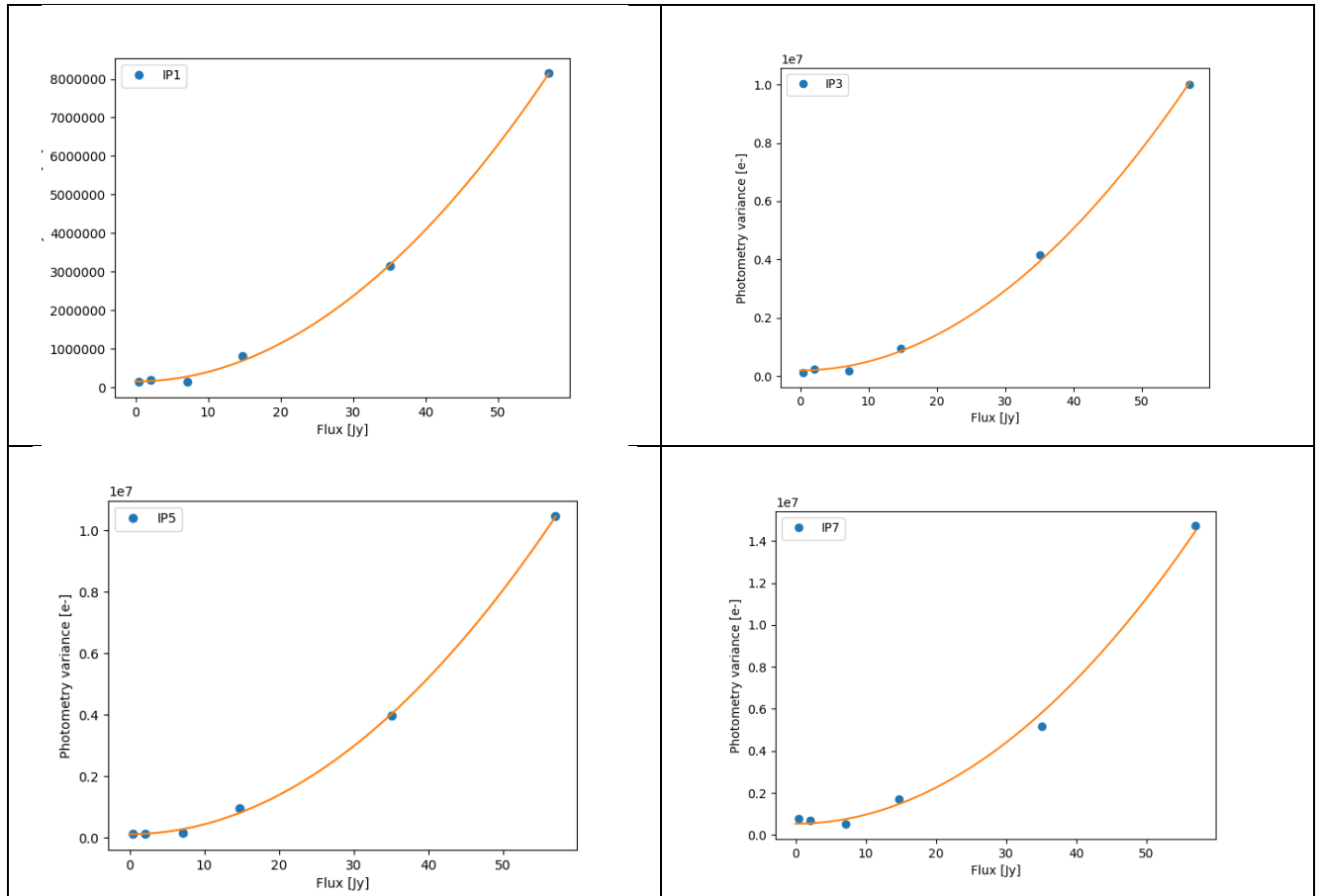


Figure 2.4: Variance of the measured flux as a function of the source catalogue flux. The fit contains a constant term that is the source independent photometric noise, a term proportional to the source flux, that is the source photon noise and a term proportional to the square of the source flux that is the residual fraction of the source in the sky image.

We used the total flux measurements provided by the DRS on chopped photometric data.

- A plot of the variance of measured flux as a function of the source catalogue flux gives the conversion between ADU (and photons) and source flux in Jy. This is also used to evaluate the flux ratios between UTs and ATs⁶.
- A plot of the variance of measured fluxes (from bins of targets with similar fluxes) as a function of the source catalogue flux allow to estimate the photometric error due to background errors, as the source flux independent term in the photometric error fit.

The photometric error is given in photons. It was correctly estimated on ATs, but we lack UT data for a good analysis. Therefore, we assumed that the UTs background is the same one as for the ATs, (similar beam etendue). The MIDI experience showed that this is conservative and pessimistic for UTs observations. However, the photometric error in photons converts differently in equivalent source brightness for UTs and ATs, since each telescope has its own photons/jansky ratio.

⁶ In RD5 these flux ratios between UTs and ATs were computed from SNR ratios. The numbers measured directly now are in remarkable agreement with these previous estimates.

The results are summarized in the following table.

Broad Band Photometric Error (Standard Deviation in Jansky)			
Band	L	M	N
Flux ratio UT/AT	14.5	12.2	29
$\epsilon_{P\ AT}$ (Jy)	0.11	0.19	2.3
$\epsilon_{P\ UT}$ (Jy)	0.008	0.016	0.08

2.5 SENSITIVITY TO SEEING CHANGES

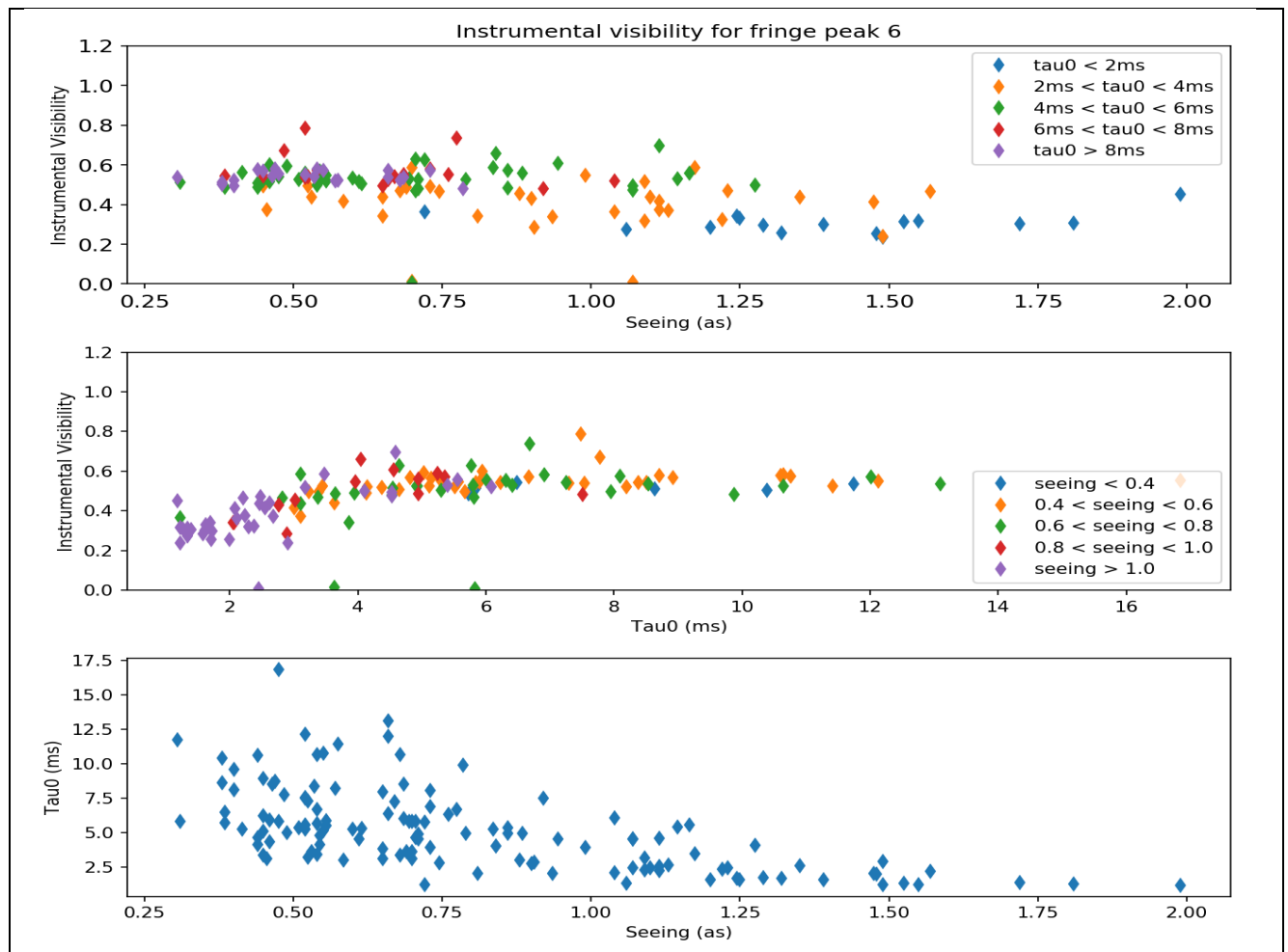


Figure 2.5: An example of the variation of instrument visibility with seeing conditions. In L band with $DIT=75\text{ ms}$. Note that we are very strongly dominated by the sensitivity to τ_{00} . After $\tau_{00}\sim 5\text{ ms}$, the sensitivity to seeing is strongly reduced. For τ_{00} lower than 3 ms, we can have a reduction in instrumental contrast by a factor 2.

The seeing changes modify the broad band calibration error. They also change the measured coherent flux. When the user requests specific seeing conditions, he has to update his coherent flux estimate and use it in all precision estimates.



Commissioning Report

The turning point both in L&M band is around $\tau_0 \sim 4$ ms for a $DIT=75$ ms. In N band we have the same τ_0 limit if we use a coherent integration over the modulation cycle, that yields an equivalent integration time of 250 ms in LR (10 frames of 20 ms plus small intervals between the frames). With 20 ms frames processed individually, the sensitivity of the N band visibility to seeing is very reduced.

2.6 SYNTHESIS OF BROAD BAND CALIBRATION ERRORS

The total error budget is derived in different ways depending on the considered MATISSE observable:

- For absolute visibility measurements we must combine the fundamental noise error per spectral channel with the broad band photometric errors following the equations given in annex 9.1.1. Then the resulting variance must be added to the broad band calibration variance due to seeing variations.
- For closure phase measurements, we add only the fundamental noise variance and the broad band calibration variance.
- For the differential measures, we consider only the fundamental noise, as the differential calibration removes broad band effects.
- The coherent flux SNR is deduced from the differential phase variance.

This process gives a measurement error as a function of the coherent flux. The coherent flux estimate has to consider the seeing conditions.

To validate our broad band calibration error estimates, we plotted the global dispersion of measurements in figures 2.6 which represent the instrument + atmosphere visibility (i.e. broad band calibrator visibility corrected from the effect of the calibrator diameter) as a function of the source flux. Each dot represents a calibrator measurement and the envelopes of the curve are set at $\pm 1\sigma$. At high flux the measurement error is completely dominated by the seeing broad band calibration error. As these plots merge many calibrators in various conditions, one can see here the calibration error made when one use a calibrator that is not close to the source in space nor in time. That median sigma is 7-8% in L and 8-9 % in M and less than 3% in N (when the data is processed frame by frame). At lower flux, we are dominated by the broad band flux dependent photometric error, as it will be seen through all section 5 and as it already clearly appears in the fact that the flux limits for absolute visibility are much higher than these for differential measures at low spectral resolution.

In L and in M, it appears that we are probably overestimating the photometric error: all the low flux points are well within the $\pm\sigma$ envelope. In N band our estimation appears to be roughly correct, but the fact that the low flux visibility tends to be systematically higher than average indicates that we are probably systematically underestimating the photometry and hence overestimating the background. However, we also see, from the dispersion of the points, that we are approaching the fundamental photometric noise dispersion. Note that these plots validate the substantial update of the N band limit for absolute visibility, from 28 Jy to 17 Jy for fair seeing conditions.

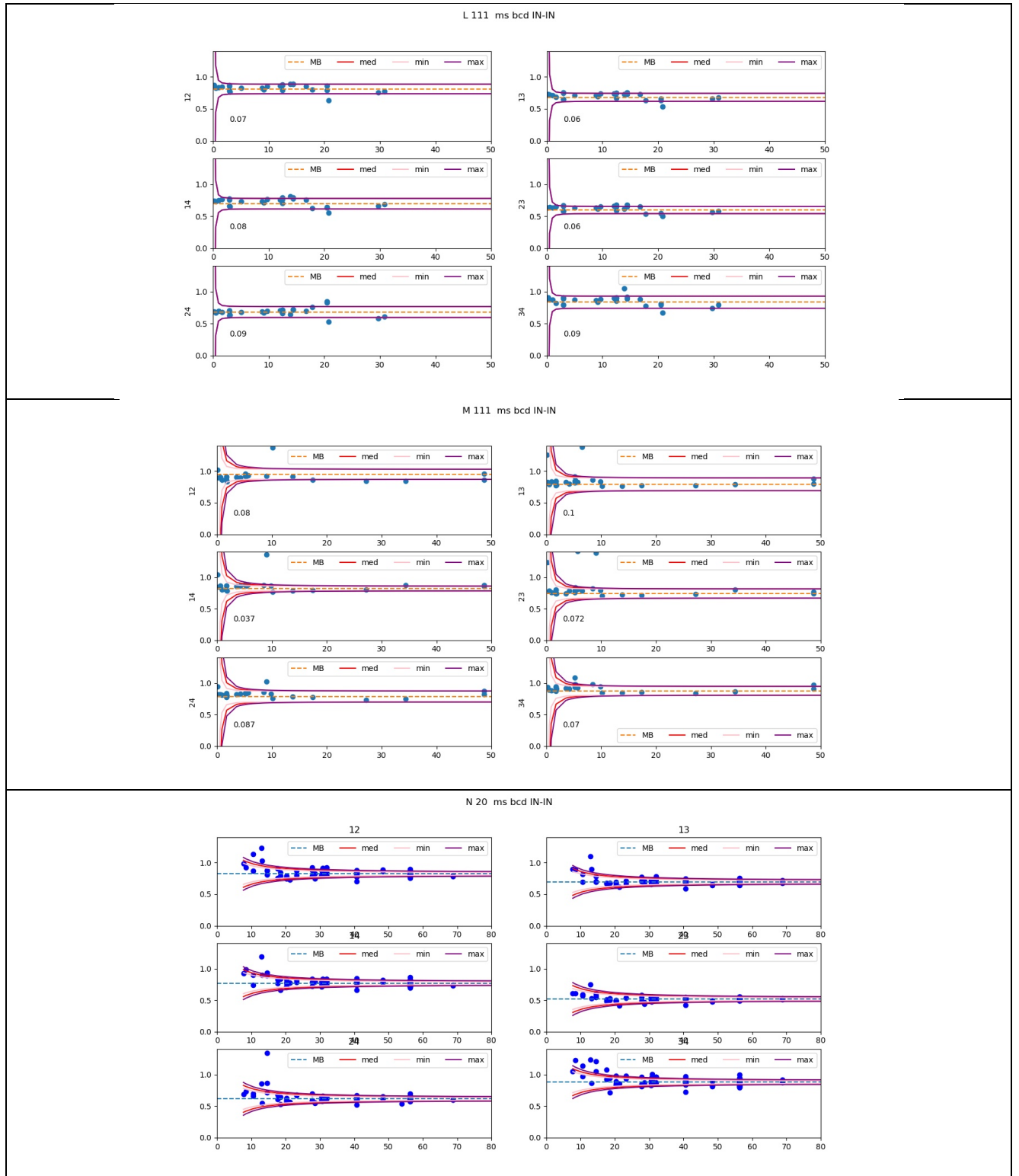


Figure 2.6: Instrument + atmosphere broad band visibility as a function of coherent flux, in L (top), M (middle) and N (bottom). Each dot represents the broad band visibility of a calibrator (corrected from the calibrator diameter effect). The dashed line is the average visibility for the baseline. The upper and lower curve represents the mean \pm the 1σ measurement error. We have considered the minimum, median and maximum values of the error, as a function of seeing conditions.



2.7 UPDATE ON THE COHERENT FLUX BIAS IN THE N BAND

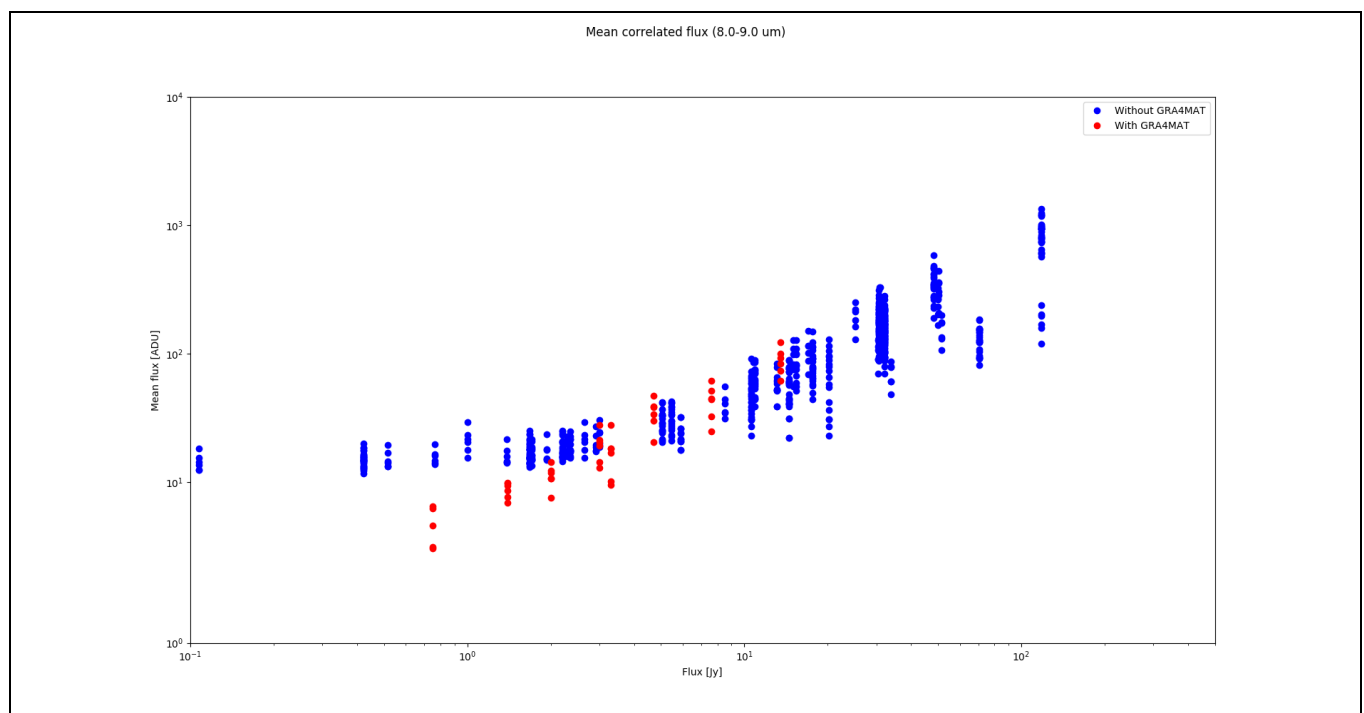
In June 2020, MATISSE users warned us about some possible biases appearing on N band coherent flux estimates, for source coherent flux somewhere between 5 and 9 Jy with ATs. An investigation confirmed that this problem appears near 5 Jy for the 8-9 μm spectral band and around 8 Jy for the 10-12 μm spectral band, as indicated by the figure 2.7a below.

This bias seems due to the error on the piston estimate. In the most performant coherent flux estimate (--coherentAlgo = 2 in MATISSE DRS), we perform a coherent integration of the N band frames after measuring and correcting the piston in each modulation cycle (i.e. in each coherence time) with the N band piston extracted from the N band data itself. Then, we use the real part of the piston corrected integrated complex coherent flux as a coherent flux estimator. When the piston errors estimate becomes large, this method introduces a bias in the coherent flux that tends to saturate to a fixed minimal value of the order of 5 Jy.

The other methods currently used to correct the CF bias do not seem to improve that situation. Computing the squared modulus of the complex coherent flux for each frame, or each coherence time, leads to a lower SNR for faint targets and is affected by a quadratic noise bias (--coherentAlgo = 1).

Several DRS improvements are considered to improve that situation, but they have not been tested yet.

We suggest correcting the limits for coherent flux measurements in the N band for MATISSE observations without GRA4MAT. We propose also to apply the same limit on the differential phase.



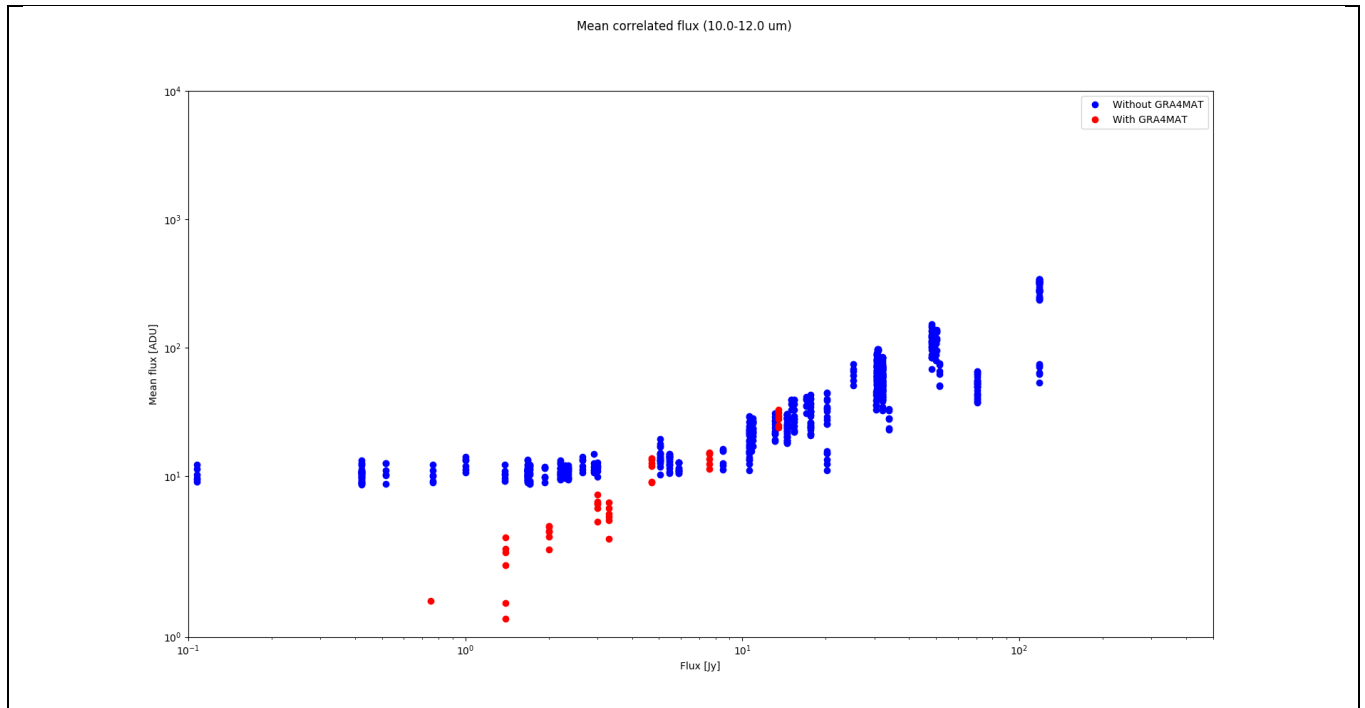


Figure 2.7a: Measured coherent flux, corrected for the source diameter and averaged between 8 and 9 μm (top) and 10-12 μm (bottom), as a function of the Wise W3 N band flux of the calibrator. The blue dots are for MATISSE alone observations N band coherent flux integration with piston correction from the N band itself (coherent algo=2). The red dots are for N band coherent integration using GRA4MAT

Based on this bias effect, we therefore propose the following limits on the coherent flux and conservatively on the differential phase in the table below. The 5 Jy limit at 8.5 μm indicated by figure 2.7a is supported by the example in figure 2.7b, showing a reasonably debiased CF with a SNR > 10 on a 5.5 Jy calibrator.

<i>Limit for N band coherent flux</i>		
	LR-N at 8.5 μm	LR-N at 11 μm
AT, fair and good seeing	5	8
AT, poor seeing	6	9
UT, fair and good seeing	0.2	0.3
UT, poor seeing	0.25	0.4

The poor seeing estimate is based on the dispersion of points in figure 2.7a and on an estimation of the sensitivity of piston estimates to seeing.

The UT values are based on the UT/AT flux ratio in N (~29). The UT numbers are very little changed with regard to previous value (which were actually showing an incoherence between UTs and ATs with a SNR ratio close to 10).

In the M band, the bias problem appears below the fundamental noise limit (M=1.1 Jy), as indicated by figure 2.7c. In L band, the problem has not been detected.

In HR-N, the limit will be the same as for LR-N, if the HR N data is binned to LR resolution. If the HR-N resolution is used, then the fundamental noise sets a much higher limit.

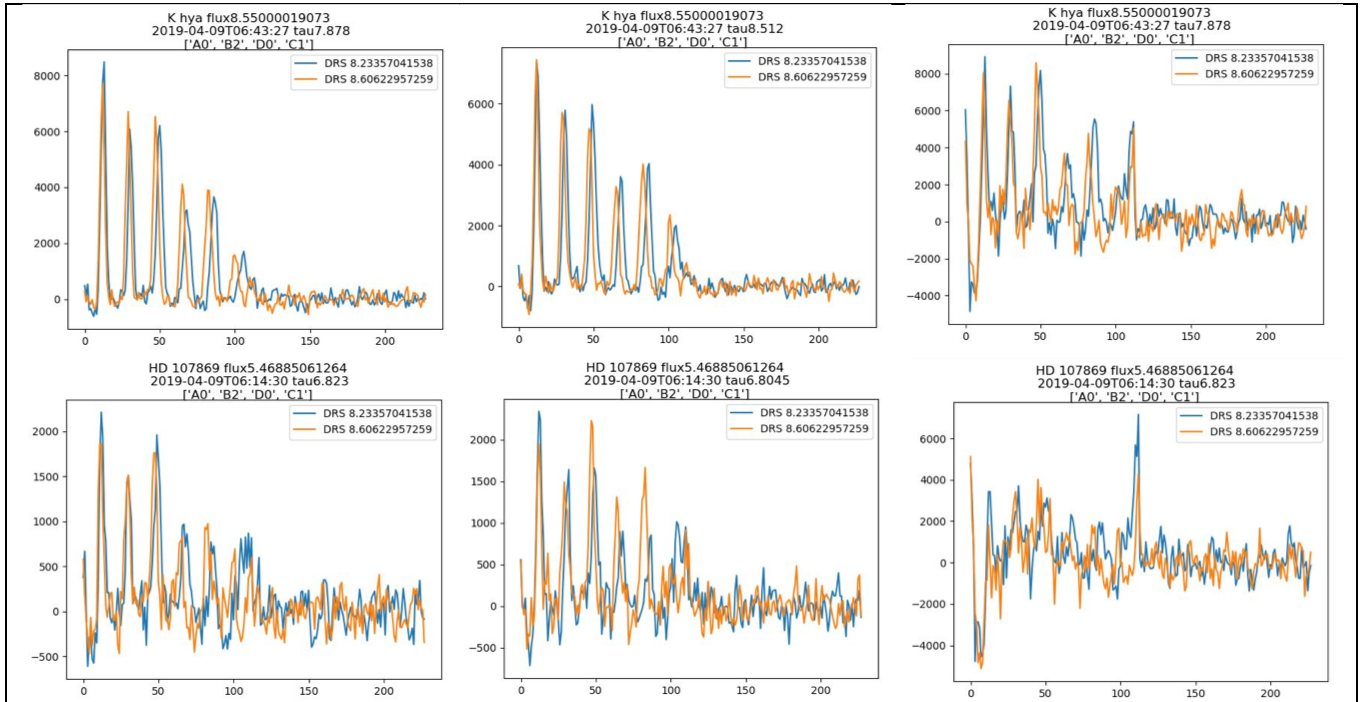


Figure 2.7b: cuts of the coherent flux amplitude in LR-N, for 2 spectral channels (8.23 μm in blue, 8.61 μm in orange), for a 8.55 Jy source (top) and a 5.47 Jy source (bottom). Left: coherent algo=1 (sum of CF squared modulus with bias correction from fit between peaks and subtraction): Centre: coherent algo =2 (coherent integration of CF after correction from the piston estimated in each modulation cycle). Right: integration frame by frame (opdmod=false). Note the strong decrease of CF from fringe peak=1 to fringe peak=6. This is due to binning without rescaling the fringes. The effect is partly reduced when the integral of the fringe peak is used (peak width increases with peak number).

We see that algo 2 is globally the most efficient. At 5.47 Jy the average CF SNR is between 15 and 30. Coherent integration over the modulation cycle (opdmod=true) is mandatory for any target fainter than ~ 25 Jy.

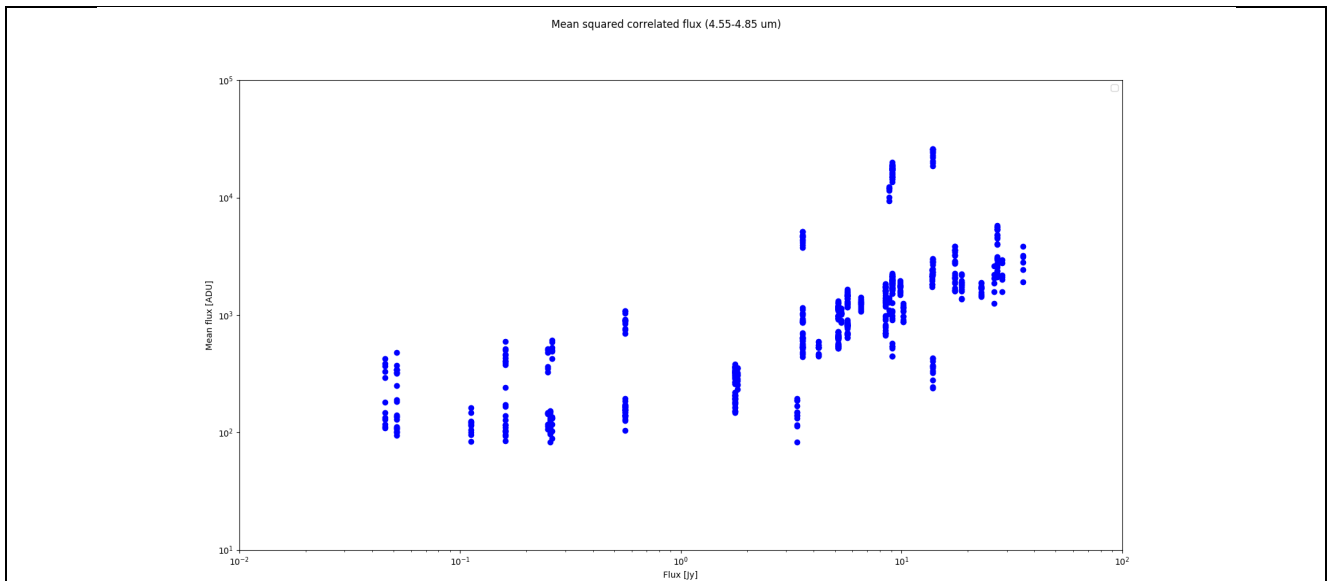


Figure 2.7c: same as figure 2.7a, for the M band averaged between 4.55 and 4.85 μm . The saturation effect appears below 1 Jy.

This problem disappears when we use GRA4MAT to allow coherent integration in N , as also indicated by figure 2.7a. The figure 2.7d below shows that with GRA4MAT the coherent flux limit is certainly below 2 Jy and probably below 1 Jy (figure 2.7e).

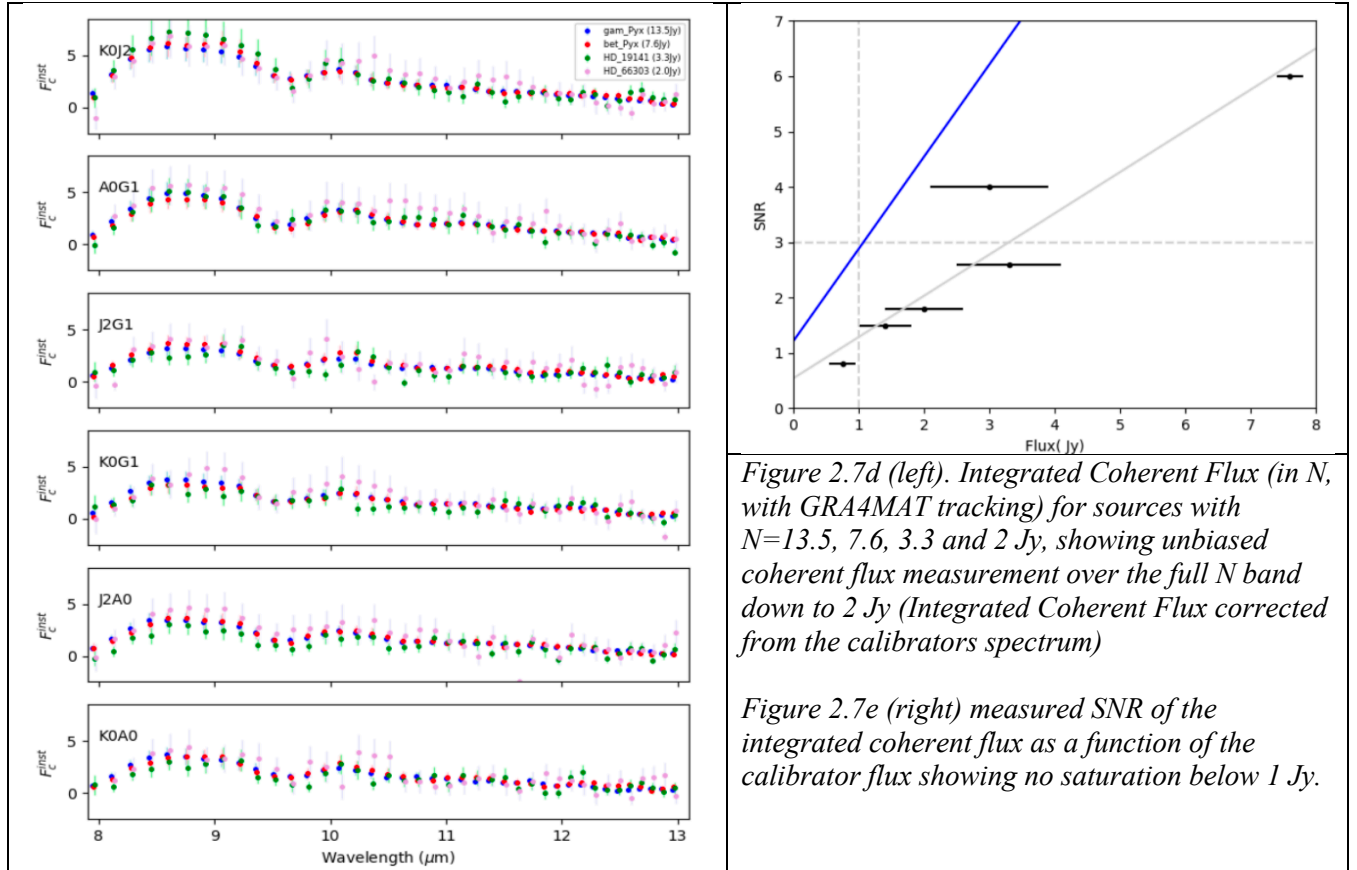


Figure 2.7d (left). Integrated Coherent Flux (in N , with GRA4MAT tracking) for sources with $N=13.5$, 7.6, 3.3 and 2 Jy, showing unbiased coherent flux measurement over the full N band down to 2 Jy (Integrated Coherent Flux corrected from the calibrators spectrum)

Figure 2.7e (right) measured SNR of the integrated coherent flux as a function of the calibrator flux showing no saturation below 1 Jy.

3 OPERATION AND DATA REDUCTION PARAMETERS

Here we give the observations and data reduction parameters that have been used to show the compliance with specifications and to set the performances offered to the users. The justification for these choices are given in the previous commissioning memos. They have to be summarized in annexes of this document.

3.1 ACQUISITION OB

The full acquisition OB with MATISSE stand-alone⁷ includes:

- Telescope and VLTI pre-set
- Check of pupils with IRIS
- Image acquisition with IRIS
- Image acquisition with MATISSE and update of IRIS reference pixels
 - Image tracking with IRIS (Coude lab guiding) for the rest of the observation
- Fringe search with MATISSE

More details about the parameters of the acquisition OB are given in §7.1

The full acquisition OB for a standard source needs 8 to 10 mn.

In practice the full OB must be executed only on the first calibrator of the night, to check the pupils, setup the IRIS reference pixels for the full night and DL offsets for fringe tracking.



Commissioning Report

For all other targets, the acquisition OB is reduced to the telescope and VLTI pre-set, that needs 4-5 mn with ATs and 5-6 mn with UTs

3.2 OBSERVATION OB

The typical OB contains

- 1 “interferometric cycle” without chopping with the 4 BCD setups: OUT-OUT; OUT-IN; IN-IN; IN-OUT
- 4 photometric observations with BCD IN-IN, with chopping
- 4 photometric observations with BCD OUT-OUT, with chopping

The OB can be reduced to the interferometric cycle if only closure phase and differential measurements are needed.

The chopped observations are needed for absolute visibility in the N and M bands (for all targets) and in the L band for targets fainter than 22 Jy⁸.

3.3 DATA REDUCTION PARAMETERS

The following data reduction options optimize the performances:

- With ATs, the IP5/AT3 photometry is replaced by the mean of the three other beams
- The L band photometry is processed with an Hampel filter, that eliminates outlying shots on the HAWAII-2RG detector
- The N band data is processed frame by frame for absolute visibility measurements and integrated coherently over the coherence time for all other measures.
- For the other measures in N band it is better to use the coherent integration over a modulation cycle.
- The spectral columns are binned in spectral channels (by 5 in L, by 7 in N).
- The closure phases are calibrated using the 4 steps BCD cycle. The closure phase calibration error given here are based on this BCD calibration.

4 COMPLIANCE WITH THE TECHNICAL SPECIFICATION

The list of Technical Specifications that had to be tested in commissioning is given in AD1 and RD1 and can be found in the table in chapter §1.4 above.

4.1 OPERATION SPECIFICATIONS

4.1.1 Number of telescopes and baselines

MATISSE is a 4 telescopes instrument.

All performance measurements given in this report are for 6 baselines.

It is possible to observe with 3 or 2 telescopes by:

- Bypassing manually the NRTS pop-ups warning about baselines without fringes
- Ignoring in the DRS results the baselines implying missing beams

We do not have an analysis of the performances with 2 or 3 telescopes.

It is strongly recommended to users to declare situations with a missing telescope as “technical losses”.

The specification SP1 stated “Operation with 4 beams and possibility to observe with 3 or 2 beams”.

MATISSE is compliant with this specification.

8 The actual limit that implies chopping in L varies with the wavelength of interest from 22 Jy for 4 μm down to about 4 Jy for 3 μm (RD7).



VRM Number	Number of telescopes	Technical Specification	Compliance
SP-1	4	4: Instrument and software designed for 4 beams 3, 2 beams: Operational	C

4.1.2 Observing modes

MATISSE has two observing modes.

- High_Sens (HSE) for High Sensitivity: all fluxes in Interferometric Channel without chopping during “interferometric observation”, then sequential photometric measurements, with chopping, in interferometric channel with all shutters closed but one.
- Si_Phot (SPH) for Simultaneous Photometry: a ~third of each beam is sent in a specific photometric channel and simultaneous observations of interferometry and photometry.

The operation of all modes has been tested in Nice before the PAE.

It has been found that SPH was not easily applicable to the N band because of the instability of the N-band “kappa-matrix” used to deduce the actual fluxes in the interferometric beams from the measurements in the photometric channels. This seems to be a problem specific to the Aquarius detector used in N band.

At the PAE it has been agreed (see RD11) that the commissioning will concentrate on the Hybrid mode, with SPH in the L-M band and HSE in the N band.

It has been found (cf RD7) that the chopped SPH observations obtained in the L-M band during the N band HSE photometry

- must be used for M band absolute visibility measurements
- improve L band absolute photometry measurements for targets fainter than 22 (Jy) for measures around 4 μm or fainter than 5 Jy for measures around 3 μm .

All L and M band absolute visibility performances given here are for chopped SPH observations, while the differential and closure phase performances in L-M can use non-chopped interferometric observations.

MATISSE is compliant with the SP44 specifications. However, the SPH mode in N and the HSE mode in L-M are not included in the current MATISSE Instrument Package agreed with Paranal.

VRM Number	Observing Mode	Technical Specification	Compliance
SP-44	Operational PAE Optimization: SiPhot in L and HighSens in N (Hybrid mode)	HighSens, SiPhot	C

4.1.3 Sensitivity

The technical specifications [AD1] for the sensitivity are: “the following flux limit numbers are intended at $SNR_C=3$ on the coherent fluxes on a few low spectral resolution individual



interferograms taken during the coherence time of the atmosphere, considering the full band”:

- In L band: 7.5Jy (L mag 3.95 and goal 1.5Jy) in SiPhot mode with 4ATs,
- In L band: 0.75Jy (L mag 6.45 and goal 0.15Jy) in SiPhot mode with 4UTs,
- In N band: 45Jy (N mag -0.25 and goal 10Jy) in High_Sens mode with 4ATs,
- In N band: 3Jy (N mag 2.7 and goal 0.75Jy) in High_Sens mode with 4UTs.

In the MATISSE Performance Analysis Report [RD13] as well as in annex 9.1.2 below, it is shown that the SNR_C on the coherent flux can be estimated from the error on the differential phase σ_ϕ using:

$$SNR_C = 2^{-1/2} / \sigma_\phi$$

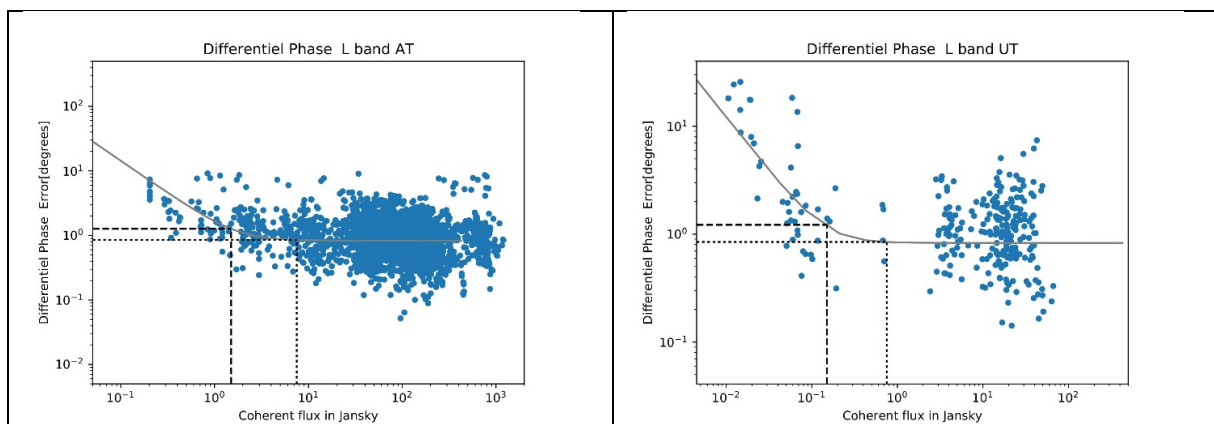
An $SNR_C=3$ corresponds to a differential phase error $\sigma_\phi=0.23$ rad.

Figure 4.1.3 gives the error σ_ϕ on the differential phase for different required limiting magnitudes for one minute of observation and one spectral channel.

Table 4.1.3a summarizes the errors on the differential phase σ_ϕ in one spectral channel for one minute of observation for the specified limiting fluxes, derived from Figure 4.1.3. It also gives the error on the differential phase when considering the full spectral band and observation during one coherence time, from the following observing characteristics: $DIT_L=111$ ms (Frame time = 222ms), $DIT_N=20$ ms (Frame time = 26ms), number of spectral channels $n_{ch}=13$ in L band and 17 in N band, observation with chopping in L and without chopping in N.

Table 4.1.3.b gives SNR_C for the flux set by the specification and the goal. This tables show that σ_ϕ is always much smaller than 0.23 rad and hence the SNR_C on the coherence flux for the specified magnitudes is always much greater than 3 and thus within specification and exceeding the goals.

Table 4.1.3.c gives the coherent flux that allows to reach $SNR_C=3$ in the nominal seeing conditions. Again, this flux limits are typically 3-4 times lower than the “goal” limits.



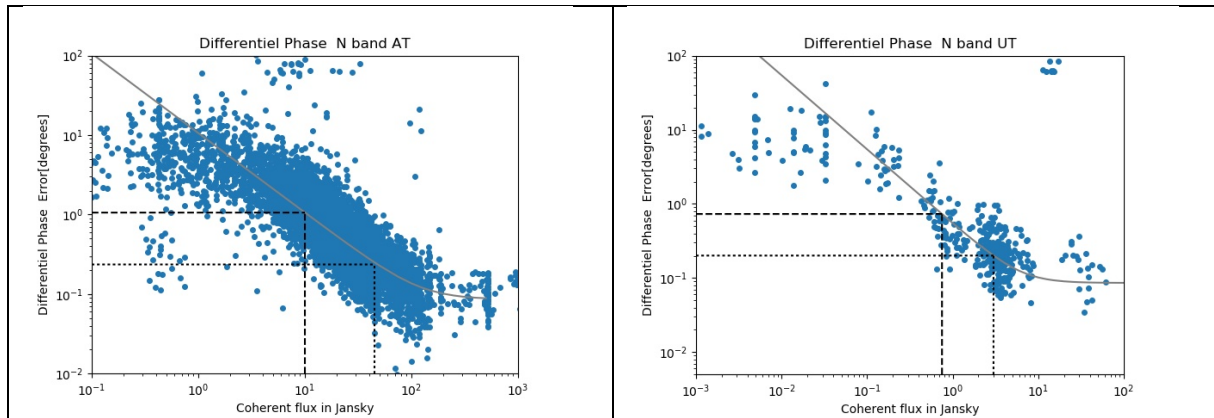


Figure 4.1.3: Error on differential phase per spectral channel vs coherent flux for observations in L band with ATs (upper left), in L band with UTs (upper right), in N band with ATs (bottom left) and in N band with UTs (bottom right). The dotted lines represent the specified limiting magnitude (in Jansky) and the dashed lines represent the goals. Every dot corresponds to measured differential phase error for a 1 minute observation.

Table 4.1.3.a Error on Differential Phase for the specified limiting magnitude

L Band	Limiting flux (Jy)	σ_ϕ (one minute one channel)	σ_ϕ (coherence time full band)
ATs	Spec: 7.5 Jy	0.85° (14.8 mrad)	47.8 mrad
	Goal: 1.5 Jy	1.27° (22.2 mrad)	71.4 mrad
UTs	Spec: 0.75 Jy	0.85° (14.8 mrad)	47.8 mrad
	Goal: 0.15 Jy	1.22° (21.3 mrad)	68.6 mrad
N Band	Limiting flux (Jy)	σ_ϕ (one minute one channel)	σ_ϕ (coherence time full band)
ATs	Spec: 45 Jy	0.24° (4.2 mrad)	15.4 mrad
	Goal: 10 Jy	1° (17.5 mrad)	64.3 mrad
UTs	Spec: 3 Jy	0.2° (3/4 mrad)	12.8 mrad
	Goal: 0.75 Jy	0.7° (12.2 mrad)	45.0 mrad

Table 4.1.3.b Coherent flux SNR at the flux set in “specification” and “goal”

VRM Number	L Band	Limiting Mag (Jy)	SNR _C	Technical Specification	Compliance
SP-25	ATs	Spec: 7.5 Jy	SNR _C = 14.8	SNR _C > 3	C
		Goal: 1.5 Jy	SNR _C = 9.9	SNR _C > 3	
SP-24	UTs	Spec: 0.75 Jy	SNR _C = 14.8	SNR _C > 3	C
		Goal: 0.15 Jy	SNR _C = 10.3	SNR _C > 3	
VRM Number	N Band	Limiting Mag (Jy)	SNR _C	Technical Specification	Compliance
SP-27	ATs	Spec: 45 Jy	SNR _C = 45.8	SNR _C > 3	C
		Goal: 10 Jy	SNR _C = 11.0	SNR _C > 3	
SP-26	UTs	Spec: 3 Jy	SNR _C = 55.0	SNR _C > 3	C
		Goal: 0.75 Jy	SNR _C = 15.7	SNR _C > 3	

Table 4.1.3.c Minimum coherent flux to achieve SNR_C=3



VRM Number	L Band	Min flux (Jy)	SNR _C	Technical Specification	Compliance
SP-25	ATs	0.45 Jy	SNR _C = 3	7.5 Jy (goal 1.5 Jy)	C
SP-24	UTs	0.04 Jy	SNR _C = 3	0.75 Jy (goal 0.15 Jy)	C
VRM Number	N Band	Min flux (Jy)	SNR _C	Technical Specification	Compliance
SP-27	ATs	<10 Jy	SNR _C = 3	45 Jy (goal 10 Jy)	C
SP-26	UTs	<0.75 Jy	SNR _C = 3	3 Jy (goal 0.75 Jy)	C

Note that figures 4.1.3 confirms that for all these minimum fluxes we are in the regime $\sigma_\phi(f) \propto 1/f$, that validates these minimum flux estimates. Targets with the corresponding coherent fluxes have indeed been observed and the data successfully reduced.

4.1.4 Fringe Sensing

From the technical specifications [AD1], MATISSE shall have a fringe sensing capability. This capability is intended primarily for fringe coherencing (group delay tracking) and shall not substitute the full fringe sensing and tracking capability of an external fringe tracker. The specifications for the MATISSE internal fringe sensing are as follows:

- Bandpass: L band only, full band (low spectral resolution)
- Frequency of sensing: lower or equal to 10 seconds
- Accuracy of coherencing: coherence length/2 (=15λ at low spectral resolution)

During MATISSE commissioning, we almost never used a coherencing frequency lower than 1 Hz (10 frames incoherently integrated with frame DIT=75 ms in L). All observed targets reported here could be tracked with MATISSE in L. Successful tracking implies that we stay well within the coherence length⁹.

The following curves (Figure 4.1.4) show the OPD residuals for an observation with ATs with poor atmospheric condition (Tau0 of 1.5ms, a seeing of 0.9) on a 2.5Jy target fainter than the specified AT sensitivity limit in L (that is 7.5 Jy). The observation is made with tracking in L (central wavelength = 3.5μm) at low resolution (R=31.5). This corresponds to a coherence length $l_c=110\mu\text{m}$. The tracking frequency was about 10 Hz (frame by frame)¹⁰. The PTV value of the OPD residuals is lower than 20μm ($l_c/5.5$) and the RMS value is about 7μm ($l_c/15.7$) which is within the specification ($l_c/2$).

Table 4.1.4. Compliance of the Fringe Sensing

VRM Number	Fringe Sensing performance	Technical Specification	Compliance
SP-38	Bandpass: Full L band low resolution Frequency: 1-10 Hz Accuracy ≤ Coherence length/15	Bandpass: Full L band low resolution Frequency ≤ Every 10s Accuracy ≤ Coherence length/2	C

9 Faintest targets successfully tracked in L : <0.2 Jy with ATs (RD3) and <50 mJy with UTs (RD7).
 10 TBC



2019-06-25T00:03:05 DIT:0.0751997 TAU0:1.348 SEEING:1.0 HD97048 2.5Jy

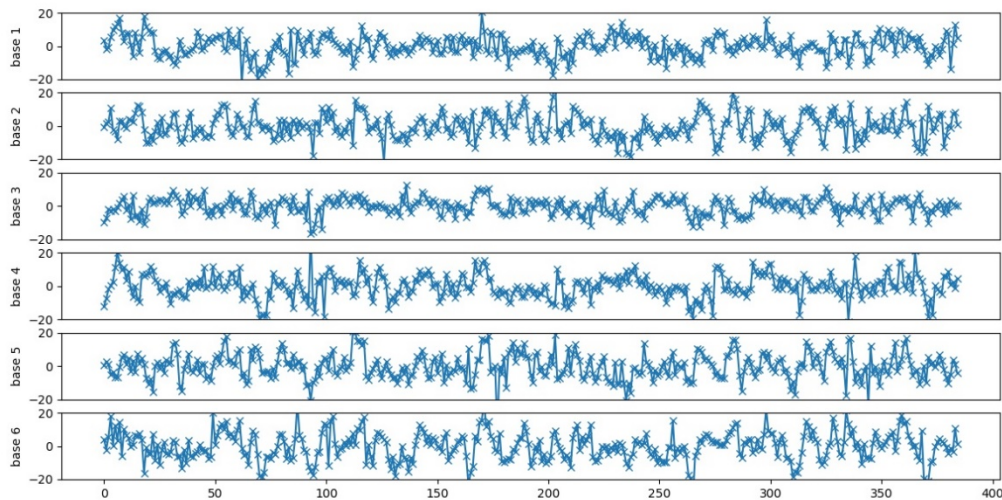


Figure 4.1.4: OPD residuals for the 6 baselines during a 1mn observation using the internal MATISSE fringe sensing.

4.1.5 Observing time efficiency

4.1.5.1 Standard OB structure

Acquisition (6mn with ATs, 7 mn with UTs)

Interferometric observation without chopping (9-10 mn), 7-8 mn when the OB is automatically started after a previous one.

Photometric observation with chopping (10-12 mn)

In practice, the acquisition is reduced to telescope and VLTI pre-set for all observations but the first calibrator of the night, this reduces the acquisition to 3-4 mn with ATs and 4-5 mn with UTs.

4.1.5.2 Observing time efficiency

From the technical specifications [AD1], “MATISSE shall produce a set of 6 calibrated visibility points, corresponding to the 6 spatial frequencies observed with 4T, in 1hr, under the condition that the overhead of tasks belonging to the VLTI and external to MATISSE is less than 40%”.

From the analysis of our log files we have the following data (example in table 4.1.5 below), for a fair night without technical or weather interruptions, in May 2018.

- Shortest full observation (with target change): 26’36’’
- Shortest full observation (without target change): 19’24’’
- Shortest Interferometric OB with photometry: 9’07’’
- Shortest full observation without photometry: 16’12’’

Average Time for a Cal-Sci calibrated observation:

- ATs: 55’14’’ (over a full fair night)
- UTs: 56’36’’ (over a full fair half night)

Table4.1.5.a Log files from fair nights



ATs		
Target (or calibrator)	TPL start	Sci-Cal cycle Duration
alf Ant	01:08:14	
HD99333	01:34:59	00:53:21
C01 Cen	02:01:35	
alpha Arae	02:36:41	00:54:30
alpha Arae	02:56:05	
HD138505	03:24:37	00:48:59
HD138505	03:45:04	
del Sco	04:16:31	00:52:07
del Sco	04:37:11	
HD142527	05:16:11	01:10:18
HD161560	05:47:29	
alpha Arae	06:14:53	00:43:46
HD171094	06:31:15	
e Aql	06:59:56	00:55:37
AV Mic	07:26:52	
HD171094	08:03:35	01:04:46
e Aql	08:31:38	
29 Cap	08:58:38	00:53:41
HD171094	09:25:19	
Average Sci-Cal cycle Duration for ATs		00:55:14
UTs		
Target (or calibrator)	Target (or calibrator)	Target (or calibrator)
HD142527	05:41:05	
HD147929	06:05:41	00:50:17
HD148255	06:31:22	
alpha Arae	06:58:23	00:54:29
G Sco	07:25:51	
HD156936	07:55:15	00:56:48
HD161849	08:22:39	
HD165413	08:57:25	01:04:48
HD182669	09:27:27	
Average Sci-Cal cycle Duration for UTs		00:56:36

This is compliant with specifications.

Table4.1.5.b Compliance of the Observing Time Efficiency

VRM Number	Observing Time Efficiency	Technical Specification	Compliance
SP-43	6 calibrated points in less than 1h, actual average on observing nights: 55'15'' with ATs and 56'40'' with UTs. Min.	MATISSE shall produce a set of 6 calibrated visibility points, corresponding to the 6 spatial frequencies observed with 4T, in 1hr.	C

4.2 COMPLIANCE OF MEASUREMENT PRECISION OR ACCURACY WITH SPECIFICATIONS

4.2.1 Absolute visibility

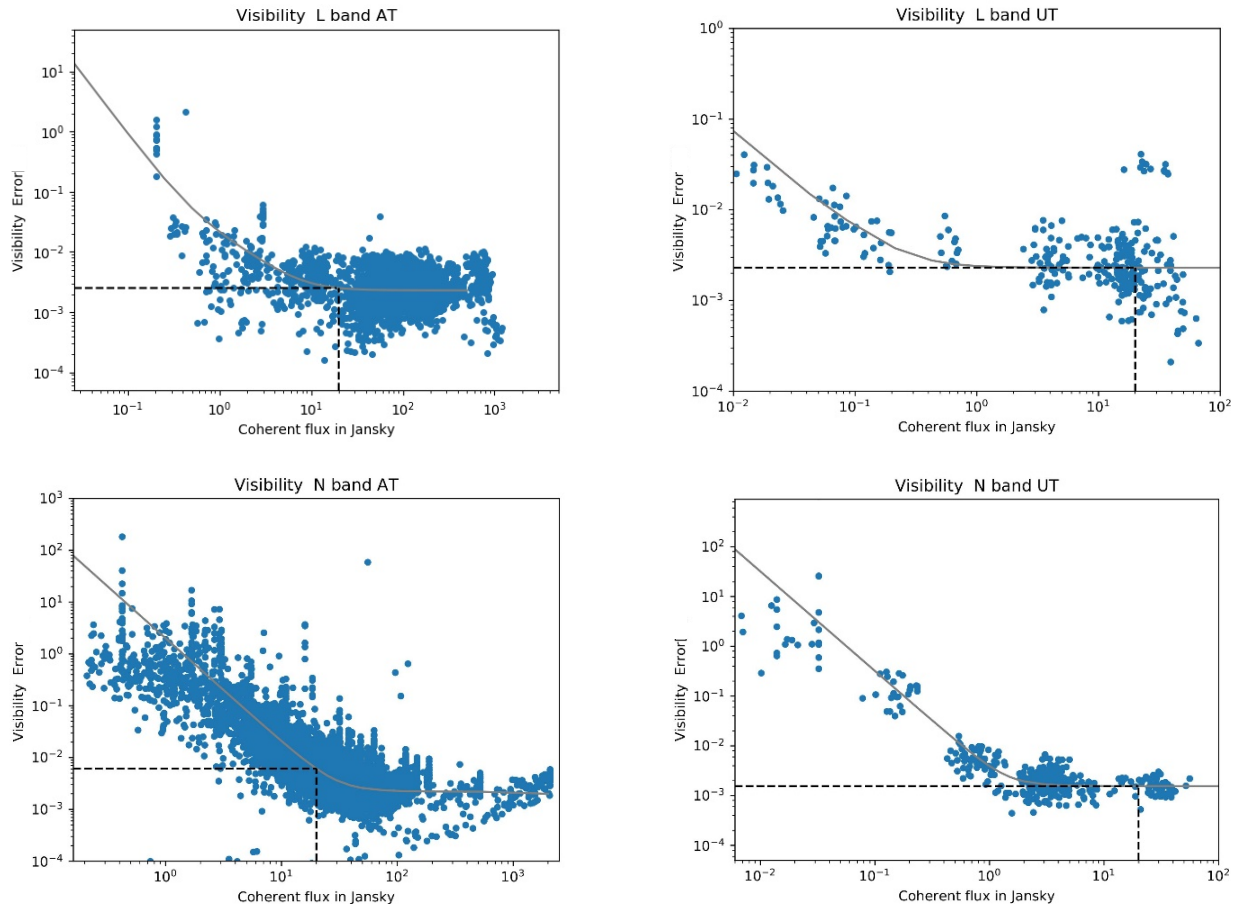


Figure 4.2.1: Relative accuracy on visibility per spectral channel vs coherent flux for observations in L band with ATs (upper left), in L band with UTs (upper right), in N band with ATs (bottom left) and in N band with UTs (bottom right).

The technical specifications [AD1] for the visibility are:

The visibility V and its error σ_v shall be computed **from a single OB** measurement in low spectral resolution, from one spectral channel at the central wavelength. The specification for the relative accuracy on the visibility, σ_v/v , is:

- In L band: $\leq 7.5\%$ (goal 2.5%) for UTs, for unresolved source, 20 Jy (L mag 2.9), Strehl 0.7.
- In L band: $\leq 7.5\%$ (goal 2.5%) for ATs, for unresolved source, 20 Jy (L mag 2.9), Strehl 0.7.
- In N band: $\leq 7.5\%$ (goal 2.5%) for UTs, for unresolved source, 20 Jy (N mag 0.66), Strehl 0.95.
- In N band: $\leq 30\%$ (goal 10%) For ATs, for unresolved source, 20 Jy (N mag 0.66), Strehl 0.95.



Figure 4.2.1 represents the relative precision σ_v/V on the visibility in L and N bands per spectral channel (corresponding to 5 spectral columns in L band and 7 spectral columns in N band), with ATs and UTs. Every point corresponds to one-minute observation on calibrators. The data used for these plots were recorded during various commissioning runs held in September 2018 and in 2019¹¹.

For each point, V is computed from the median visibility value computed over the 3.2 - 3.8 μm range in L band, and over the 8.2 - 8.9 μm range for the N band.

To obtain σ_v a second order polynomial fit is first applied to the visibility $V(\lambda)$. Then this fit is subtracted from $V(\lambda)$ and σ_v is the RMS over wavelength of this residual. This yields the fundamental noise contribution to the visibility error but removes the broad band calibration errors.

The solid line corresponds to a MATISSE ETC curve scaled to match at best the data. It is used to visualize the average trend of the visibility precision as a function of the calibrator coherent flux, and thus to derive our visibility accuracy for a 20 Jy source. The dashed line corresponds to a non-resolved source of 20Jy.

From Figure 4.2.1, the fundamental noise precisions on the visibility for a 20 Jy source are: 0.0025 in L band for both UTs and ATs, and 0.0015 in N band for UTs and 0.006 for ATs. It should be noted that these values are pessimistic since they based on a one-minute exposure instead of a single complete OB (four exposures for the interferometric part).

This fundamental noise precision per spectral channel must be combined with the broad band errors from the global photometric errors and the seeing variations described in the methodology chapter. It is a little bit tricky to give a calibrated visibility accuracy from a single OB, as the calibration process implies several OBs. However, the broad band visibility error due to seeing is the rms of the difference between individual OBs and a global fit through all calibrators of the night, which has been shown to be also close to a local fit using two calibrators in a Cal-Sci-Cal sequence. So we consider that taking it into account gives a correct estimation of the absolute visibility accuracy. Using the values for “fair seeing” (0.74 ± 0.2) given in section 2.3 and the broad band photometric errors from section 2.4, gives the accuracy on calibrated visibility given in table 4.2.1 below. The results are compliant with all specifications and exceed all the goals.

Table 4.2.1. Compliance of the Visibility accuracy

VRM Number	L Band	Relative accuracy on Visibility	Technical Specification	Compliance
SP-14	ATs	$\sigma_v/v = 0.8\%$	$\leq 7.5\%$ (goal 2.5%)	C
SP-12	UTs	$\sigma_v/v = 0.25\%$	$\leq 7.5\%$ (goal 2.5%)	C
VRM Number	N Band	Relative accuracy on Visibility	Technical Specification	Compliance
SP-15	ATs	$\sigma_v/v = 8.5\%$	$\leq 30\%$ (goal 10%)	C
SP-13	UTs	$\sigma_v/v = 0.35\%$	$\leq 7.5\%$ (goal 2.5%)	C

These are accuracies for 1 mn exposures from one OB. Note that the fundamental noise precision improves like $\sqrt{n_{exp}}$ where n_{exp} is the number of interferometric exposures in one

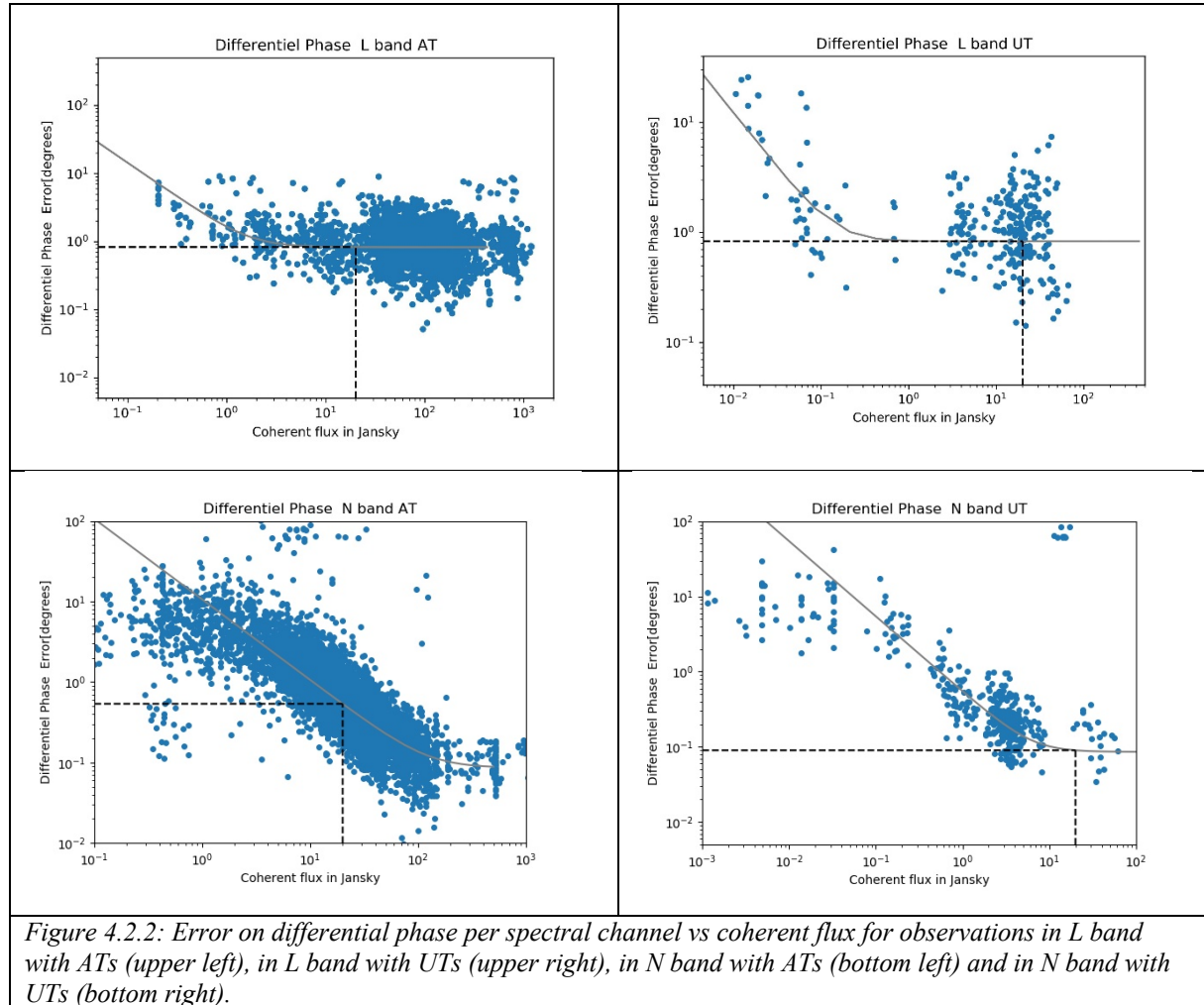
11 The implementation of NAOMI in November 2018 has not introduced any significant difference on this relative precision, but for small changes in the instrumental visibility and hence the coherent flux, that cannot appear in figure A plotting precision as a function of the coherent flux.

Commissioning Report

OB (typically 4 exposures), at least down to the high flux precision plateau. The broad band calibration errors improve, at best, with $\sqrt{n_{COB}}$ where n_{COB} is the number of independent calibrated OBs.

Hence, the values given here are a pessimistic and hence safe estimation of the accuracy on one OB.

4.2.2 Differential phase



The technical specifications [AD1] for the differential phase accuracy are:

- In L band: ≤ 30 mrad (goal ≤ 1 mrad) for UTs, for unresolved source, 20 Jy, Strehl 0.7.
- In L band: ≤ 60 mrad for ATs, for unresolved source, 20 Jy (L mag 2.9), Strehl 0.7.
- In N band: ≤ 30 mrad (goal 1 mrad) for UTs, for unresolved source, 20 Jy, Strehl 0.95.
- In N band: ≤ 60 mrad for ATs, for unresolved source, 20 Jy (N mag 0.66), Strehl 0.95.

Figure 4.2.2 represents the error σ_ϕ on the differential phase in L and N bands per spectral channel (corresponding to 5 spectral columns in L band and 7 in N band), with the ATs and UTs. Every point corresponds to σ_ϕ obtained from 1mn observation on calibrators.

For each point, σ_ϕ is the RMS value of $\phi(\lambda)$ computed over the 3.2-3.8 μm interval in L band, and over the 8.2-8.9 μm interval in N band. The solid line corresponds to a MATISSE ETC



curve scaled to match at best the data. The dashed line corresponds to a non-resolved source of 20Jy.

From Figure 4.2.2, the accuracies of the differential phase are: 0.83° (14.5mrad) in L band for both UTs and ATs, 0.086° (1.5 mrad) in N band for UTs and 0.5° (9mrad) for ATs. They are within the technical specifications. It should be noted that these values are pessimistic since they based on a one-minute exposure instead of a single complete OB; one single OB consisting of four exposures of one minute.

The differential phase is not sensitive to broad band calibration errors. The accuracy given here applies for the difference between the phase in one spectral channel and the average phase of the reference channel, defined in the intervals [3.2-3.8 μm] in L and [8.2-8.9 μm] in N.

The differential phase over broader spectral channels, as well as for channels very close to the band limits (i.e. outside the intervals above) are sensitive to calibration errors due to the variation of the chromatic OPD. There are no specifications for these specific conditions and calibrating those chromatic OPD effects is a work in progress.

Table 4.2.2. Compliance of the Differential Phase

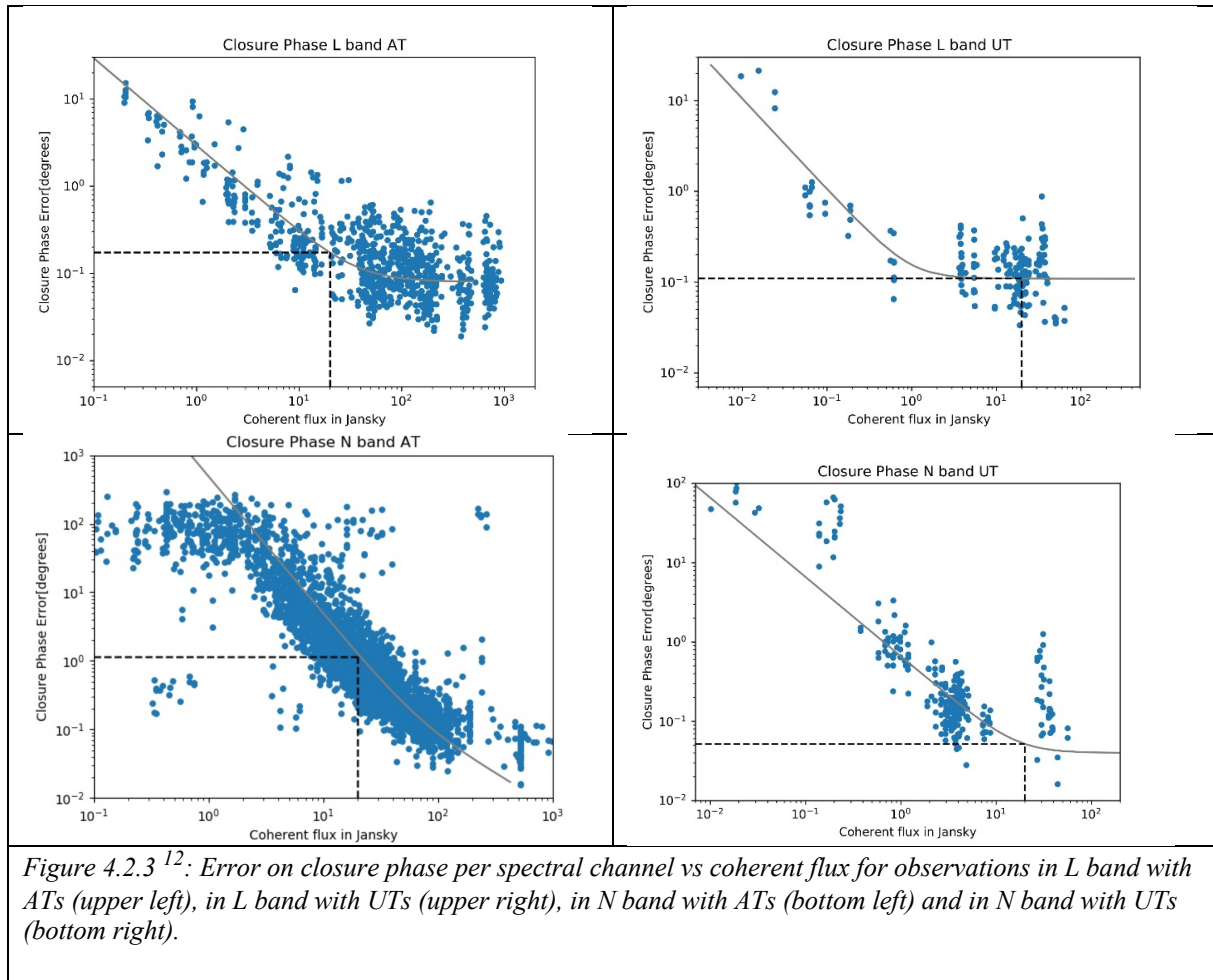
VRM Number	L Band	Accuracy on Differential Phase	Technical Specification	Compliance
SP-17	ATs	$\sigma_\phi = 14.5\text{mrad}$	$\leq 60\text{mrad}$	C
SP-16	UTs	$\sigma_\phi = 14.5\text{mrad}$	$\leq 30\text{ mrad}$	C
VRM Number	N Band	Accuracy on Differential Phase	Technical Specification	Compliance
SP-19	ATs	$\sigma_\phi = 9\text{mrad}$	$\leq 60\text{mrad}$	C
SP-18	UTs	$\sigma_\phi = 1.5\text{mrad}$	$\leq 30\text{ mrad}$	C

4.2.3 Closure phase

The technical specifications [AD1] for the closure phase accuracy are:

- In L band: $\leq 40\text{ mrad}$ (goal $\leq 1\text{ mrad}$) for UTs, for unresolved source, 20 Jy, Strehl 0.7.
- In L band: $\leq 80\text{ mrad}$ for ATs, for unresolved source, 20 Jy (L mag 2.9), Strehl 0.7.
- In N band: $\leq 40\text{ mrad}$ (goal 1 mrad) for UTs, for unresolved source, 20 Jy, Strehl 0.95.
- In N band: $\leq 80\text{ mrad}$ for ATs, for unresolved source, 20 Jy (N mag 0.66), Strehl 0.95.

Figure 4.2.3 represents the error σ_ϕ on the closure phase in L and N bands per spectral channel with the ATs and UTs. Every point corresponds to σ_ϕ obtained from 1mn observation on calibrators.



From Figure 4.2.3, the fundamental noise precision on the closure phase for a 20 Jy coherent flux are: 0.11° (1.9mrad) in L band with UTs and 0.17° (2.9mrad) with ATs, and 0.05° (0.9mrad) in N band with UTs and 1.2° (19mrad) with ATs. Here there is no photometric broad band calibration error. The seeing broad band calibration error has been computed from closure phases calibrated using the BCD cycle internal to 1 OB. This broad band calibration error ($0.26^\circ=4.5$ mrad in L and $0.49^\circ=8.5$ mrad in N in fair seeing conditions) has to be included in the closure phase accuracy estimate. The results are given in the table **Erreur ! Source du renvoi introuvable.** They are compliant with specifications.

Table 4.2.3. Compliance of the Closure Phase Accuracy

VRM Number	L Band	Precision on Closure Phase	Technical Specification	Compliance
SP-21	ATs	$\sigma_\phi = 5.4\text{mrad}$	$\leq 80\text{mrad}$	C
SP-20	UTs	$\sigma_\phi = 4.9\text{mrad}$	≤ 40 mrad	C
VRM Number	N Band	Precision on Closure Phase	Technical Specification	Compliance
SP-23	ATs	$\sigma_\phi = 21\text{mrad}$	$\leq 80\text{mrad}$	C
SP-22	UTs	$\sigma_\phi = 8.5\text{mrad}$	≤ 40 mrad	C



4.2.4 Differential visibility

The technical specifications [AD1] for the differential visibility are:

The differential visibility shall be computed from a single OB measurement in low spectral resolution. The differential visibility will be the ratio of the visibility V in each channel against the reference visibility V_{ref} . The error σ_V/V_{ref} is computed from one spectral channel at the central wavelength. The specification for the relative accuracy on the differential visibility, $(\sigma_V/V_{ref})/(V/V_{ref})$, is:

- In L band: $\leq 1.5\%$ (goal 0.5%) for UTs, for unresolved source, 20 Jy (L mag 2.9), Strehl 0.7.
- In L band: $\leq 3\%$ (goal 1%) for ATs, for unresolved source, 20 Jy (L mag 2.9), Strehl 0.7.
- In N band: $\leq 5\%$ (goal 2%) for UTs, for unresolved source, 20 Jy (N mag 0.66), Strehl 0.95.
- In N band: $\leq 30\%$ (goal 10%) For ATs, for unresolved source, 20 Jy (N mag 0.66), Strehl 0.95.

The differential visibility V_{dif} is defined as:

$$V_{dif} = V/V_{ref}$$

From the MATISSE Performance Analysis Report [RD1], as the reference channel is made up of all the spectral channels, we consider the error on V_{ref} to be negligible. As a consequence, we have:

$$SNR_{V_{dif}} \sim SNR_V$$

The relative accuracy on the differential visibility is thus the same as the one obtained for the absolute visibility. As the differential visibility is a relative measurable, the broad band errors do not have to be considered.

Table 4.2.4. Compliance of the Differential Visibility

VRM Number	L Band	Relative accuracy on Diff. Visibility	Technical Specification	Compliance
SP-30	ATs	$\sigma_{V_{diff}}/V_{diff} = 0.25\%$	$\leq 3\%$ (goal 1%)	C
SP-28	UTs	$\sigma_{V_{diff}}/V_{diff} = 0.25\%$	$\leq 1.5\%$ (goal 0.5%)	C
VRM Number	N Band	Relative accuracy on Diff. Visibility	Technical Specification	Compliance
SP-31	ATs	$\sigma_{V_{diff}}/V_{diff} = 0.6\%$	$\leq 30\%$ (goal 10%)	C
SP-29	UTs	$\sigma_{V_{diff}}/V_{diff} = 0.15\%$	$\leq 5\%$ (goal 2 %)	C



5 OFFERED PERFORMANCES

5.1 INTRODUCTION

This section summarizes the limiting magnitudes of MATISSE for the different observing modes offered to the users in the calls for proposal.

It has been agreed with the Paranal MATISSE instrument scientists (T. Rivinius and C. Paladini) that these limits are defined by the following measurement precision *per 1-minute exposure and per spectral channel*:

- Absolute visibility: $\sigma_V = 0.1$
- Closure phase: $\sigma_{CP} = 5^\circ$
- Differential phase: $\sigma_\phi = 4^\circ$
- Coherent flux $SNR_C = 10$.

An error of 4° on the Differential phase corresponds to a $SNR = 10$ on the coherent flux according to the formula $\sigma_\phi = \frac{c}{\sqrt{2}\sigma_C} = \frac{1}{\sqrt{2}SNR_C}$, which is valid if $SNR_C \gtrsim 1$.

Through different plots, we will highlight the *coherent* minimum fluxes (in Jy) needed to achieve the above-mentioned precisions for each band, resolution and telescope used. In the following sections, the left curves (with blue dots) represent the error due to the fundamental noise. The right curves show the different error contributions (errors per spectral channel due to the fundamental noise, broad-band calibration errors due to seeing changes, broad-band photometric error due to a wrong background correction), as summarized in sections §2.3 and §2.4, along with the total error (square root of the sum of the variances of the different errors).

- The absolute visibility plot and sensitivity estimate combine the fundamental noise (fitted blue dots), the flux dependent broad band photometric error (yellow curve) and the flux independent broad band calibration error due to atmospheric changes (cyan curves).
- The closure phase plot and sensitivity estimate combine the fundamental noise and the flux independent broad band calibration error, estimated from BCD calibration of the closure phase.
- The differential phase and the coherent flux SNR are read directly from the fundamental noise plot.

The impact of seeing conditions on the broad band calibration errors is used to derive the good-seeing and bad-seeing values. The user should also remember that the seeing variations change the coherent flux of the source as explained in section 2.5.

The performances have been measured for the following wavelengths:

L Band	Wavelengths
Low resolution	$\lambda_0 = 3.5\mu\text{m}$, $\Delta\lambda = [3.2 - 3.8] \mu\text{m}$
Medium resolution	λ_0 between 3.2 and 4.1 μm , $\Delta\lambda = 0.2 \mu\text{m}$
High resolution	λ_0 between 3.9 and 4.2 μm , $\Delta\lambda = 0.1 \mu\text{m}$
M Band	Wavelengths
Low resolution	$\lambda_0 = 4.75\mu\text{m}$, $\Delta\lambda = [4.55 - 4.95] \mu\text{m}$
Medium resolution	λ_0 between 4.55 and 4.95 μm , $\Delta\lambda = 0.2 \mu\text{m}$
N1 Band	Wavelengths
Low resolution	$\lambda_0 = 8.5\mu\text{m}$, $\Delta\lambda = [8.1 - 8.9] \mu\text{m}$
High resolution	$\lambda_0 = 8.5\mu\text{m}$, $\Delta\lambda = [8.1 - 8.9] \mu\text{m}$

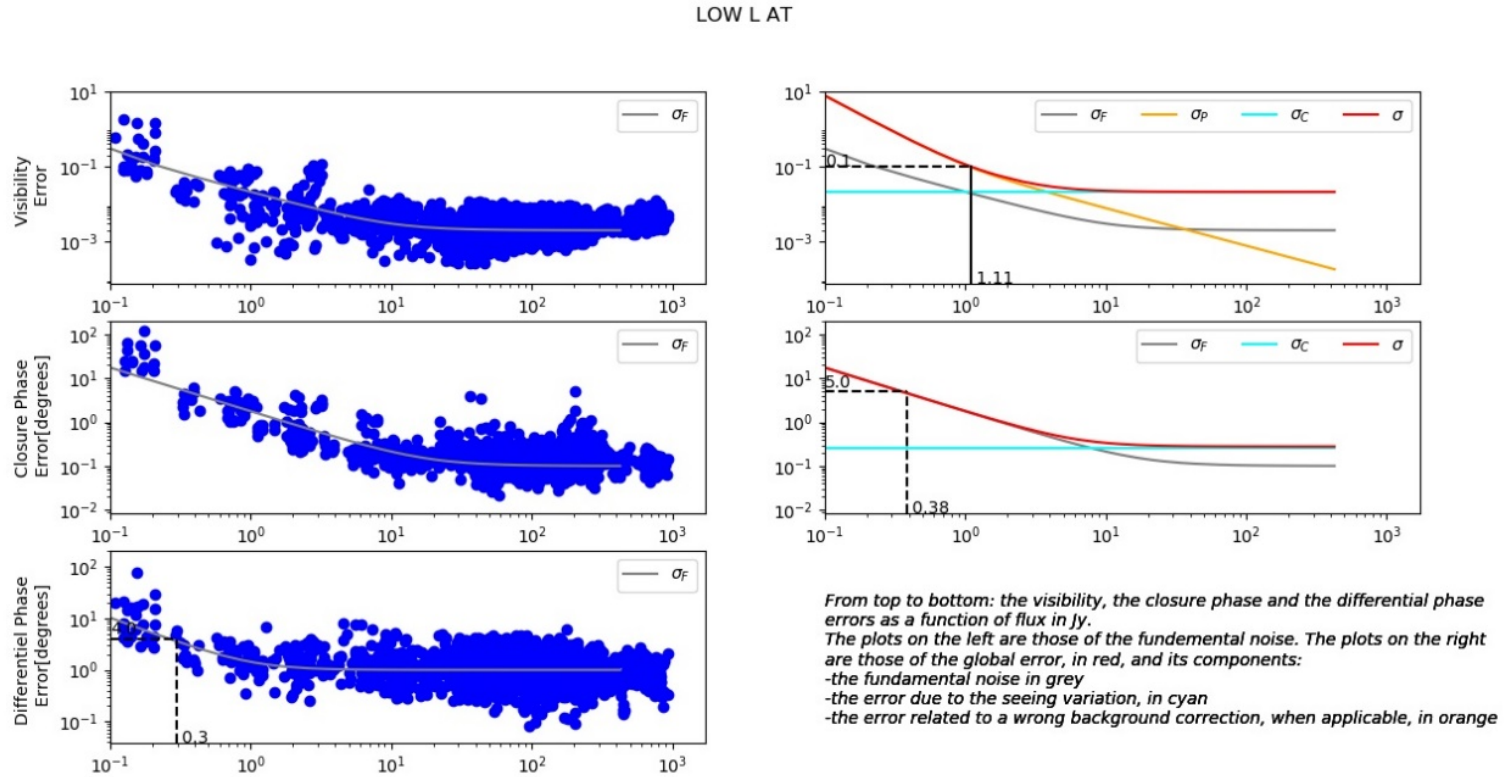
**Commissioning Report**

The following plots involve observations taken during the commissioning runs of the years 2018 and 2019. The errors curves of the plots, σ_F , σ_C and σ_P , are derived for so called fair seeing conditions. The tables at the end of the chapter summarize the achievable magnitudes for all seeing conditions: bad, fair and good. From bad to fair to good conditions, the seeing is the following: 0.95, 0.75 and 0.55. Only tables with fair and bad conditions will be shown since the results in good or fair conditions are very similar.

5.2 L BAND¹³

5.2.1 Low Resolution

5.2.1.1 ATs

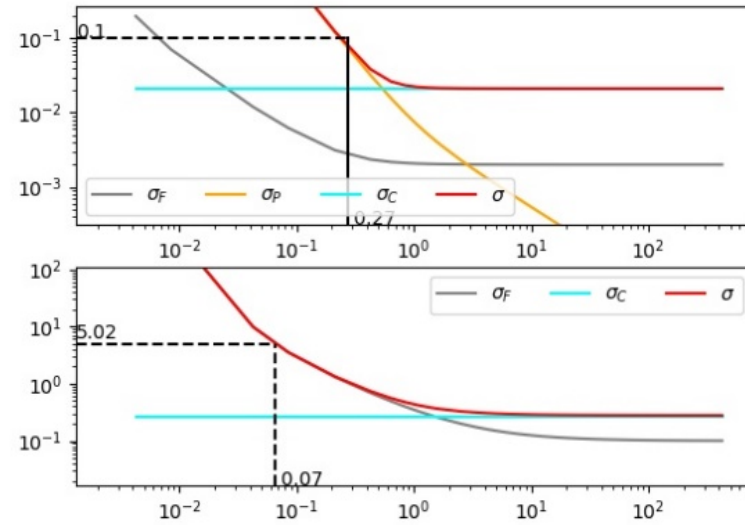
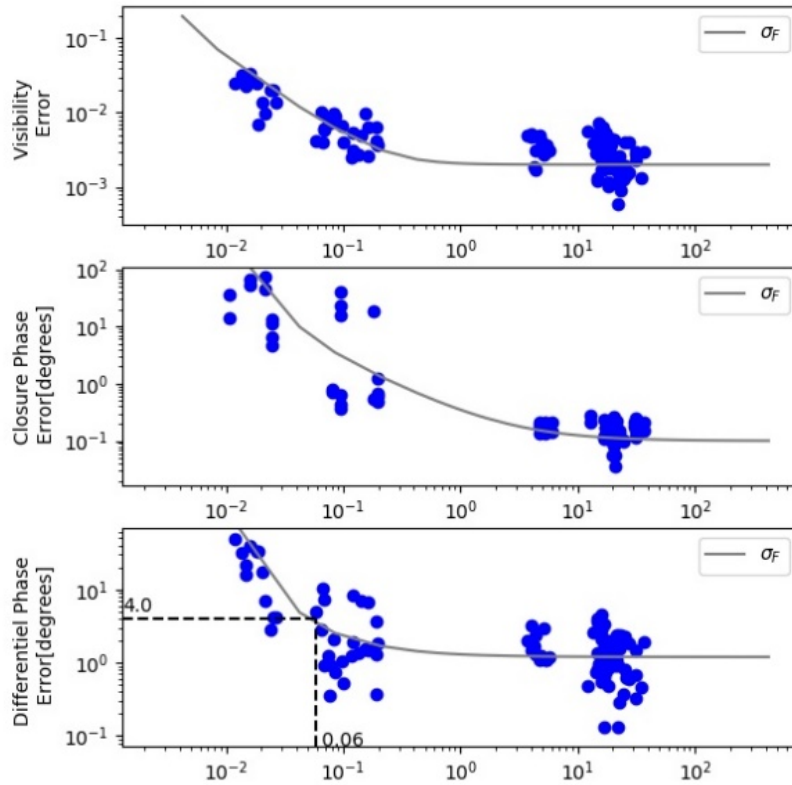


¹³ All plots are as a function of the coherent flux of the source. The broad band calibration error has been estimated from a “fair seeing” data set with seeing= 0.75 ± 0.25 arcsec and $\tau_0 = 7 \pm 2$ ms.



5.2.1.2 UTs

LOW L UT



From top to bottom: the visibility, the closure phase and the differential phase errors as a function of flux in Jy.

The plots on the left are those of the fundamental noise. The plots on the right are those of the global error, in red, and its components:

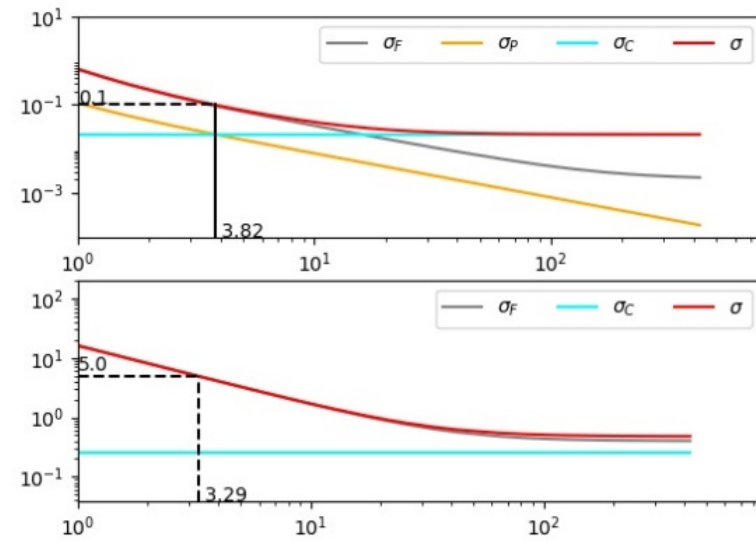
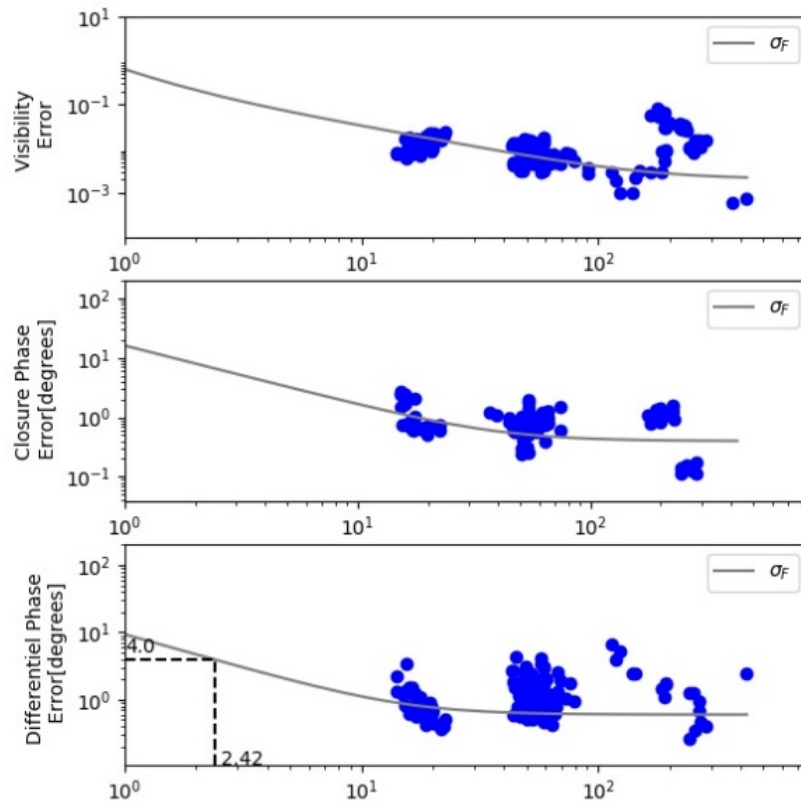
- the fundamental noise in grey
- the error due to the seeing variation, in cyan
- the error related to a wrong background correction, when applicable, in orange



5.2.2 Medium Resolution

5.2.2.1 ATs

MED L AT

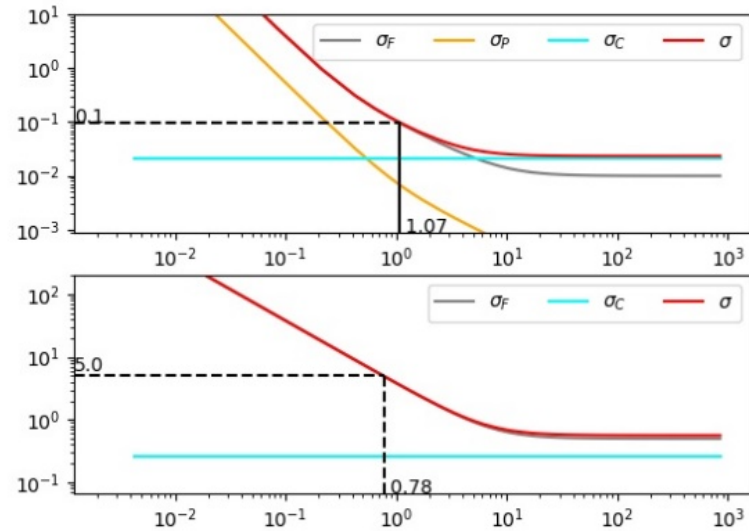
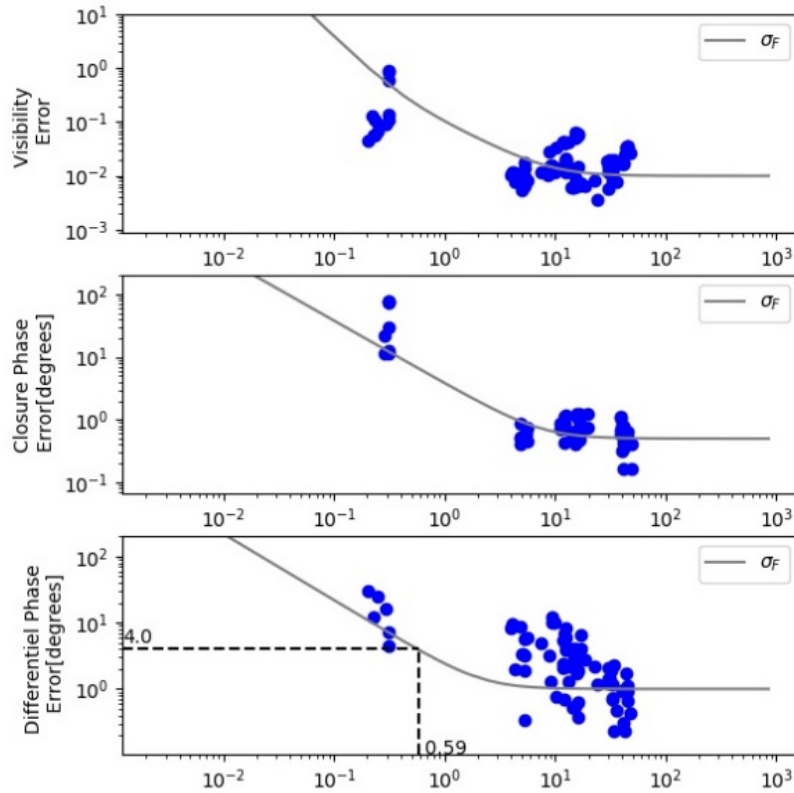


From top to bottom: the visibility, the closure phase and the differential phase errors as a function of flux in Jy.
 The plots on the left are those of the fundamental noise. The plots on the right are those of the global error, in red, and its components:
 -the fundamental noise in grey
 -the error due to the seeing variation, in cyan
 -the error related to a wrong background correction, when applicable, in orange



5.2.2.2 UTs

MED L UT



From top to bottom: the visibility, the closure phase and the differential phase errors as a function of flux in Jy.

The plots on the left are those of the fundamental noise. The plots on the right are those of the global error, in red, and its components:

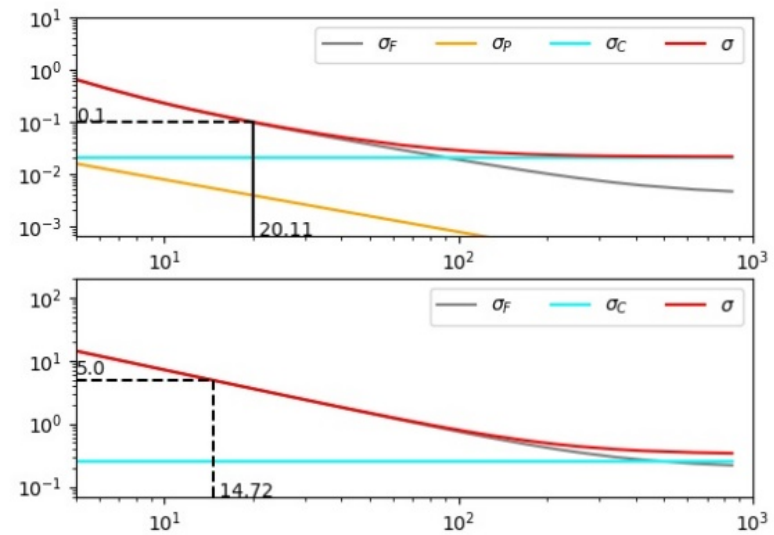
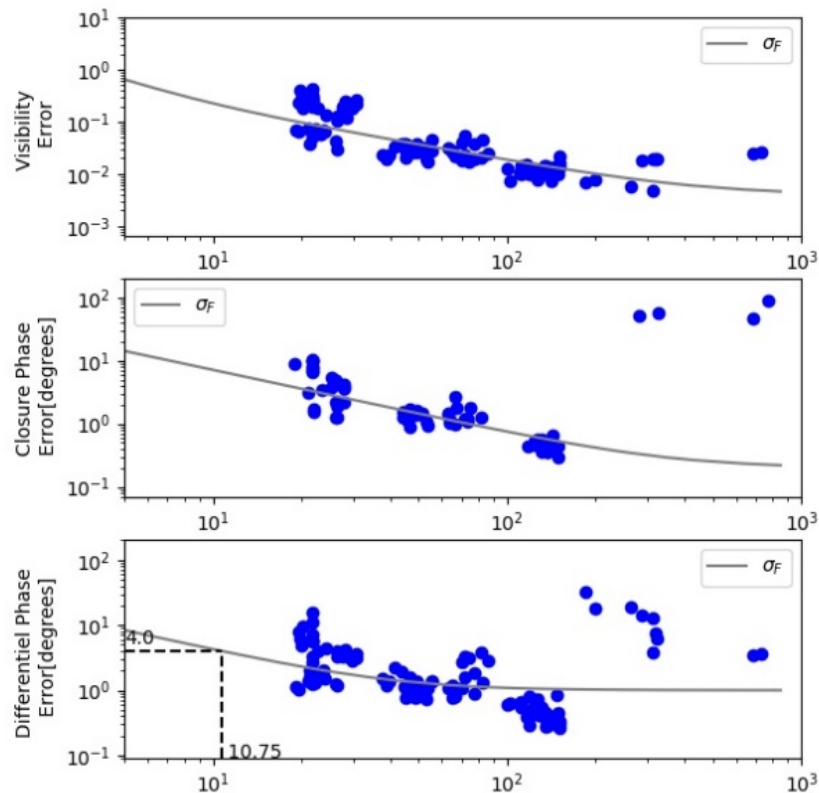
- the fundamental noise in grey
- the error due to the seeing variation, in cyan
- the error related to a wrong background correction, when applicable, in orange



5.2.3 High Resolution

5.2.3.1 ATs

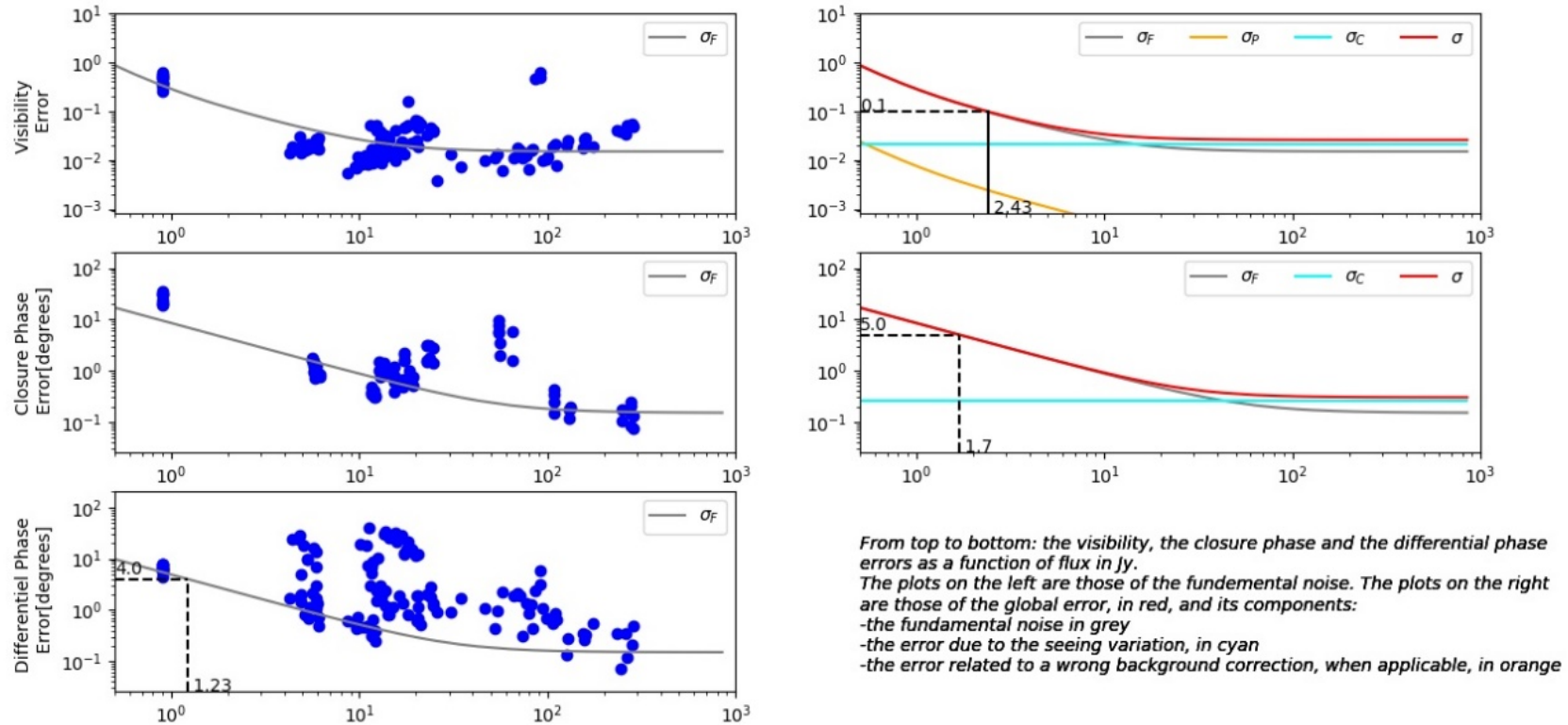
HIGH L AT



From top to bottom: the visibility, the closure phase and the differential phase errors as a function of flux in Jy.
 The plots on the left are those of the fundamental noise. The plots on the right are those of the global error, in red, and its components:
 -the fundamental noise in grey
 -the error due to the seeing variation, in cyan
 -the error related to a wrong background correction, when applicable, in orange

5.2.3.2 UTs¹⁴

HIGH L UT



14 There is a clear deficit of low flux calibrators in our HR-L data with UTs. The fundamental noise fits are also supported by the comparison with AT data. The differential phases are abnormally noisy, probably because the very small window available in HR-L is an end of band zone, around 4.05 μm strongly affected by chromatic OPD very variable feature. The fundamental noise fit is also made in coherence with the cleaner closure phase data.

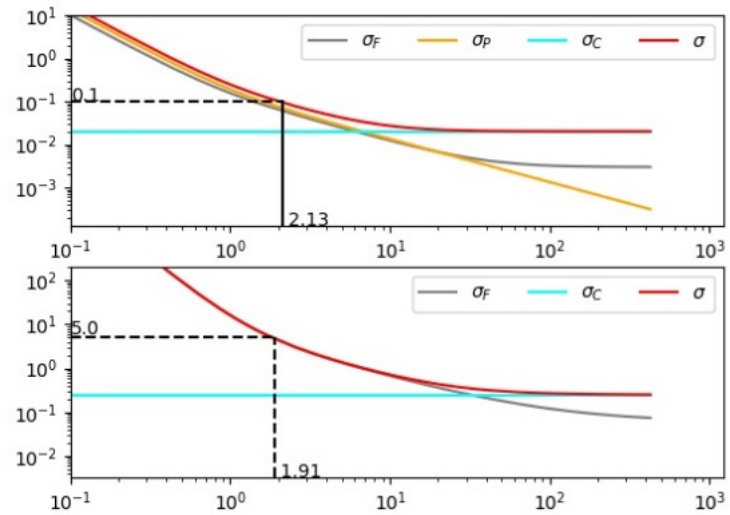
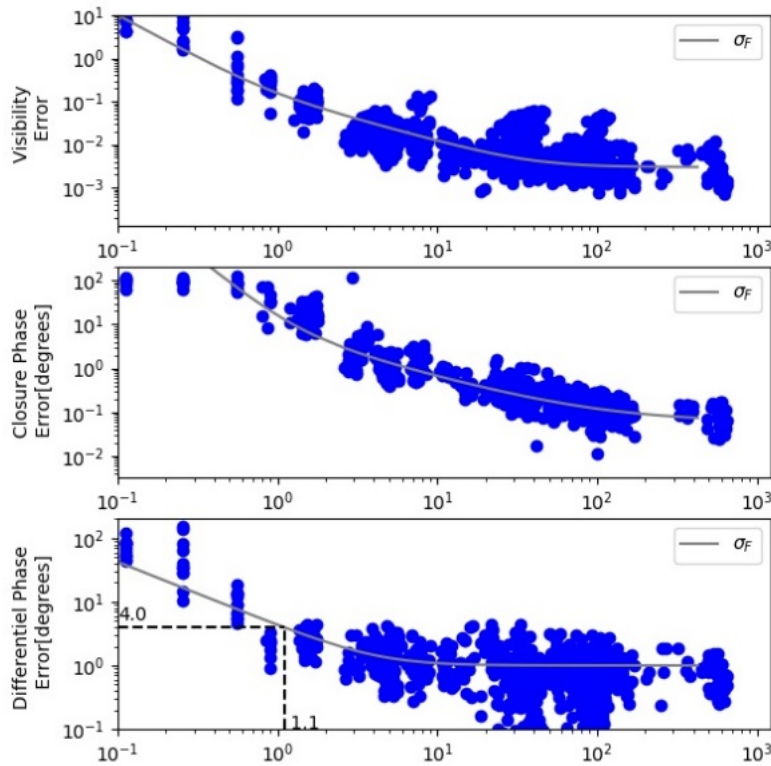


5.3 MBAND

5.3.1 Low Resolution

5.3.1.1 ATs

LOW M AT

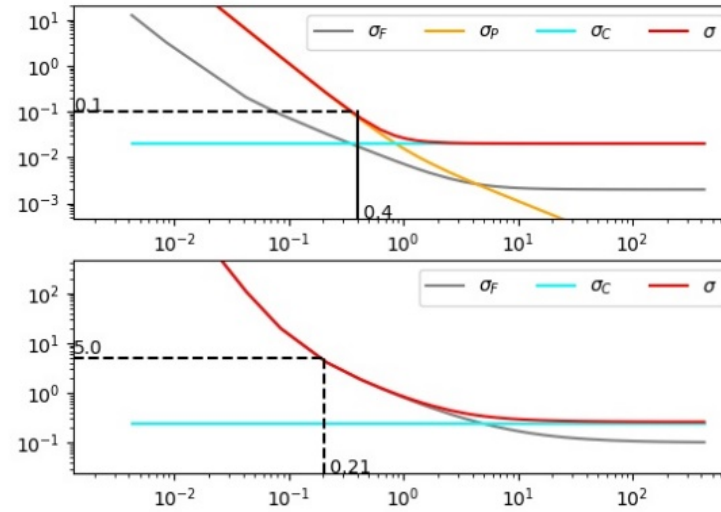
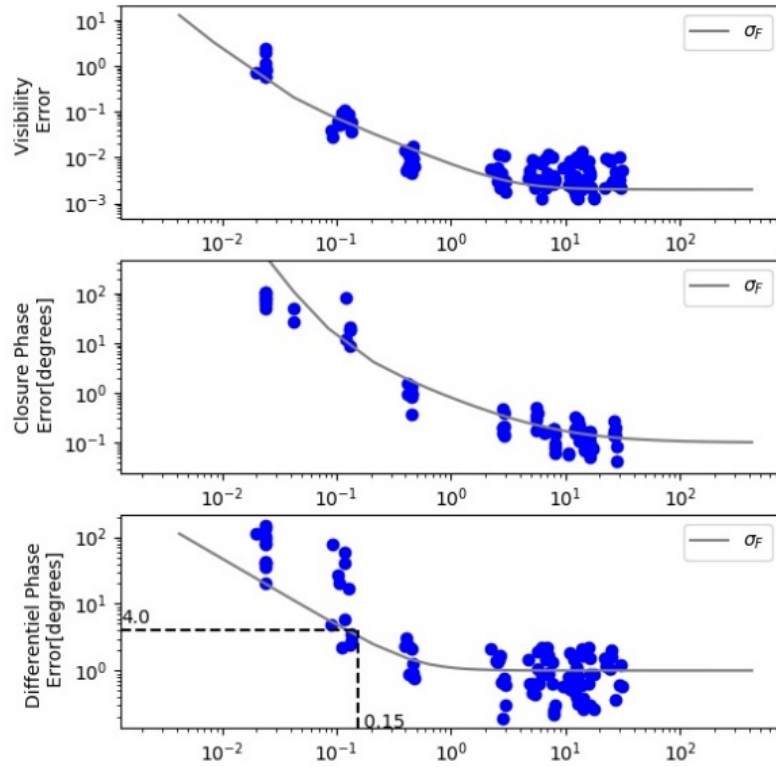


From top to bottom: the visibility, the closure phase and the differential phase errors as a function of flux in Jy. The plots on the left are those of the fundamental noise. The plots on the right are those of the global error, in red, and its components: -the fundamental noise in grey -the error due to the seeing variation, in cyan -the error related to a wrong background correction, when applicable, in orange



5.3.1.2 UTs

LOW M UT

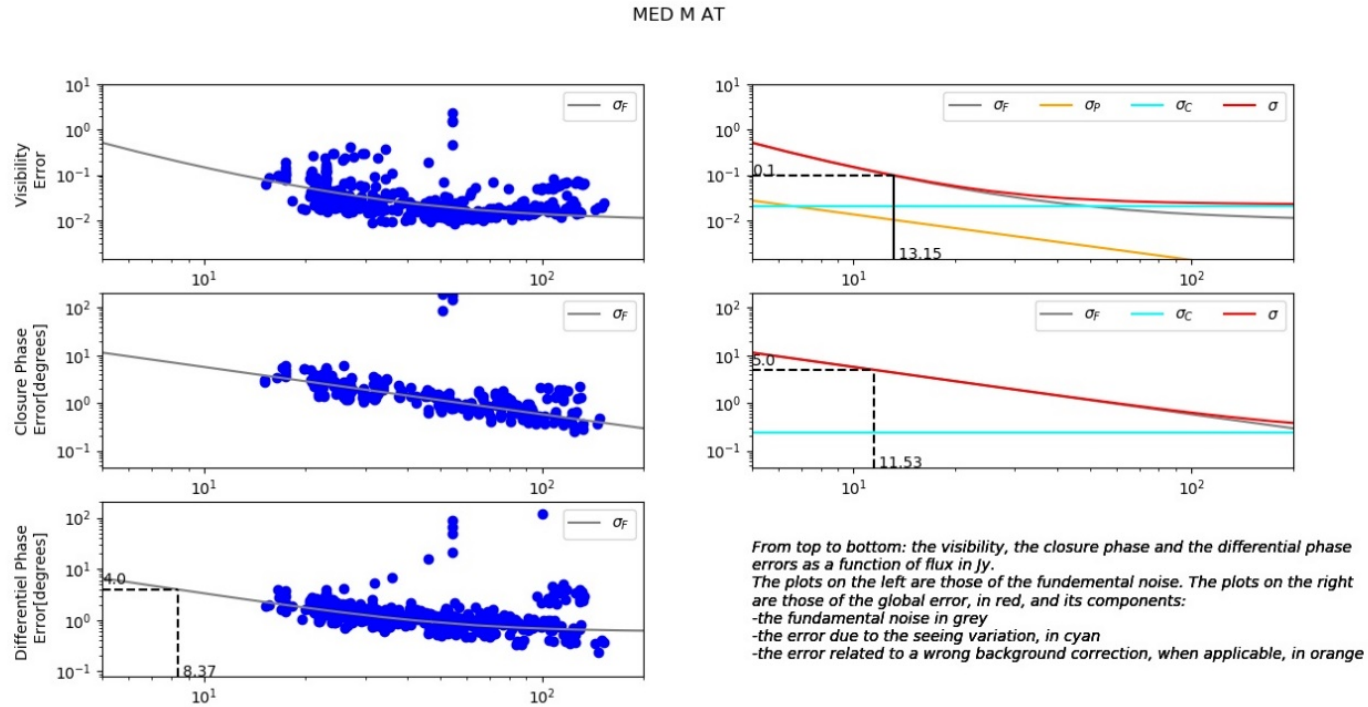


From top to bottom: the visibility, the closure phase and the differential phase errors as a function of flux in Jy. The plots on the left are those of the fundamental noise. The plots on the right are those of the global error, in red, and its components: -the fundamental noise in grey -the error due to the seeing variation, in cyan -the error related to a wrong background correction, when applicable, in orange



5.3.2 Medium Resolution

5.3.2.1 ATs



5.3.2.2 UTs

No data has been yet recorded for the medium resolution in M band with UTs, but we can give an estimation from the UT/AT flux ratio in M that has been measured to be ~ 12.2 . The comparison of UT and AT plots in L and N bands, detailed in [RD6, figure 10 page 11 and figure 14 page 14] and checked here indicate that applying the measured flux ratios given in section §2.4 is a correct way to scale limiting sensitivity from ATs to UTs.

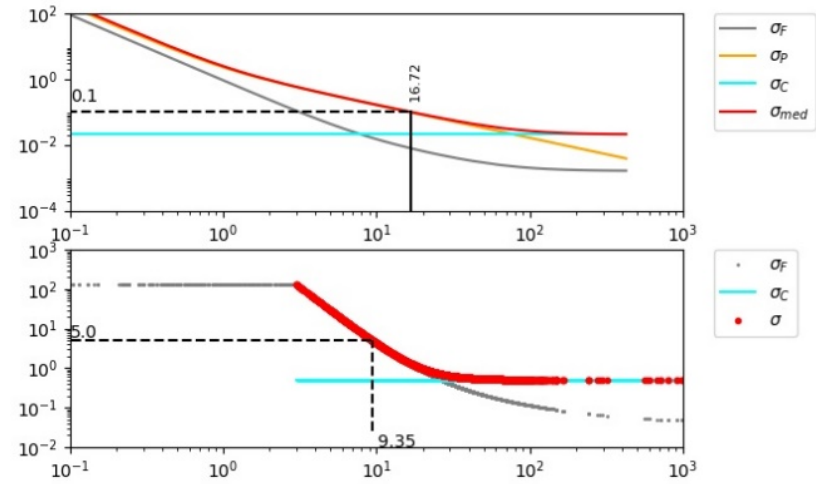
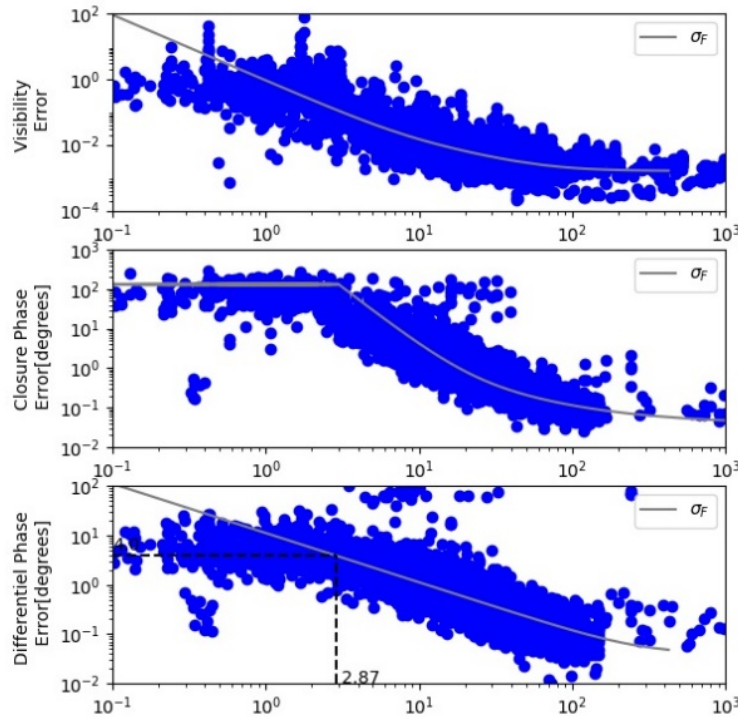


5.4 N1 BAND¹⁵

5.4.1 Low Resolution

5.4.1.1 ATs

LOW N1 AT



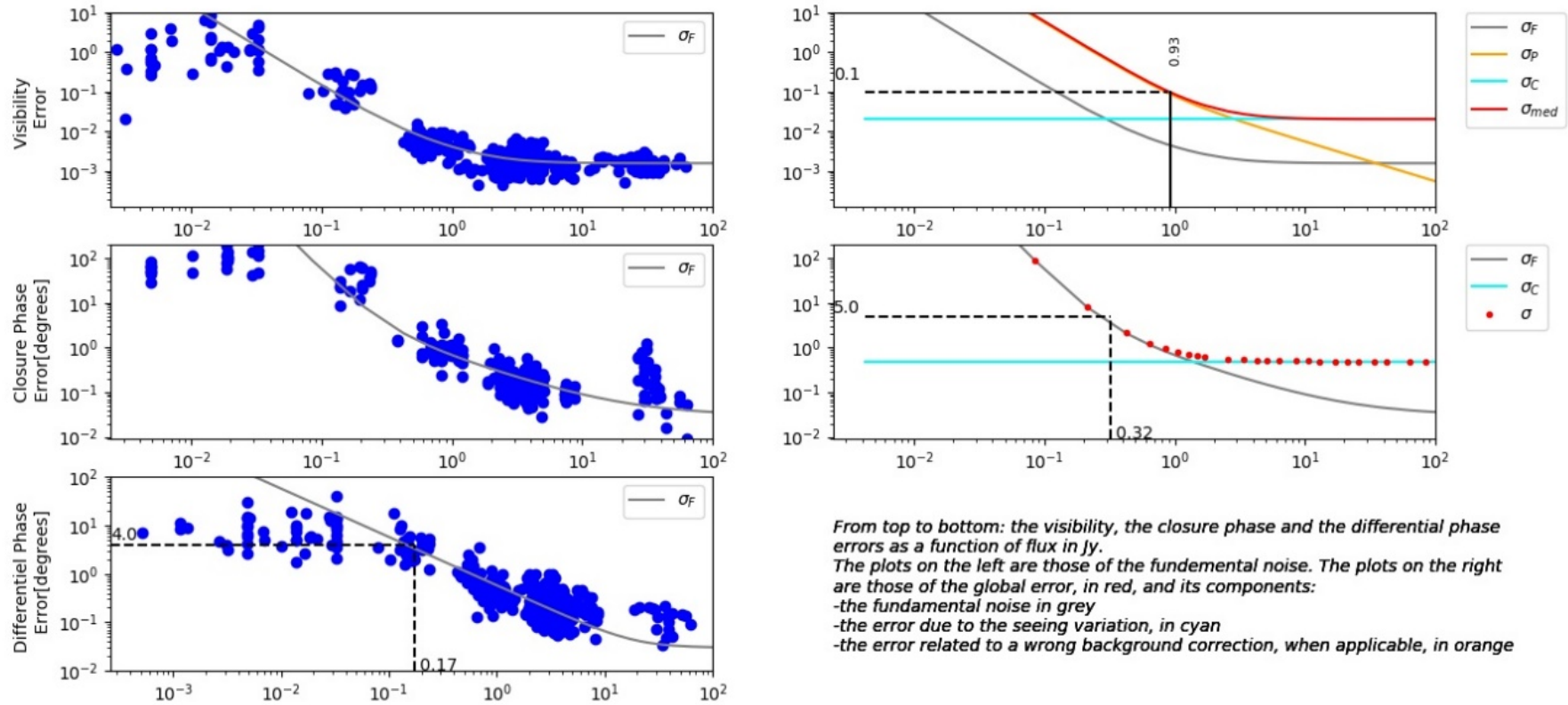
From top to bottom: the visibility, the closure phase and the differential phase errors as a function of flux in Jy.
 The plots on the left are those of the fundamental noise. The plots on the right are those of the global error, in red, and its components:
 -the fundamental noise in grey
 -the error due to the seeing variation, in cyan
 -the error related to a wrong background correction, when applicable, in orange

 The logo for MATISSE, featuring a stylized white 'M' on a dark blue square background with three small white stars above it. The word 'MATISSE' is written in white capital letters at the bottom of the square.	MATISSE Instrument Performance Report: Commissioning Report	Doc. : Issue : Date : Page :	VLT-TRE-MAT-15860-9141 2.0 15.07.22 52 of 131
---	---	---------------------------------------	--



5.4.1.2 UTs¹⁶

LOW N1 UT



From top to bottom: the visibility, the closure phase and the differential phase errors as a function of flux in Jy. The plots on the left are those of the fundamental noise. The plots on the right are those of the global error, in red, and its components:
 -the fundamental noise in grey
 -the error due to the seeing variation, in cyan
 -the error related to a wrong background correction, when applicable, in orange

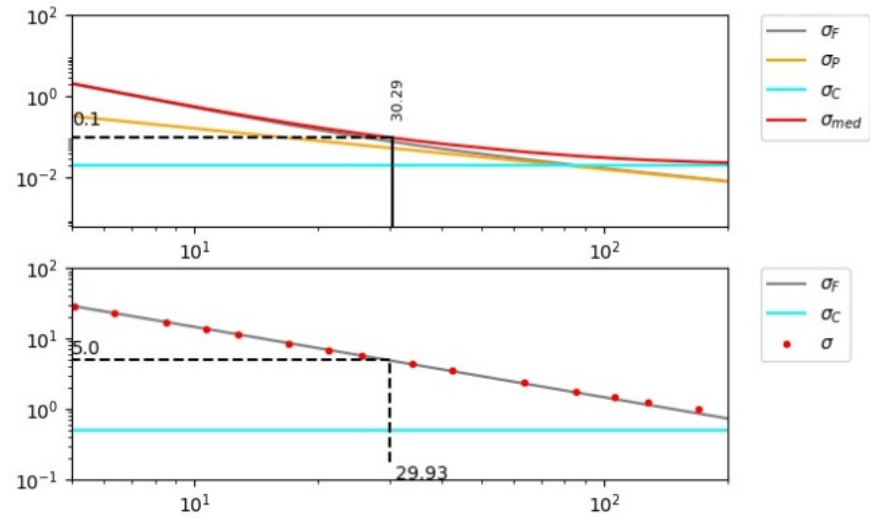
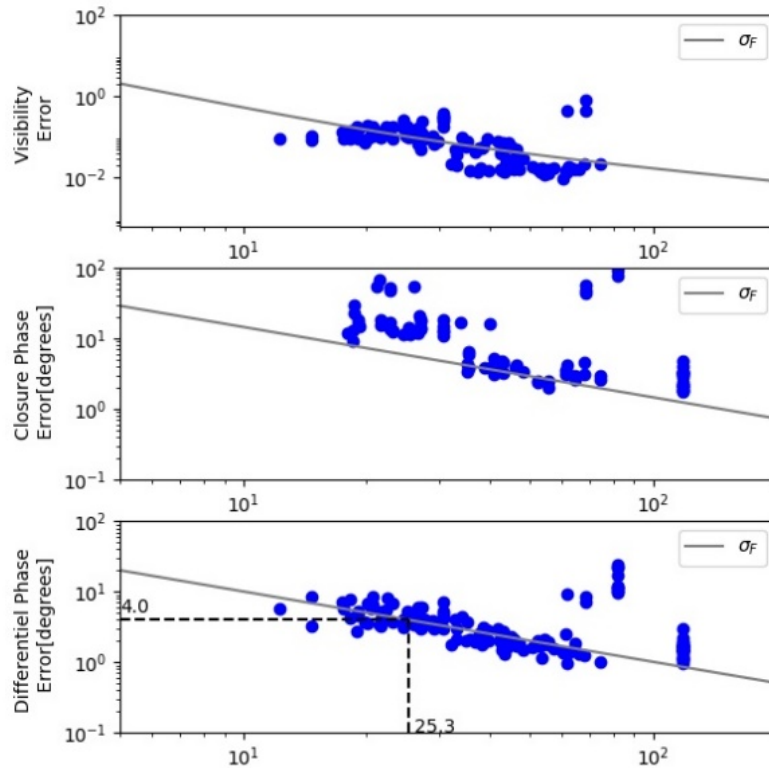
16 The saturation of the fundamental error phase error around a value of 10° in LR-N with UTs and ATs, is not understood and still under investigation. However, the fit for lower noise and higher flux seems correct and in agreement with the visibility and closure phase fits. As the limit of sensitivity is set at 4°, the estimate seems correct.



5.4.2 High Resolution

5.4.2.1 ATs

HIGH N1 AT

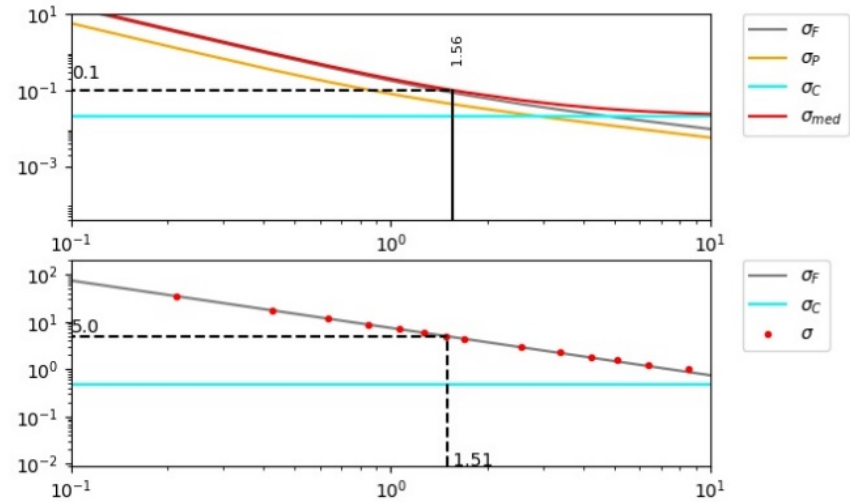
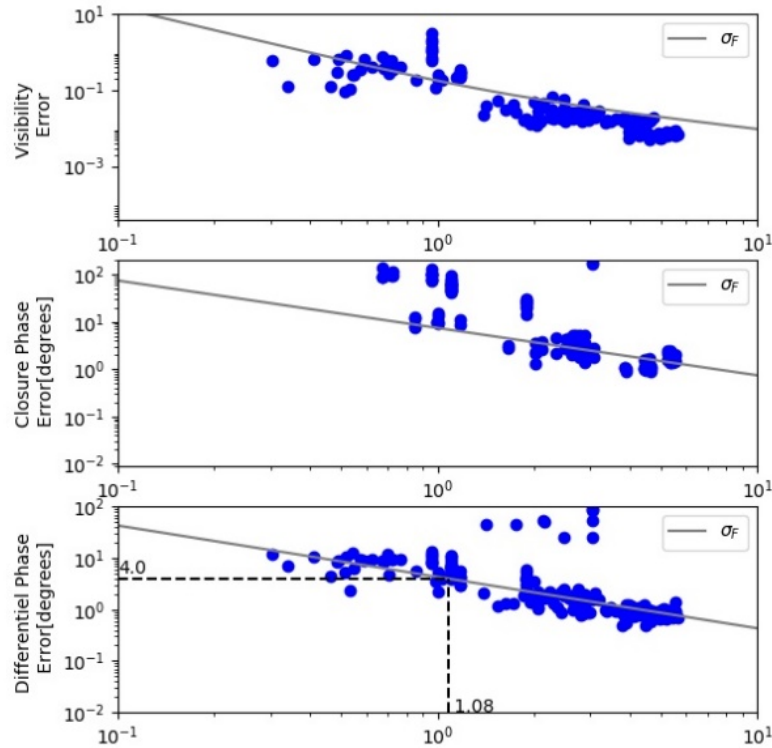


From top to bottom: the visibility, the closure phase and the differential phase errors as a function of flux in Jy.
 The plots on the left are those of the fundamental noise. The plots on the right are those of the global error, in red, and its components:
 -the fundamental noise in grey
 -the error due to the seeing variation, in cyan
 -the error related to a wrong background correction, when applicable, in orange



5.4.2.2 UTs

HIGH N1 UT



From top to bottom: the visibility, the closure phase and the differential phase errors as a function of flux in Jy.
 The plots on the left are those of the fundamental noise. The plots on the right are those of the global error, in red, and its components:
 -the fundamental noise in grey
 -the error due to the seeing variation, in cyan
 -the error related to a wrong background correction, when applicable, in orange

5.5 SUMMARY TABLE FOR THE V1.1 VERSION¹⁷

5.5.1 L, M and N1 bands

The following tables collect all the numbers extracted from the plots in section §0 and give the minimum coherent flux in Jy to achieve the limits agreed with Paranal on visibility (0.1 per spectral channel per minute), closure phase (5° per spectral channel per minute), differential phase (4° per spectral channel and per minute) that should also yield a coherent flux measure SNR=10 per spectral channel and per minute. The first table, from the plots above is in fair and good seeing conditions.

For « Fair and Good » seeing conditions (seeing<0.9 arcsec, $\tau_0>5$ ms)¹⁸.

Limiting Coherent flux in Jy										
Telescopes	Resolution	Visibility			Closure Phase			Differential Phase Coherent Flux SNR		
		L	M	N	L	M	N	L	M	N1
ATs	LOW	1.1	2.1	16.8	0.4	1.9	9.4	0.3	1.1	2.9
	MED	3.8	13.2	na	3.3	11.5	na	2.4	8.4	na
	HIGH	20.1	na	30.3	14.7	na	29.9	10.7	na	25.3
UTs	LOW	0.3	0.4	0.9	0.07	0.15	0.3	0.06	0.15	0.2
	MED	1.1	1.1 ¹⁹	na	0.8	0.9	na	0.6	0.7	na
	HIGH	2.4	na	1.6	1.7	na	1.5	1.2	na	1.1

The second table is from similar plots with the flux independent broad calibration error estimated on a poor seeing data set.

For « Poor » seeing conditions (seeing=0.9±0.2 arcsec and $\tau_0=3.6±1.6$ ms)

Limiting Coherent flux in Jy										
Telescopes	Resolution	Visibility			Closure Phase			Differential Phase Coherent Flux SNR		
		L	M	N	L	M	N	L	M	N1
ATs	LOW	2.8	4.0	18.5	0.4	1.5	9.4	0.3	1.1	2.9
	MED	7.8	15.7	na	3.3	11.5	na	2.42	8.4	na
	HIGH	31.4	na	32.2	14.7	na	29.9	10.7	na	25.3
UTs	LOW	0.5	0.6	1	0.07	0.15	0.3	0.06	0.15	0.2
	MED	1.7	1.3	na	0.8	0.9	na	0.6	0.7	na
	HIGH	3.8	na	1.7	1.7	na	1.5	1.3	na	1.1

At the higher spectral resolution, we give the limit for absolute visibility and closure phase accuracy per spectral channel, where the broad band errors are assumed independent from the resolution.

¹⁷ As in V1.1 but with the correction of some typos and the extension of N band results to the bands N2 and N3

¹⁸ The numbers for the « fair seeing » data set (seeing=0.75±0.2 arcsec and $\tau_0=7±2$ ms) are very similar to those for a “good seeing” data set (seeing=0.55±0.1 arcsec and $\tau_0=8±2$ ms). The limit between “good” and “bad” conditions for MATISSE is fundamentally set by $\tau_0\sim 4$ ms)

¹⁹ The values given in MR_M with UTs are estimated from the measured UT/AT flux ratio in M. They are not yet supported by observations, which we could not perform so far.



In practice, it is strongly recommended to use LR observations for absolute measurements and to reserve the higher spectral resolution for differential measures. So, the relevant number for all higher spectral resolutions is the one given for the differential phase limit, that corresponds also to a differential visibility precision of 5%. However, for targets brighter than the coherent fluxes given here, higher spectral resolution can also be used for absolute measurements.

5.6 PROPOSED PERFORMANCES IN VERSION 1.1

Due to bias problem uncovered in N band (see section 2.7), the limiting fluxes for N band differential phase and coherent flux measurements derived in section 5.5 are to be replaced, in the present status of the DRS, by the bias limit described in section 2.7. This yields the following final tables

For « Fair and Good » seeing conditions (seeing<0.9 arcsec, $\tau_0>5$ ms)²⁰.

Limiting Coherent flux in Jy										
Telescopes	Resolution	Visibility			Closure Phase			Differential Phase Coherent Flux SNR		
		L	M	N	L	M	N	L	M	N1
ATs	LOW	1.1	2.1	16.8	0.4	1.9	9.4	0.3	1.1	5
	MED	3.8	13.2	na	3.3	11.5	na	2.4	8.4	na
	HIGH	20.1	na	30.3	14.7	na	29.9	10.7	na	25.3
UTs	LOW	0.3	0.4	0.9	0.07	0.15	0.3	0.06	0.15	0.2
	MED	1.1	1.1 ²¹	na	0.8	0.9	na	0.6	0.7	na
	HIGH	2.4	na	1.6	1.7	na	1.5	1.2	na	1.1

For « Poor » seeing conditions (seeing=0.9±0.2 arcsec and $\tau_0=3.6±1.6$ ms)

Limiting Coherent flux in Jy										
Telescopes	Resolution	Visibility			Closure Phase			Differential Phase Coherent Flux SNR		
		L	M	N	L	M	N	L	M	N1
ATs	LOW	2.8	4.0	18.5	0.4	1.5	9.4	0.3	1.1	6
	MED	7.8	15.7	na	3.3	11.5	na	2.42	8.4	na
	HIGH	31.4	na	32.2	14.7	na	29.9	10.7	na	25.3
UTs	LOW	0.5	0.6	1	0.07	0.15	0.3	0.06	0.15	0.25
	MED	1.7	1.3	na	0.8	0.9	na	0.6	0.7	na
	HIGH	3.8	na	1.7	1.7	na	1.5	1.3	na	1.1

5.7 COMPLEMENT TO N-BAND PERFORMANCES: N2 AND N3 BANDS

Here we provide the requested additional performance estimates in the two other parts of N-band, i.e. N2 and N3, defined by:

	Wavelengths
--	--------------------

20 The numbers for the « fair seeing » data set (seeing=0.75±0.2 arcsec and $\tau_0=7±2$ ms) are very similar to those for a “good seeing” data set (seeing=0.55±0.1 arcsec and $\tau_0=8±2$ ms). The limit between “good” and “bad” conditions for MATISSE is fundamentally set by $\tau_0\sim 4$ ms)

21 The values given in MR_M with UTs are estimated from the measured UT/AT flux ratio in M. They are not yet supported by observations, which we could not perform so far.



N1 Band	$\lambda_0 = 8.5\mu\text{m}, \Delta\lambda = [8.1 - 8.9] \mu\text{m}$
N2 Band	$\lambda_0 = 10.5\mu\text{m}, \Delta\lambda = [10 - 11] \mu\text{m}$
N3 Band	$\lambda_0 = 11.5\mu\text{m}, \Delta\lambda = [11 - 12] \mu\text{m}$

The estimation procedure applied to N2 and N3 is the same as for the other bands. The corresponding performance plots are shown in annex 12.

For All conditions²²

Limiting Coherent flux in Jy										
Telescopes	Resolution	Visibility			Closure Phase			Differential Phase Coherent Flux SNR		
		N1	N2	N3	N1	N2	N3	N1	N2	N3
ATs	LOW	16.8	31.4	44.0	9,4	23.6	36.7	2,9	7.5	11.7
	HIGH	30.3	51.3	83.7	29.9	194	218	25,3	45.9	58.9
UTs	LOW	0.9	1.4	1.9	0.3	0.8	1.3	0.2	0.55	0.6
	HIGH	1.6	3.4	4.1	1.5	4.9	13.1	1.1	3.5	3.7

²² In the N band there is no significant difference between the different seeing conditions for these performance limits.



Commissioning Report

6 ANNEX: COMMISSIONING RUNS AND TEAM

6.1 COMMISSIONING RUNS

The initial commissioning plan has been updated to adapt to the VLTI availability. Here we summarize the updated schedule, goals and key results of the runs.

6.1.1 Operations (March 2018)

Its main goals were:

- To commission the operation of MATISSE in the VLTI environment.

This has been fully achieved, from the operation of MATISSE with the standard VLTI instrument OS environment, using the Broker of Observing Blocks (BOB) in which we fetch OB prepared with the Visitor Observing Tool (VOT). MATISSE is ready to be operated as any operational VLTI instrument.

- To make a first set of sensitivity estimates.

This is detailed in the next chapter, indicating that MATISSE is performing better than its goals and therefore much better than its contractual specifications

- To test the MATISSE pipeline.

MATISSE pipeline was usable almost from the beginning of the first commissioning run, but we detected a lot of software bugs and many needs to adapt the data reduction to the actual behavior of the instrument on the VLTI. This is discussed for each measurement presented above.

6.1.2 Measurement accuracy in LR L&N (May 2018)

The initial goal of the run was to evaluate the performance of the LR observing modes in L and in N, in order to report to ESO early enough (June 2018) to allow considering offering MATISSE in LR on the VLTI in the September 2018 "Call for Proposal" for the ESO observing period P103.

This run allowed to implement and to validate many corrections in the Operating System, NRTS and DRS.

The NRTS is now able to process all frames, while in March it was too slow to process more than one out of 4 to 5 frames. This allows to actually add coherently typically 10 frames in N and improves the fringe detection sensitivity.

The overheads have been quite substantially reduced and now a typical observation, with 4 interferometric exposures and 8 photometric exposures in N (and therefore 12 interferometric exposures in L) takes 20 mn, for 12 mn open shutter time.

Changing the spectral resolution of the instrument can be done in less than 2 mn and does not require repeating instrument calibration. We therefore decided to combine LR and HR (or MR) observation after the acquisition of the target and of the fringes. Therefore, we could make a preliminary evaluation of the HR mode performances during this run.

6.1.3 Higher spectral resolutions (July and September 2018)

Update the sensitivity limits, mainly with UTs because we had only 2 half nights with 4UTs so far, that were dedicated in priority to an evaluation of the measurement accuracy.

More detailed study of the higher spectral resolutions, HR in N and MR and HR in L.

Investigate the performances in the M band → moved to the April 2019 run.



Commissioning Report

6.1.4 Imaging and NAOMI update (December 2018)

Many repeated calibrators → substantial update of performances in LR.

First image reconstructions. See the image reconstructions memos.

- Image reconstruction during a run is possible in L, which allows to check the quality of the data
- The Image quality in L is strongly improved after the run with careful calibration and data selection.
- The N band images produced during the run were almost too poor to be usable.
- After the run, good N band images have been obtained after
 - o Systematic processing with telescope substitute and spectral binning, that were not standard part of the DRS at the time. Now they have been included in the default pipeline options.
 - o Careful verification of absolute visibility in N

6.1.5 M Band (April 2019)

The M band performances have been commissioned and that mode has been offered.

We found that M band observations must be made in SiPhot with chopping. Actually, we found that this applies also in L for faint targets.

6.1.6 VHR (December 2019)

The Very High Spectral resolution mode has been commissioned at the end of the November 2019 technical run after the replacement of the VHR grism. The VHR mode is non-contractual and has been defined after the MATISSE FDR. Its performances with ATs are reported here.

6.1.7 GRA4MAT (from 2019 to 2022)

GRA4MAT (GRAVITY for MATISSE) is the use of the GRAVITY Fringe Tracker for MATISSE observations. GRA4MAT is not part of the initial MATISSE agreement, and it is an additional project led by ESO in collaboration with the MATISSE consortium.

GRA4MAT has been developed and tested by ESO's Julien Woillez and Gerard Zins during technical runs in June, September, October 2019, and January 2020 with MATISSE's Anthony Meilland. The MATISSE consortium participated in the implementation runs in 2019 and in the commissioning runs in 2020 and 2021, remotely from Europe after March 2020 due to the Covid-19 crisis. A final GRA4MAT run is foreseen mid-July 2022.

6.1.8 L band dispersive wheel recovery (February 2022)

Beginning of 2021, after the restart of the instrument after the Covid-19 crisis, the DIL wheel (the wheel in the L band cryostat composed of grisms and prism) has shown problematic behavior until being completely stuck in "low resolution". A plan was made to replace the faulty wheel and implement several mechanical improvements, and an intervention took place in February 2022. This intervention was a success and was followed by few on sky testing night observations.



6.1.9 Final update run (April 2022)

A final commissioning and technical run were first scheduled in April-May 2020. It was rescheduled after the covid-19 crisis; it has been executed in April 2022 to complement the performance limit values based on extrapolations or on scaling from ATs. The very bad atmospheric conditions did not allow us to achieve these goals and some observations will be inserted in the July 2022 GRA4MAT run.

6.2 COMMISSIONING TEAM

The following table lists the direct participants at Paranal to the MATISSE commissioning runs (green boxes), GRA4MAT commissioning runs (blue boxes) or for technical activities just before or during a commissioning run (orange boxes). Due to the Covid-19 crisis, the runs of 2021 and April 2022 has made remotely from Europe:

Year		2018						2019				2020		2021			2022		
Month		3	5	7	9	12	4	6,9	10	12	1	3	3	6	9	2	4	7	
Participants	Institut																		
F. Allouche	OCA	Green	Green		Green	Green	Green			Green						Green			
Ch. Bailet	OCA								Orange										
F. Bettonvil	ASTRON								Orange										
Y. Bresson	OCA								Orange										
L. Burtscher	Leiden			Green															
A. Chelli	OCA		Green																
P. Cruzalèbes	OCA	Green		Green		Green													
E. Elswijk	ASTRON				Orange				Orange										
Y. Fanteï	OCA		Orange																
K.-H. Hofmann	MPIfR					Green													
W. Jaffe	Leiden	Green		Green															
S. Lagarde	OCA	Green	Green		Green	Green	Green			Green							Green		
W. Laun	MPIA								Orange										
M. Lehmitz	MPIA								Orange										
B. Lopez	OCA				Green	Green	Green			Green									
A. Matter	OCA		Green		Green	Green	Green			Green									
A. Meilland	OCA	Green	Green	Green	Green	Green	Green	Blue	Blue	Green		Blue					Green		
K. Meisenheimer	MPIA		Green																
F. Millour	OCA	Green		Green		Green					Blue								
R. Petrov	OCA	Green	Green	Green	Green	Green	Green		Blue	Green		Blue					Green		
S. Robbe-Dubois	OCA	Green		Green		Green				Green									
S. Rousseau	OCA	Orange																	
D. Schertl	MPIfR				Green	Green													
J. Varga	Leiden	Green									Blue								
Remote session	All												Blue	Blue	Blue		Green	Blue	



7 ANNEX: OBSERVING PARAMETERS

7.1 PARAMETERS OF ACQUISITION OB

The typical parameters for image acquisition are:

- N band DIT=5ms (to avoid saturating the detector with background in non-dispersed mode)
- L band DIT=5ms. We could use longer DITs but this has not been tested
- NDIT for acquisition: to have acquisition times between 1 s and 10 s. To acquire difficult targets like the Circinus galaxy, we have tried one minute acquisition exposures.
- TADC: transverse atmospheric dispersion correction: off with ATs, on with UTs.
 - o The TADC correctly compensates the difference between L and N bands in MATISSE
- Chopping: Yes.
- Chopping frequency: 1 Hz with ATs. 0.5 Hz so far with UTs. During the last UT half night we have used successfully 1 Hz with UTs

The first calibrator of the night

- bright enough for pupil check ($K < 6$ on ATs) and
- close to zenith ($z < 30^\circ$) to correctly initialize the IRIS tracking and the transverse differential correction by MATISSE.

The typical parameters for fringe search and acquisition are

- L band DIT=50 ms in LR, 100 ms in MR
- N band DIT=20 ms in LR, 100 ms in HR (not tested nor optimized)
- MR for the first fringe search of the night, or to face unexpected fringe jumps.
- LR has always been sufficient to reacquire the fringes with UTs and with ATs in the small configuration. After a long break with ATs on a large quadruplet, it is recommended to use MR for fringe search if the target allows it.
- LADC: no, in fringe search

After a change of configuration, the first fringe search should be done in MR.

7.2 PARAMETERS OF OBSERVATION OB

This report is based on the following set of parameters

7.2.1 DIT and NDIT

- L band, LR: 75 ms,
- L-M band, LR: 111 ms
- L or M, Higher spectral resolution: 111 ms
- N, LR: 20 ms. Modulation over 10 steps
- N, HR, 75 ms. Modulation over 6 steps.

7.2.2 Chopping parameters

- ATs: 1 Hz
- UTs: mostly 0.5 Hz, as we had problems for most of the runs with chopping on UTs. Lately, 1 Hz is OK but we have very little commissioning data with 1 Hz
- Chopping stroke: 5 as with ATs, 4.5 as with UTs



Commissioning Report

7.2.3 Spatial filters

- 1.5 λ/D in L-M
- 2 λ/D in N

7.2.4 Modulation

- The observations are modulated in 10 steps both in L and N (6 steps in HR-N). In L we process frame by frame and the modulation has no effect (but for the NRTS). In N, the fundamental noise results are reported with coherent integration over the modulation cycle. They are only marginally modified by the modulation. The modulation/demodulation slightly improves the closure phase stability and degrades the absolute visibility sensitivity to seeing. The N band broad band calibration error on the visibility is given for a frame-by-frame processing.

8 ANNEX: DATA REDUCTION OPTIONS

All data shown in this report has been reduced with the following parameters. This annex illustrates the choice of this options by the gain they provided.

8.1 REPLACETEL

With ATs, the photometric measurement from IP5 (AT3) is replaced by the mean of the other photometric measures. It is shown that this substantially reduces the dispersion of measures and stabilizes the transfer function.

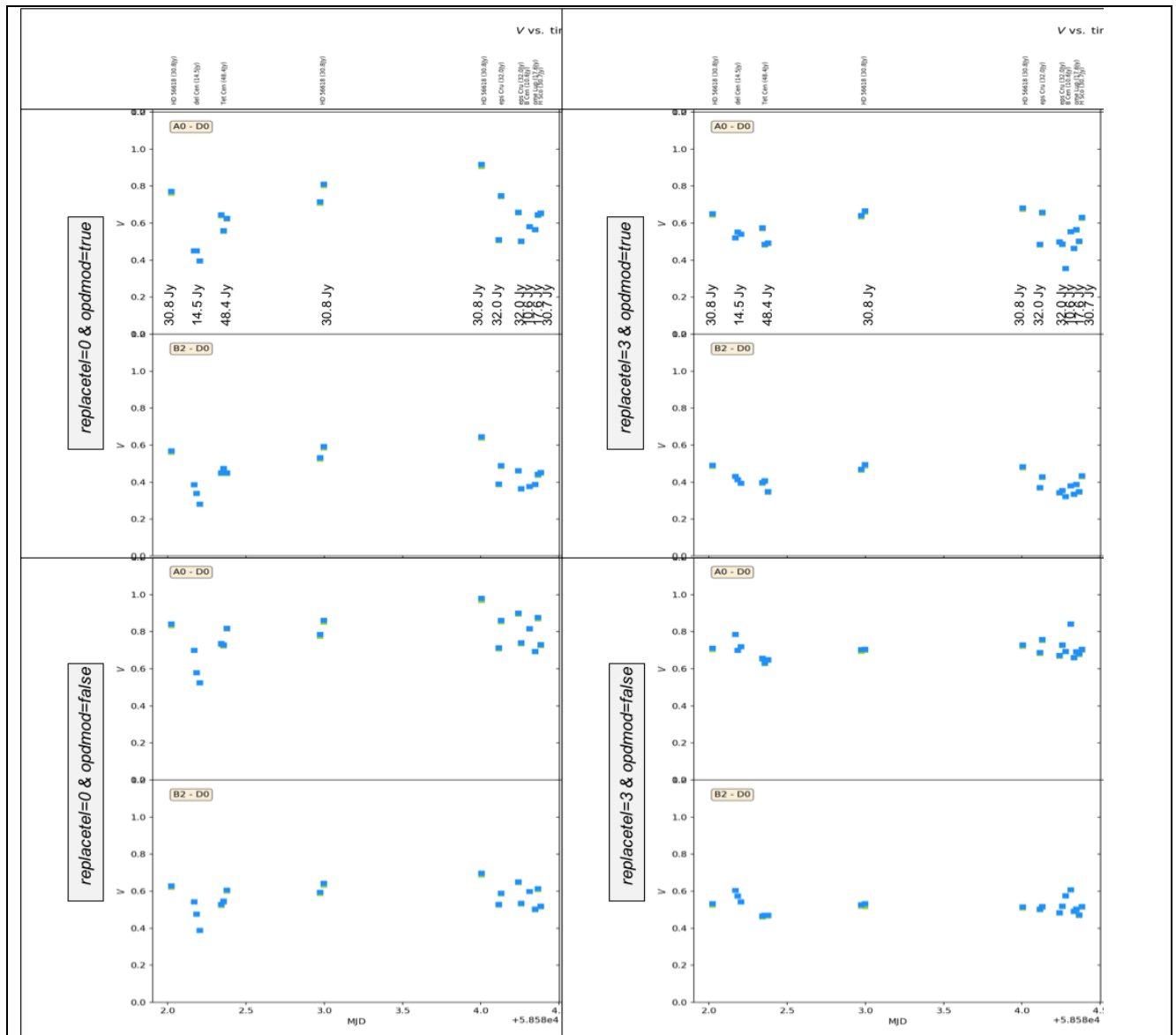
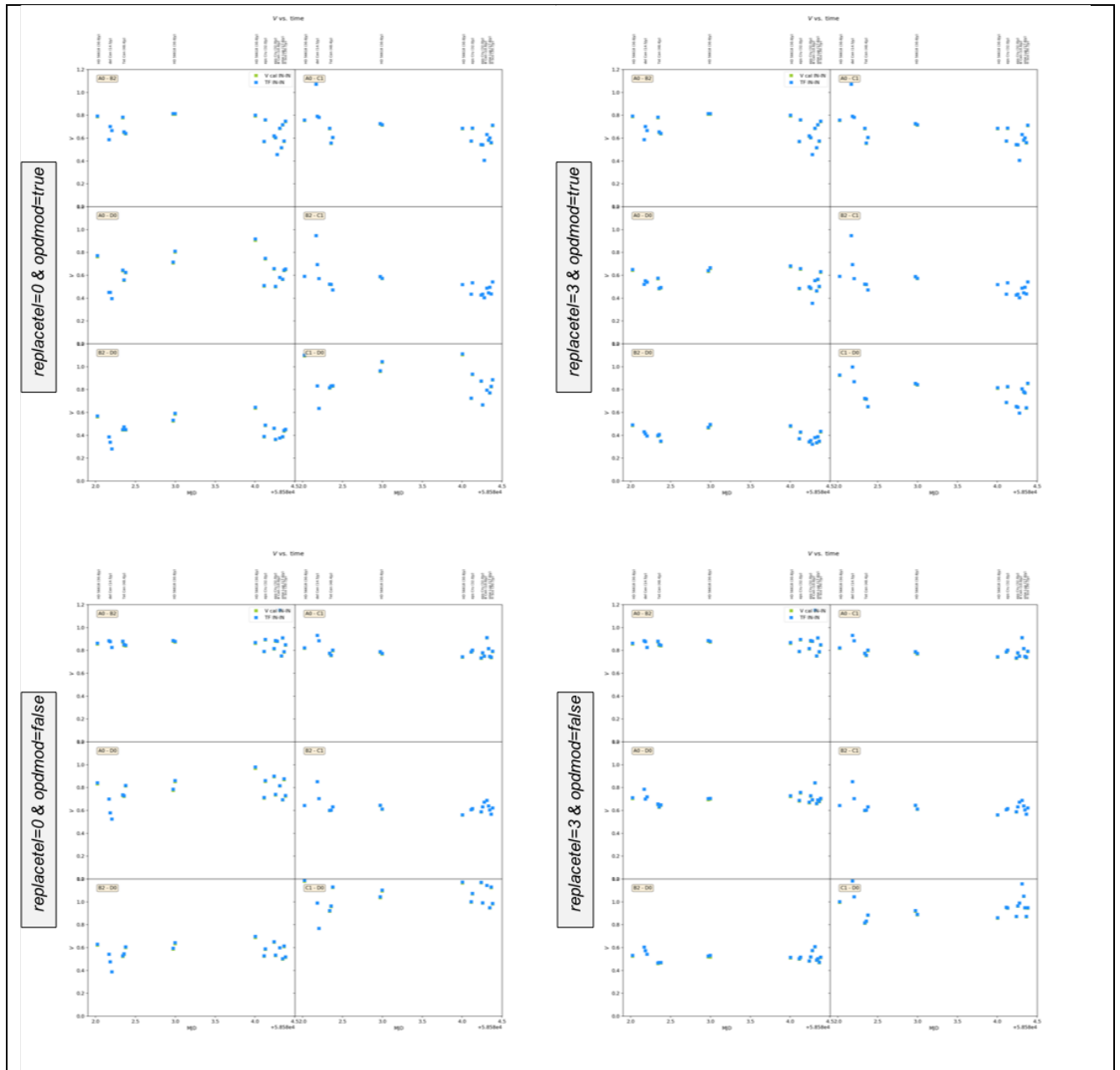


Figure 8.1: effect of `replacetel` and of `opdmod` parameters in LR-N on the instrument + atmosphere visibility (corrected from the calibrator diameter) as a function of time (MJD). Top line: data processing with coherent integration over the modulation cycle (`opdmod=true`). Bottom line: processing frame by frame (`opdmod=false`). Left column, processing using all the photometric measurements as they are obtained (`replacetel=0`). Right column, processing where the photometry in IP5 (tel 3) is replaced by a combination of the other photometric beams (`replacetel=3`). Above, we zoom on baselines A0-D0 and B2-D0. Below, we see all baselines of the small AT quadruplet.



The integration over a modulation cycle (~ 240 ms) strongly increases the sensitivity to seeing, on all baselines, and the processing frame by frame clearly reduces the broad band calibration error, even for relatively faint targets (14 Jy) where the fundamental noise per spectral channel is clearly increased by the frame-by-frame processing.

The replacement of the photometry in beam 3 by a combination of the other ones improves the broad band calibration on the 3 baselines affected by this photometry (here the AT at position D0).

8.2 HAMPEL FILTER

With the Hawaii detector (L and M bands), outlying pixels are eliminated in the photometry by a MAD clipping filter applied over typically ten frames. This is applied since the July 2019 commissioning memo (RD7). It has reduced the equivalent photometric noise in L from ~ 0.5 Jy (with ATs) to less than 0.1 Jy. This sets the L band limits explained in section 5.2.1.

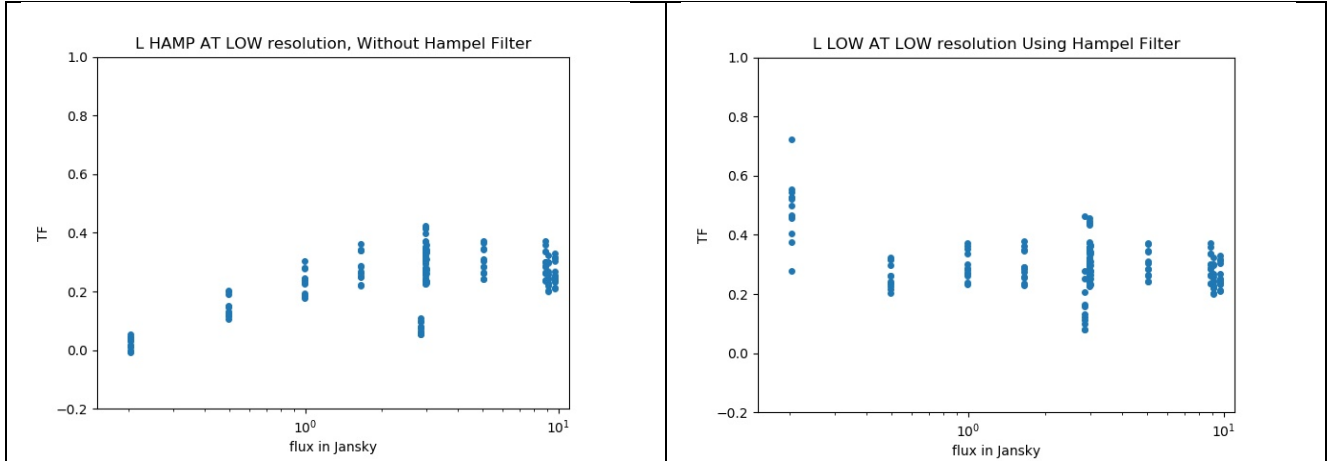


Figure 8.2: TF (broad band visibility corrected from the calibrator diameter) as a function of the calibrator flux in Jy, without (left) and with (right) the application of an Hampel filter on the photometry. Each point stands for an exposure. Without the Hampel filter, we had a visibility drop that was explained by the equivalent of a photometric broad band noise of the order of 0.5 Jy. With the use of the Hampel filter this effect disappears.

8.3 MODULATION/DEMODULATION

The modulation has been shown to improve substantially the N band instrument response in laboratory before the PAE. Now, we find that the gain provided seems marginal on the closure phase (except maybe for very high accuracy measures that are beyond the scope of a general commissioning report) and make the absolute visibility more sensitive to seeing (if we integrate coherently over a demodulated modulation cycle). The gain on the coherent flux reliability still has to be evaluated.

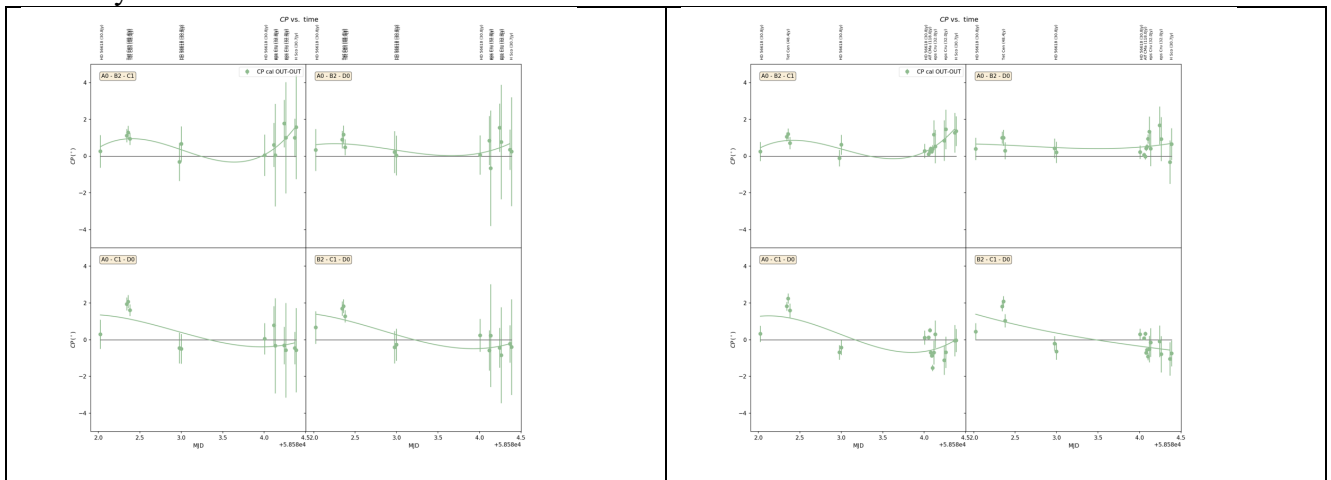


Figure 8.3: Impact of the N band modulation on the closure phase. Left CP transfer function [CP(MJD)] obtained with “opdmod=false”, i.e. frame by frame without impact of the demodulation. Right, same transfer function obtained with “opdmod=true” i.e. computed with a coherent integration on each modulation cycle after demodulation. We see that “opdmod=true” improves the error bars of individual exposures but does not have a measurable effect on the broad band CP calibration.

8.4 BCD CALIBRATION OF CLOSURE PHASE

In the first commissioning memo (RD3) we showed that the BCD improves the closure phase as a function of wavelength in the L band. Figure 8.4a shows another example from 2019 April data with 4-step BCD cycle. The “science” and “calibration” targets are IRAS10153-5540 (L=73 Jy) and VV396Cen (L=81 Jy). A From the figure, we see that a calibration with the calibrator alone (blue, red, orange and green lines) yields wavelength dependent errors of up to 3° . A calibration with the BCD alone (purple line) reduces the errors by a factor of 3. Then a calibration combining both the BCD and a calibrator (brown line) yields even slightly better results.

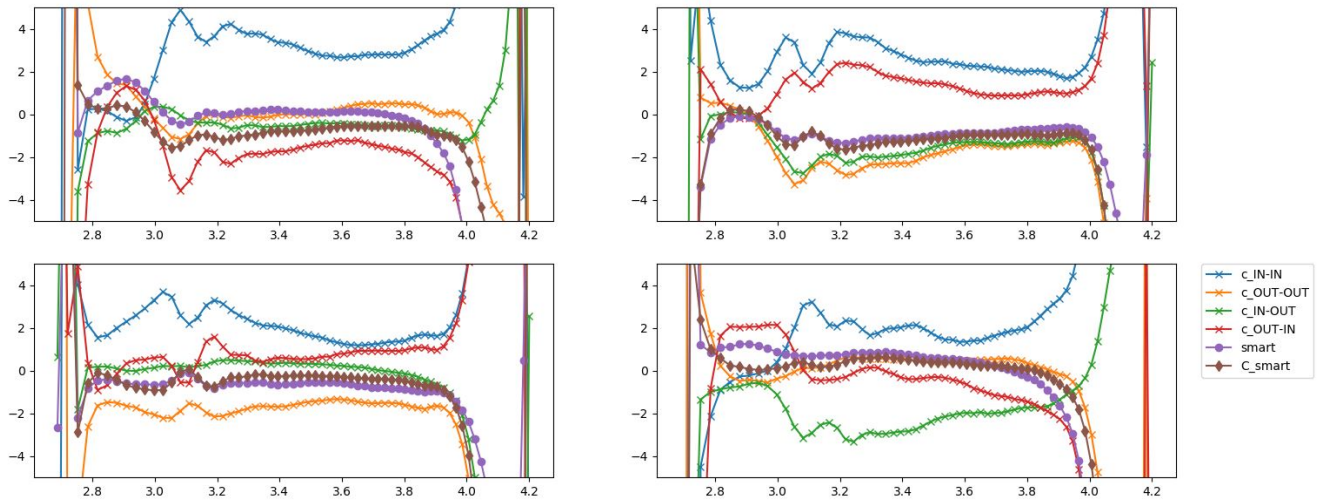


Figure 8.4a. Calibration of the closure phase in the L band with one calibrator for the four BCD positions (c_{IN-IN} , $c_{OUT-OUT}$, c_{IN-OUT} , c_{OUT-IN}). with the BCD alone (purple line; smart) and with both the BCD and calibrator (brown; C_{smart})

Here we analyze the contribution of the BCD to the stability of the broad band closure phase, in L, M and N.

In L, the BCD improves the broad band closure phase calibration and could reduce the frequency of calibrators observation to a few per night, but it does not substantially decrease the dispersion of measurements.

In N the BCD calibration strongly reduces the broad band calibration error, by a factor 2 to 3, and allows to reach in good seeing the 0.3° broad band calibration error presented in section 2.3.

In M, we have a combination of the two situations: an improvement of the global calibration and a reduction of the dispersion.

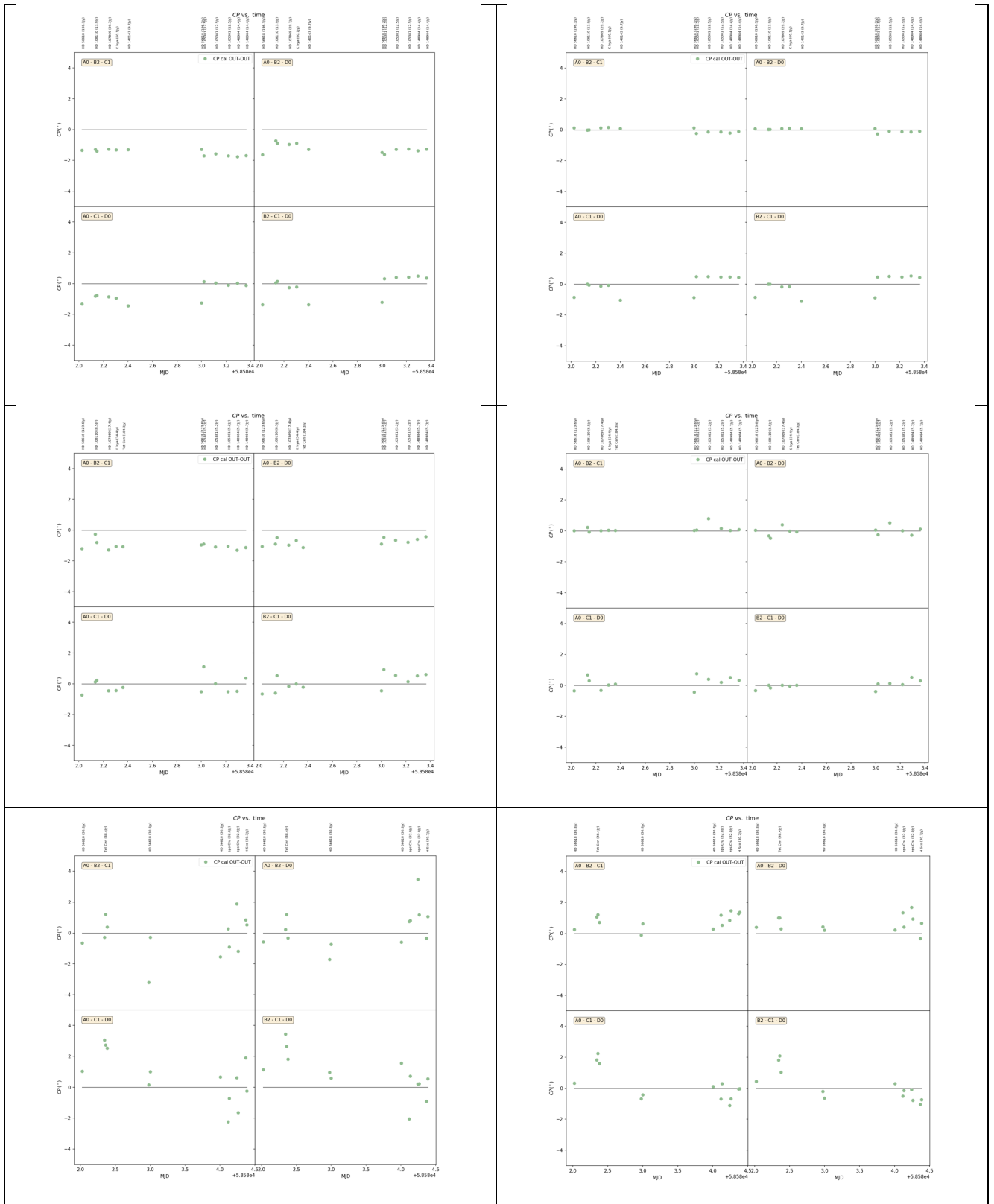
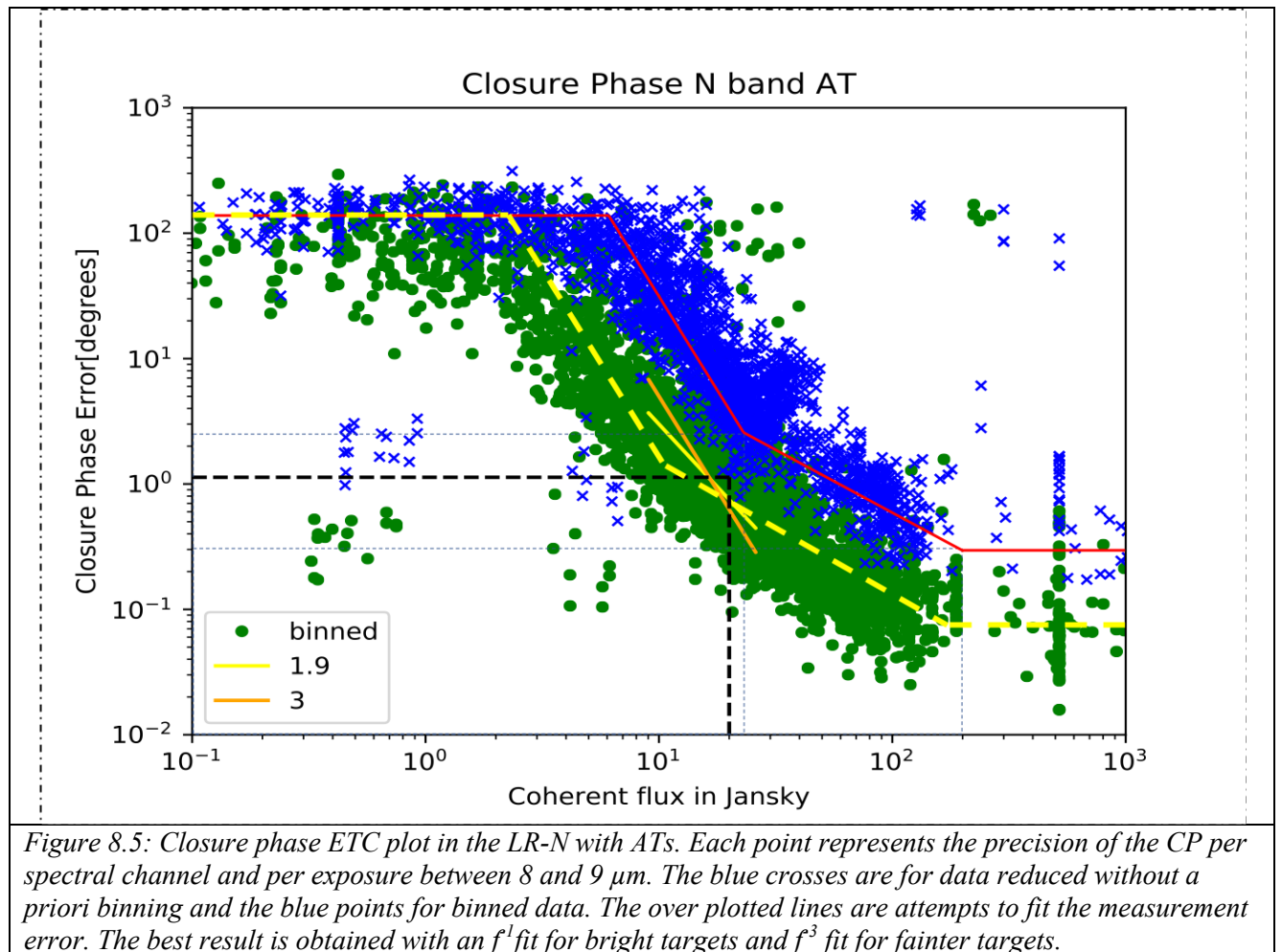


Figure 8.4b. Closure phase as a function of time without BCD calibration (left) and with BCD calibration (right), in L (top), M (middle) and N (bottom)

8.5 SPECTRAL BINNING

The binning of spectral columns in spectral channels “a priori”, i.e. before Fourier processing but after demodulation has a strong impact on the precision of all measurements and above all on the closure phase fundamental noise. It is substantially more efficient than the binning “a posteriori” of the measurements obtained in each spectral column. It has been systematically used for all results showed in this commissioning report.

However, note that currently the spectral binning is done without correcting the change of fringe spacing with wavelength. Even within a spectral channel this has a substantial impact on the instrument visibility, that increases with the fringe peak number. This does not erase the SNR gain due to binning, but it could be improved in a new DRS version.



8.6 HR-N BINNED TO LR-N

We have shown [RD10] that the HR-N grism is less efficient than the LR-N one below $\sim 10 \mu\text{m}$ and more efficient above. Hence, we would expect that the measurement precision from HR-N spectral columns binned in LR-N spectral channels is slightly better than in direct LR-N spectral channels, because, in the N band we are dominated by background photon noise.

However, the HR-N frames require longer DITs (75 ms instead of 20 ms) and imply longer modulation cycles (~ 500 ms instead of ~ 250 ms). This yields a seeing dependant loss in instrument + atmosphere visibility and hence in coherent flux. The much larger data volume also makes the off line processing of the data shortly after observations almost impossible. We have also been discussing the possibility to have a lower “ELFIN²³” noise on the Aquarius detector with lower illumination on each individual pixel, which would bring an advantage to the HR-N binned LR-N processing.

The figures below show a systematic comparison of these two options. We see that the performances are comparable, although with a clear advantage for direct LR-N measures but for Closure phase above $10 \mu\text{m}$ in the frame-by-frame processing.

Conclusion:

- If HR-N is required by the science goals, observing the same source in LR-N is not necessary.
- If only LR-N is needed, then the observation should be made in LR-N only.

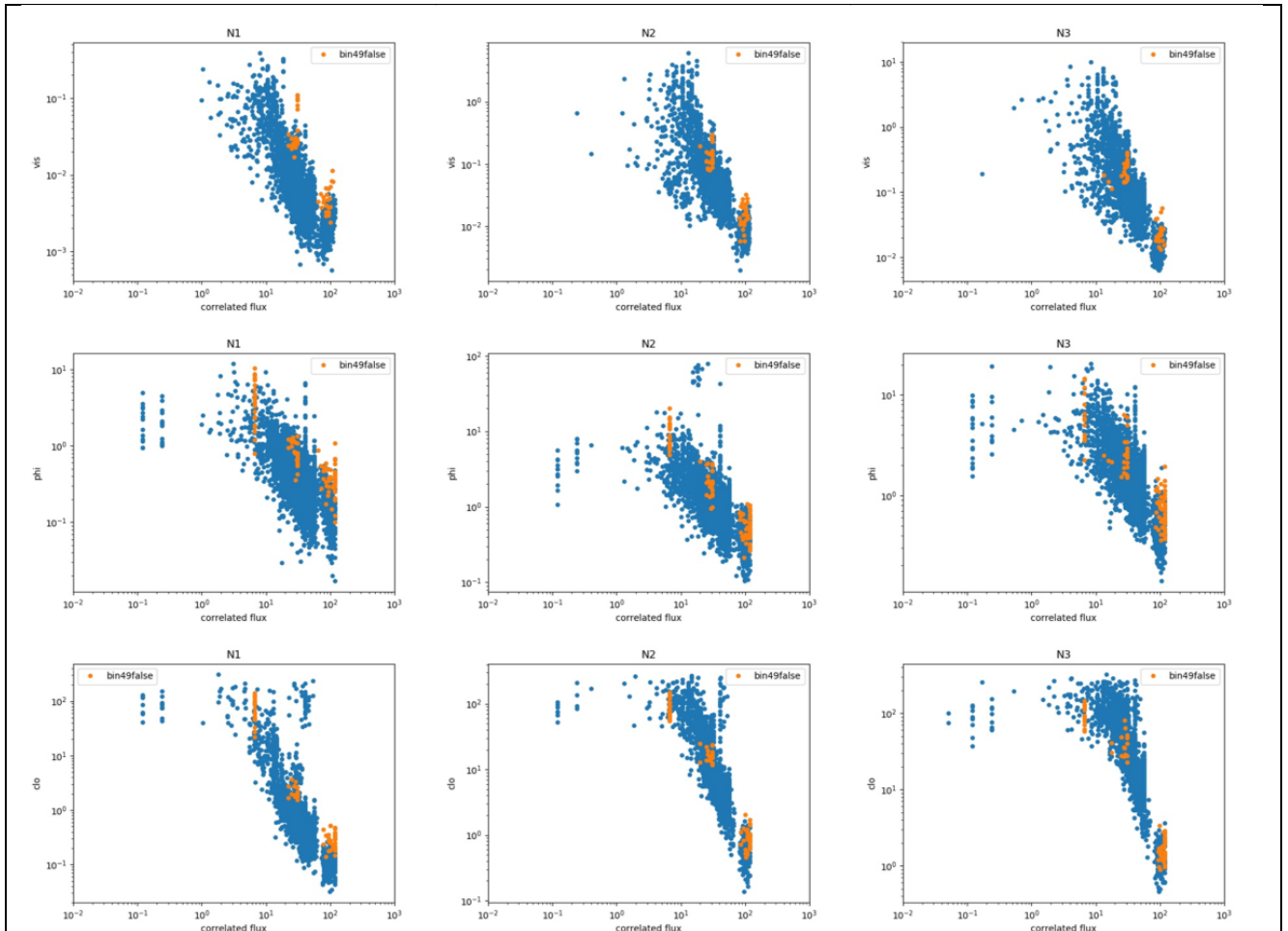


Figure 8.6a: Comparing the precision of LR-N measurements (blue dots) with HR-N ones binned down to LR-N resolution (orange dots). The plots show the measured precision per LR-N spectral channel en per exposure as a function of the coherent flux. The top line is for visibility, the middle one for differential phase and the bottom one for closure phase. From left to right are measures around $8.5 \mu\text{m}$ (N1), $11 \mu\text{m}$ (N2) and



12 μm (N3). The data has been reduced frame by frame, with the “*opdmod=false*” options. We see that the performances are comparable, although with a clear advantage for direct LR-N measures but for Closure phase above 10 μm . Note that there is a possible selection bias, as the HR-N observations are much less numerous and cover a smaller range of observing conditions, although they have mostly been obtained in fair or good conditions.

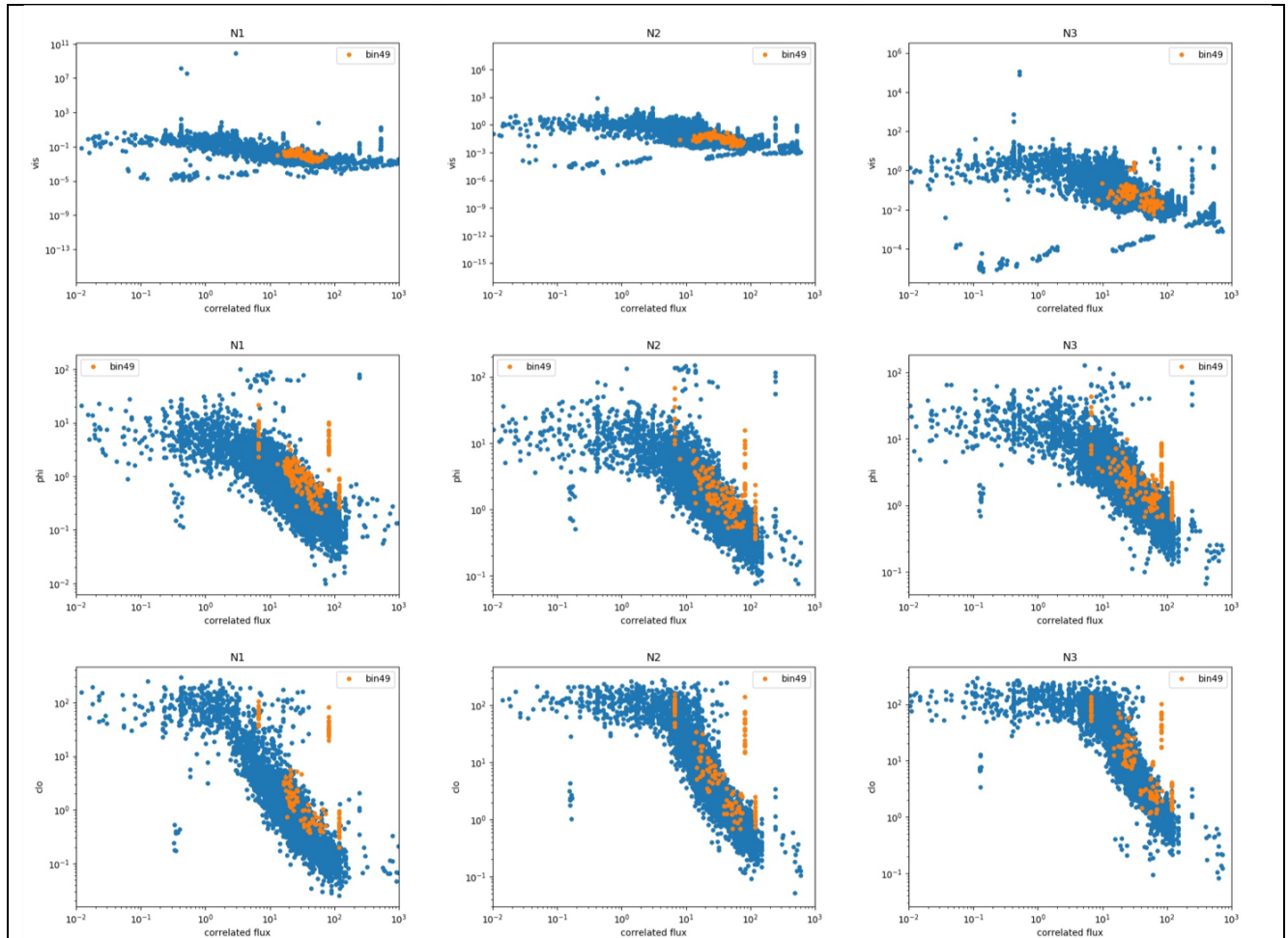


Figure 8.6b: Same as figure 8.6a with a processing by modulation cycle (*opdmod=true*).



9 ANNEX: FUNDAMENTAL NOISE ESTIMATION

9.1 EXPECTED FUNDAMENTAL NOISE FROM THE EXPOSURE TIME

CALCULATOR

The expected MATISSE measurement precisions were computed from the MATISSE ETC reference tool, which is at the basis of the ESO MATISSE ETC. This reference tool computes the error and corresponding SNR on the squared visibility, the visibility, the differential phase, and the closure phase. So far, the errors only include the contribution from the fundamental noises (source photon noise, readout noise, thermal background photon noise), in agreement with the MATISSE ETC specifications (RD9: VLT-SPE-MAT-15860-9304) that describes the ESO ETC tool and details the underlying error and SNR expressions. In the current report, this ETC tool has been used to check and fit the fundamental noise errors on the measurements as described in chapter 2.2. Below, we summarize the key error and SNR expressions, and refer to RD9 for demonstrations.

The present commissioning report, that characterizes the broad band calibration errors that have to be combined with the fundamental noise errors provides the necessary inputs for an updated, full exposure time calculator that integrates all error causes.

9.1.1 Visibility observable

- **Squared coherent flux:**

Per frame, the SNR of the squared coherent flux estimation is:

$$\text{SNR}_{C^2} = \frac{n_T^2 V^2 V_{\text{inst}}^2}{\sigma_{C^2}} [5],$$

where σ_{C^2} is the standard deviation on the squared coherent flux. Following e.g. Tatulli et al. (2004), the variance of the squared coherent flux can be written as :

$$\begin{aligned} \sigma_{C^2}^2 = & (n^I V V_{\text{inst}})^2 [2n_T (n_b^I + n^I) + 2n_p' \text{RON}^2 + 4] \\ & + n_T^2 (n_b^I + n^I)^2 + n_T (n_b^I + n^I) (1 + 2n_p' \text{RON}^2) \\ & + (3 + n_p') n_p' \text{RON}^4 \end{aligned}$$

where n_T is the number of telescopes, n_p' is the number of pixels used to analyze the signal in the interferometric channel (for a given spectral channel), RON is the read-out-noise of the detector, V is the object visibility and V_{inst} is the instrumental visibility. In the case of a total observation time on the fringes t_{obs} (excluding observational overheads), the SNR is:

$$\text{SNR}_{C^2,t} = \text{SNR}_{C^2} \sqrt{\frac{R_{\text{chop}} t_{\text{obs}}}{\Delta t}} [6],$$

where Δt is the frame time for one coherent flux estimation, and R_{chop} is the chopping ratio (R_{chop} can be 1).

- **Photometry**

Per frame, the SNR of the estimation of the photometry is:

$$\text{SNR}_n = \frac{n^p}{\sqrt{2n_b^p + n^p + 2n_p'' \text{RON}^2}} [7],$$

where n_p'' is the number of pixels used to analyze the signal in the photometric channels (for a given spectral channel) in *Si_Photo* mode. In *High_Sens* mode, n_p'' must be replaced by n_p' since the optional photometry of each beam is measured, after the interferometric fringes, on the interferometric channel.



In the case of a total observation time on one beam photometry $t_{obs,p}$, the SNR is:

$$SNR_{n,t} = SNR_n \sqrt{\frac{R_{chop} t_{obs,p}}{\Delta t}} \quad [8],$$

where Δt is the frame time for one photometry estimation.

● **Squared visibility:**

The estimator of the squared visibility is:

$$V^2 = \frac{C^2}{n_i n_j},$$

where V^2 is the visibility, C^2 is the coherent flux and n_i and n_j are the photometries of the two corresponding beams. Assuming $n_i = n_j$, the relative error on the squared visibility can be written as :

$$\frac{\sigma_{V^2}}{V^4} = \frac{\sigma_{C^2}}{C^2} + 2 \frac{\sigma_n}{n^2}$$

So the SNR of the squared visibility estimation, containing only the contribution from fundamental noises, is:

$$SNR_{V,t} = \frac{1}{\sqrt{\frac{1}{SNR_{C,t}^2} + \frac{2}{SNR_{n,t}^2}}} \quad [9]$$

The error on $V = \sqrt{V^2}$ is given by : $\sigma_V = \frac{\sigma_{V^2}}{2V}$

9.1.2 Phase observables

● **Coherent flux**

Per frame, the SNR of the coherent flux estimation is:

$$SNR_C = \frac{n^l V V_{inst}}{\sqrt{n_T n_b^l + n_T n^l + n_p^l RON^2}},$$

where n_T is the number of telescopes, n_p^l is the number of pixels used to analyze the signal in the interferometric channel, RON is the read-out-noise of the detector. V is the object visibility and V_{inst} is the instrumental visibility. In the case of a total observation time on the fringes t_{obs} (excluding observational overheads) the SNR is:

$$SNR_{C,t} = SNR_C \sqrt{\frac{R_{chop} t_{obs}}{\Delta t}},$$

where Δt is the frame time, and R_{chop} is the chopping ratio (R_{chop} can be 1).

● **Differential phase**

The fundamental error on the differential phase in the case of an observation time t_{obs} can be approximated by:

$$\sigma_\phi \approx \sqrt{\left(\frac{\Delta t}{2R_{chop} t_{obs}}\right) \left(\frac{1}{SNR_C^2}\right)} = \frac{1}{\sqrt{2} SNR_{C,t}}$$

This approximation is only for small to moderate phase errors (< 1 rad).

● **Closure phase**

The fundamental error on the closure phase in the case of an integration time t_{obs} is:

$$\sigma_\psi \approx \sqrt{\left(\frac{\Delta t}{2R_{chop} t_{obs}}\right) \left(\frac{3}{SNR_C^2}\right)} = \frac{\sqrt{3}}{\sqrt{2} SNR_{C,t}}$$



Commissioning Report

where the coherent flux provided by the 3 fringe signals involved in the closure phase, is assumed to be the same. This is an approximation valid only when the phase error per spectral channel and per coherent integration time is smaller than ~ 1 rad.

9.1.3 Parameters and assumptions

The assumptions and parameters values used for all the ETC calculations shown in this document are :

- The Strehl ratio and the instrumental visibility are assumed constant over a spectral band. The instrumental visibility values correspond to the instrumental visibilities measured in lab during the test phase (ref to instrument performance report), while the Strehl ratios are assumed to be 0.7 in L-band, 0.8 in M-band, and 0.9 in N-band (ref to performance analysis report)
- The nominal VLTI+MATISSE transmission was also assumed constant over the spectral band, and was taken from the performance analysis report (ref to performance analysis report). The relative transmissions between the different spectral resolutions were updated on the basis of the last commissioning results. 2 'extreme' transmissions (nominal transmission multiplied by 2 and divided by 2) were also considered to include a possible discrepancy between the nominal transmission and the true one.
- The atmospheric transmission profiles in LM and N bands were computed, for the various spectral resolutions, using the Skycalc tool and assuming median humidity conditions at Paranal.
- The error and SNR values were computed per spectral channel, which covers 5 pixels in LM band and 7 pixels in N band, at a given reference wavelength: 3.5 μm for the L-band, 4.75 μm for the M-band, and 8.5 μm for the N-band.
- The error and SNR values were computed for a 1 mn exposure. The DIT values considered for a single frame followed the actual ones, namely:
 - DIT=111ms in LM band for the low and medium resolutions
 - DIT=111ms in L band for the high resolution
 - DIT=20ms in N band for the low resolution
 - DIT=75ms in N band for the high resolution

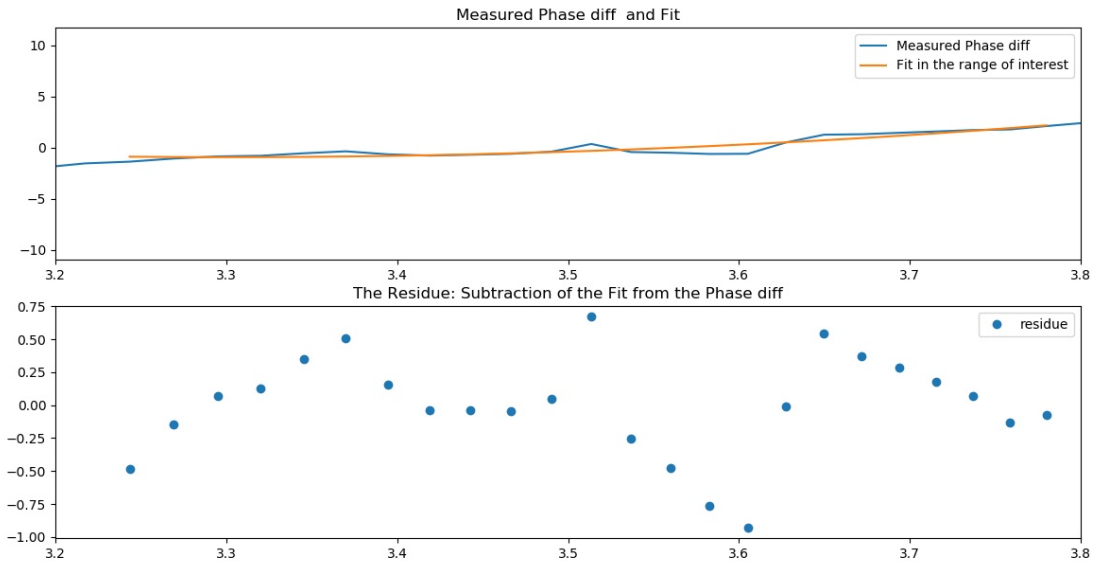
9.2 MEASURED FUNDAMENTAL NOISE

The figures below illustrate the method used to estimate the contribution of fundamental noise to the measurement error. The measurements (in blue) are fitted by a 2nd degree polynomial function (in orange) and the standard deviation of the residual (blue points) is used as an estimator of the fundamental noise.

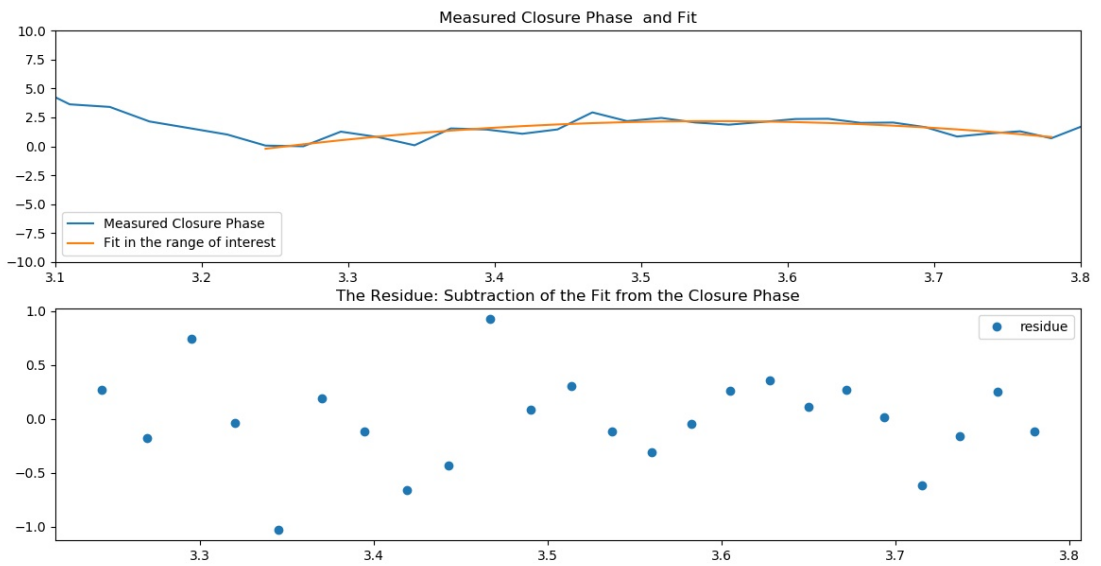
In practice we use the Median Absolute Deviation (MAD) to eliminate outliers, and scale it to a standard deviation, assuming gaussian noise distribution. The validity of this estimate has been checked in a substantial number of examples and is in good general agreement with ETC predictions (the ETC computes Standard deviations).



L band AT, rms of the phase diff



L band AT, rms of the Closure Phase



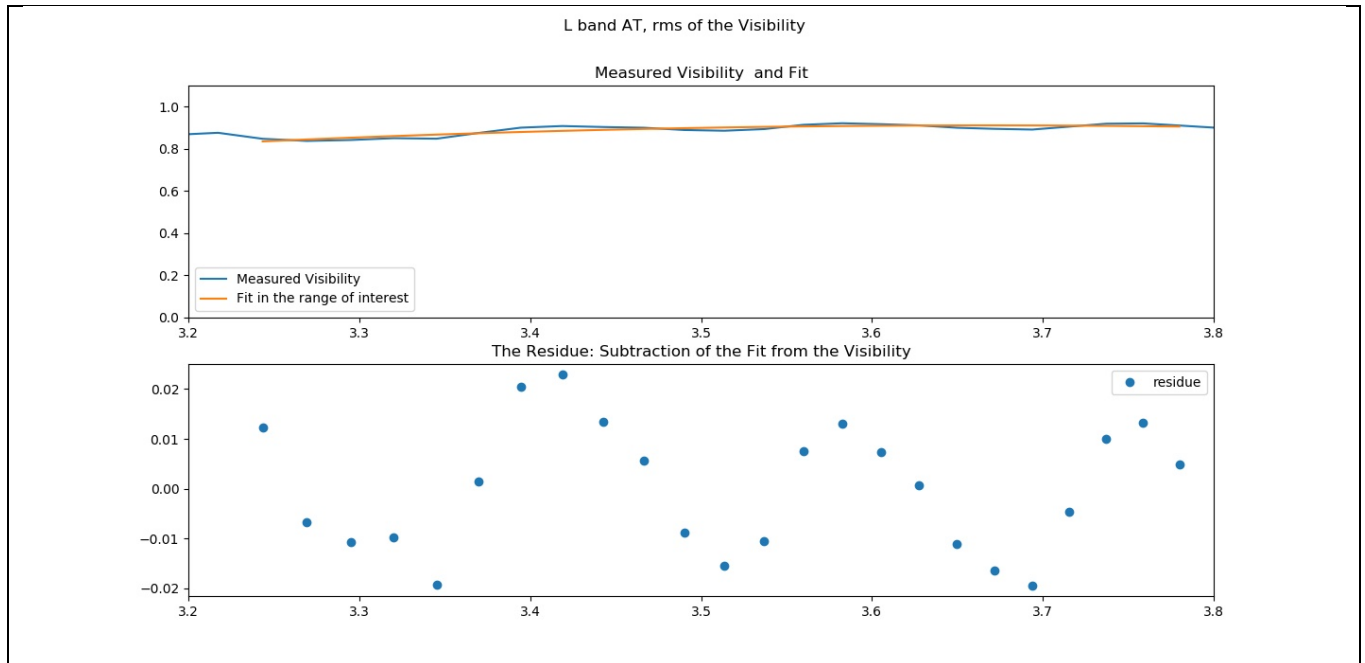


Figure 9.2. Measured (blue), Fitted (orange) and residual=Measured-Fit (dots) values for the differential phase (top), the closure phase (middle) and the visibility (bottom) in the L band in Low Resolution, on a 1 Jy calibrator (HD148441). The rms of the residual function is used as an estimate of the measurement error. Note that the data in that example is processed with a sliding binning of 5 spectral columns before processing. Hence only points separated by 5 intervals are statistically independent.

10 ANNEX: EXAMPLES OF MEASURES NEAR THE LIMITS

Here we show some outputs of the python routine “mat_showOiData.py” that is part of the MATISSE python package.

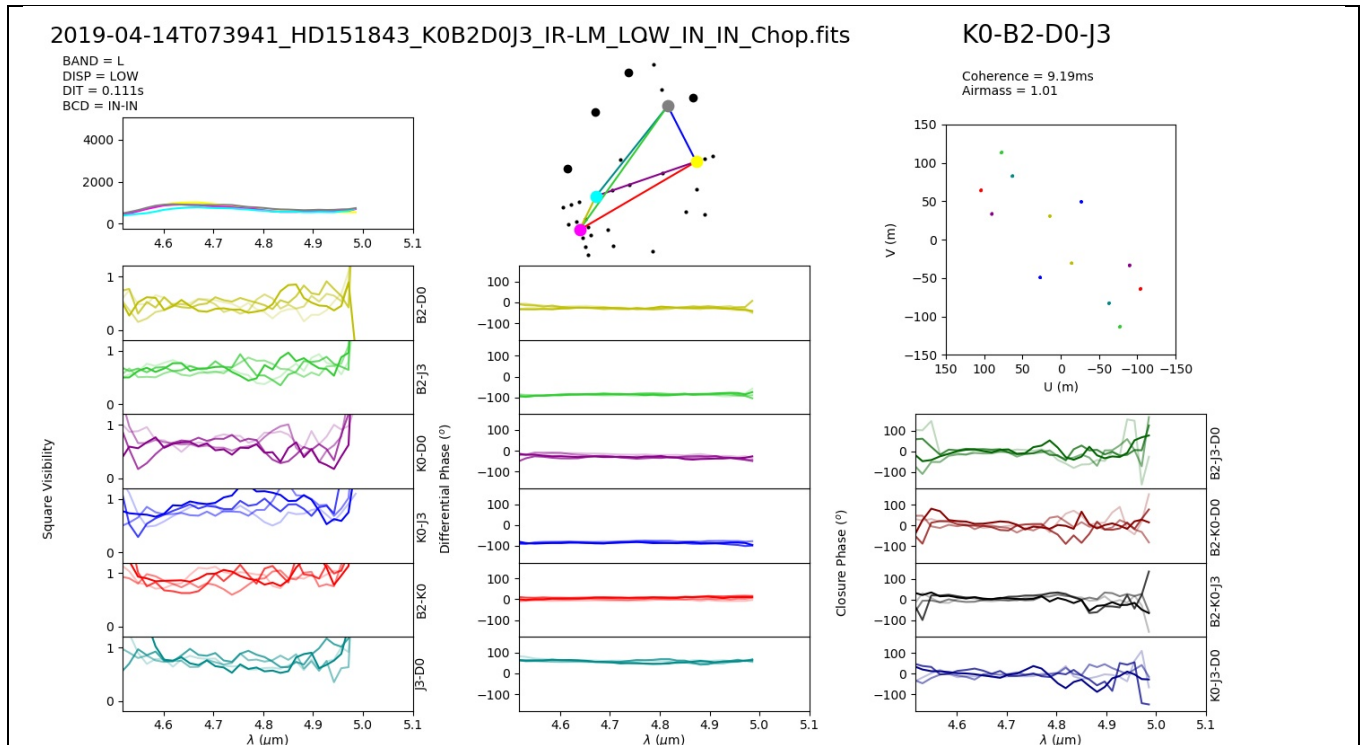
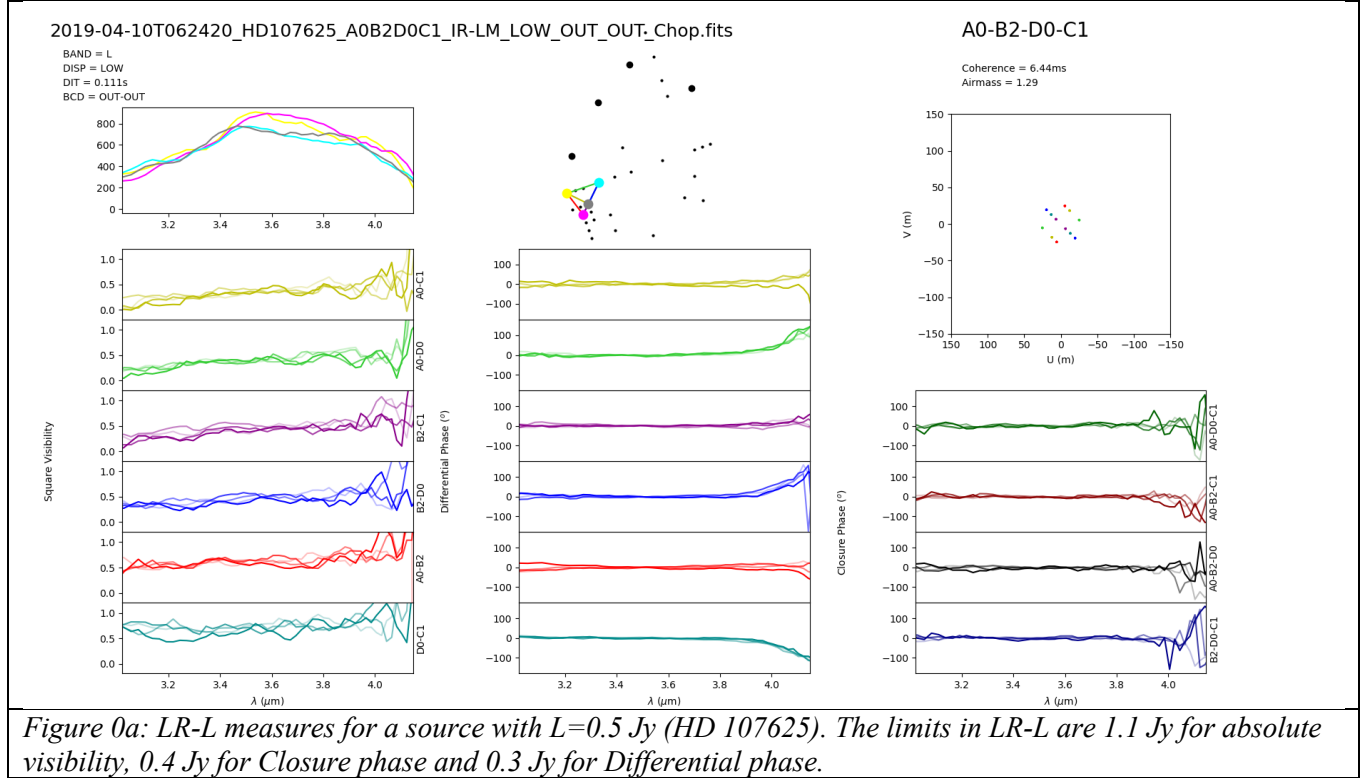


Figure 0b: LR-M measures for a source with $M=1.8$ Jy (HD 151843). The limits in LR-M are 2.1 Jy for absolute visibility, 1.9 Jy for Closure phase and 1.1 Jy for Differential phase.

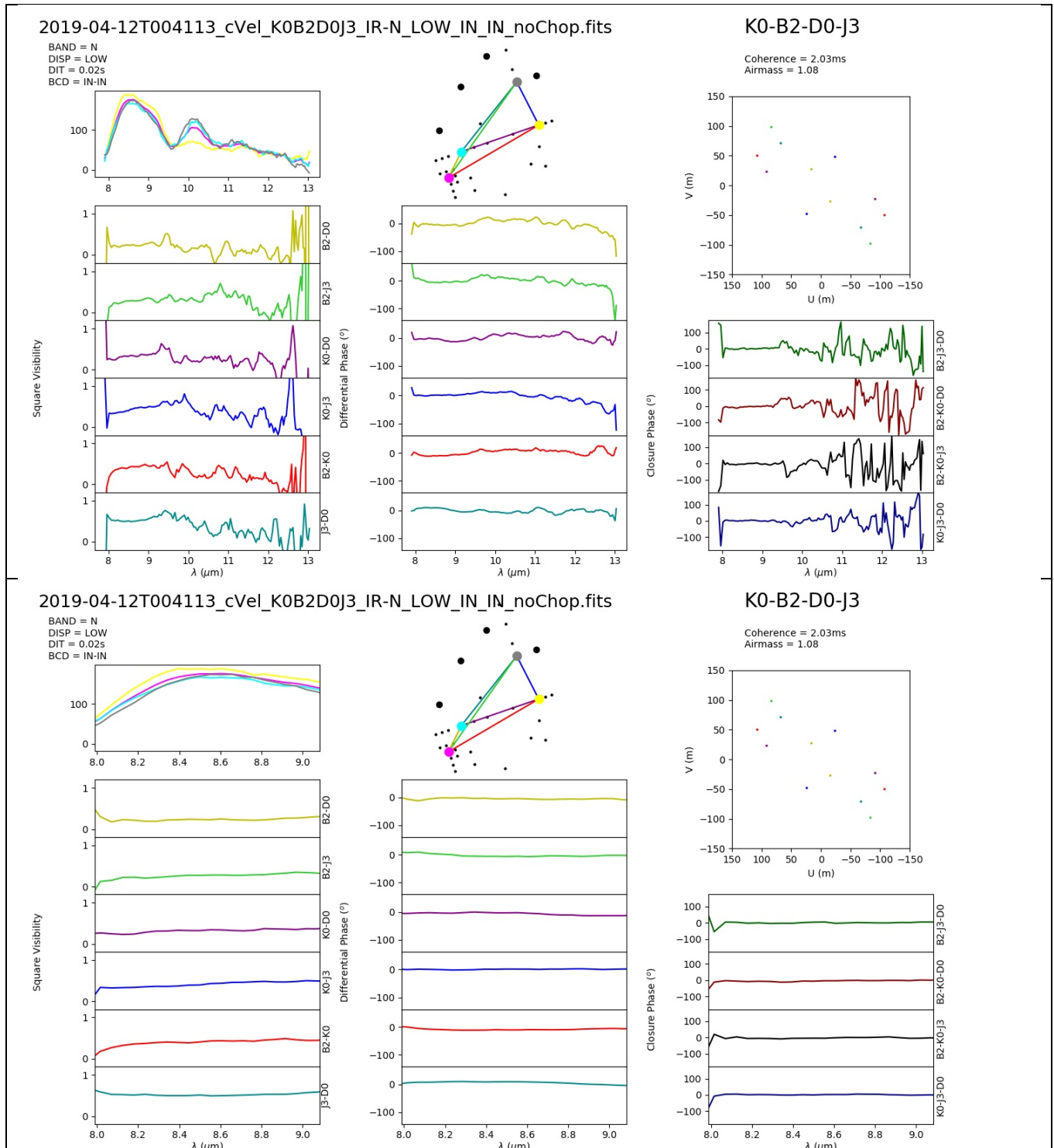
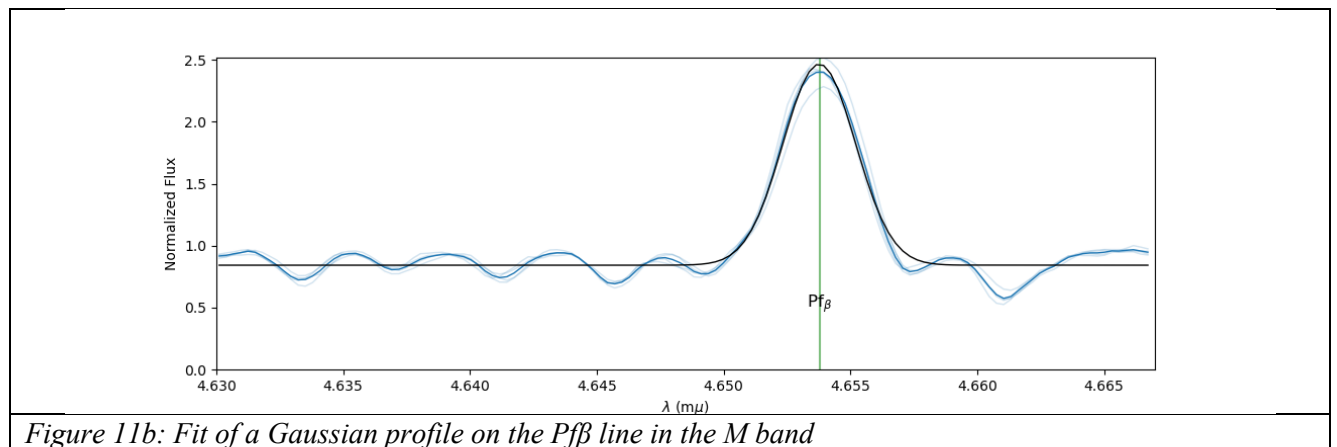
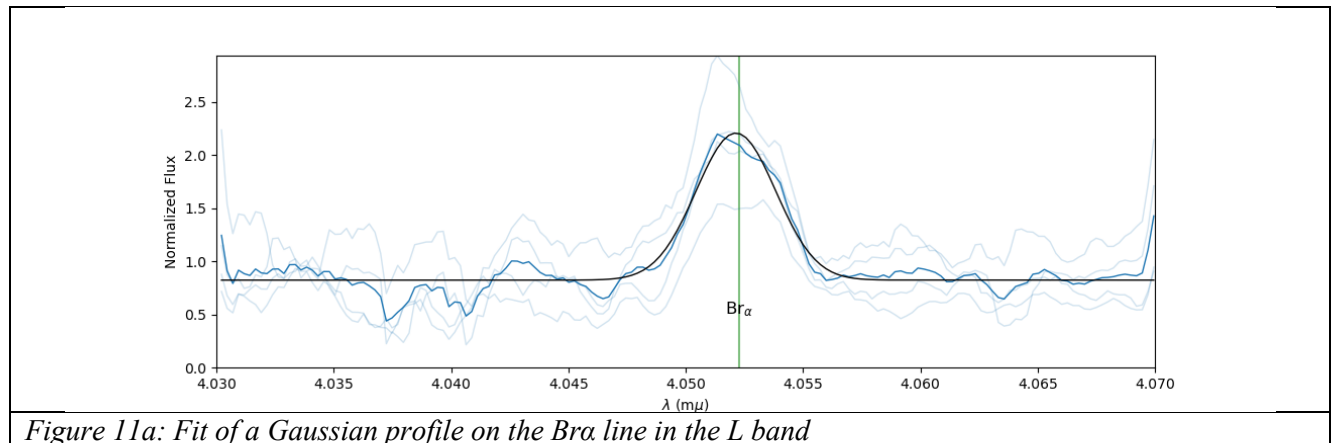


Figure 0c: LR-N measures for a source with $N=15.4$ Jy (c Vel), for the full N band (top) and for the 8-9 μm window (bottom). The limits in LR-N, at 8.5 μm , are 16.8 Jy for absolute visibility, 9.4 Jy for Closure phase and 6 Jy for Differential phase.

11 ANNEX: VHR CALIBRATION IN L AND M BAND

To verify the spectral calibration recipe for the HIGH+ mode in both the L and M bands, we observed two classical Be stars from the list we have given SciOps: β CMi (in the L band) and δ Cen (in the M band).

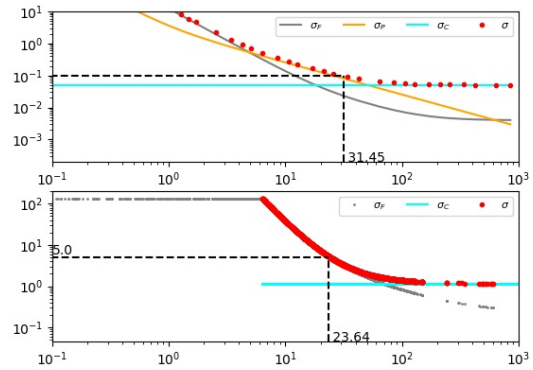
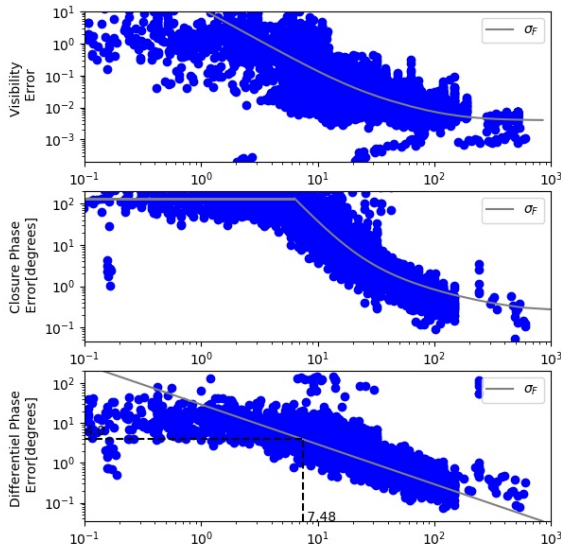
To measure the shift in wavelength we used the $Br\alpha$ line (40522.6Å) and $Pf\beta$ (46537.7 Å). We performed fit of Gaussian profiles on the normalized flux for each of the photometric beam. We found a shifted of $0.9\pm 2.3\text{\AA}$ in L (Figure 11a) and $0.0\pm 1.1\text{\AA}$ in M (Figure 11b). The shifts are smaller than the uncertainties and they are of the order of a tenth of the spectral channel (about 12-15 Å).



12 ANNEX: N2 AND N3 PERFORMANCE ESTIMATES

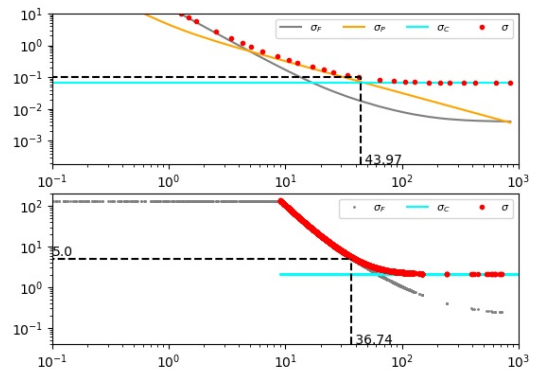
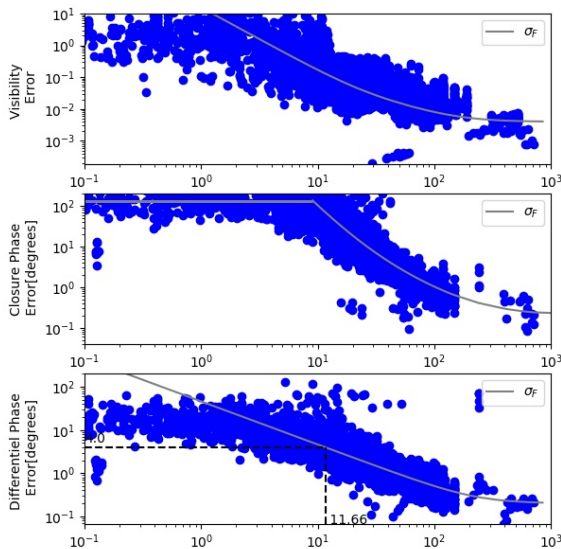
12.1 LOW RESOLUTION

LOW N2 AT



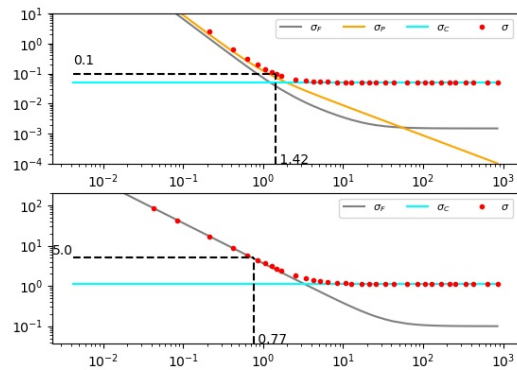
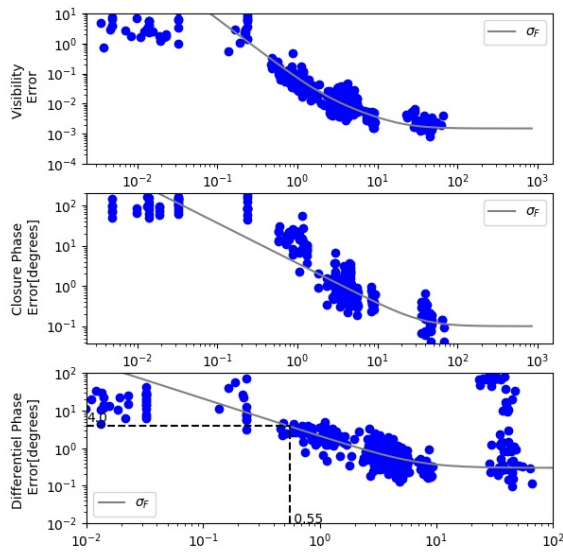
From top to bottom: the visibility, the closure phase and the differential phase errors as a function of flux in Jy. The plots on the left are those of the fundamental noise. The plots on the right are those of the global error, in red, and its components: -the fundamental noise in grey -the error due to the seeing variation, in cyan -the error related to a wrong background correction, when applicable, in orange

LOW N3 AT



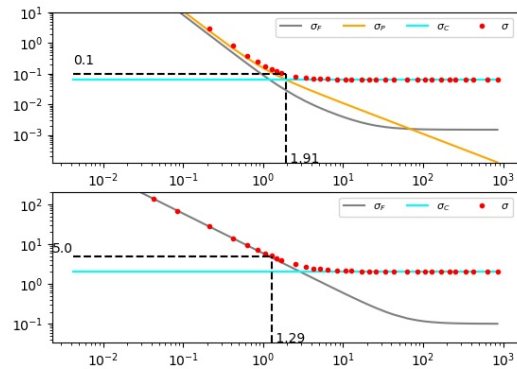
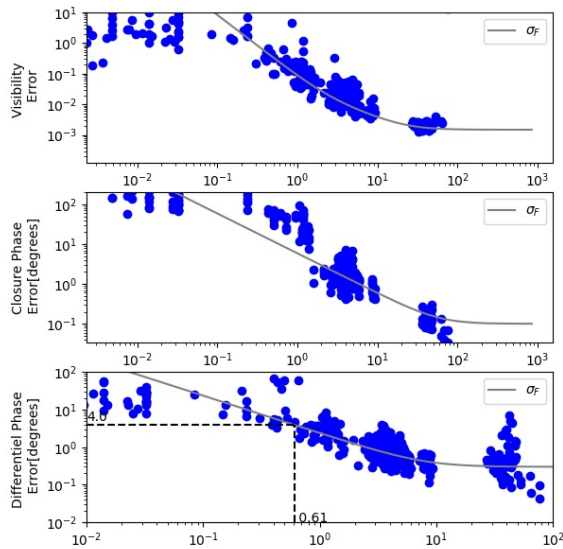
From top to bottom: the visibility, the closure phase and the differential phase errors as a function of flux in Jy. The plots on the left are those of the fundamental noise. The plots on the right are those of the global error, in red, and its components: -the fundamental noise in grey -the error due to the seeing variation, in cyan -the error related to a wrong background correction, when applicable, in orange

LOW N2 UT



From top to bottom: the visibility, the closure phase and the differential phase errors as a function of flux in Jy.
 The plots on the left are those of the fundamental noise. The plots on the right are those of the global error, in red, and its components:
 -the fundamental noise in grey
 -the error due to the seeing variation, in cyan
 -the error related to a wrong background correction, when applicable, in orange

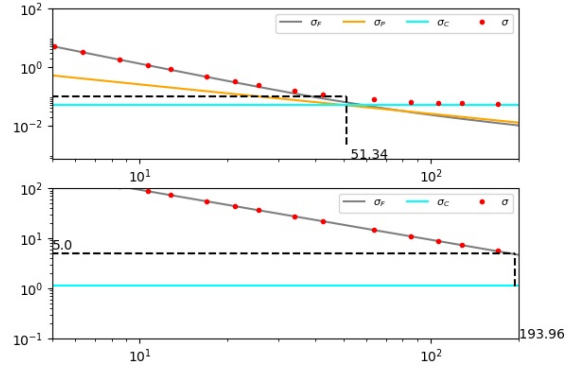
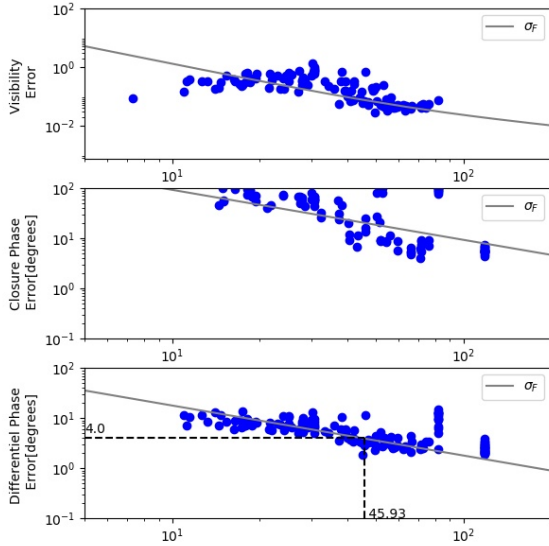
LOW N3 UT



From top to bottom: the visibility, the closure phase and the differential phase errors as a function of flux in Jy.
 The plots on the left are those of the fundamental noise. The plots on the right are those of the global error, in red, and its components:
 -the fundamental noise in grey
 -the error due to the seeing variation, in cyan
 -the error related to a wrong background correction, when applicable, in orange

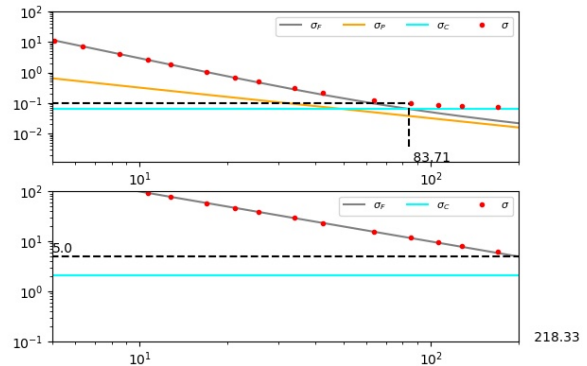
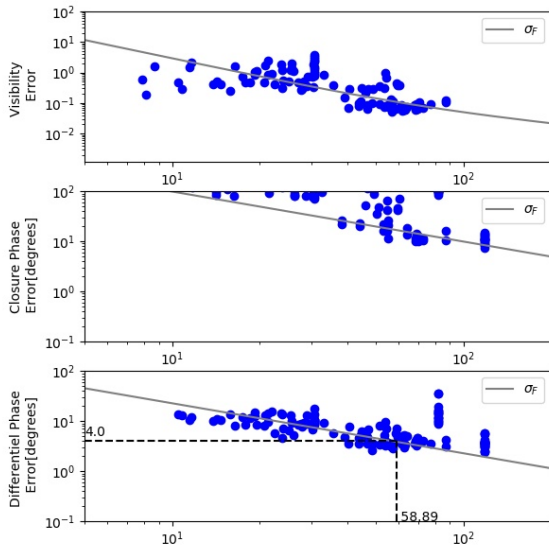
12.2 HIGH RESOLUTION

HIGH N2 AT



From top to bottom: the visibility, the closure phase and the differential phase errors as a function of flux in Jy.
 The plots on the left are those of the fundamental noise. The plots on the right are those of the global error, in red, and its components:
 -the fundamental noise in grey
 -the error due to the seeing variation, in cyan
 -the error related to a wrong background correction, when applicable, in orange

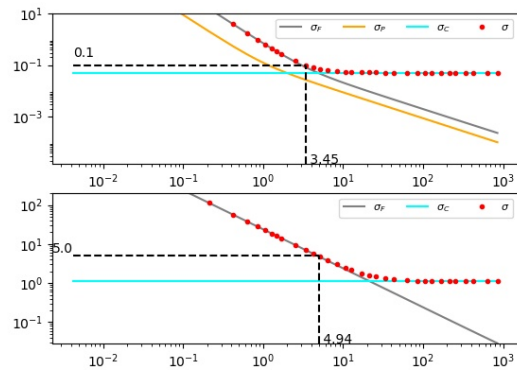
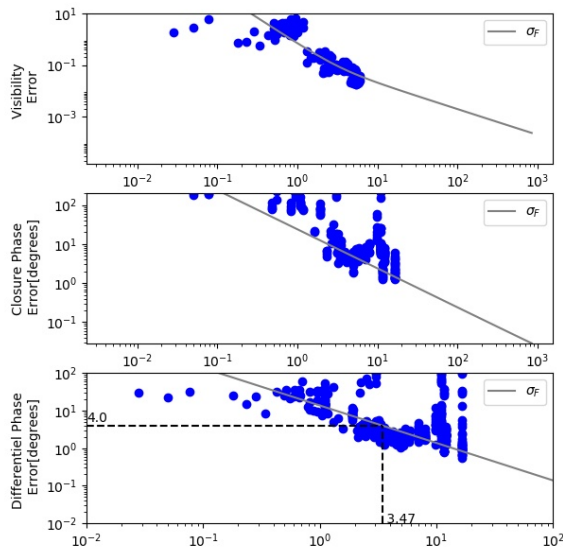
HIGH N3 AT



From top to bottom: the visibility, the closure phase and the differential phase errors as a function of flux in Jy.
 The plots on the left are those of the fundamental noise. The plots on the right are those of the global error, in red, and its components:
 -the fundamental noise in grey
 -the error due to the seeing variation, in cyan
 -the error related to a wrong background correction, when applicable, in orange

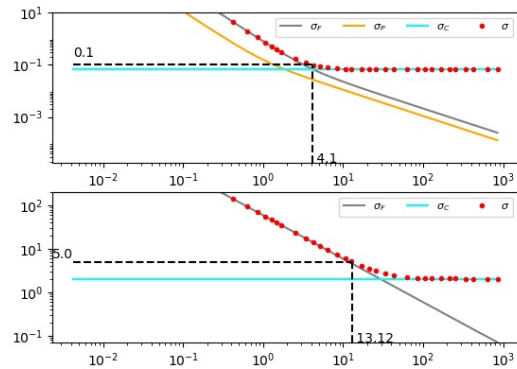
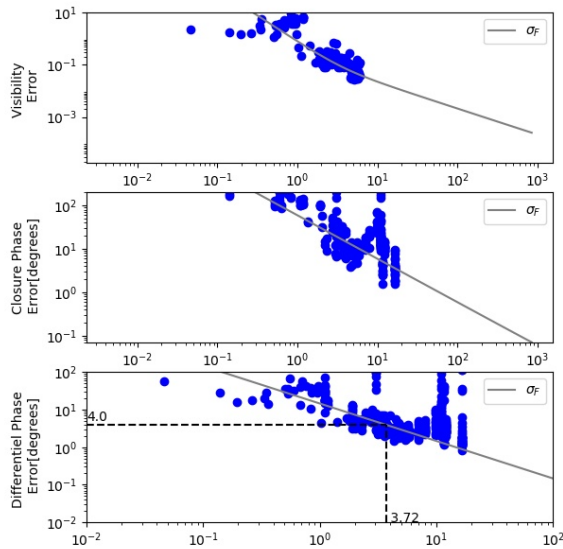


HIGH N2 UT



From top to bottom: the visibility, the closure phase and the differential phase errors as a function of flux in J_y .
 The plots on the left are those of the fundamental noise. The plots on the right are those of the global error, in red, and its components:
 -the fundamental noise in grey
 -the error due to the seeing variation, in cyan
 -the error related to a wrong background correction, when applicable, in orange

HIGH N3 UT



From top to bottom: the visibility, the closure phase and the differential phase errors as a function of flux in J_y .
 The plots on the left are those of the fundamental noise. The plots on the right are those of the global error, in red, and its components:
 -the fundamental noise in grey
 -the error due to the seeing variation, in cyan
 -the error related to a wrong background correction, when applicable, in orange

13 ANNEX: CHOPPING FREQUENCY

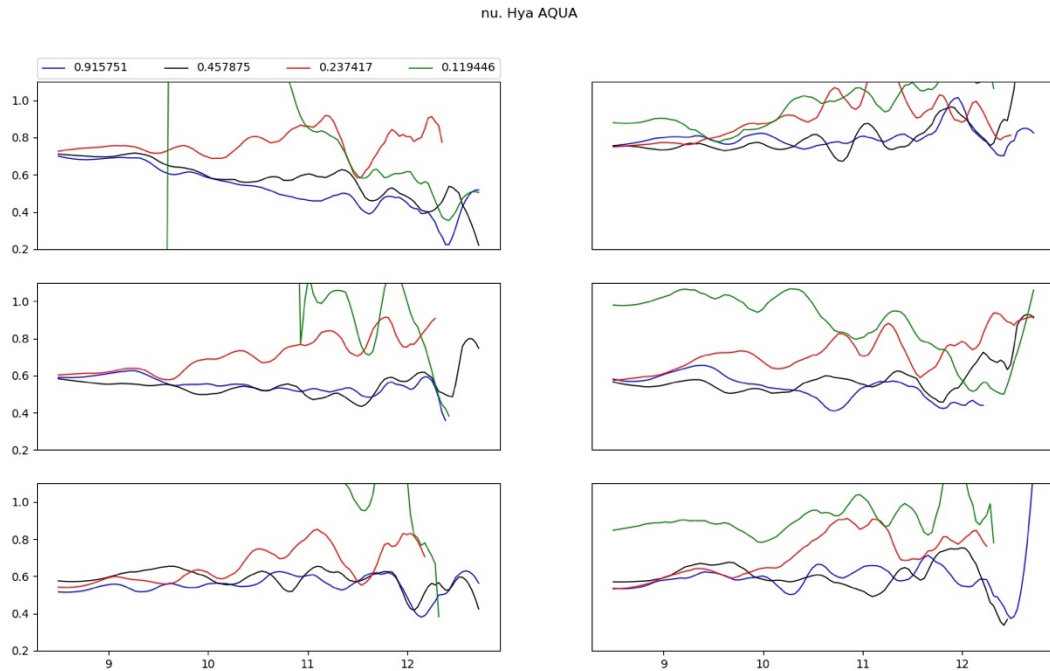


Figure 13.1: The six N band Aquarius visibilities obtained on nu Hya for 4 different chopping frequencies: 0.92 (blue), 0.46 (green), 0.24 (red) and 0.12 (green) Hz. These nu Hya data were obtained with ATs.

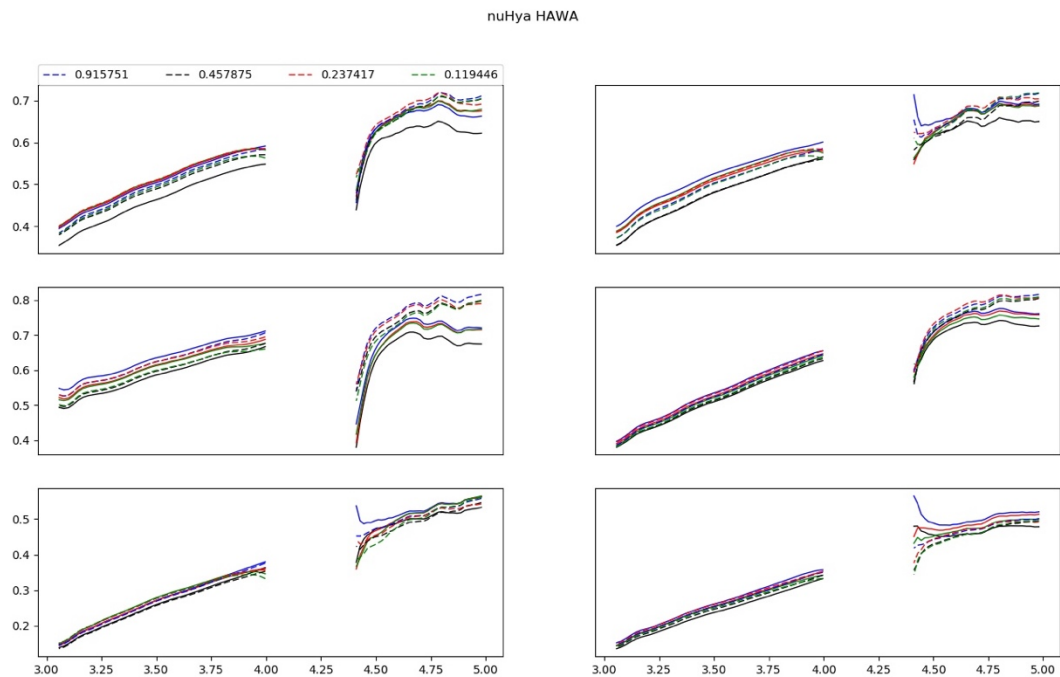


Figure 13.2: The six L&M band Hawaii2RG visibilities obtained on nu Hya for 4 different chopping frequencies, chopping data refer to the dashed lines: 0.92 (blue), 0.46 (green), 0.24 (red) and 0.12



Commissioning Report

(green) Hz. Non-chopped data are displayed for comparison and refer to the continuum line. These nu Hya data were obtained with ATs.

As illustrated in Figure 13.1 by the six visibilities obtained on nu Hya with ATs, a chopping frequency above 0.5 Hz allows for a stable transfer function ‘atmosphere + instrument’. The six N band Aquarius visibilities were obtained on nu Hya for 4 different chopping frequencies: 0.92 (blue), 0.46 (green), 0.24 (red) and 0.12 (green) Hz. The blue and green visibilities corresponding to ~1 Hz and ~0.5 Hz chopping frequencies provide consistent values. Chopping frequencies < 0.5 Hz display randomly affected transfer functions meaning that these low chopping frequencies are not fast enough.

A side note is that we know that on UTs, with the current MACAO AO and chopping equipment, a chopping frequency of 1 Hz is often problematic with UTs, **we therefore recommend that the chopping frequency for MATISSE standalone is set to 0.5 Hz by default both on ATs and on UTs.**

In L and M bands, as displayed on Figure 13.2, all chopping frequency seem to provide correct results (see the dashed line : 0.92 (blue), 0.46 (green), 0.24 (red) and 0.12 (green) Hz). The chopping is necessary in M band to provide stable results compared to the non-chopped observation (continuous lines of Figure 13.2).

To further project us on the perspective of the use of GRA4MAT:

- The chopping capability of MATISSE operating with GRA4MAT has been demonstrated with ATs (not shown in this report),

The chopping capability of MATISSE with GRA4MAT has not been yet demonstrated with UTs. It is possible that for observations at spectral resolutions higher than LR in LM: higher spectral resolution with GRA4MAT without chopping will be performed coupled with chopping observations in LR LM with MATISSE standalone.

The specific conclusion that can be drawn for the use of MATISSE standalone is:

- **in N: chopping ≥ 0.5 Hz is required**
- **in L&M: chopping as low as 0.1 Hz is sufficient**

14 ANNEX: BCD INFLUENCE ON VISIBILITY

Depending on the BCD configuration, four input baselines are switched to different fringe peaks, ie output baselines. Each fringe peak is associated with a given instrumental visibility. Thus, except of fringe peaks 1 and 2, a BCD configuration cannot be directly used to calibrate another one. The standard calibration procedure corrects the BCD configuration one by one by applying the calibrator on the science then averages the input baselines that have been measured on different output baselines in the different BCD configurations. When it is necessary to use faint calibrators it is much more efficient to combine the different BCD configurations on the science and on the calibrator before performing the Sci/Cal operation. In the broadband case, such an instrumental visibility change can be described by one fixed and stable number as shown in Fig.14.1

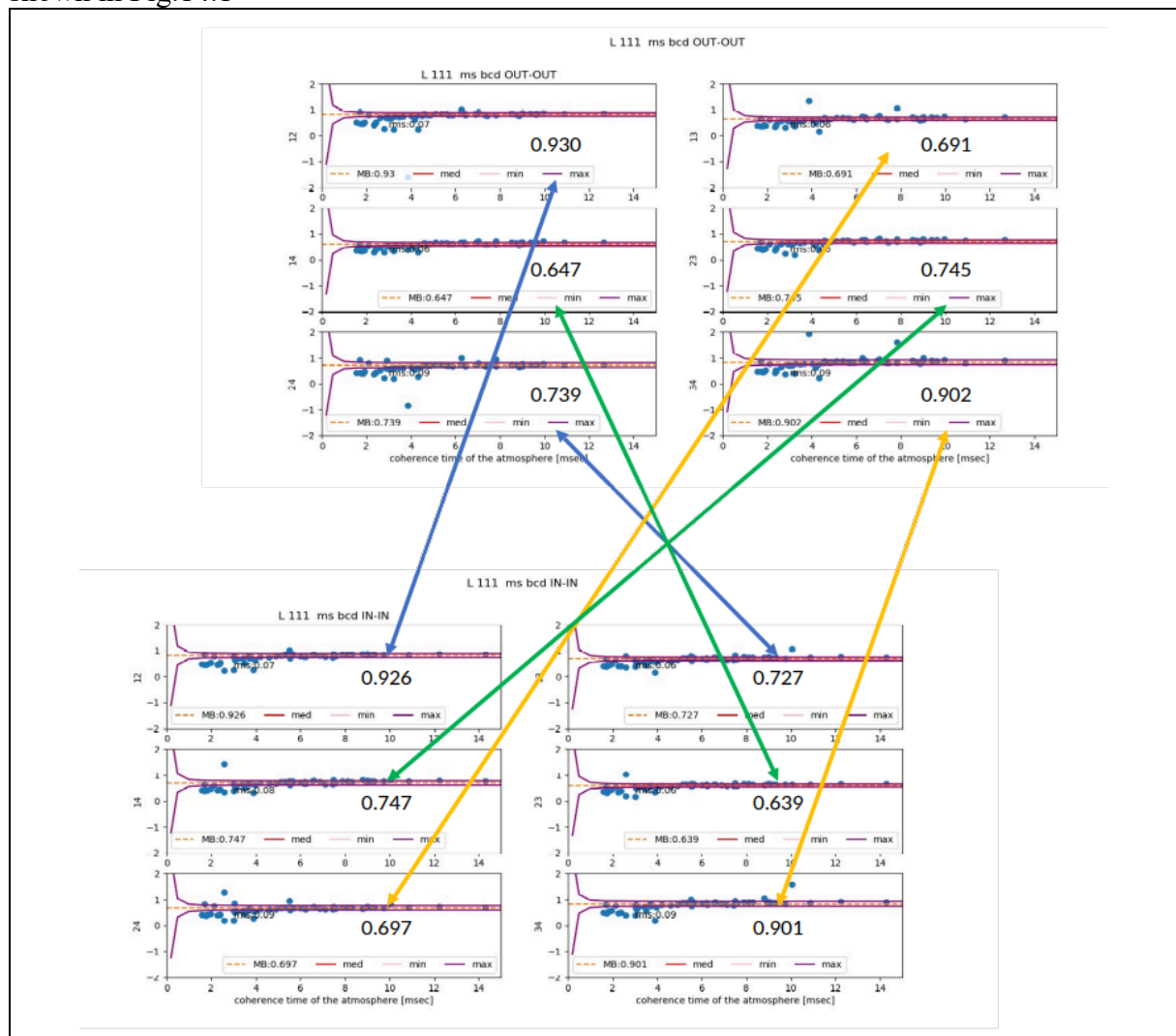


Figure. 14.1: Broadband L-band instrumental visibility plotted as a function of the coherence time for the two BCD configurations OUT-OUT and IN-IN. The average visibility level for every baseline is indicated in bold font. This average visibility has been estimated from a large number of observations over more than 18 months



We define the correction as the ratio between OUTOUT and the BCD configuration which can be ININ, INOUT or OUTIN. Ergo, multiplying the appropriate observable by the provided correction produces the OUTOUT equivalent value. We find the correction to be chromatic and linear with wavelength to first order with the following form: $V_{\text{corr}}(\lambda) = m \cdot \lambda + c$, with λ in meter. We therefore provide the coefficients of the linear fit to the L, M corrections in Table 14.1.

Band	OUT-OUT Fringe peak	BCD configuration	m	c
L	1	IN_IN	17855,33	0,934
M	1	IN_IN	40981,87	0,810
L	2	IN_IN	1585,76	1,001
M	2	IN_IN	-12155,63	1,082
L	3	IN_IN	-442130,25	3,113
M	3	IN_IN	-17532,45	1,330
L	4	IN_IN	-84923,15	1,441
M	4	IN_IN	80916,31	0,649
L	5	IN_IN	32355,58	0,797
M	5	IN_IN	22219,89	0,884
L	6	IN_IN	178739,57	0,053
M	6	IN_IN	-84838,566	1,225

Table 14.1 Coefficients of the linear fit to the L, M corrections.

We provide an example of the correction on the IN-IN transfer function in Figure 14.2. We can see that the OUT-OUT visibilities (blue and orange dots) overlap well with the IN-IN visibilities (blue and orange squares), except for one problematic observation of one of the science targets.

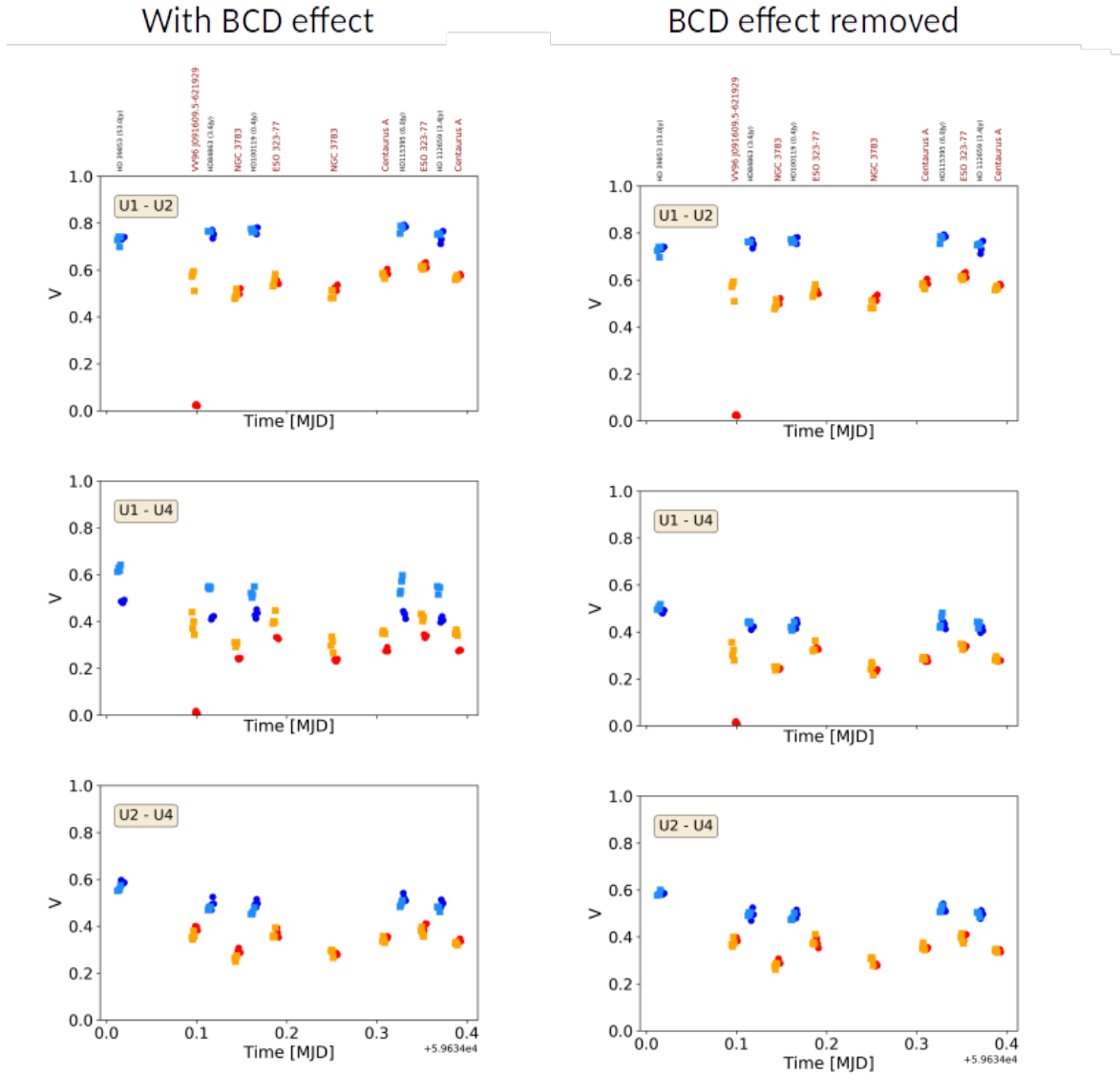


Figure 14.2: Plot of the broadband L-band transfer function (between 3.1 and 3.9 μm) for the night of Feb 23, 2022, with the effect of the BCD (Left) and with the BCD effect removed by the chromatic correction factor applied to the IN-IN visibilities (Right). The dots and squares correspond to the OUT-OUT and IN-IN configurations, respectively. Blue (dark and light) and red/orange colors correspond to calibrator and science targets.



15 ANNEX: CHROMATIC PHASE CORRECTION

The differential phase is a powerful tool for modelling and image reconstruction. However, it is contaminated by a chromatic OPD effect that makes the calibration difficult except for the simplest continuum-line-continuum case. Here we discuss the basic calibration method that applies the chromatic index estimated on calibrators to correct the differential phase on a science target after correction of the air path differences that have changed between the observation of the science and calibrators. The BCD provides us with the opportunity to improve this calibration method with regard to what was implemented on MIDI. As a first step, the BCD inverts the first two phase terms for the first two fringe peaks, allowing the removal of the instrumental term.

From this, if we assume the atmospheric component is dominant over the VLTI component, we can calculate the atmospheric index:

$$n(\lambda) - 1 \simeq \frac{\lambda}{2\pi} \frac{\varphi_{d_{out}}(\lambda) - \varphi_{d_{in}}(\lambda)}{\Delta E_{out} + \Delta E_{in}}$$

where $n(\lambda)$ is the atmospheric index, and $\varphi_{d_{out}}(\lambda)$, $\varphi_{d_{in}}(\lambda)$, ΔE_{out} , ΔE_{in} are the BCD out phase, BCD in phase, absolute BCD out optical path difference, and absolute BCD in optical path difference, respectively. This can only be calculated for fringe peak 1 and 2. We then calculate for the target source and apply the calculated atmospheric index from the calibrator. For the first two fringe peaks, we apply directly $n(\lambda) - 1$ estimated on the same peaks from the calibrator; for the remaining peaks we apply the average of these two values. This method is sufficient for the first two peaks but leaves the instrumental phase term in the remaining four. To remove this, we apply the average $n(\lambda) - 1$ to the latter four peaks of the calibrator. The remaining phase is used as the instrumental term for those peaks and subtracted from the target. To evaluate the method, we have selected commissioning calibrators close in time (less than 90') and in space (less than 20°). The following figures give the average rms of the residual phase errors. We have considered the Cal-Sci case (the differential phase on Cal2 -the mock science target- corrected from these estimated on Cal1) and the Cal1-Sci-Cal2 case where the differential phase on the mock Sci target is computed from a $n(\lambda)$ value interpolated between Cal1 and Cal2.

We find that if this method is applied using a single nearby calibrator within 2 hours to calibrate a calibrator, we get the RMS of the residual plotted in Fig. 15.1. When we interpolate between the calibrators either side of the target with the same criteria, we get the RMS of residuals seen in Fig. 15.2. The interpolation method shows improvement over the single calibrator method although both yield less than a degree of error over most of the L band and M band (the 2022 nights were remarkably stable in atmospheric quality which improved the calibration).

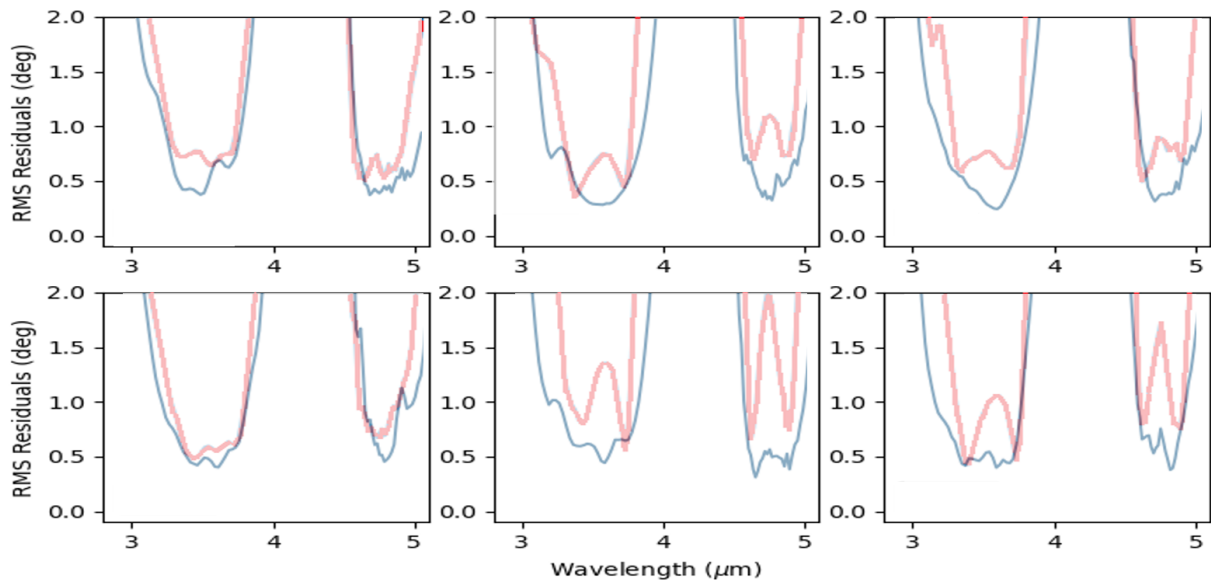


Figure 15.1: RMS of residuals when calibrating zero phase sources using the Call-Sci-Cal2 method based on an interpolation between Cal1 and Cal2 (in blue). It has been overplotted with the results of a basic calibration where the differential phases from cal1 and cal2 are directly subtracted (in red). For these carefully selected calibrators, the basic procedure was giving fairly good results but the calibration procedure using the index estimation yields a clear improvement in the center and the edges of the bands.

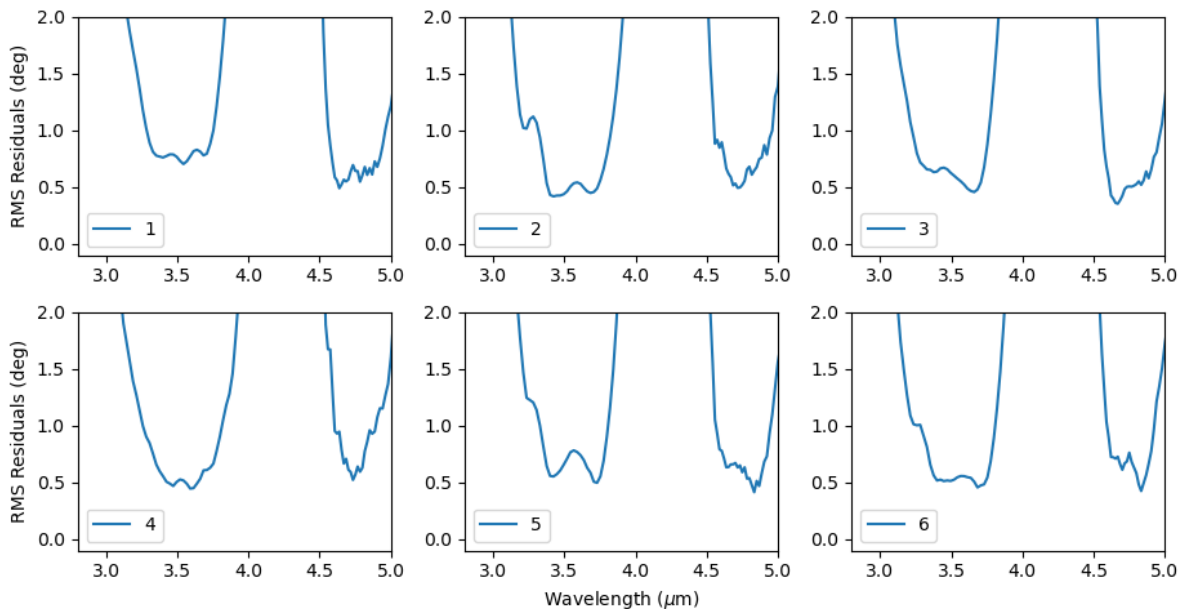


Figure 15.2: RMS of the residuals after calibrating zero phase sources using the Cal-Sci method. The results are comparable to the Call-Sci-Cal2 method but slightly inferior.

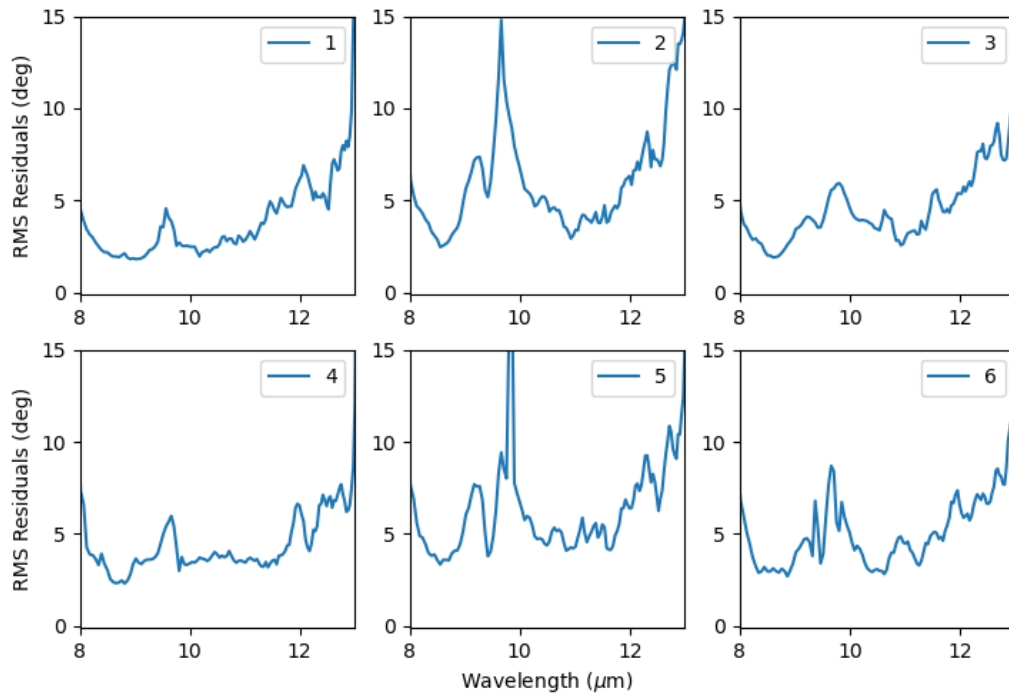


Figure 15.3 : RMS of residuals when calibrating zero phase sources in N by interpolating between two nearby calibrators

Repeating this method in the N band also yields the results in Fig. 15.3 and Fig. 15.4. A caveat with the N band is that sometimes the phases are wrapped due to an incorrect group delay analysis. This stems from the choice of wavelength reference. The wavelength range used in the group delay calculation is the entire N band (8-13 microns). Should there be a particularly large uncertainty towards the edge of the band or a strong $\sim 9.6 \mu\text{m}$ atmospheric feature this can introduce a slope in the differential phase. In this case it is difficult or impossible to reliably calibrate the differential phase. For the figures given here, we have removed cases of wrapping.

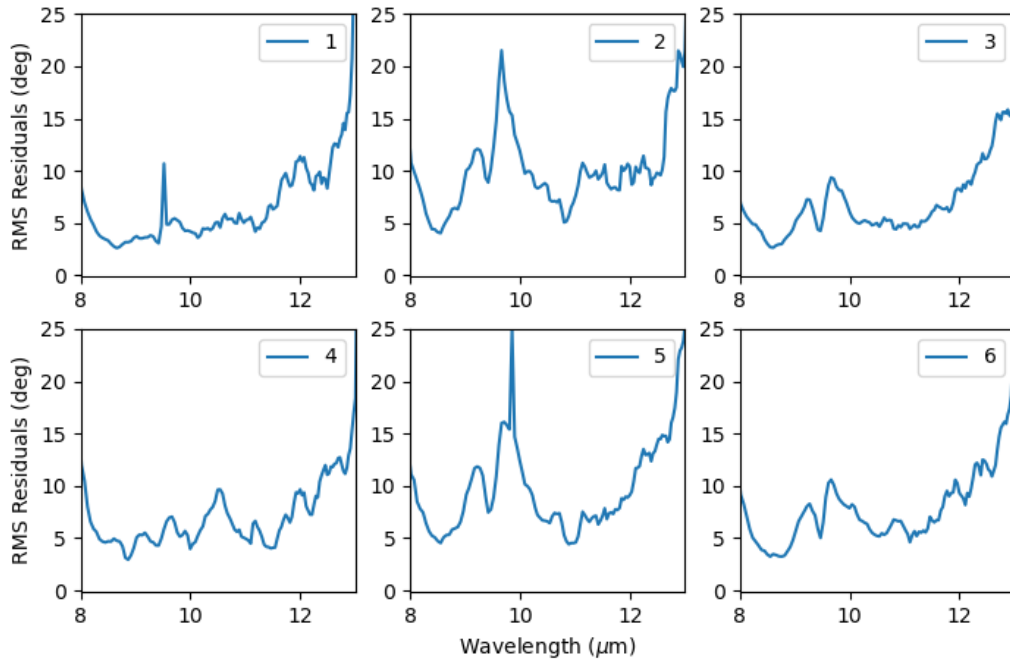


Figure 15.4 RMS of residuals when calibrating zero phase sources in N with a single nearby calibrator

We find that narrowing the N band reference to both 8.2-8.8 microns and 9.8 to 10.8 microns prevents wrapping for a night that was heavily wrapped in the standard pipeline. This came at the expense of S/N for the differential phase. Selecting a wide window with the removal of the atmospheric feature and band edges may provide the best compromise in future pipeline improvements.

Currently, the L, M, and N band are all independent in terms of phase. This is because the group delay is calculated separately for each. An improvement for the future is to use chromatic atmospheric models to calculate the intra-band phase.

16 ANNEX: IMPACT OF THE PWV ON VISIBILITY

The Precipitable Water Vapor (PWV) impact the differential phase near the band edges as briefly discussed in the previous section. There are no specifications nor performance estimates in these bands. We have evaluated the influence of the PWV on the broad band measurements of visibility. The plots below show that the visibility is much less sensitive to the PWV than to coherence time or even seeing.

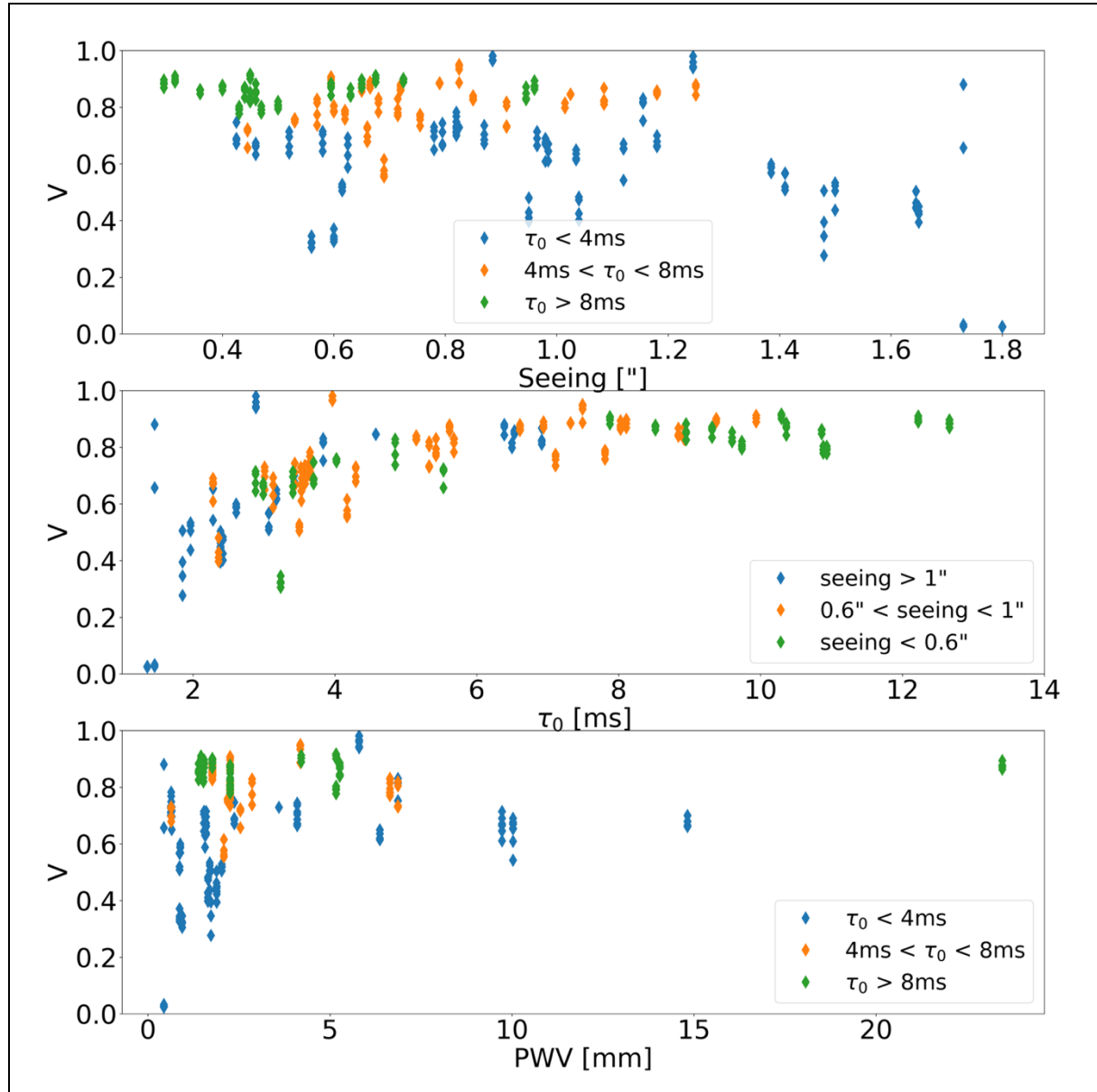
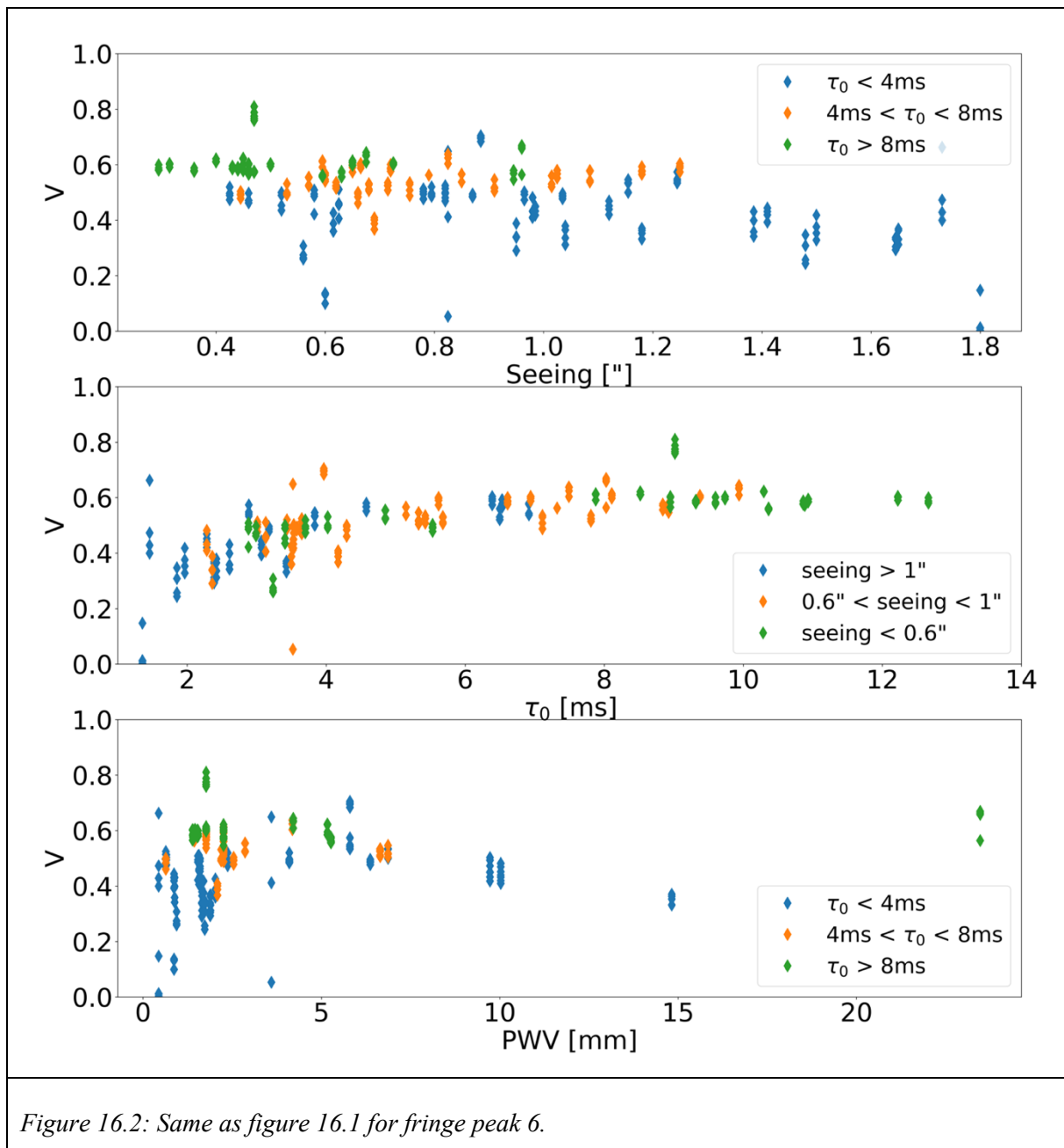


Figure 16.1: Instrument Visibility (measured on calibrators with a correction from the calibrator uniform disk diameter) as a function of seeing (top), coherence time (middle) and PWV (bottom) on fringe peak 1. The dominant parameter is coherence time and there is no indication of PWV requirement for any Visibility and hence coherent magnitude requirement.





17 ANNEX: UPDATE OF MATISSE STANDALONE PROPOSED

PERFORMANCES

17.1 NEW MEASUREMENTS

The previous versions of the commissioning reports as well as the MATISSE publications contained a few sensitivity limits based on extrapolation because of the lack of data. As we are dealing mostly with higher spectral resolution modes, we focused mainly on the differential phase error (from observations without photometry and hence chopping) that is also directly related to the coherent flux SNR.

The following table summarizes the findings in differential phase accuracy:

Mode	Target	L	M	Tau 0	seeing	sigma_phi	Conclusion on mode limit (4°)
MR-L-UT	BD-13 2169 02 :09 :59	0.8		5.4	0.7	1.5°	Coherent with 0.3 Jy limit
MR-L-UT	HD 150071 05 :12 :38	0.3		3.2	0.8	9°	Coherent with 0.7 Jy, but coherent flux loss between 1.5 and 2
MR-L-AT	Del For 03 :42 :45	2		3.0	1.0	21° (18-26)	Compatible 10 Jy (5 Jy if 50% Vis loss)
MR-L-AT	Mu Cen 06:29:36	9.1	6.5	3.7	0.7	2°	Compatible 5 Jy (despite not so good seeing)
MR-L limit for diff phase 0.3 to 0.5 Jy in coherent flux → 0.4 Jy on UTs, 0.6 in V, 0.6 in CP → 5.6 Jy on ATs, 6 to 8 in V							
HR-L-AT	HD 6629 07:46:19	16		6.6	0.38	9-23	After 4.02 Would give 32 Jy for 4°
HR-L-AT	HD 138938 23:41:42	22	17	9.8	0.49	2°	Would give 11 Jy
The HR-L-AT situation is confusing and missing data, by coherence with the well-established limit ~1.1 Jy on UTs, we will conclude to a limit ~15 Jy							
LR-L-AT	HD 107625 06:24:20	0.5	0.25	9	0.6	2°	Compatible 0.25 Jy Pushing the LR-L limit is still possible. 0.25 Jy ATs corresponds to 20 mJy UTs in outstanding conditions
LR-M-AT	HD 151843 07:39:41	3	1.8	8	0.55	2.5°	Compatible 1 Jy, supports the previous MATISSE values
LR-N-AT	c Vel 00:41:13	109	N=15. 4	2.03	1.35	1°	
MR-M	No usable new data						



17.2 SENSITIVITY LIMIT UPDATES FROM NEW MEASUREMENTS

The LR-M and LR-L values given in the previous versions of the report are basically confirmed. An update of the ESO web page values might be considered. They are slightly optimistic in L (for visibility) and clearly pessimistic in M). In LR-M UTs we need the check that will be performed in the July run.

Setup	AT, visibility measurements					
	ESO		MATISSE previous		Update	
	Good/Fair	Poor	Good/Fair	Poor	Good/Fair	Poor
LR-L	1	1.5	1.1	2.8	1.1	2.8
LR-M	5	9	2.1	4.0	2.1	4

Setup	UT, visibility measurements					
	ESO		MATISSE previous		Update	
	Good/Fair	Poor	Good/Fair	Poor	Good/Fair	Poor
LR-L	0.1	0.15	0.3	0.5	0.08	0.1
LR-M	0.5	1	0.4	0.6	0.17	0.2

For the higher spectral resolutions and relative measurements, in MR-L both the ESO and previous MATISSE numbers are wrong. Here we have clear evidence of a limit in L around 6 Jy on ATs, well supported by the value measured on UTs that converges near 0.4 Jy in coherent flux. We remind that for differential phase there is no seeing calibration effect for a given coherent flux. The seeing (mostly the coherence time) change the coherent flux of a target. The calibration effect due to chromatic OPD changes is shown in the new section ... to be well below 1° between 3.2 and 3.9 μm where the values given here are defined

Setup	AT, differential phase					
	ESO		MATISSE previous		Update	
	Good/Fair	Poor	Good/Fair	Poor	Good/Fair	Poor
MR-L	1	1.5	1.1	2.8	5.6	5.6
MR-M	5	9	2.1	4.0	No usable new data	
HR-L	10	15	10.7	10.7	10.7	10.7

Setup	UT, differential phase					
	ESO		MATISSE previous		Update	
	Good/Fair	Poor	Good/Fair	Poor	Good/Fair	Poor
MR-L	0.2	0.3	0.6	0.6	0.4	0.4
MR-M	0.7	0.7	0.7	0.7	No usable new data	

Finally, in HR-L-AT, we find some new evidence supporting a L=10.7 Jy limit, but there is a strong dispersion between our sparse data on that mode.



17.3 GLOBAL SYNTHESIS OF PERFORMANCES

Here we combine the V1.1 values, with the corrections of typos, the updates from measurements made after March 2020 and the computation of the performances in N2 and N3 to cover the full N band. This synthesis is the one presented in the section 1.5.

For « Fair and Good » seeing conditions (seeing<0.9 arcsec, $\tau_0>5$ ms)²⁴.

Limiting Coherent flux in Jy							
Telescopes	Resolution	Visibility		Closure Phase		Differential Phase	
		L	M	L	M	L	M
ATs	LOW	1.1	2.1	0.4	1.9	0.3	1.1
	MED	8.0	TBC ²⁵	7.0	TBC	5.6	TBC
	HIGH	20.1	na	14.7	na	10.7	na
UTs	LOW	0.08	0.17	0.07	0.16	0.06	0.15
	MED	0.6	TBC ²⁶	0.6	TBC	0.4	TBC
	HIGH	2.4	na	1.7	na	1.2	na

For « Poor » seeing conditions (seeing=0.9±0.2 arcsec and $\tau_0=3.6±1.6$ ms)

Limiting Coherent flux in Jy							
Telescopes	Resolution	Visibility		Closure Phase		Differential Phase	
		L	M	L	M	L	M
ATs	LOW	2.8	4.0	0.4	1.5	0.3	1.1
	MED	8.0	TBC	7.0	TBC	5.6	TBC
	HIGH	31.4	na	14.7	na	10.7	na
UTs	LOW	0.1	0.15	0.07	0.16	0.06	0.15
	MED	0.6	TBC	0.6	TBC	0.4	TBC
	HIGH	3.8	na	1.7	na	1.3	na

As already well established in the V1.0 and 1.1 of the commissioning report for 8.5 μ m and completed here for 10.5 and 12.5 μ m, the limits for visibility measurements in LR-N are:

Limiting Coherent flux in Jy													
Telescopes	Resolution	Visibility			Closure Phase			Differential Phase Coherent Flux SNR			Combined Bias and fundamental noise limit on the CF		
		N1	N2	N3	N1	N2	N3	N1	N2	N3	N1	N2	N3
ATs	LOW	16.8	31.4	44.0	9,4	23.6	36.7	2,9	7.5	11.7	6	8	12
	HIGH	30.3	51.3	83.7	29.9	194	218	25,3	45.9	58.9	25,3	45.9	58.9
UTs	LOW	0.9	1.4	1.9	0.3	0.8	1.3	0.2	0.55	0.6	0.5	0.7	0.8
	HIGH	1.6	3.4	4.1	1.5	4.9	13.1	1.1	3.5	3.7	1.1	3.5	3.7

24 The numbers for the « fair seeing » data set (seeing=0.75±0.2 arcsec and $\tau_0=7±2$ ms) are very similar to those for a “good seeing” data set (seeing=0.55±0.1 arcsec and $\tau_0=8±2$ ms). The limit between “good” and “bad” conditions for MATISSE is fundamentally set by $\tau_0\sim 4$ ms)

25 The MR-M band values were based on extrapolation from sparse data. We could not confirm these values as our new measurements are incoherent. We prefer to declare this values “TBC” until we obtain new data, hopefully in July 2022 if weather permits.

26 The values given in MR_M with UTs were estimated from the measured UT/AT flux ratio in M. As we could not confirm the AT values, the UT values are also declared “TBC”.

**Commissioning Report**

The coherent flux bias limits set by noise on the group delay correction have been estimated to be of the order of 5-6 Jy in N1 and 8-9 Jy in N3. As the group delay is estimated from the full N band, this bias is less dependent from the wavelength than the fundamental noise. In fact, it represents a specific limit only in and near N1, the other bands remaining dominated by fundamental noise. In HR-N, the fundamental noise completely dominates over the bias limit.

**Commissioning Report****18 ADDITIONAL MEMO: VHR AND GRA4MAT MATISSE
PERFORMANCES****19 ADDITIONAL MEMO: GRA4MAT WITH UTS**

The Very High Spectral Resolution mode and the use of MATISSE with GRAVITY as a fringe tracker are not contractually part of the MATISSE PAC documents. However, as these modes are partially commissioned and offered to the general user (on ATs since P108 and on UTs in P110) we include here the two MATISSE commissioning memos that provided the information allowing these achievements. The commissioning of MATISSE with GRA4MAT has been delayed by the Covid-19 crisis and by bad observing conditions during the July 2022 run on UTs, which was supposed to be the final one. The final performances of MATISSE with GRA4MAT on UTs should be known by the end of 2022.

MATISSE Memo

MAT-COM-2020-01-16

From: R. G. Petrov, F. Allouche, A. Matter, A. Meilland, P. Berio, P. Cruzalèbes, S. Lagarde, F. Millour, J. Varga, J. Woillez and the MATISSE Commissioning Team



To: C. Paladini, M. Schöller, ESO, MATISSE Consortium

Sent: February 25, 2020

Version: 1.2

Subject: **VHR and GRA4MAT MATISSE performance update**

MATISSE COMMISSIONING TEAM

Fatmé Allouche, Philippe Berio, Leonard Burtscher, Alain Chelli, Pierre Cruzalèbes, Yann Fanteï, Karl-Heinz Hofmann, Walter Jaffe, Stéphane Lagarde, Bruno Lopez, Alexis Matter, Anthony Meilland, Klaus Meisenheimer, Florentin Millour, Sébastien Morel, Romain Petrov, Sylvie Robbe-Dubois, Sylvain Rousseau, Dieter Schertl, Jozsef Varga.

1	Scope	103
2	Summary of conclusions	103
2.1	Propositions	103
2.2	GRA4MAT operation limits	103
2.3	Coherent flux, closure phase and differential measures	103
2.4	Absolute visibility measures	103
2.5	Execution times with GRA4MAT	104
2.6	Future improvements	104
2.7	Data reduction of MATISSE data with GRA4MAT	104
3	GRA4MAT operation	105
3.1	Observation preparation	105
3.2	Operation sequence	105
3.3	MATISSE DITs with GRA4MAT	105
3.3.1	<i>In Low Resolution: DIT=1s</i>	105
3.3.2	<i>Higher spectral resolutions: DIT=10s</i>	106
4	Limits of MATISSE with GRA4MAT	106
4.1	Methodology	106
4.1.1	<i>Flux dependent calibration error</i>	106
4.1.2	<i>Seeing dependent calibration error</i>	107
4.1.3	<i>Fundamental noise errors</i>	108
4.2	VHR mode	108
4.3	VHR-L differential phase: 20 Jy limit	109
4.4	VHR-L closure phase: 25 Jy	109
4.5	VHR-L Differential Visibility: 18 Jy	110
4.6	VHR-L illustration	110
4.7	VHR-M differential phase: 17 Jy	111
4.8	VHR-M closure phase: 25 Jy	111
4.9	VHR-M differential visibility: 15 Jy	112
4.10	HR-L Differential phase: 2 Jy	113
4.11	HR-L Closure phase: 3 Jy	113
4.12	HR-L Differential visibility: 3 Jy but SiPhot shift problem	114
4.13	HR-L illustration	115
4.14	MR-L Differential phase: 1 Jy	115
4.15	MR-L Closure phase: 1.5 Jy	116
4.16	MR-L Illustration	116
4.17	MR-M Differential phase	117
4.18	MR-M Closure phase	117

4.19	LR-L Differential phase: 0.17 Jy.....	118
4.20	LR-L Closure phase: 0.5 Jy.....	118
4.21	LR-M Differential phase: 0.7 Jy.	119
4.22	LR-M Closure phase: 4 Jy.....	119
4.23	LR-M Illustration	120
5	Annex: transmission of VHR grisms	121

CHANGE RECORD			
Issue	Date	Section/page	Reason
1.0	16/01/20	All	First Issue
1.1	20/01/20	§2/p1 §4.17/p18	Typo in perf flux table: VHR-L limit=20 Jy Legend of figure
1.2	25/02/20	§2.3/p4 and §4.18/p19	Correction of an error on the limit for Closure Phase in MR-M with GRA4MAT (DIT=10s). Now 20 Jy. Old value: 10 Jy.

1 SCOPE

We report the successful implementation of

- the GRA4MAT extension of MATISSE that uses the GRAVITY fringe tracker to stabilize the fringes observed by MATISSE
- the Very High Spectral Resolution mode of MATISSE in the L and M bands.

We give the performances of MATISSE with GRA4MAT in all spectral resolutions in the L and M bands, including the newly installed VHR mode.

We propose to include the GRA4MAT and VHR options in the March 2020 Call for Proposals for P106. GRA4MAT should be offered on ATs and without chopping.

2 SUMMARY OF CONCLUSIONS

2.1 PROPOSITIONS

- Observations with MATISSE and GRA4MAT without chopping have been successfully commissioned on ATs for all spectral resolutions in the L and M bands, including the newly installed “Very High Spectral” one (VHR, $R \sim 3300$).
- For P106, offer MATISSE with GRA4MAT on ATs and without chopping, in all spectral resolutions in L&M with the performance limits given in the next three paragraphs.

2.2 GRA4MAT OPERATION LIMITS

To consider the specific problems of GRA4MAT (risk of fringe jumps during long frames) we propose to use the GRAVITY FT limits with an additional margin of 1 magnitude. This yield:

Seeing conditions	T \leq 10% Seeing \leq 0.6” $\tau_0 > 5.2$ ms	T \leq 50% Seeing \leq 1.0” $\tau_0 > 3.2$ ms	T \leq 85% Seeing \leq 1.4” $\tau_0 > 1.6$ ms
K coherent magnitude limit	8.5	7.5	6.5

Table 1: K band coherent magnitude limit for GRA4MAT operation

We have indeed observed successfully at K up to 8.5.

2.3 COHERENT FLUX, CLOSURE PHASE AND DIFFERENTIAL MEASURES

The following tables illustrates the performances of MATISSE on ATs with GRA4MAT in all modes including VHR. The performances are given for observations without chopping, nor “N band photometry”.

Resolution	Band	L		M	
		CF & Dif. Ph.	Clos. Ph.	CF & Dif. Ph.	Clos. Ph.
LR	DIT=1s	0.2	0.5	1	4
MR	DIT=10s	1	1.5	14	20
HR	DIT=10s	2	3	--	--
VHR	DIT=10s	20	25	17	25

Table 2: estimated limits in Jy for performances of MATISSE with GRA4MAT. We use the standard criteria: differential phase precision=4°/spectral channel \Leftrightarrow coherent flux SNR=10/spectral channel and Closure Phase precision=5°/spectral channel

The gain in N band precision for these measures has not been fully evaluated, and we do not propose any change in the N band performance limits.

2.4 ABSOLUTE VISIBILITY MEASURES

Without chopping, the use of GRA4MAT excludes:

- Absolute visibility measures in the M band
- Absolute visibility measures in L for targets²⁷:
 - o Fainter than L=10 Jy for broad band (3.1 to 3.8 μ m) visibility estimates
 - o Fainter than L=20 Jy for visibility estimates in all individual spectral channels

The DITs selected for MATISSE with GRA4MAT exclude N band photometry with standard MATISSE chopping frequencies²⁸.

Thus, MATISSE with GRA4MAT allows absolute visibility measures only in the L band with the current limiting fluxes (for a visibility precision =0.1/spectral channel):

Resolution	LR	MR	HR	VHR
Limit in Jy	10	20	20	20

Table 3: flux limit in Jy for absolute visibility measures without chopping in the L band

Above these limits, the use of GRA4MAT for absolute visibility measures in L is recommended because GRA4MAT improves the MATISSE instrument + atmosphere visibility and makes it much less sensitive to seeing changes.

Below these limits in L and for all N and M observations, absolute visibility measures require chopping and thus, for the time being, stand-alone MATISSE observations.

2.5 EXECUTION TIMES WITH GRA4MAT

The current duration of MATISSE operation with GRA4MAT are:

- Acquisition of Image and Fringes: 8 mn
- Observation without photometry: 12 mn

This yields for a complete OB (acquisition + observation): 20 mn.

2.6 FUTURE IMPROVEMENTS

The following points are under investigation:

- The operation of GRA4MAT and in particular
 - o The additional overheads implied by switches from MATISSE alone and MATISSE with GRA4MAT modes.
 - o An acquisition procedure, similar to the one used for MATISSE with IRIS, that avoids repeating field acquisition for each target.
- The gain in sensitivity in N band from coherent integration.
- The compatibility of GRA4MAT with N band photometry chopped at low frequencies.

The current GRA4MAT run (January 10 to 17) is expected to provide new data on these three points. The preliminary results are encouraging.

2.7 DATA REDUCTION OF MATISSE DATA WITH GRA4MAT

The current version of the MATISSE pipeline (1.5.0) has been used to reduce MATISSE data with GRA4MAT, for all resolutions including VHR. It has provided the performance estimates given in this report.

Several additional DRS developments are in progress:

- The flagging of MATISSE frames affected by GRA4MAT fringe jumps.
- The coherent integration of MATISSE, including a correction of the chromatic differences between K and the MATISSE bands.

²⁷ See memo MAT-COM-2019-07-31 and section 4.1.1

²⁸ The DIT=1s selected for LR with GRA4MAT should be compatible with a chopping frequency of about 0.25 Hz. The quality of the corresponding N band data has not been fully evaluated yet. The possibility to offer MATISSE with GRA4MAT in LR and to execute the photometric sequence with a chopping frequency of 0.25 or 0.2 Hz is an open question.

- The correction of spectral variable distortions between photometric and interferometric channels that affect the high spectral resolution observations over large bands permitted by GRA4MAT
- The use of GRA4MAT data to improve the calibration of MATISSE measures.

3 GRA4MAT OPERATION

3.1 OBSERVATION PREPARATION

For the user, the GRA4MAT operation is very straightforward: in P2 he has to use an acquisition template with GRA4MAT (MATISSE_img_acq_ft) instead of the standard acquisition template (MATISSE_img_acq).

Then the GRAVITY FT, acquisition and fringe search, is operated in the standard GRAVITY way.

The MATISSE observation template (in MATISSE_hyb_obs) and its parameters are as usual, but for the DITs.

3.2 OPERATION SEQUENCE

- In the template MATISSE_img_acq_ft
 - Image acquisition with MATISSE with the Field Separation Mirror (FSM).
 - Optimization injection GRAVITY (with internal optics)
 - Field tracking by GRAVITY with the FSM
 - Search and lock fringes with GRAVITY
- In the template MATISSE_hyb_obs
 - Center fringes in MATISSE (with MATISSE internal DL)
 - Store the offsets
 - Make sky observation (opening GRAVITY tracking loops)
 - Closing the GRAVITY loops when back on target
 - MATISSE Observation with specific GRA4MAT DITs

A prior operation is to align GRAVITY and MATISSE using MARCEL²⁹.

If the cophasing between GRAVITY and MATISSE using MARCEL has not been executed recently (in daytime before the observations), the offset between GRAVITY and MATISSE zero OPD might be larger than the coherence length of MATISSE in Low Resolution in L (100 μm). It is then recommended to make the first GRA4MAT fringe acquisition with MATISSE at least in Medium Resolution.

3.3 MATISSE DITS WITH GRA4MAT.

3.3.1 In Low Resolution: DIT=1s

The proposed 1s limit is set by the saturation of the Hawaii detector. With DIT=1s we estimate the saturation of the detector to be reached around:

- L=300 Jy
- M>2000 Jy (~no limit)

These estimates have to be checked.

For brighter targets with GRA4MAT, it is advised to switch to a higher spectral resolution mode.

The performances of MATISSE in LR_M and LR_L with GRA4MAT are given for DIT=1s.

²⁹ MATISSE is aligned on MARCEL (cf. MATISSE maintenance manual). Then, for GRA4MAT, GRAVITY is aligned on the same MARCEL beams and OPD.

3.3.2 Higher spectral resolutions: DIT=10s

The risk of saturation is limited at DIT=10s, even in MR³⁰. In our GRA4MAT experience, the risk of fringe jumps, is much less than once per mn, and least within the proposed GRA4MAT K band limits. On the other hand, a DIT larger than 10s would reduce too strongly the number of independent measures per 1 mn OB.

Thus, we have selected a 10 s DIT for all higher spectral resolution modes and all performance estimates are given for this value.

4 LIMITS OF MATISSE WITH GRA4MAT

4.1 METHODOLOGY

We have used the performance evaluation methodology defined in the previous commissioning reports and memos.

The goal is to define coherent flux limits that ensure, for each mn of observation:

- Coherent flux SNR>10 per spectral channel that is equivalent to differential visibility precision<4° per spectral channel
- Closure phase precision<5° per spectral channel
- Absolute visibility precision<0.1 per spectral channel, when this is applicable

We combine

- The fundamental noise error per spectral channel from source and background photon noise and detector noise.
- The magnitude independent calibration error that is mainly due to seeing variations. This is deduced from the analysis of the time variations of measures on calibrators.
- The flux dependent calibration errors on the photometry and hence visibility estimates that result from errors in the background estimation.

4.1.1 Flux dependent calibration error.

As we observe without chopping and without HiSens photometry, we consider only the photometric error in the L band that results from SiPhot photometric measures without chopping corrected by Sky measurements made 1 to 10 mn before.

This effect is described in the memo MAT-COM-2019-07-31.

In M band it makes the photometry useless and hence the absolute visibility measures impossible.

In the L band it introduces a flux limit for 0.1 visibility precision per spectral channel that increases regularly from L=2 Jy, that still allow precise measures at 3 μm, to L~22 Jy that are needed for a precise measure at 4 Jy. A linear estimate of the limit $L(\lambda)$ for an accurate observation at λ (in μm) would be:

$$L(\lambda) = 20(\lambda - 3) + 2 \text{ with } \lambda \text{ in } \mu\text{m}$$

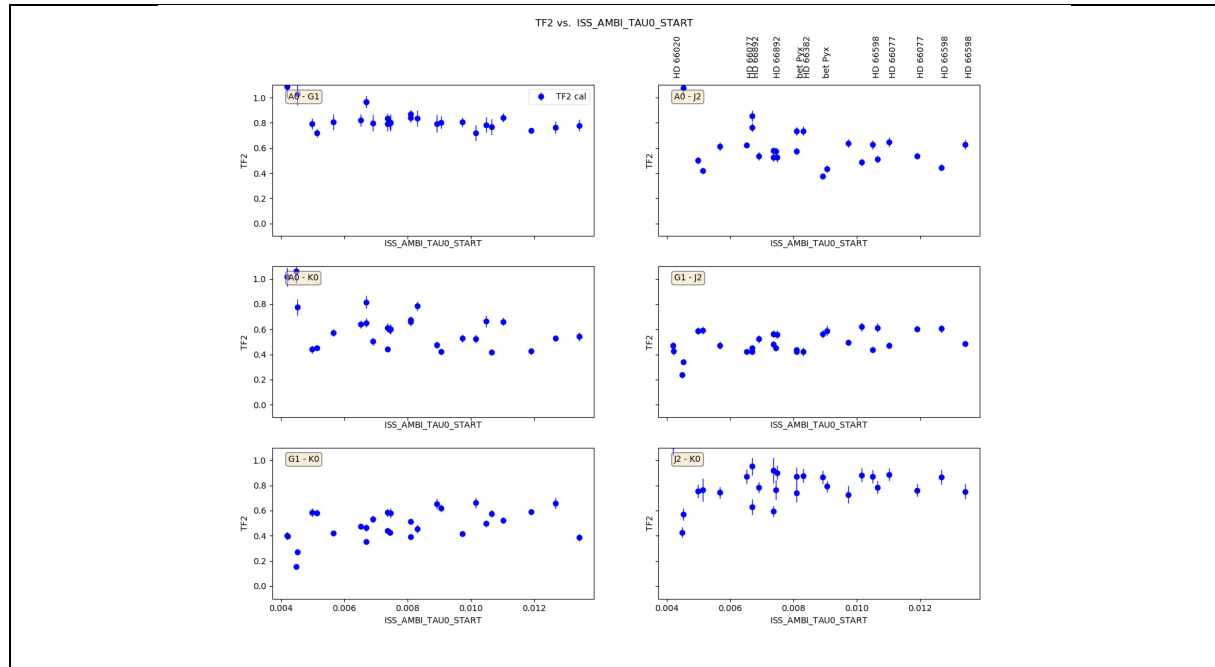
For simplicity, we could use a 10 Jy limit for a broad band visibility estimate and a 20 Jy limit for estimates in all L band spectral channels.

We are not reporting on N band absolute visibility measures with GRA4MAT. As their accuracy is strongly dominated by photometric errors, GRA4MAT cannot significantly improve it.

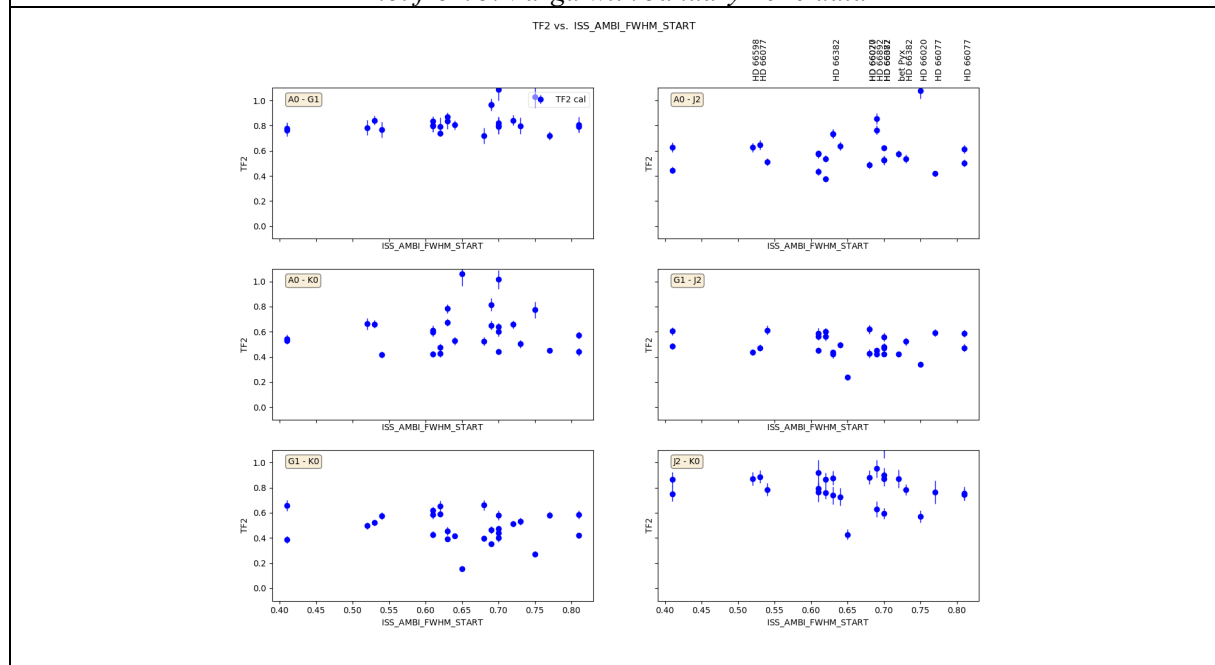
³⁰ The numbers given in 3.3.1 correspond to saturation limits in MR of L~1000 Jy (TBC)

4.1.2 Seeing dependent calibration error

As GRA4MAT stabilize the fringes and drastically reduces the piston residual, it strongly decreases the variation of MATISSE instrument + atmosphere visibility, as illustrated by the following plots:

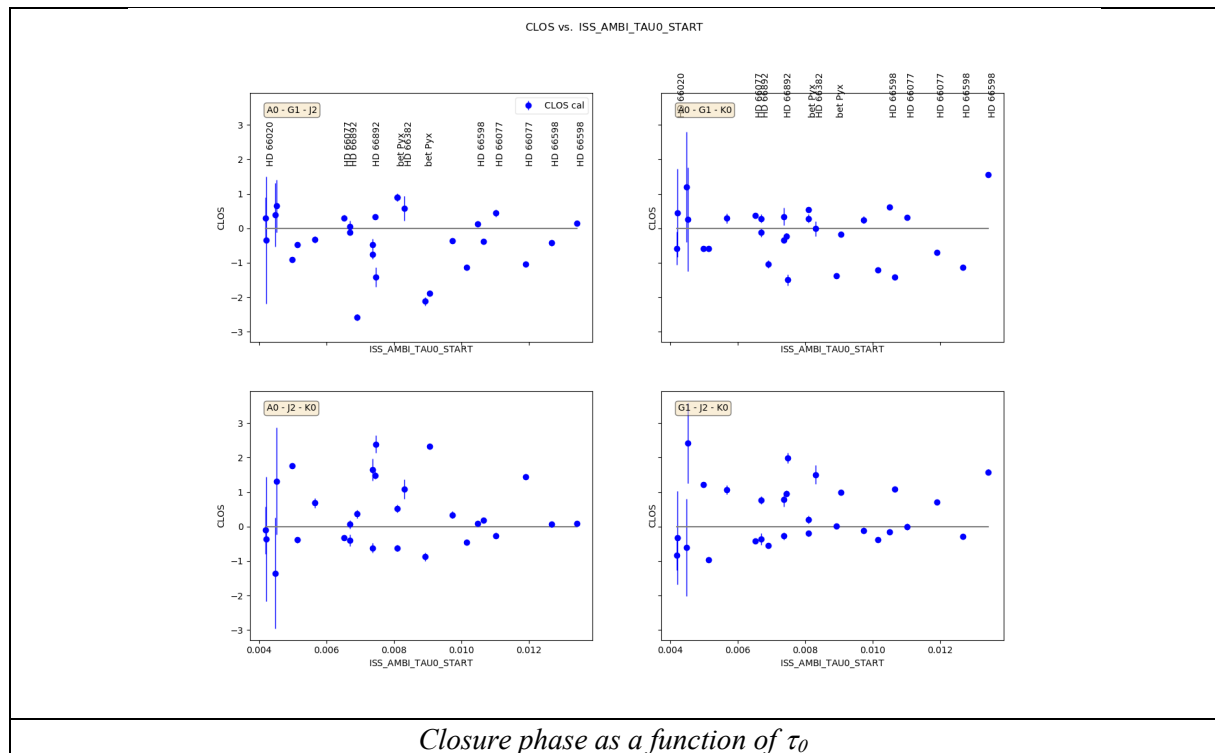


*V^2 measured on calibrators as a function of τ_0 (above) and seeing (bellow). The dispersion of points is due to non-chopped L band observations on faint or even very faint targets. However, the average instrument response is remarkably independent from seeing conditions.
Plot from J. Varga with January 2020 data*



However, from the October and December 2019 runs, we do not have enough homogeneous TF data to assess new calibration errors, and we decide to keep the MATISSE alone values. They are confirmed so far by the data set that we have. A more complete analysis will be necessary to detect possible specific problems for long DITs. However, our current and provisional observation is that fringe jumps are rare enough and should have a minor impact

on measurement stability. This is completed by the high stability of the closure phases illustrated below.



4.1.3 Fundamental noise errors

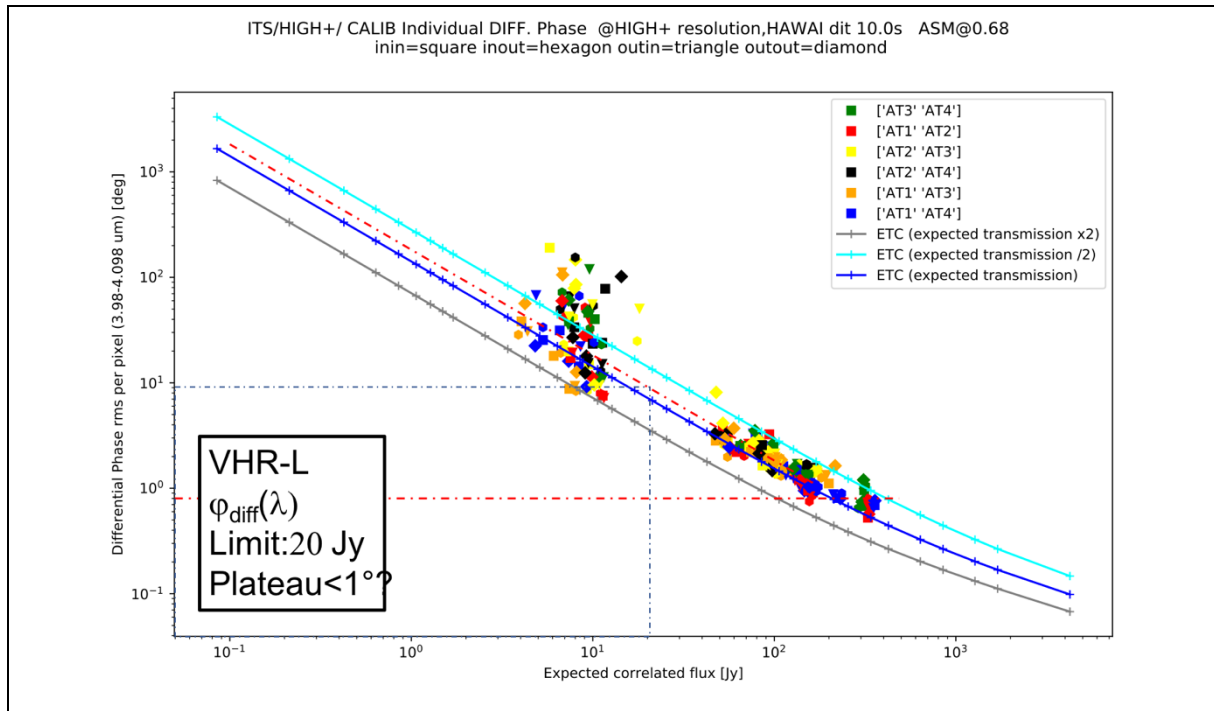
The fundamental noise is estimated from the dispersion of measurement values in the spectral direction after removal of calibration errors by a polynomial fit of the data. Then it is compared to the Exposure Time Calculator (ETC) prediction. Eventually, the parameters of the ETC (mainly the transmission of the mode) are adjusted to fit the experimental date, if necessary.

In the following we show the plots of actual measurement precision as a function of flux, over plotted with ETC predictions. This is used to propose a limiting flux for each mode. We have also tried to confirm this limit by plotting one measure obtained on a target near the limit. Comments about each specific resolutions and measurements are given below the figures.

4.2 VHR MODE

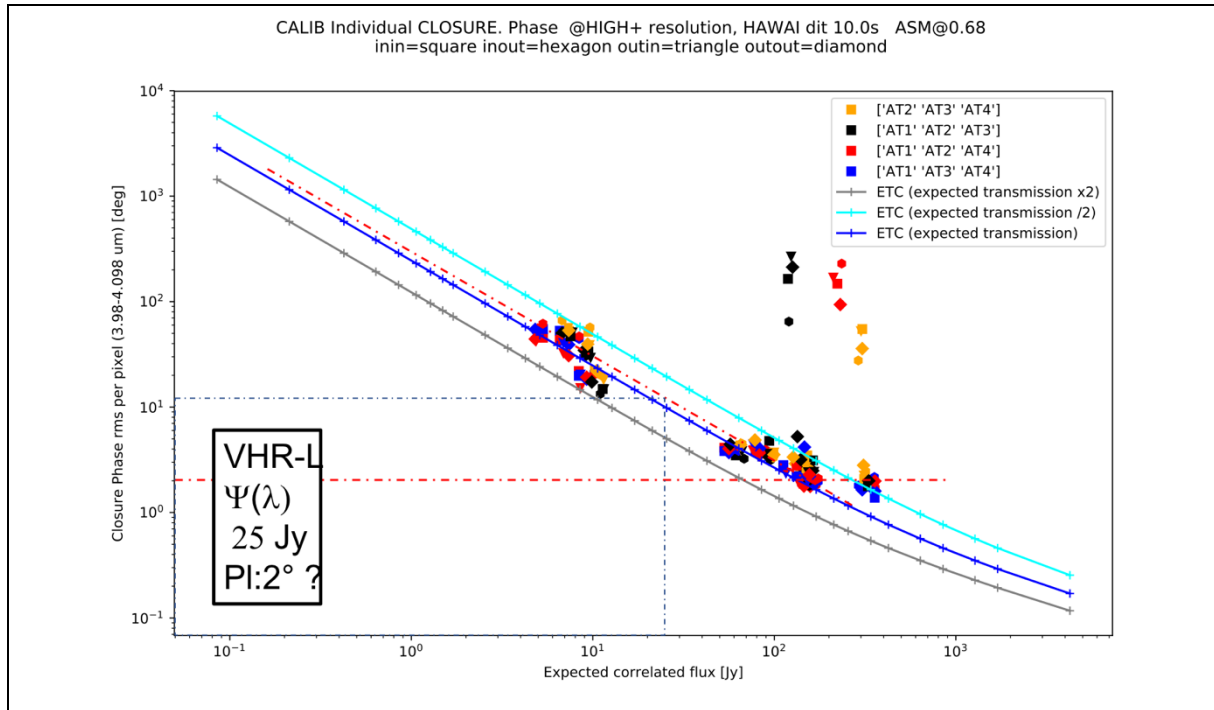
The VHR mode is offered in the full M band and in L around Br_α . As shown in Annex 0, the transmission in L very rapidly drops at short wavelengths, because of the order sorting filter. In M, the transmission of the VHR grism is better than this of the MR one.

4.3 VHR-L DIFFERENTIAL PHASE: 20 JY LIMIT



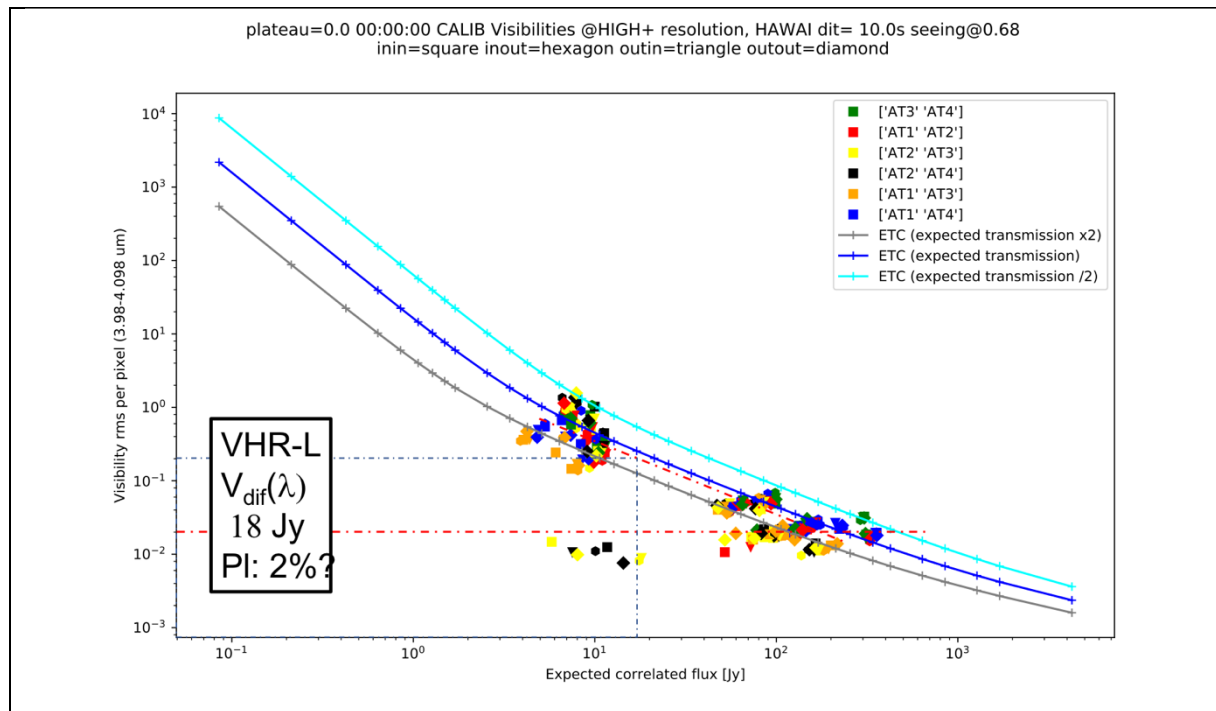
Differential phase precision, per spectral pixel, in $^{\circ}$ as a function of correlated flux in Jy. DIT=10s. Precision estimated over the 3.98 to 4.098 μm window. Each point represents a 1 mn exposure. The colors of the points refer to baselines and the shapes to BCD positions. The blue lines are the ETC predictions. The red dash-dotted line is a median ETC update fitted through the data. A precision of 4° /spectral channel is equivalent to 9° /spectral pixel (~ 5 pixels/channel). This equivalent to a coherent flux SNR=10 per spectral channel. This is achieved for a 20 Jy source.

4.4 VHR-L CLOSURE PHASE: 25 JY



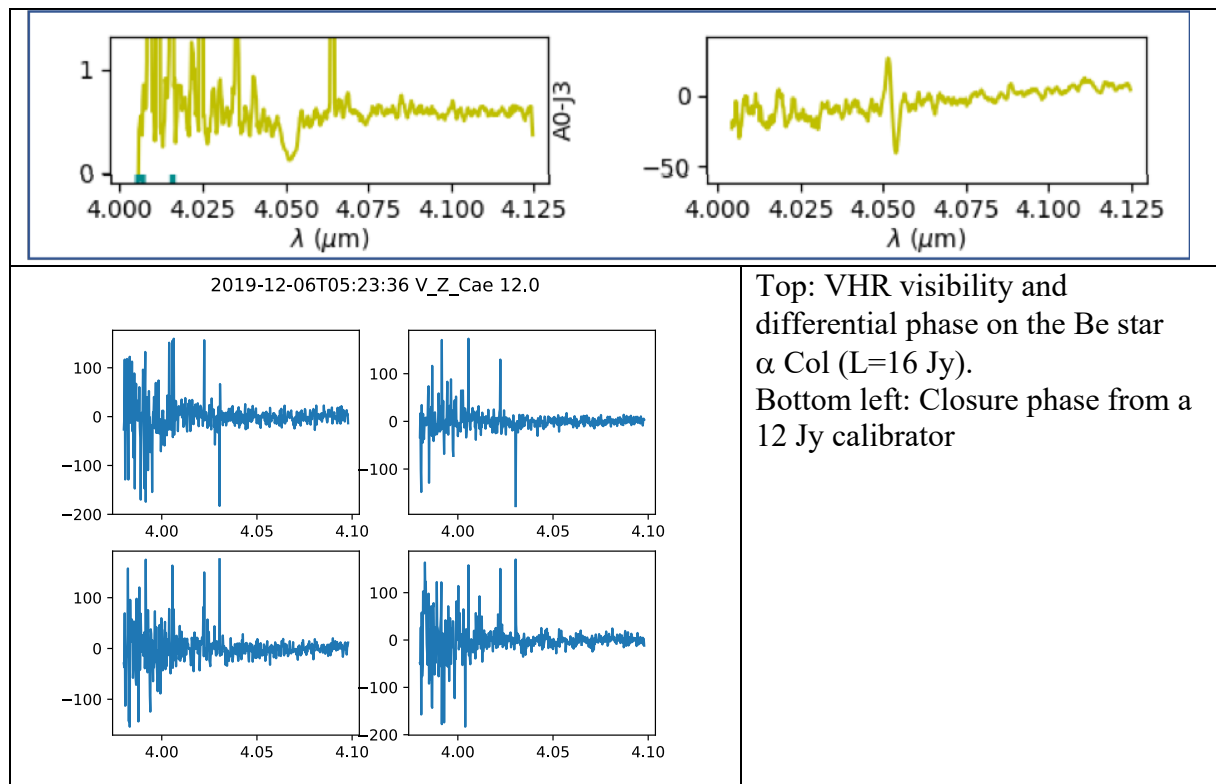
Same plot for the Closure phase, yielding a 25 Jy limit

4.5 VHR-L DIFFERENTIAL VISIBILITY: 18 JY

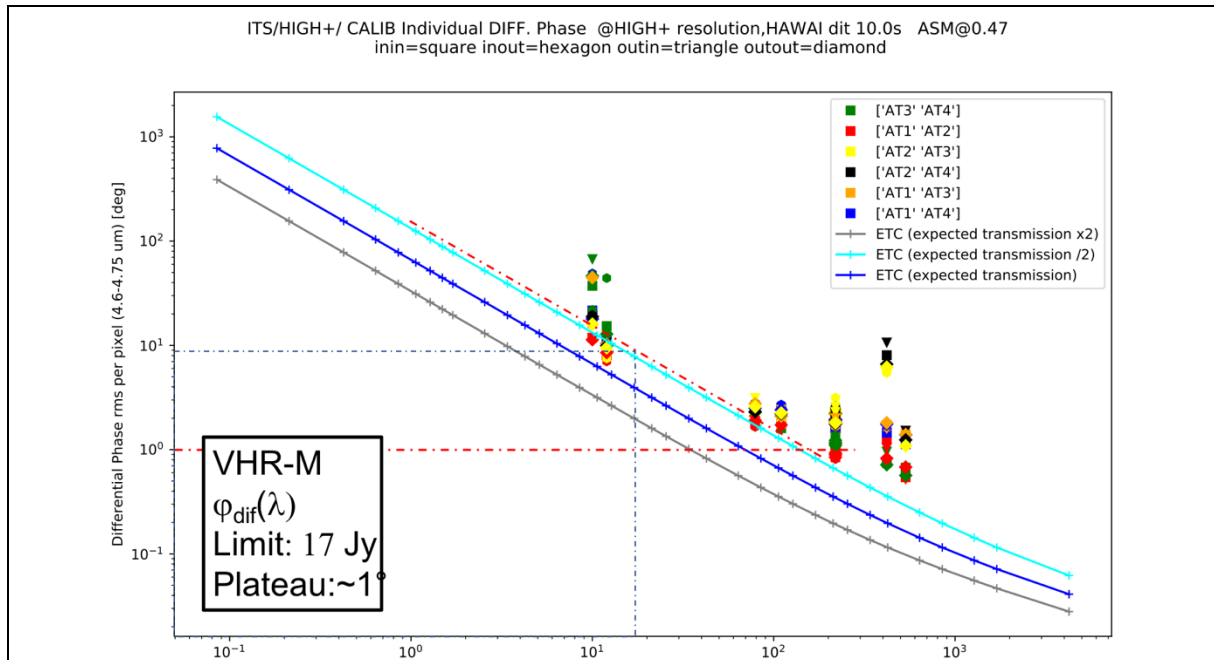


Same plot for the Differential Visibility, yielding a 18 Jy limit.

4.6 VHR-L ILLUSTRATION

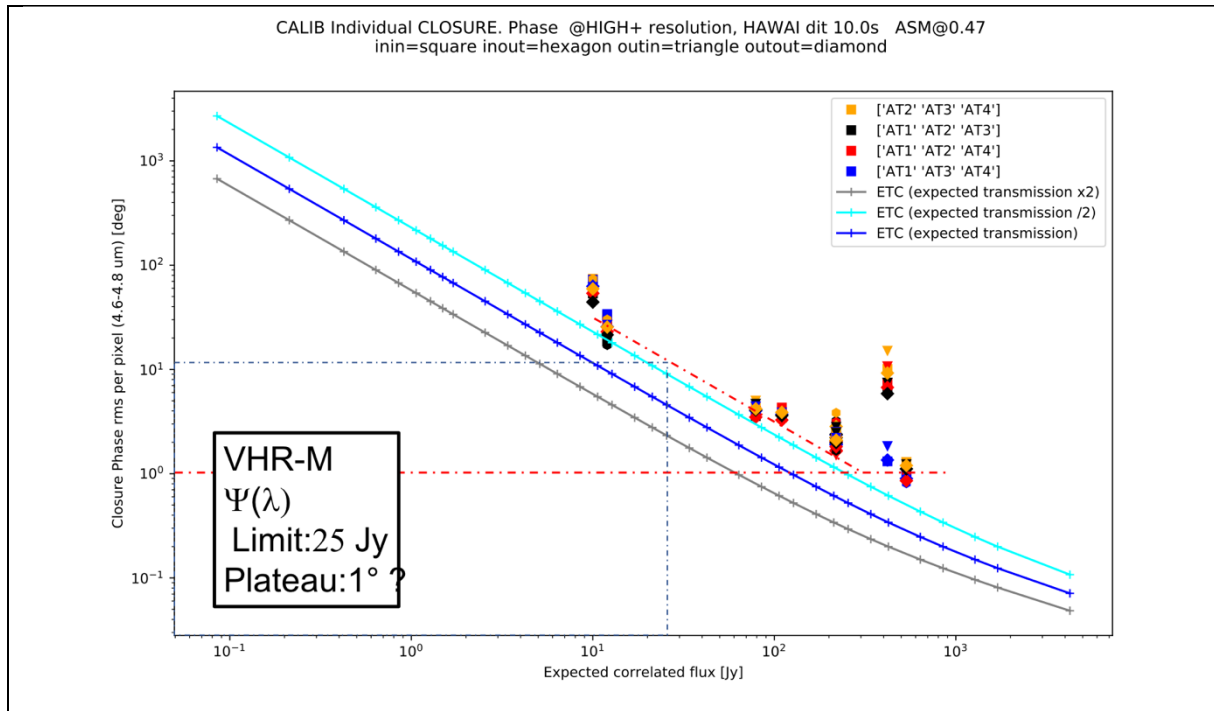


4.7 VHR-M DIFFERENTIAL PHASE: 17 JY



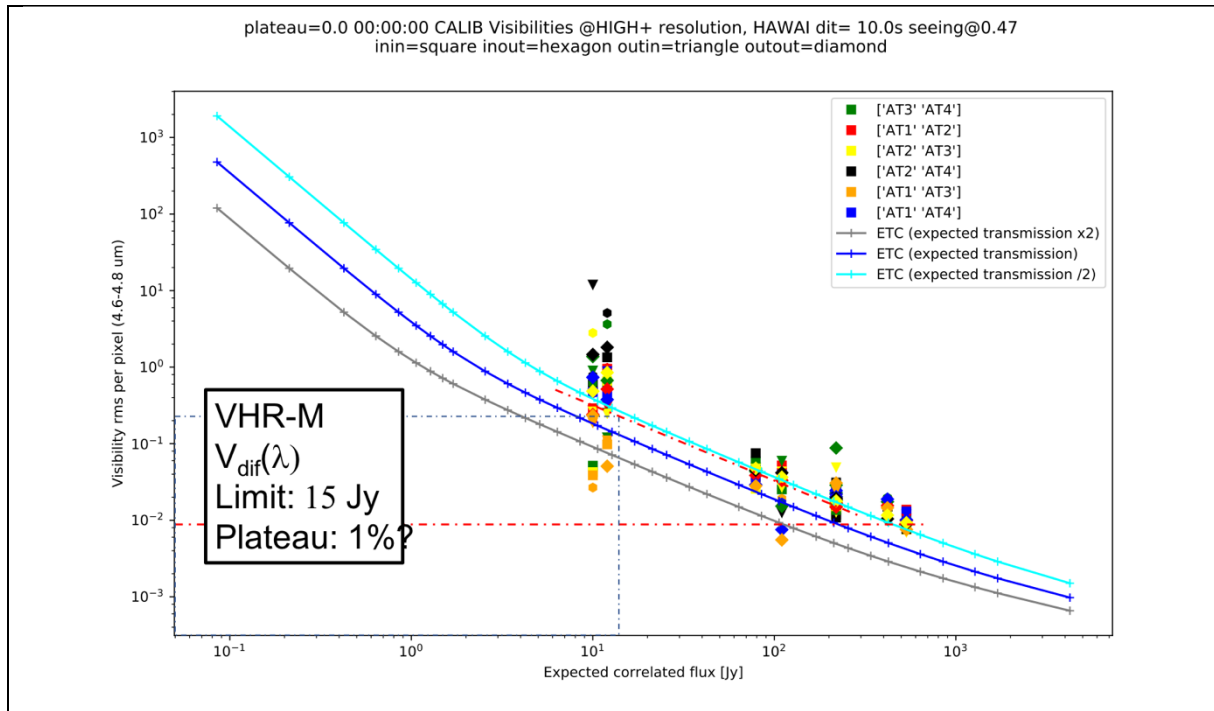
Differential phase precision in VHR-M, here as a function of the flux in Jy (because the correlated flux estimates, based on the visibility measured from non-chopped M data, are not available). The limit is M~18 Jy

4.8 VHR-M CLOSURE PHASE: 25 JY

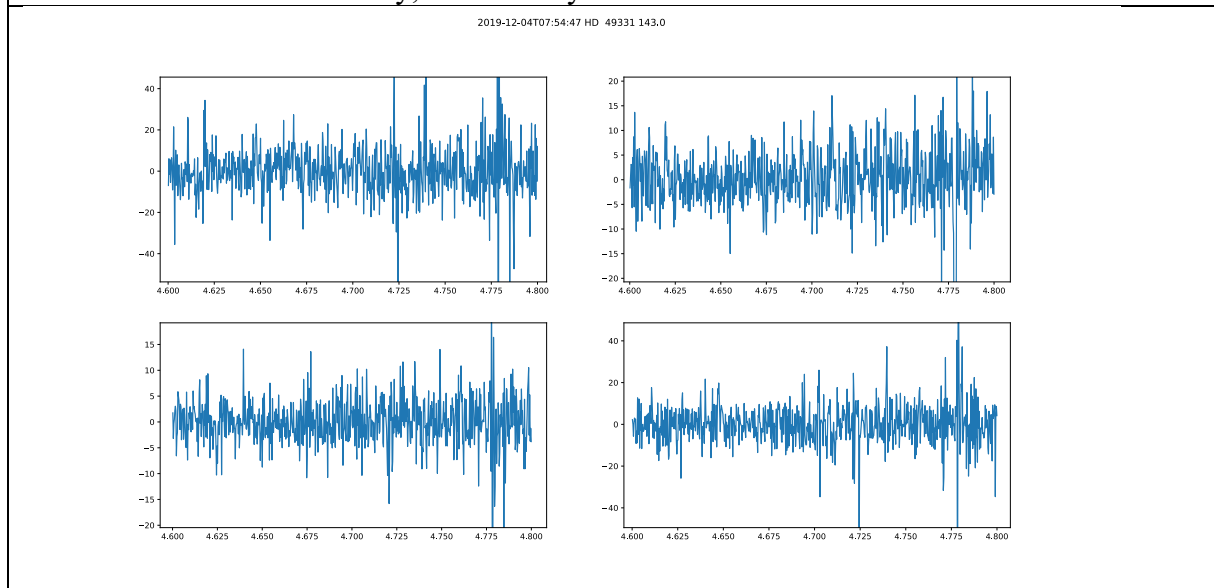


Same for Closure Phase, yielding a 25 Jy limit for VHR-M

4.9 VHR-M DIFFERENTIAL VISIBILITY: 15 JY

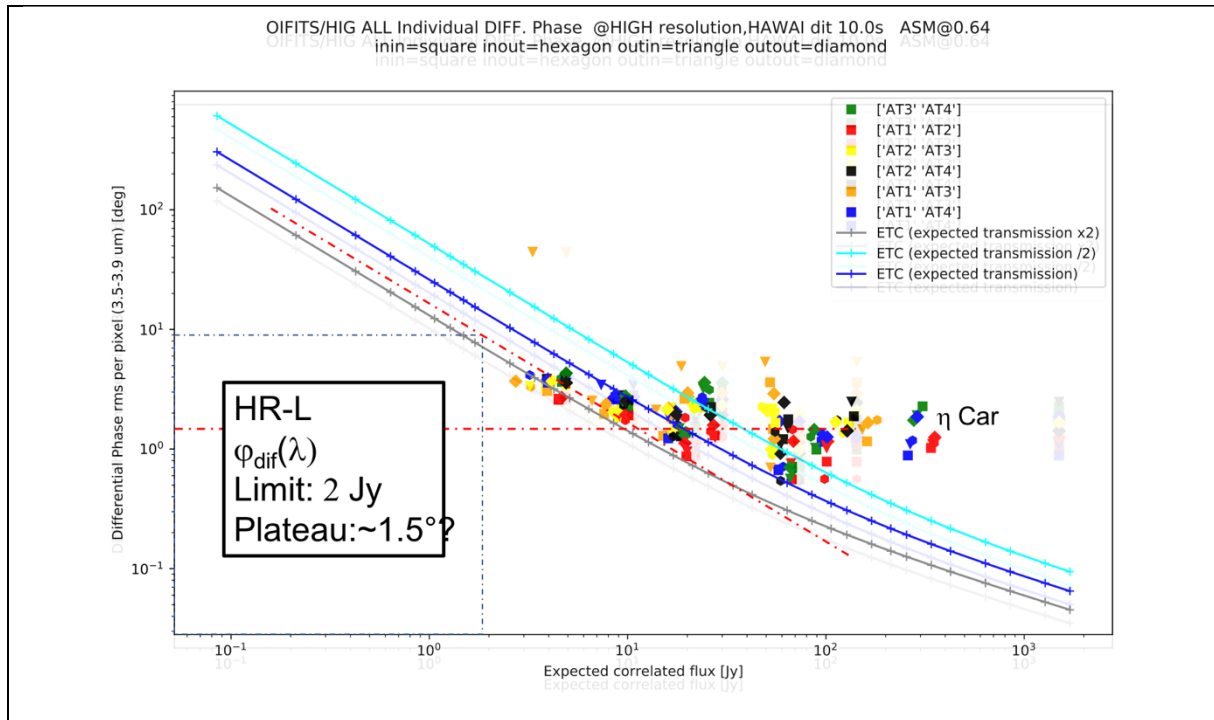


Same for differential visibility, with a 15 Jy limit.



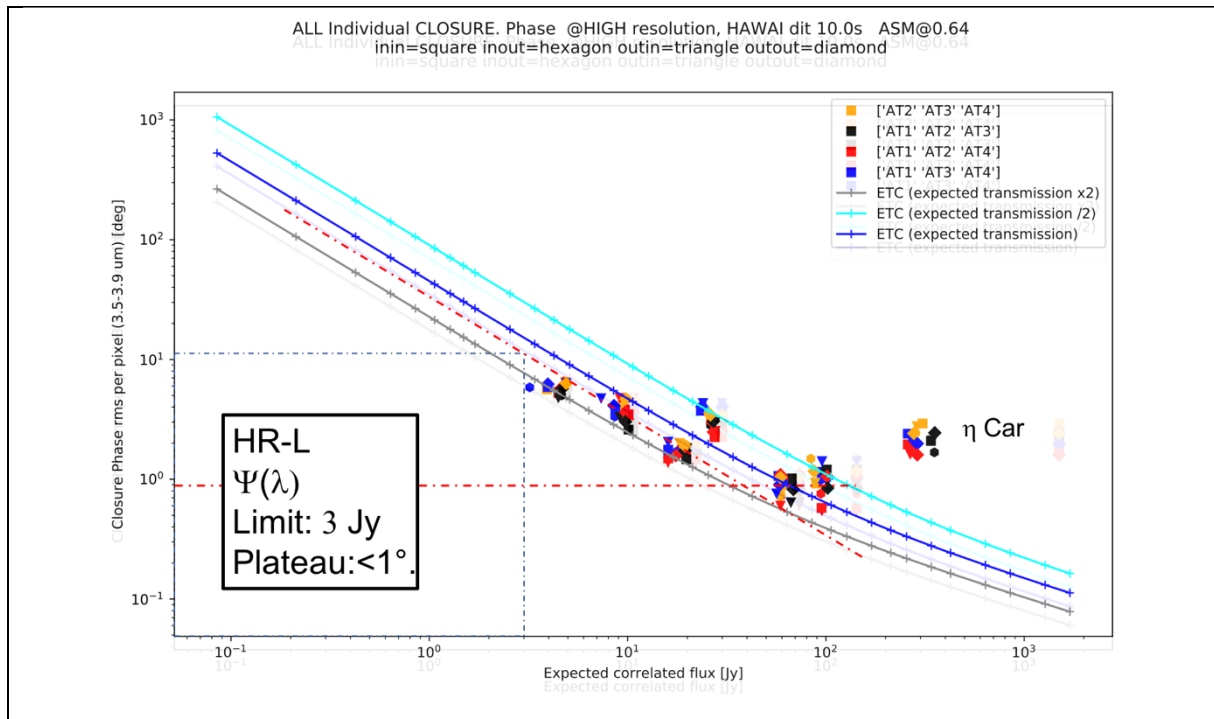
Closure phase on the calibrator HD 49331 ($M \sim 66 \pm 24 Jy$)

4.10 HR-L DIFFERENTIAL PHASE: 2 JY



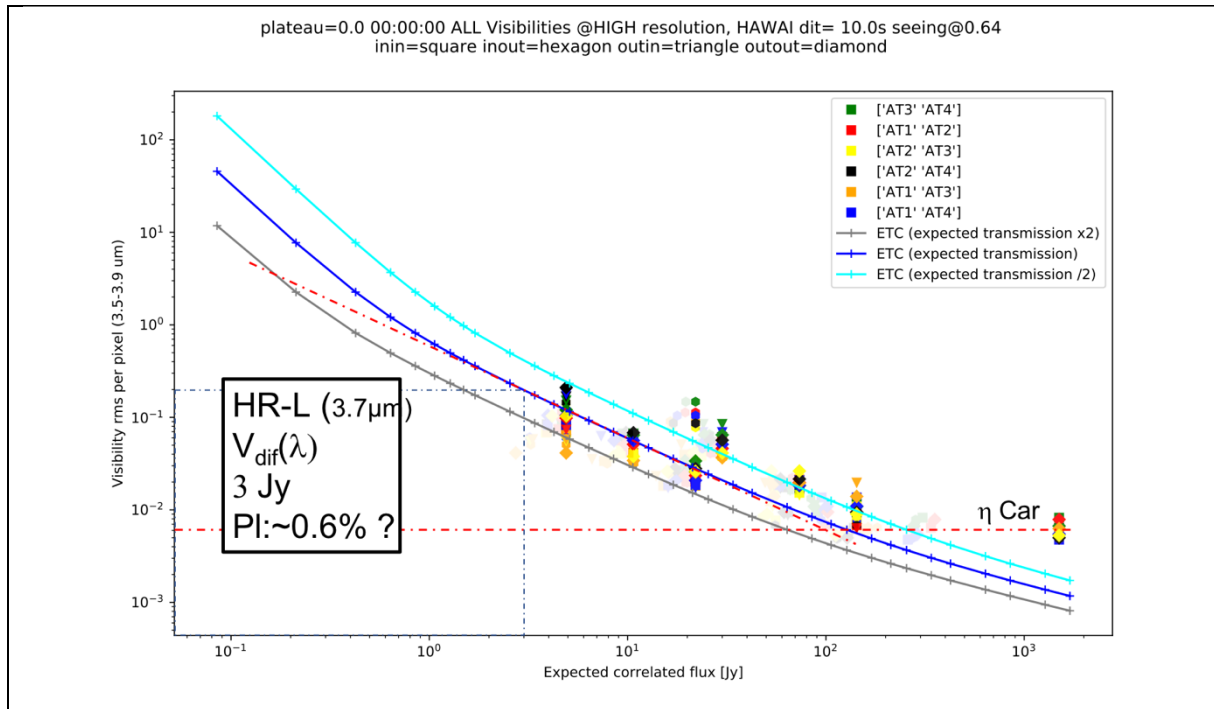
Differential phase precision in HR-L, as a function of correlated flux for 3 calibrators and 4 stars with Hydrogen lines. The dots as a function of absolute flux appear dimmed. From a fit through the calibrators we get a 2 Jy limit.

4.11 HR-L CLOSURE PHASE: 3 JY

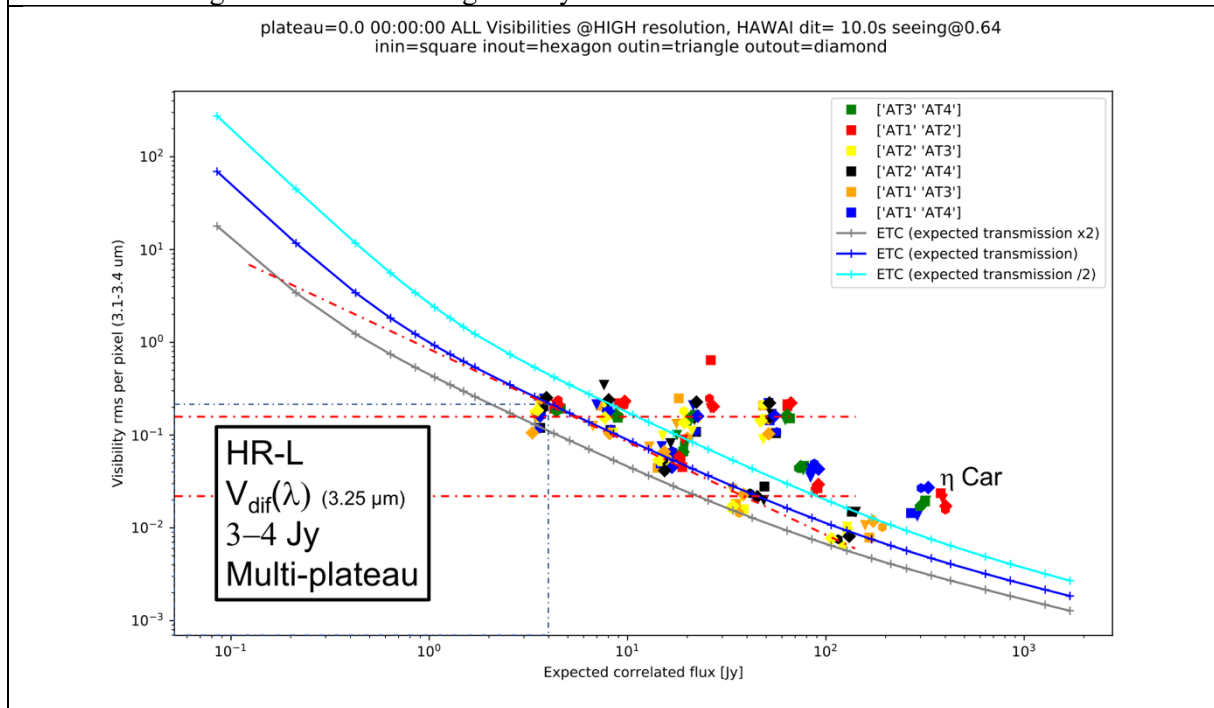


Closure phase precision in HR-L, as a function of flux (and correlated flux for the dimmed points) for 3 calibrators and 4 stars with Hydrogen lines. From a fit through the calibrators we get a 3 Jy limit.

4.12 HR-L DIFFERENTIAL VISIBILITY: 3 JY BUT SIPHOT SHIFT PROBLEM

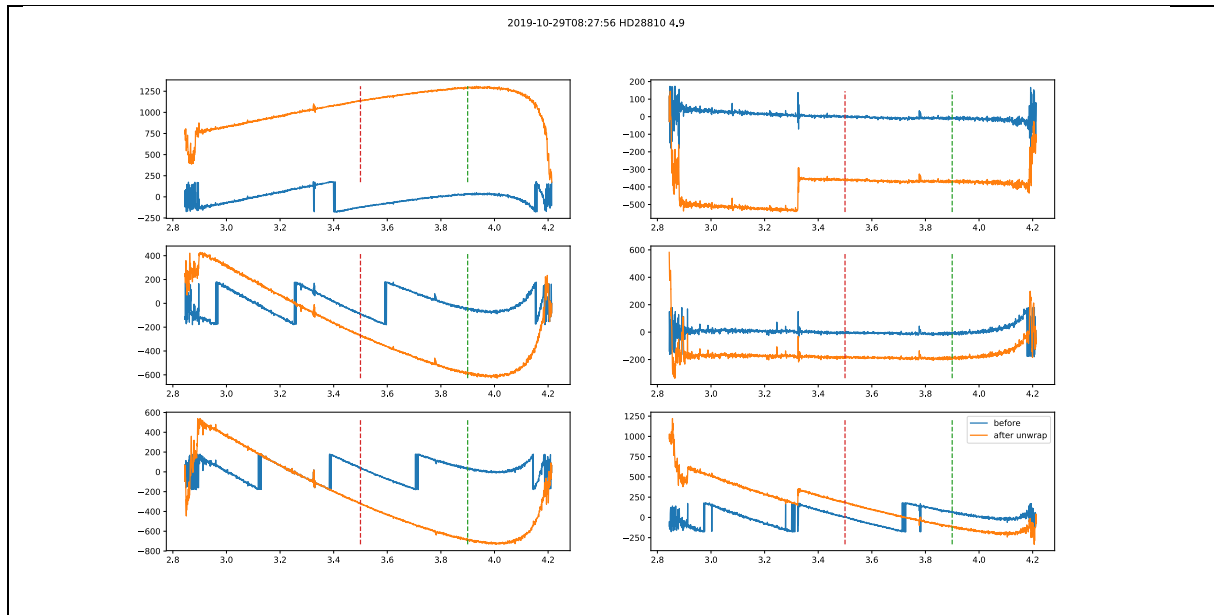


Differential visibility precision in HR-L, in the 3.5-3.9 μm range, as a function of flux for 3 calibrators and 4 stars with Hydrogen lines. The dots as a function of absolute flux appear dimmed. From a fit through the calibrators we get a 3 Jy limit.



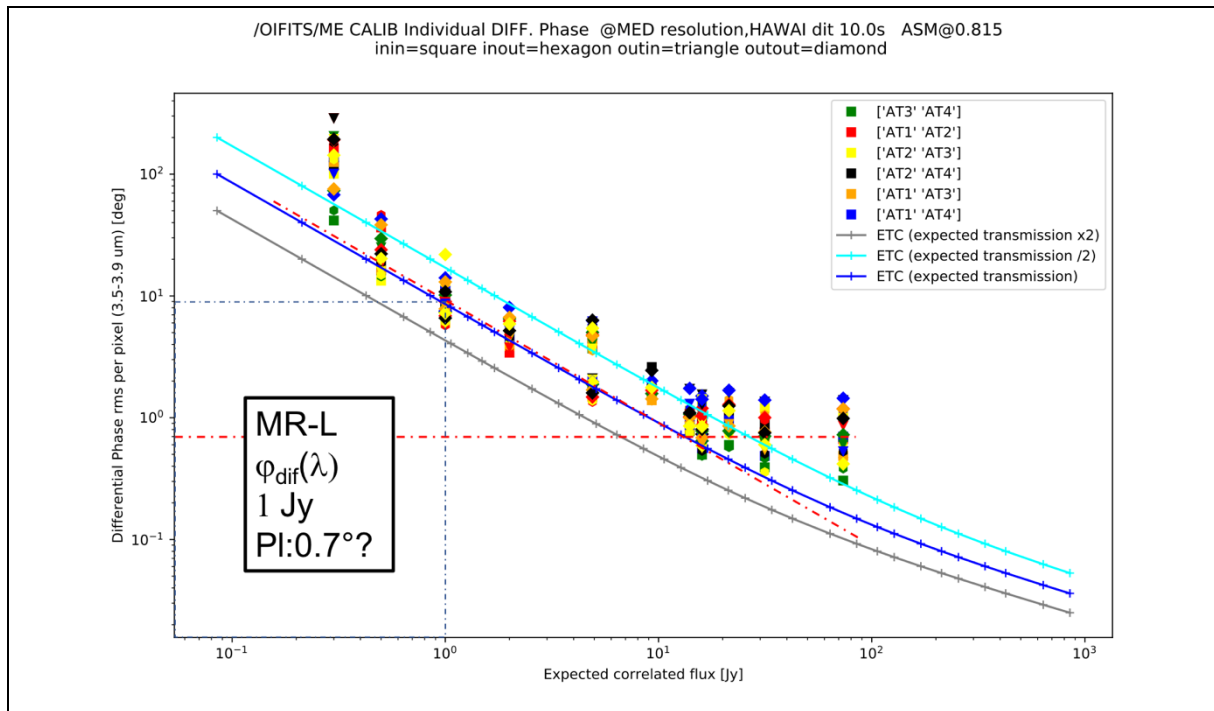
Differential visibility precision in HR-L, in the 3.1-3.4 μm range, as a function of flux for 3 calibrators and 4 stars with Hydrogen lines. A fit through the calibrators could give a 4 Jy limit. But there are a lot of weird points from a spectral region without stellar lines. This is produced by the very dense atmospheric lines that are slightly shifted between interferometric and photometric channels. This subpixel variable shift biases the visibility estimates in this regime. We are working on a software correction of this problem, and we have to implement it before Visibility observations with this resolution. The same problem exists in MR-L and MR-M for visibility measurements.

4.13 HR-L ILLUSTRATION



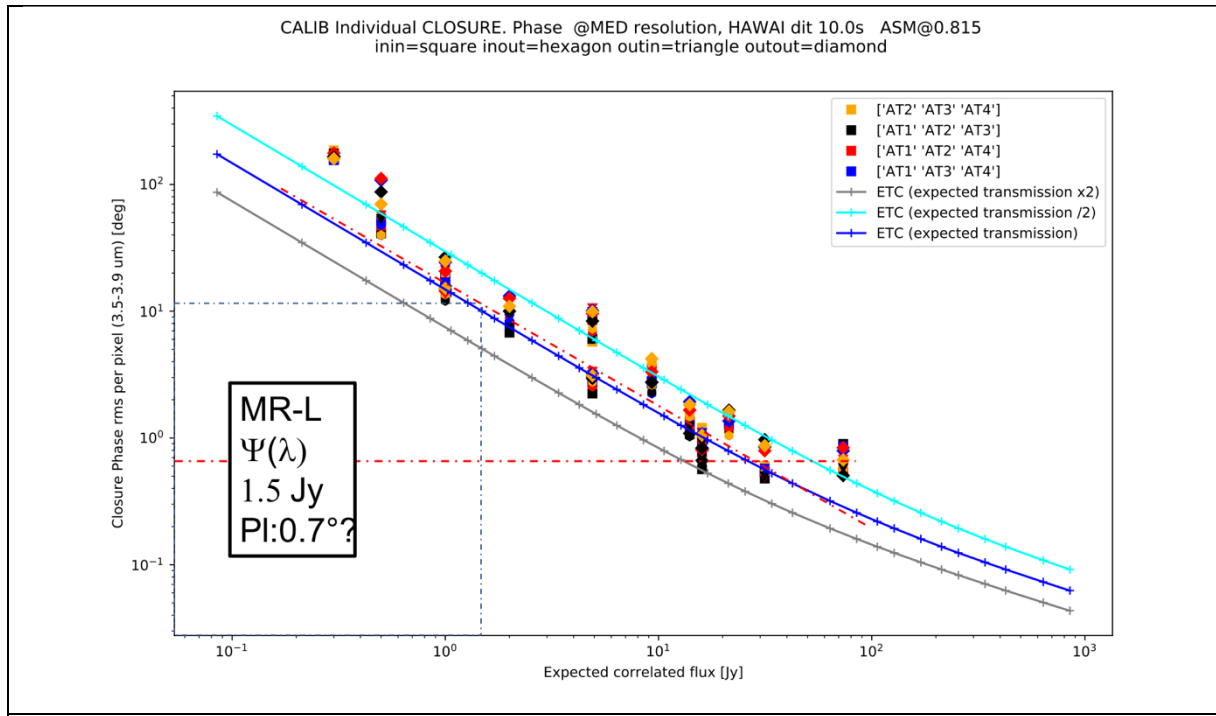
HR-L differential phase on a L=5 Jy calibrator. The measured phase is wrapped and shows 2π jumps. We use an unwrapping python function before applying the ETC procedure. We see here that the unwrapping can partially fail or need to be iterated. The user should be aware of this phase wrapping problem, even if we plan to correct this in the DRS. This problem is not critical for local continuum-line-continuum measurements.

4.14 MR-L DIFFERENTIAL PHASE: 1 JY



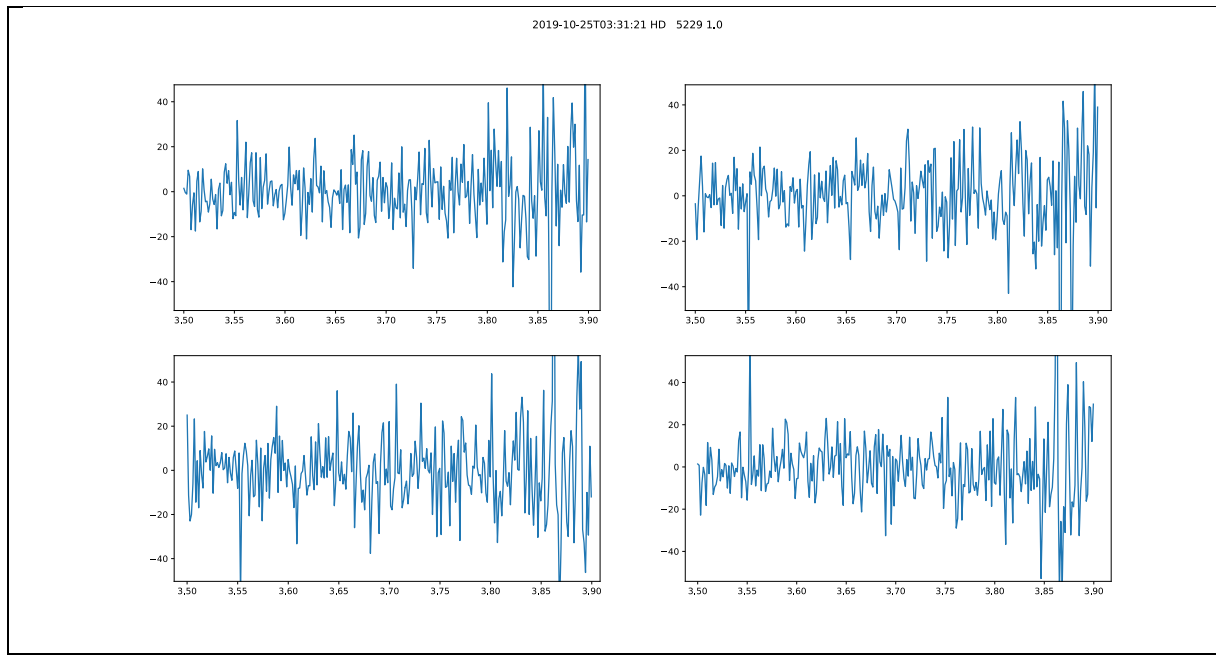
MR-L differential phase precision as a function of flux. Limit 1 Jy.

4.15 MR-L CLOSURE PHASE: 1.5 JY



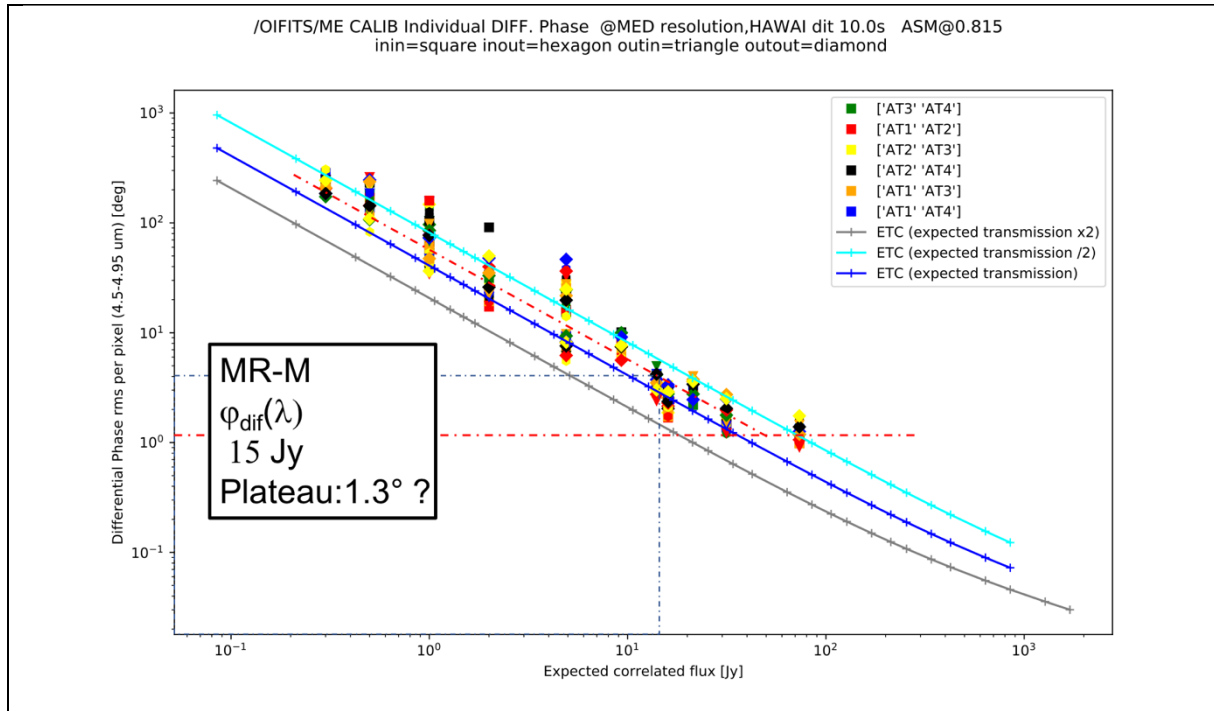
MR-L closure phase precision as a function of flux. Limit 1.5 Jy.

4.16 MR-L ILLUSTRATION



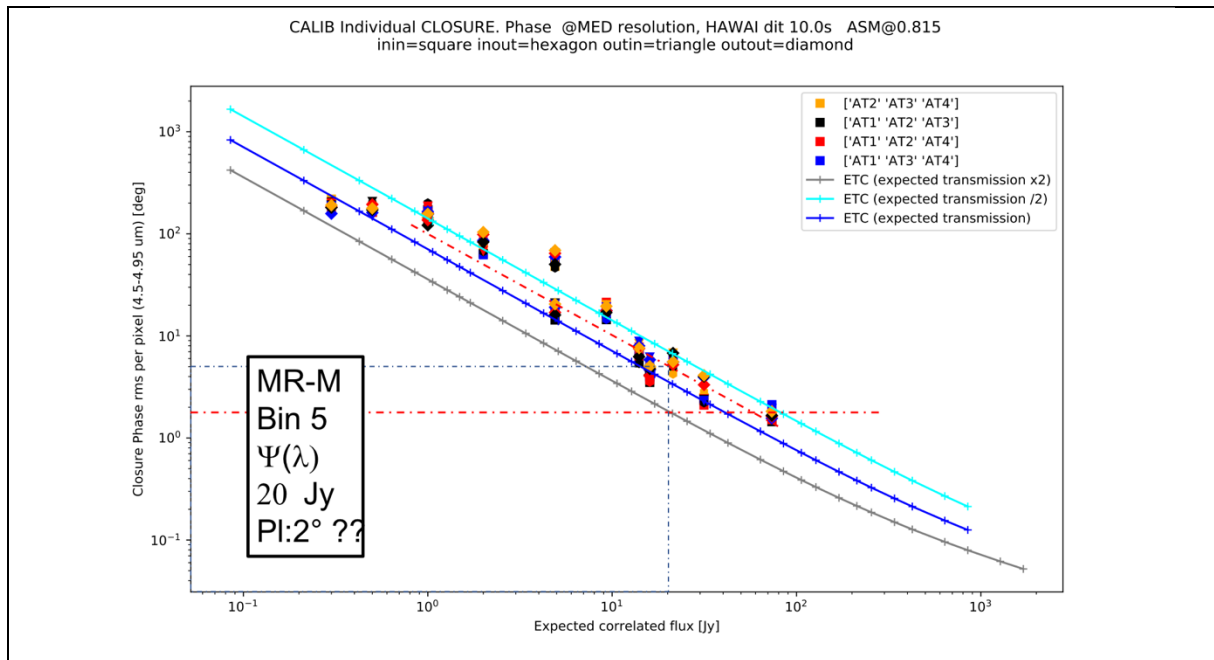
Closure Phase in MR L on the calibrator HD 5229 (L=0.9 Jy)

4.17 MR-M DIFFERENTIAL PHASE



MR-M differential phase precision as a function of flux. Limit 15 Jy. Unlike all other plots, here de spectral pixels have been binned 5 by 5 to get the precision on a spectral channel. Then the specification is directly 4° per spectral channel that yields a limit M~15 Jy.

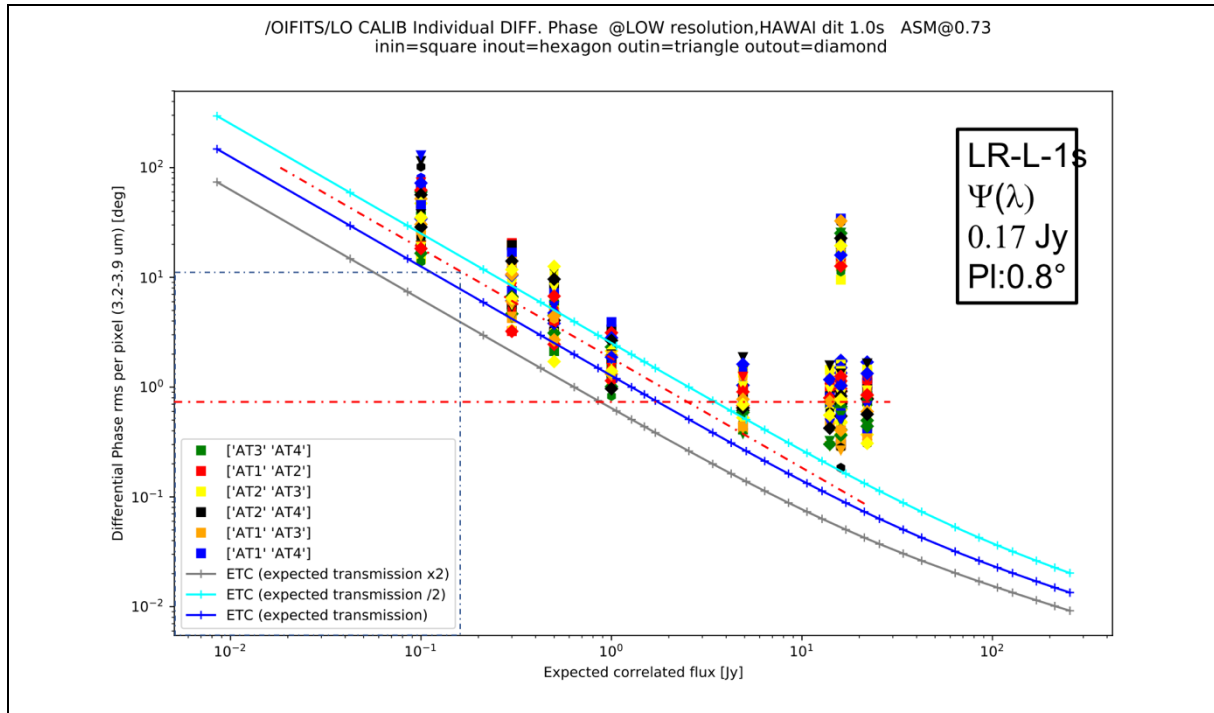
4.18 MR-M CLOSURE PHASE



MR-M closure phase precision as a function of flux. Here the spectral pixels have been binned by 5 in spectral channels before the Fourier processing. Then, the criteria CP precision=5° per spectral channel and per exposure yields a 20 Jy limit.

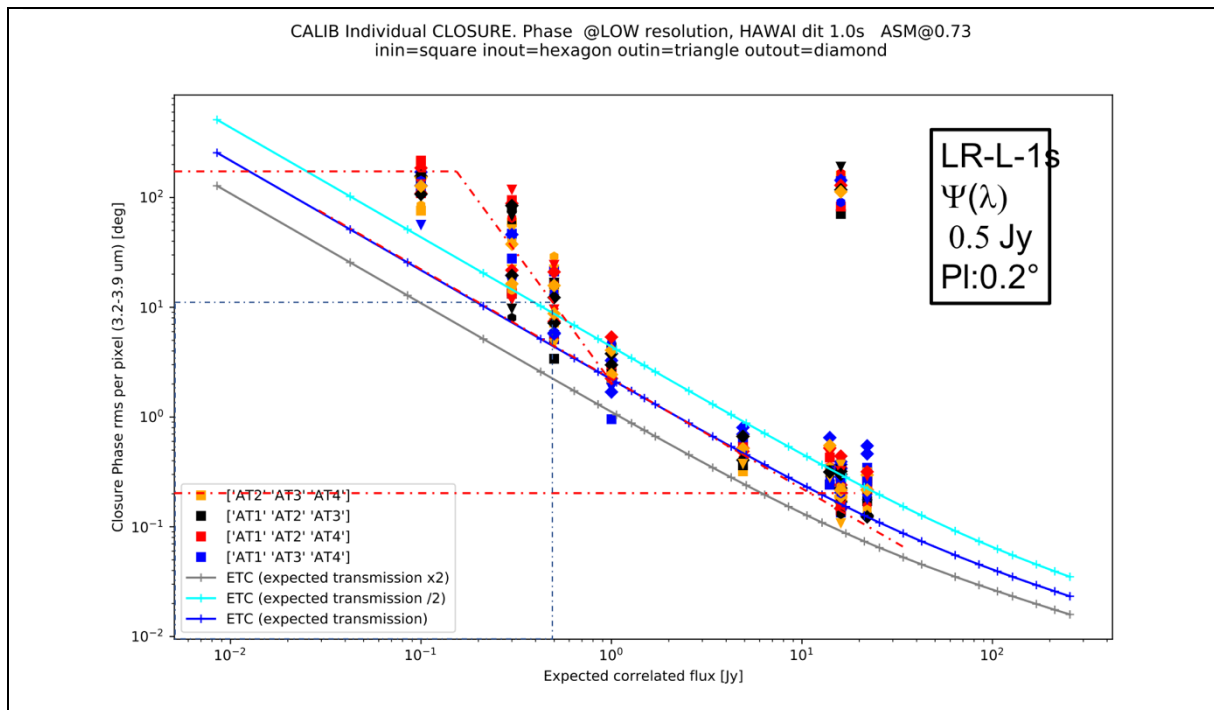
The very small limiting sensitivity difference between MR-M and VHR-M indicates that, when GRA4MAT is available, it is worth to observe in VHR-M and to bin the spectral channels to the MR-M resolution. In addition, the VHR-M allows cleaning the spectrum for the complex atmospheric features before processing, although this is not part of standard DRS so far.

4.19 LR-L DIFFERENTIAL PHASE: 0.17 JY



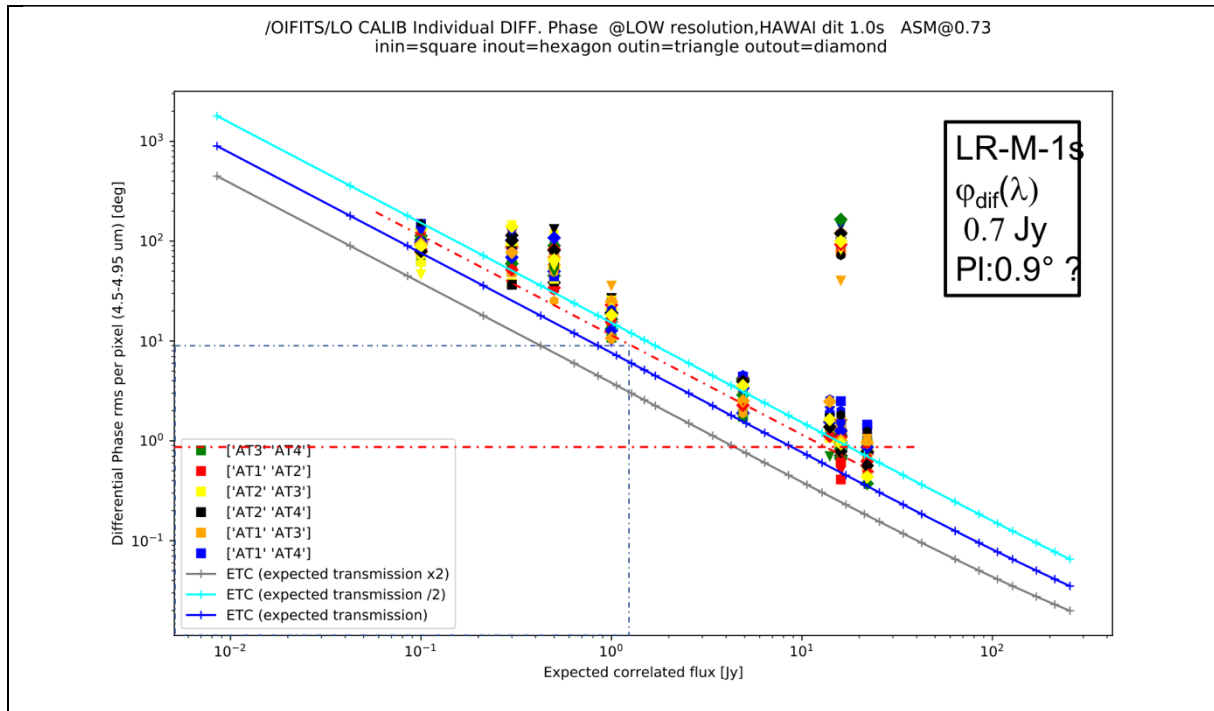
LR-L differential phase precision as a function of flux. Limit 0.17 Jy.

4.20 LR-L CLOSURE PHASE: 0.5 JY



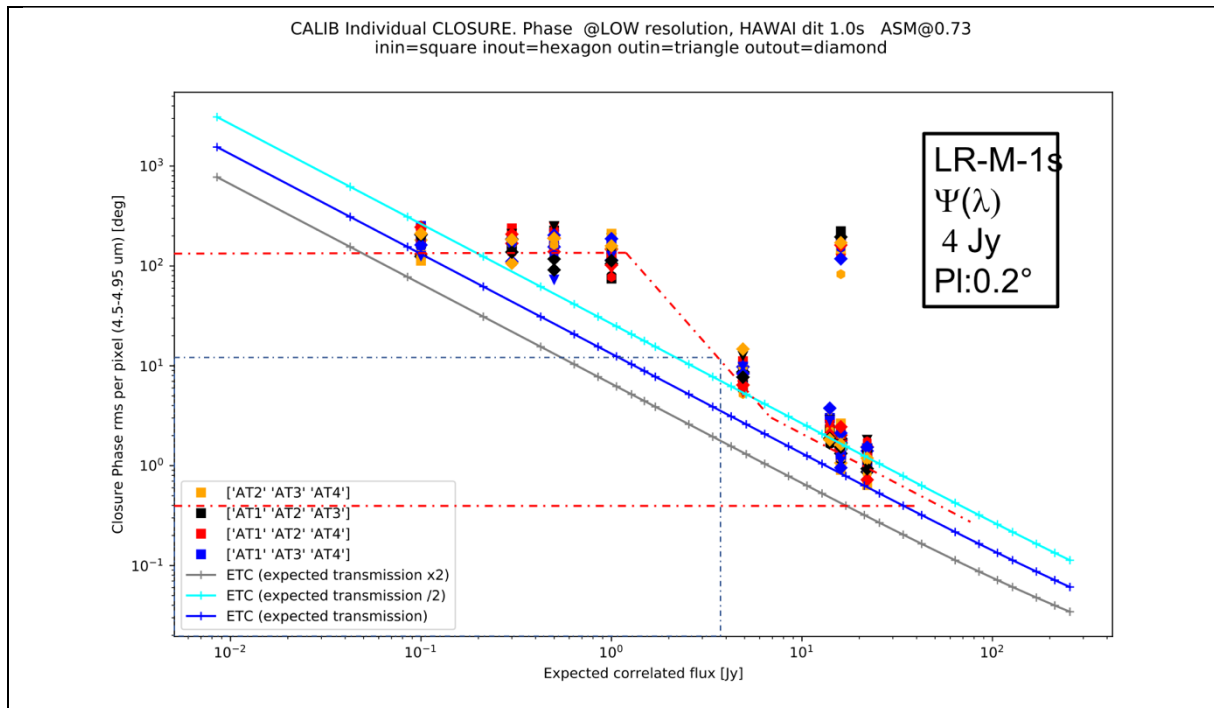
LR-L Closure phase precision as a function of flux. Limit 0.5 Jy. From the differential phase precision, we see that an important gain can be expected on the closure phase precision by spectral binning before processing.

4.21 LR-M DIFFERENTIAL PHASE: 0.7 JY.



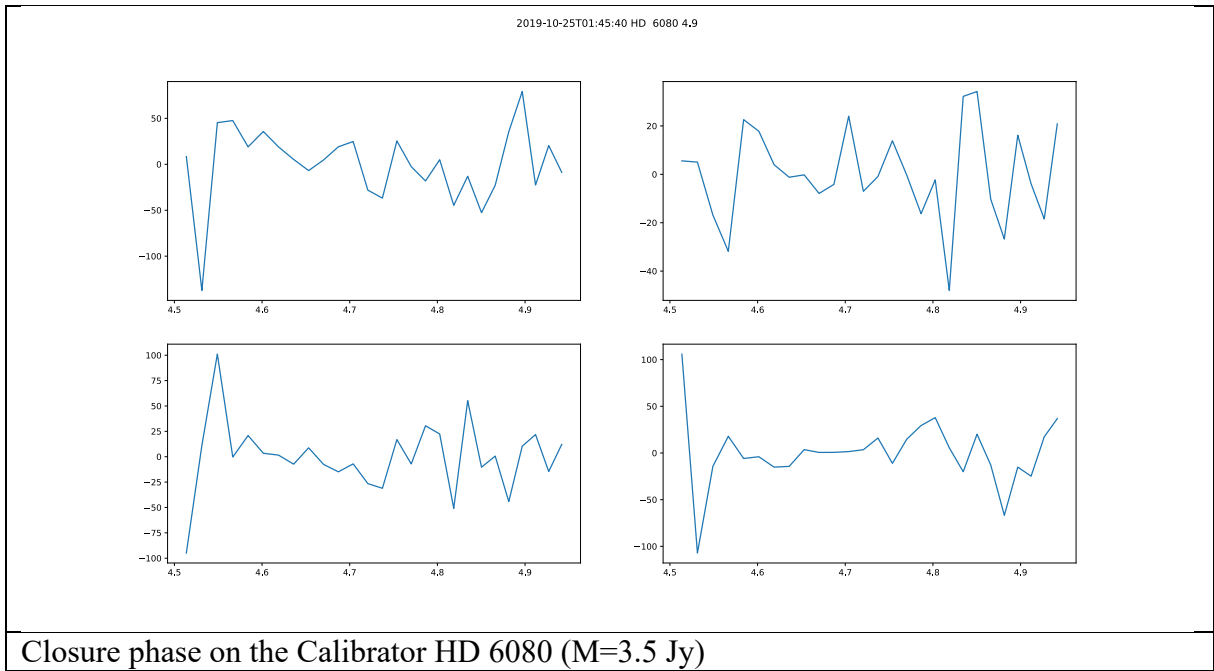
LR-M differential phase precision as a function of flux. Limit 0.7 Jy.

4.22 LR-M CLOSURE PHASE: 4 JY.



LR-M Closure phase precision as a function of flux. Limit 4 Jy. Like in the L band, from the differential phase precision, we see that an important gain can be expected on the closure phase precision by spectral binning before processing. We should update this rapidly.

4.23 LR-M ILLUSTRATION



5 ANNEX: TRANSMISSION OF VHR GRISMS

The table A gives the maximal flux per pixel (in ADU) in the interferometric image for the different grisms with the same instrumental set-up (by using the artificial source):

Grism	Medium		High	Very High	
Filter	L	M	L	L	M
DIT (s)	3	3	6	6	6
Resolution	500	500	950	3400	3400
Flux (ADU)	46000 ³	33000 ³	24000 ³	8800 ¹	16000 ²

Table A: Relative flux per pixel (in ADU) for different grisms.

- ¹: Maximal value for pixel=50 corresponding to $\lambda=4.128\mu\text{m}$ (see figure A).
²: Value at the central part of the detector. The transmission is relatively equal all wavelengths.
³: Maximal flux around $4.05\mu\text{m}$ for the L band and $4.65\mu\text{m}$ for the N band.

The transmissions of all the grisms are relatively identical for all wavelength. But this is not the case for the VHR grism in L band due to the coating necessary to eliminate the photons of the low wavelengths. The figure A gives the relative transmission of the VHR grism according to the wavelength:

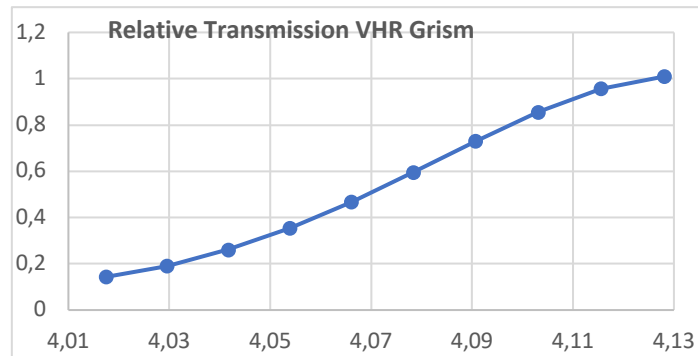


Figure A: Relative transmission of the VHR grism in L band.
 At $4.052\mu\text{m}$ ($B\alpha$) the transmission is 35% of the one at $4.128\mu\text{m}$.

The relative transmission of the different grisms taking as reference the medium resolution grism is given in table B1 and B2:

Grism	Medium	High	VHR ($4.128\mu\text{m}$)	VHR ($4.05\mu\text{m}$)
Transmission	1	0.50	0.65	0.23

Table B1: Relative transmission of the grisms in L band

Grism	Medium	VHR
Transmission	1	1.65

Table B2: Relative transmission of the grisms in M band

MATISSE Memo MAT-COM-2021-07-23

From: R. G. Petrov, F. Allouche, Ph. Berio, J. Leftley, A. Matter, A. Meilland, S. Lagarde and the MATISSE Commissioning Team.

With Julien Woillez, Gérard Zins and the ESO GRA4MAT team



To: J. Woillez, Th. Rivinius, C. Paladini ESO, MATISSE Consortium

Sent: July 23, 2021

Version: Draft

Subject: **GRA4MAT with UTs**

MATISSE COMMISSIONING TEAM

Fatmé Allouche, Philippe Berio, Leonard Burtscher, Alain Chelli, Pierre Cruzalèbes, Yann Fanteï, Karl-Heinz Hofmann, Walter Jaffe, Stéphane Lagarde, James Leftley, Bruno Lopez, Alexis Matter, Anthony Meilland, Klaus Meisenheimer, Florentin Millour, Sébastien Morel, Romain Petrov, Sylvie Robbe-Dubois, Sylvain Rousseau, Dieter Schertl, Jozsef Varga.

1	Scope.....	124
2	Summary of conclusions	124
2.1	Status of observations.....	124
2.2	Propositions	124
2.3	GRA4MAT operation limits	124
2.4	Coherent flux limit in the N	124
2.5	DIT for LM band observations with GRA4MAT on UTs	125
2.6	Absolute visibility measures	126
2.7	Execution times with GRA4MAT.....	127
2.8	Data reduction of MATISSE data with GRA4MAT.....	127
3	Targets successfully reduced in N with the K for N coherent flux bias correction.	128
4	Fringe jump rates as a function of observing conditions.....	131

CHANGE RECORD

Issue	Date	Section/page	Reason
1.0	23/07/2021	All	Draft

1 SCOPE

We report the analysis of the data collected about the use of GRA4MAT on UTs and we discuss about what we currently know about the possibilities and limits of this mode.

2 SUMMARY OF CONCLUSIONS

2.1 STATUS OF OBSERVATIONS

In March 2020, February 2021 and June 2021, we had 6.5 half nights on UTs to test GRA4MAT. We could actually observe during a little bit less than 3 half nights, the rest being lost to weather or extremely bad seeing conditions.

2.2 PROPOSITIONS

- GRA4MAT should be offered on UTs without chopping for coherent flux observations of faint targets in the N band, without chopping, in the 0.1-1 Jy range.
- The software package developed for GRA4MAT observations in the N band with ATs is applicable to UTs. This includes the detection of fringe jumps and the flagging of frames or modulation cycles affected by fringe jumps and the use of K band information to correct the chromatic OPD effects between K and N and hence allow coherent integration in N.
- When GRA4MAT is used for the N band, the DIT in the L-M bands can be either the short MATISSE standalone DIT (111 ms) or a longer DIT=0.5 s, depending on seeing and airmass as explained below. The DIT=0.5 s can be used to increase the spectral windows in higher spectral resolution modes, but the performances in L and M have not been consolidated and we should conservatively use the MATISSE standalone sensitivity limits.
- On UTs, it is not yet possible to offer GRA4MAT with chopping. Any observations requiring chopping for photometry and hence absolute visibility calibration should be executed with MATISSE standalone.

2.3 GRA4MAT OPERATION LIMITS

We have not detected a significant gap between the V and K magnitudes given for the GRAVITY Fringe Tracker alone and GRA4MAT. We have successfully observed AGNs with compact source magnitudes $K=10\pm 0.3$ in good and fair conditions, including the detection of fringe jumps and the correction of chromatic effects between K and N. Although we do not have enough data to set a precise bad seeing limit, we consider that GRA4MAT should not be used for seeing $>1''$ and $\tau_0 < 2.5$ ms

Seeing conditions	$T \leq 10\%$ Seeing $\leq 0.6''$ $\tau_0 > 5.2$ ms	$T \leq 50\%$ Seeing $\leq 1.0''$ $\tau_0 > 3.2$ ms	$T \leq 85\%$ Seeing $\leq 1.4''$ $\tau_0 > 1.6$ ms
K coherent magnitude limit	10.5	9.5	Don't use GRA4MAT

Table 1: K band coherent magnitude limit for GRA4MAT operation

2.4 COHERENT FLUX LIMIT IN THE N

With MATISSE standalone the coherent flux is biased for targets fainter than 0.5 Jy and $8.5 \mu\text{m}$ and 0.8 Jy at $12 \mu\text{m}$. Improvements of MATISSE standalone DRS will probably divide these limits by at least a factor 2, but the relevant tests are in progress and we cannot yet set

final numbers. With GRA4MAT we have sufficient evidence that this bias limit is lowered down to at least 0.1 Jy

2.5 DIT FOR LM BAND OBSERVATIONS WITH GRA4MAT ON UTs

On UTs we observe a much large number of fringe jumps than with ATs. The fringe jump histograms give the following frame loss rate estimates for selected conditions:

- $\tau_0 > 4$ ms; *seeing* < 1 arc"; *airmass* < 1.5
 - DIT=1 s \rightarrow ~50% frames lost
 - DIT=0.5 s \rightarrow ~15% frames lost
- All conditions [
 - DIT=1 s \rightarrow ~75% frames lost
 - DIT=0.5 s \rightarrow ~50% frames

We therefore recommend to use a DIT=0.5 s and to restrict the use of GRA4MAT to fair seeing conditions $\sim \tau_0 > 3$ ms; *seeing* < 1 arc"; *airmass* < 1.5

DIT=0.5 s restricts the spectral windows to 0.6 μ m in MR, 0.3 μ m in HR and 0.1 μ m in VHR. This yields the following central wavelengths (numbers to be checked, selected among existing values):

MR: 3.3 μ m, 3.88 μ m, 4.78 μ m

HR: 3.17 μ m, 3.4 μ m, 3.52 μ m, 3.77 μ m, 3.95 μ m, 4.65 μ m

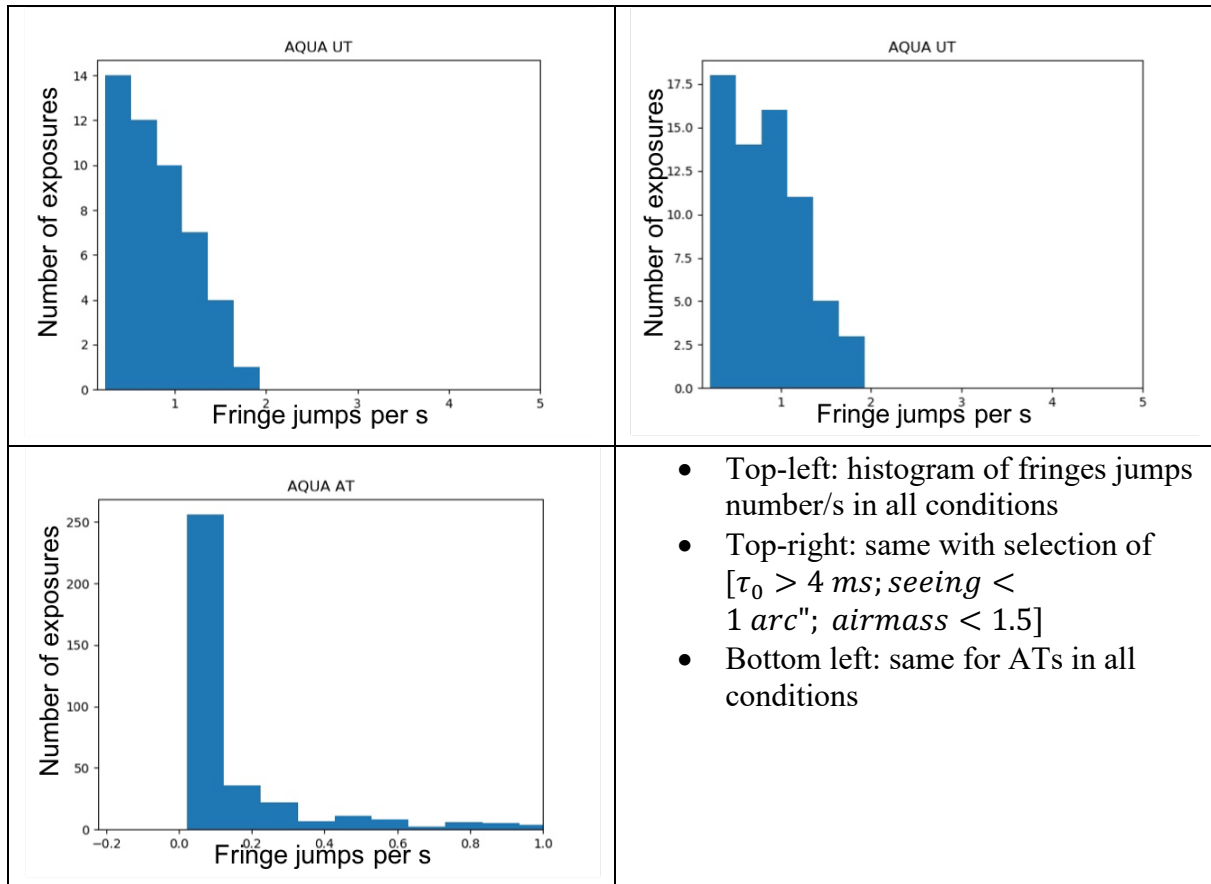
VHR: 3.88 μ m, 3.95 μ m, 4.0 μ m, 4.05 μ m, 4.65 μ m, 4.78 μ m

Limiting performances in LM bands for GRA4MAT with UTs and DIT=0.5 s.

The following numbers are deduced from MATISSE standalone with DIT=0.111 s. They have not been checked experimentally. In L band we should be dominated by detector noise and hence gain like \sqrt{DIT} . In M, we should be limited by background photon noise except, maybe, for VHR.

UT		Closure Phase			Differential Phase & Coherent Flux			CF bias limit
Resolution	DIT	L	M	N	L	M	N	N
Low	0.5 s	0.03	0.1	0.1	0.02	0.07	0.1	0.1
Medium	0.5 s	0.5	1.5	--	0.3	1	--	--
High	0.5 s	1	--	0.7	0.7	--	0.5	<0.5
Very High	0.5 s	8	8	--	6	6	--	--

The numbers in red have been measured on actual reduced and calibrated data. The other numbers are SNR extrapolation using the SNR variations with DIT and telescope diameter.



2.6 ABSOLUTE VISIBILITY MEASURES

GRA4MAT cannot be used on UTs with chopping. This impacts the photometric calibration and hence excludes:

- Absolute visibility measures in the N and M band
- Absolute visibility measures in L for targets³¹:
 - o Fainter than L=1 Jy for broad band (3.1 to 3.8 μm) visibility estimates
 - o Fainter than L=2 Jy for visibility estimates in all individual spectral channels

The DITs selected for MATISSE with GRA4MAT exclude N band photometry with standard MATISSE chopping frequencies³².

Thus, MATISSE with GRA4MAT allows absolute visibility measures only in the L band with the current limiting fluxes (for a visibility precision = 0.1/spectral channel):

Resolution	LR	MR	HR	VHR
Limit in Jy	1	2	2	2

Table 3: flux limit in Jy for absolute visibility measures without chopping in the L band

Above these limits, the use of GRA4MAT for absolute visibility measures in L is recommended because GRA4MAT improves the MATISSE instrument + atmosphere visibility and makes it much less sensitive to seeing changes.

³¹ See memo MAT-COM-2019-07-31 and section 4.1.1

³² The DIT=1s selected for LR with GRA4MAT should be compatible with a chopping frequency of about 0.25 Hz. The quality of the corresponding N band data has not been fully evaluated yet. The possibility to offer MATISSE with GRA4MAT in LR and to execute the photometric sequence with a chopping frequency of 0.25 or 0.2 Hz is an open question.

Below these limits in L and for all N and M observations, absolute visibility measures require chopping and thus, for the time being, stand-alone MATISSE observations.

2.7 EXECUTION TIMES WITH GRA4MAT

The current duration of MATISSE operation with GRA4MAT are:

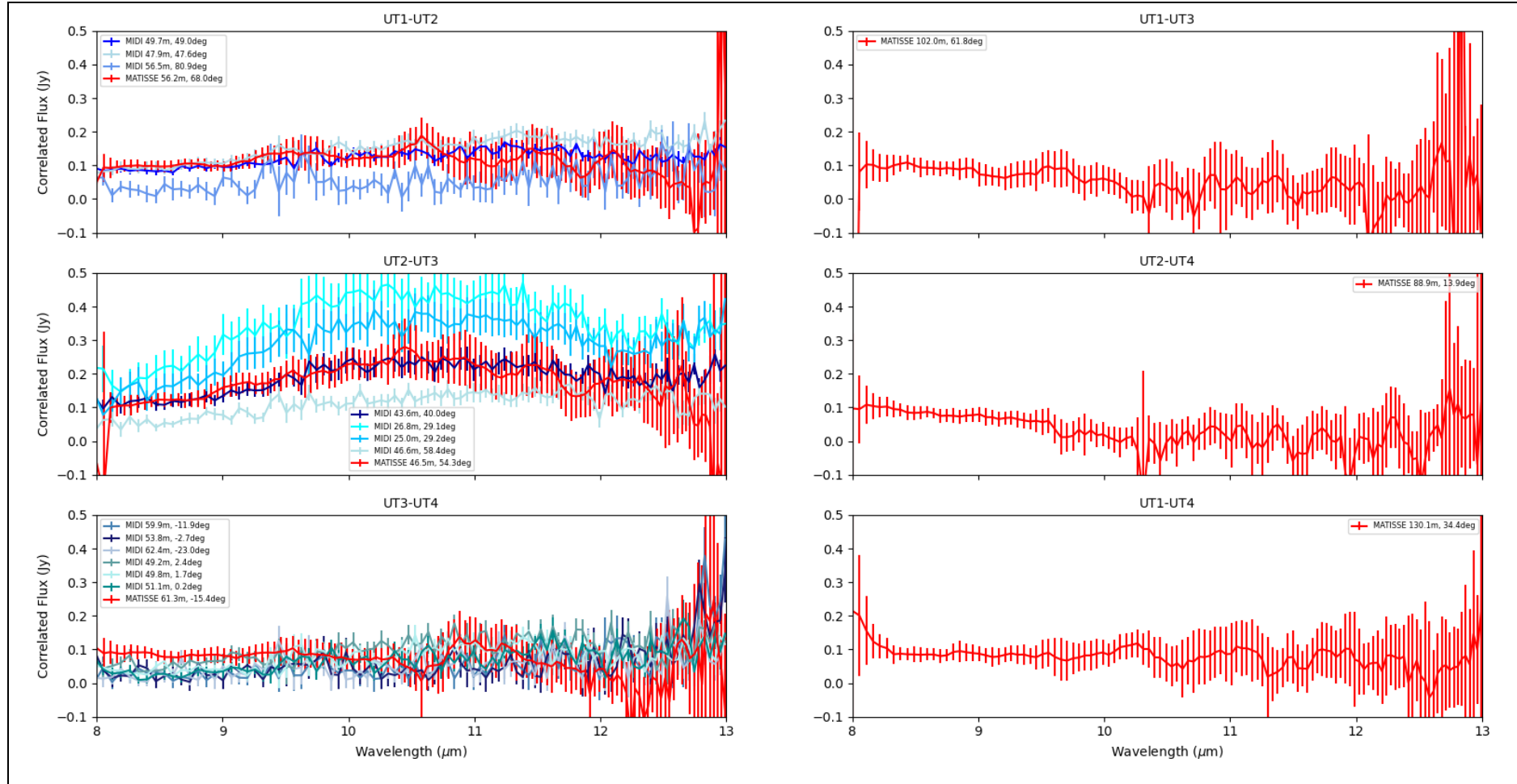
- Acquisition of Image and Fringes: 8 mn
- Observation without photometry: 12 mn

This yields for a complete OB (acquisition + observation): 20 mn.

2.8 DATA REDUCTION OF MATISSE DATA WITH GRA4MAT

- The L and M data can be reduced with the current MATISSE pipeline.
- The detection of fringe jumps and the flagging of L and M band frames and N band modulation cycles affected by fringe jumps and hence excluded from the data processing is included in the current version of the pipeline. The fringe jumps statistics displayed here have been produced by this tool from a count of the number of flagged modulation cycles.
- The use of K band GFT data for coherent integration in N requires the use of an additional Python script both with ATs and UTs. As GRA4MAT is offered to the general user in P108, this feature should be integrated in the pipeline by the start of P108.

3 TARGETS SUCCESSFULLY REDUCED IN N WITH THE K FOR N COHERENT FLUX BIAS CORRECTION.



Coherent flux of the YSO TW Hya and comparison with MIDI data. A clean MATISSE signal can be observed below 0.1 Jy at least up to 11 μm .

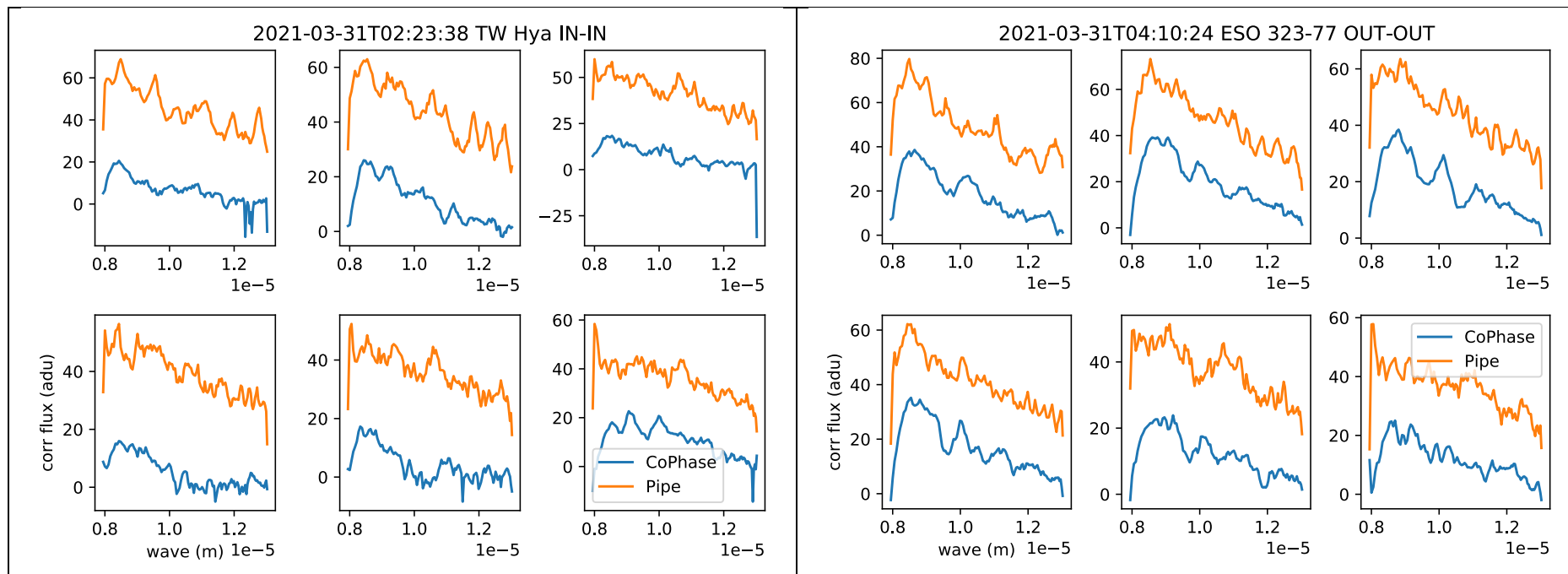
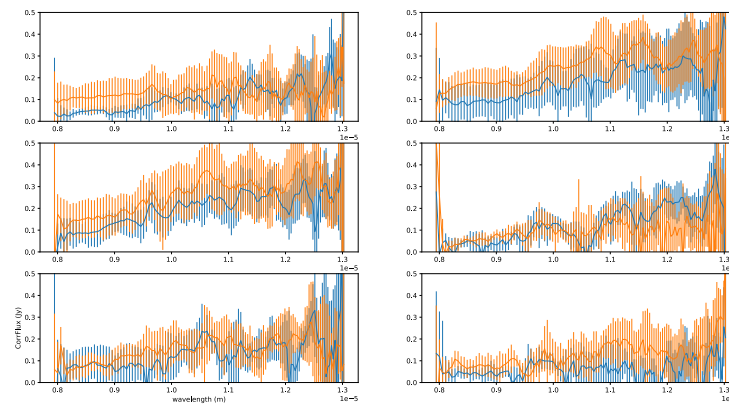
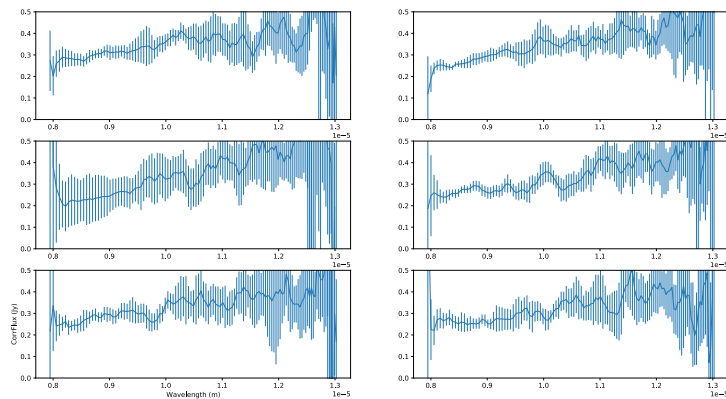
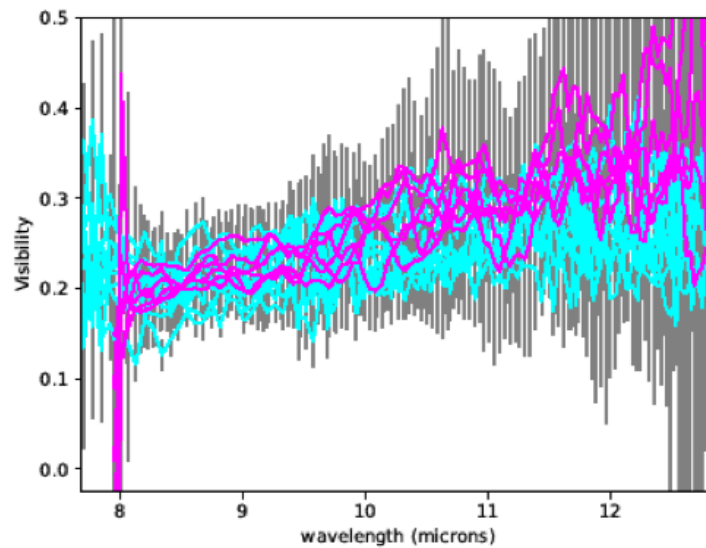


Illustration of the effect of the “K for N” bias correction algorithm, on TW Hya (left) and ESO 323-G77 (right). The standard pipeline reduction (orange lines) shows a bias of the order of 0.3 to 0.5 Jy.

Clock wise:

- ESO 323-G77 calibrated visibility from MATISSE (cyan) and MIDI (purple)
- NGC 3783 calibrated coherent flux for 2 different hour angles. This one shows some good signals well below 0.1 Jy
- 3C273 calibrated coherent flux.

These 3 AGNs have a K band magnitude for the core injected in the GRAVITY FT fibers of $K=10.1 \pm 0.3$ as estimated by GRAVITY observations.



4 FRINGE JUMP RATES AS A FUNCTION OF OBSERVING CONDITIONS

Number of fringe jumps per s (color index) as a function of, clockwise:

- the MACAO wavefront variance and the ASM coherence time in ms
- the ASM seeing in arcsec and the airmass
- the MACAO wavefront variance and the airmass

Each point represents one exposure. The numbers near the points are the K band magnitude indicated in the OB.

There are no clear correlations, except that low airmass seems to be favored.

The proximity of the calibrators in time and sky area appears to be far more important than the similarity in K magnitude.

